Reversing antimicrobial resistance with inhibitors of drug efflux pumps

Submitted in accordance with the requirements for the degree of Masters by Research

by

Yang Chen



University of South Australia

Principal Supervisor: A/Prof. Rietie Venter

Co-Supervisors: Dr. Susan Semple, Dr. Steven Polyak

Health and Biomedical Innovation, Clinical and Health Sciences,

University of South Australia

February 2023

Table of Contents

List of Figures *5*

List of Tables *7*

Abbreviations *9*

Thesis Abstract *11*

Declaration *14*

Publications arising from the project and statement of contributions *15*

Acknowledgement *16*

CHAPTER 1 Review of the literature *17*

1.1 Introduction **17**

1.2 The health and economic burden of AMR **18**

1.3 The antibiotic pipeline is running dry **19**

1.4 Reversing resistance as an alternative option for antibiotic development **20**

1.5 Antimicrobial resistance and mechanisms **20**

1.5.1 Antimicrobial resistance 20

1.5.2 General mechanisms of resistance 21

1.5.3 Gram-negative bacteria and AMR 22

1.6 Bacterial Drug Efflux Pumps **23**

1.6.1 Role of efflux pumps in virulence 25

1.6.2 Role of efflux pumps in biofilm formation and resistance 25

1.6.3 RND type drug efflux pumps of Gram-negative bacteria 26

1.6.4 Molecular mechanism of drug efflux by RND-type drug efflux pumps 27

1.6.5 The inhibition of efflux pumps 29

1.7 Representative EPIs of Gram-negative bacteria identified so far **30**

1.8 Tools for studying efflux pump inhibitors **34**

1.9 Studying mechanism of action of EPIs: Kinetic analysis of EPIs binding to AcrB **36**

1.10 Research goal and aims **37**

CHAPTER 2 General Materials and Methods 38

2.1 General Materials 38

2.1.1 General Materials, Growth Medium and Antimicrobial Agents 38

2.1.2 Synthetic compounds and repurposed drug tested as efflux pump inhibitors, and antimicrobial agents 38

2.1.3 Preparation of compounds, antimicrobials, and membrane permeabilisers 39

2.2 General Microbiology 40

2.2.1 Growth media and buffers for incubation 40

2.2.2 Preparation and storage of stock cultures of bacteria 40

2.2.3 Inoculation of a culture from the frozen stock 40

2.2.4 Bacterial strains used for assays 40

2.3 Functional assays 42

2.3.1 Antimicrobial activity assay 42

2.3.2 Checkerboard titration assay 42

2.3.3 Nile red efflux assay 43

2.3.4 Nitrocefin assay 44

2.3.5 $DiOC_2(3)$ assay 45

2.3.6 *In vivo* cytotoxicity assay 46

2.4 Protein techniques 47

2.4.1 Preparation of inside out vesicles (ISOVs) 47

2.4.2 Determination of protein concentration 48

2.4.3 Purification of His-tagged proteins 48

2.5 Surface plasmon resonance 51

2.5.1 Buffers and reagents 51

2.5.2 Preparation of the ligand 52

2.5.3 Immobilisation of protein 52

2.5.4 Determination of kinetic (equilibrium dissociation) constants 53

CHAPTER 3 Design and Synthesis of Benzochromene and Flavonoid Derivatives as AcrB Inhibitors for the Reversal of Bacterial Multidrug Resistance 58

3.1. Introduction 59

3.2 Design and Synthesis of Benzochromene Derivatives as AcrB Inhibitors for the Reversal of Bacterial Multidrug Resistance 62

3.3 Design and Synthesis of Flavonoid Derivatives as AcrB Inhibitors for the Reversal of Bacterial Multidrug Resistance **85**

3.3.1 On-target effect of compound S4 85

3.3.2 Off-target effects of compound S4 88

3.3.3 Conclusion 90

CHAPTER 4 Evaluation of Ivacaftor as MexB efflux pump inhibitor 91

4.1 Introduction **91**

4.2 Results and discussion **94**

4.2.1 Determining the kinetics of ivacaftor binding to MexB using Surface Plasmon Resonance (SPR) 94

4.2.2 Antibacterial activity 100

4.2.3 Ability to reverse drug resistance 100

4.2.4 Nile Red efflux 110

4.3 Conclusion **111**

CHAPTER 5 General Discussion, Conclusions and Future Directions 113

5.1 Introduction **113**

5.2 Synthetic efflux pump inhibitors **114**

5.3 Repurposed efflux pump inhibitor, ivacaftor **117**

5.4 Conclusion **120**

References ***122***

Appendices ***131***

Appendix 1. Chapter 3 Names and structures of benzochromene and flavonoid derivatives (39 compounds) **131**

Appendix 2. Supplementary of paper in Chapter 3 ..... **137**

Appendix 3. Checkerboard assay results for synthetic compounds not reported in Chapter 3 . **200**

Appendix 4. Copyright permission **203**

List of Figures

Figure 1.1 The priority pathogens in most urgent need for antimicrobial development according to the WHO (WHO, 2017). 17

Figure 1.2 Mechanisms of bacterial resistance. 22

Figure 1.3 The typical structures of multidrug transporters and representative tripartite assemblies (Du et al., 2018) (SAV1866, MdFA, DinF-BH, EmrE, AcrAB-TolC, and MacAB are examples of efflux pumps in these families). 24

Figure 1.4 Schematic representation of a tripartite drug efflux pump (Venter et al., 2015). 26

Figure 1.5 Drug pathways in AcrB (Kobylka et al., 2020). 28

Figure 1.6 Chemical structures of a) PAβN, b) MBX2319 and c) ABI-PP. 31

Figure 1.7 Structure of example phytochemicals and synthetic drugs investigated as EPIs.. 33

Figure 1.8 Workflow for efflux pump inhibitor development 34

Figure 2.1 Process for the purification of His-tagged proteins 50

Figure 2.2 Preparation of serial dilution of compounds 55

Figure 2.3 Reagent rack 2 attached to 96-well plate used in Biacore S200. 56

Figure 3.1 Chemical structure of PAβN 59

Figure 3.2 Structures of compounds MBX2319, A3, and quercetin. 60

Figure 3.3 Compound S4 was not able to inhibit Nile Red efflux. 87

Figure 3.4 S4 permeabilised the bacterial outer membrane. 88

Figure 3.5 Effect of compound S4 on survival of *C. elegans* nematodes. 89

Figure 4.1 Structure of ivacaftor 92

Figure 4.2 SDS-PAGE analysis of purified protein AcrB, GalP and MexB (each lane was loaded with 5 μg pure protein). 95

Figure 4.3 Immobilisation of (A) Blank (B) AcrB (C) MexB and (D) GalP on the CM5 chip surface..... 97

Figure 4.4 Kinetics of binding of PAβN and ivacaftor to purified AcrB and MexB using SPR. 99

Figure 4.5 Inhibition of Nile Red efflux by ivacaftor. 111

Figure A.1 Structures of thirty-five benzochromene derivatives. 135

Figure A.2 Structures of four flavonoid derivatives. 136

Figure A.3 Effect of the compounds on outer membrane permeabilization.

BW25113 wild-type cells were treated with 10 μM CCCP to inhibit the efflux of nitrocefin. 141

Figure A.4 ^{1}H NMR and ^{13}C NMR Spectra..... 182

Figure A.5 HPLC spectra of representative compounds. 198

List of Tables

Table 2.1 A list of synthetic compounds, antimicrobial agents, membrane permeabilisers, and their abbreviations and supplier. 39

Table 2.2 Descriptions and sources of *E. coli* strains used. 41

Table 2.3 Descriptions and sources of *P. aeruginosa* strains used. 41

Table 2.4 Components of buffers for purifying His-tagged AcrB and MexB 49

Table 2.5 Components of buffers for purifying His-tagged GalP 49

Table 2.6 The components of the solutions used for the SDS-PAGE gel..... 50

Table 2.7 Buffers and solutions used in SDS-PAGE 51

Table 2.8 Buffers, solvents and reagents used in different stages of SPR 52

Table 2.9 Solvent correction stock solutions 54

Table 2.10 Preparation of solvent correction working solutions..... 54

Table 3.1 The effect of flavonoid derivative(S4$^{\#}$) with different antimicrobial agents against the wild-type E. coli BW25113 alone and in the presence of membrane permeabiliser colistin. 86

Table 3.2 The effect of flavonoid derivative S4 with different antimicrobial agents against the drug sensitive E. coli BW25113 strain with a deletion in genomic acrB (E. coli BW25113 ΔAcrB). 87

Table 4.1 MICs for a panel of antibiotics against *P. aeruginosa* PAM 1020 (*P. aeruginosa* wild type), PAM 1032 (*P. aeruginosa* with MexAB-OprM overexpressed) and PAM 1626 (*P. aeruginosa* lacking the mexAB-oprM, mexEF-oprN and mexCD-oprJ genes). 102

Table 4.2 The minimum inhibitory concentration for ERY, LEV, MIN, and TOB against the wild-type *P. aeruginosa* (PAM 1020) at different concentrations of ivacaftor and EPI control PAβN. 104

Table 4.3 The minimum inhibitory concentration for ERY, LEV, MIN, and TOB against the efflux pump overexpressed strain of *P. aeruginosa* (PAM 1032) at different concentrations of test ivacaftor and EPI control PAβN. 105

Table 4.4 The minimum inhibitory concentration for colistin, and PMBN against PAM 1020, PAM 1032, and PAM 1626. 106

Table 4.5 The MIC concentrations for ivacaftor in the presence of colistin or PMBN. 107

Table 4.6 The minimum inhibitory concentration for ERY, LEV, MIN, and TOB against the wild-type P. aeruginosa (PAM 1020) at different concentrations of ivacaftor in the presence of 0.5 μg/mL colistin. 108

Table 4.7 The minimum inhibitory concentration for ERY, LEV, MIN, and TOB against the wild-type *P. aeruginosa* (PAM 1020) the efflux pump overexpressed strain of *P. aeruginosa* (PAM 1032) at different concentrations of ivacaftor in the presence of 1 μg/mL PMBN.... 109

Table A.1 The inherent antibacterial activities of benzo[*h*]chromene derivatives (series H, G and Y) against wild-type *E. coli* BW25113 and the BW25113 ΔAcrB mutant. 137

Table A.2 The effect of benzo[*h*]chromene derivatives (series H and G) with different antimicrobial agents against the BW25113 ΔAcrB mutant. 139

Table A.3 Minimum inhibitory concentration (MIC) of erythromycin (ERY), levofloxacin (LEV) and minocycline (MIN) against *E. coli* BW25113 in the presence of synthetic compounds (G, H, Y and S series) and positive control phenylalanine-arginine beta-naphthylamide (PAβN). 200

Abbreviations

AMR	Antimicrobial resistance
CCCP	Carbonyl cyanide m-chlorophenylhydrazone
CF	Cystic fibrosis
CFTR	Cystic fibrosis transmembrane conductance regulator
DBP	Distal binding pocket
DMSO	Dimethyl sulfoxide
DDM	Dodecyl-B-D-maltoside
EPI	Efflux pump inhibitor
ERY	Erythromycin
FDA	Food and Drug Administration
FIC	Fractional inhibitory concentration
IM	Inner membrane
IMP	Inner membrane protein
LEV	Levofloxacin
MDR	Multidrug resistance
MIC	Minimum inhibitory concentrations
MIN	Minocycline
OM	Outer membrane
OMP	Outer membrane protein

p.m.f	Proton motive force
PMBN	Polymyxin B nonapeptide
PAβN	Phe-Arg-β-naphthylamide
RND	Resistance nodulation division
SPR	Surface plasmon resonance
TEMED	Tetramethylethylenediamine
TOB	Tobramycin
R.U.	Response units
WHO	World Health Organization

Thesis Abstract

Antimicrobial resistance is an urgent and global threat that imposes a heavy burden on our health and economy. To tackle this issue, we need to develop antibiotics that can treat resistant pathogens. Of particular importance is therapies for the most critical category of Gram-negative pathogens in need of antimicrobial drug development according to the World Health Organization such as *Escherichia coli* and *Pseudomonas aeruginosa*. In these organisms, multidrug efflux pumps confer resistance to a wide range of antibiotics from various classes. The substrate range of multidrug efflux pumps is not confined to antibiotics but they are also responsible for transporting bacterial substances necessary for pathogenesis, quorum sensing chemical messages and components of biofilms. Hence multidrug efflux pumps are promising targets for the reversal of antibiotic resistance with efflux pump inhibitors (EPIs). Among the different classes of efflux pumps, the resistance nodulation division (RND) superfamily play an important role in conferring multidrug resistance phenotypes to Gram-negative bacteria such as *E. coli* and *P. aeruginosa*. Progress on the structural and functional analysis of members of the RND-family has significantly contributed to our understanding of the mechanism of transport and the options for inhibition of efflux, allowing us to develop potential EPIs. In this study, the analysis of inhibitors of AcrB from *E. coli* and MexB from *P. aeruginosa* were undertaken.

Chapter 3 presents the evaluation of designed, synthesised novel benzo[h]chromene and flavonoid compounds for their biological activity as AcrB inhibitors. The ability of the compounds to potentiate the antimicrobial activity of antibiotics and to inhibit substrate efflux was determined first. Compounds that displayed activity were further evaluated for potential off-target effects such as non-specific interaction with the *E. coli* outer- and inner membranes and for cytotoxicity. As a result, six compounds were identified to reduce the MIC values of tested antibiotics by at least 4 folds, and to further reduce the MICs in the presence of the membrane permeabiliser colistin. The identified compounds were also able to inhibit Nile Red efflux at concentrations between 50 µM and 200 µM, and neither disrupted the outer membrane nor displayed toxicity to *Caenorhabditis elegans*. Distinctively, compound G6 possessed the most potent antibacterial potentiation with erythromycin by 8-fold even in

the absence of a membrane permeabiliser. The presence of colistin as membrane permeabiliser increased the efficacy of the compounds so that they were able to synergise with antibiotics at lower concentrations than required in the absence of colistin. Furthermore, compounds G6, G10, G11, and H6 completely abolished the Nile Red efflux at a concentration as low as 50 µM. The 3,4-dihydro-2H-benzo[h]chromen-5-yl)(morpholino)methanone core of benzo[h]chromene derivatives appears to be a very promising chemical skeleton to be further studied in the discovery of more putative AcrB inhibitors.

Drug repurposing is also a possible strategy to find new therapeutic options to combat disease that would significantly reduce the discovery and development time. For this purpose, a previous study in our laboratory undertook *in silico* screening of Food and Drug Administration (FDA) approved drugs as potential EPI inhibitors. Ivacaftor was selected as a drug that fulfilled all the criteria of a potential EPI against AcrB from *E. coli.* Ivacaftor is used as a membrane potentiator in the treatment of cystic fibrosis however, it was observed that ivacaftor treatment can also reduce infection by common cystic fibrosis pathogens. We hypothesised that this 'secondary' effect of ivacaftor could be due to its ability to inhibit drug efflux pumps in these pathogens.

Chapter 4 reports on our investigation into this hypothesis. For this purpose, we studied the ability of ivacaftor to synergise with antibiotics against *P. aeruginosa*; a pathogen that commonly colonises the lungs of patients suffering from cystic fibrosis. The ability of ivacaftor to inhibit MexB, the most prominent drug efflux protein in *P. aeruginosa* was investigated. Though we were able to observe binding of ivacaftor to purified MexB with an affinity comparable to that of the known efflux pump inhibitor PAβN, ivacaftor was not able to synergise with any of the antibiotics tested. We speculated that this lack of efficiency was most probably the result of the outer membrane permeability barrier of *P. aeruginosa* that prevented ivacaftor from reaching the MexB. Accordingly, in the presence of either colistin or polymyxin B nonapeptide to permeabilise the outer membrane, ivacaftor became a highly effective MexB efflux pump inhibitor that synergised with antibiotics at a concentration of 4 µg/mL ivacaftor (10.2 µM). This activity is comparable to other EPIs in current development where the inhibitors with the highest efficacy are reported to fully potentiate antimicrobial activity at 3 µM. Moreover, as colistin is an antibiotic of choice for the treatment of infections

in cystic fibrosis patients, the synergism between colistin and ivacaftor and consequent efficacy of ivacaftor as an EPI is highly significant for the treatment of multidrug resistant infections in people suffering from cystic fibrosis and warrants further study.

Declaration

I declare that:

This thesis presents work carried out by myself and does not incorporate without acknowledgment any material previously submitted for a degree or diploma in any university.

To the best of my knowledge, it does not contain any materials previously published or written by another person except where due reference is made in the text; and all substantive contributions by others to the work presented, including jointly authored publications, is clearly acknowledged.

Print name: Yang Chen

Signed:



Date: 09/02/2023

Publications arising from the project and statement of contributions

1. Research article

The data presented in **Chapter 3** section 3.2 is a manuscript published in *The European Journal of Medicinal Chemistry*.

Guo T*, Chen Y*, Chen W, Semple SJ, Gua X, Polyak SW, Suna G, Venter H, Ma S (2023) Design and Synthesis of Benzochromene Derivatives as AcrB Inhibitors for the Reversal of Bacterial Multidrug Resistance. *Eur J Med Chem*. 249:115148

*Joint first authors

Statement of contributions: This article resulted from a collaboration between Shandong University, China and the University of South Australia, Australia (China-Australia Centre for Health Sciences Research). Ting Guo, Department of Medicinal Chemistry, School of Pharmaceutical Sciences, Shandong University was primarily responsible for the synthesis and chemical characterisation of the synthetic compounds. Yang Chen, Clinical and Health Sciences, University of South Australia, was primarily responsible for all the biological work and analysis.

Acknowledgement

I acknowledge an Australian Government Research Training Program Scholarship (RTP) for the successful completion of this degree.

I would like to sincerely acknowledge the great supervision and daily support from all my supervisors, my principal supervisor A/Professor Rietie Venter, my co-supervisors Dr. Susan Semple and Dr. Steven Polyak. Your supervision and support during my research have allowed me to challenge myself and achieve more than I set out for. I cannot fully express my thanks for all your help and support, especially Rietie, for not only teaching me various knowledge and laboratory skills, but also supporting me physically and emotionally. It is my honour to have you to be my supervisors.

I would also like to extend my deep thanks to my lovely colleagues in our lab, Dr. Sylvia Sapula, Mr. Jon Whittall, Mr Jack Blaikie, Ms Naomi Siderius, Ms Yu Wang, and Ms Sida Liu, and all other members. I feel warmed and beloved in our 'Venter lab-family'. You are not only my colleague but also my dearest friends. I will memorise the precious time while I study here. I would especially like to thank Profession Shutao Ma and his group (Department of Medical Chemistry School of Pharmaceutical Science, Shandong University) for the design and synthesis of novel compounds for biological testing, which is an important part of this thesis.

I also owe my family and especially my husband a huge thank you for supporting me while I undertook this study, committing to long hours and a tight budget during my time spent in school and in writing. Undertaking a research degree with a two-year old young child and a new baby in tummy is very hard and I cannot get it without my husband's support.

CHAPTER 1 Review of the literature

1.1 Introduction

Antimicrobial resistance (AMR) has been identified as one of the biggest threats to modern medicine and public health by the World Health Organization (WHO) (WHO, 2021). It was estimated that nearly 5 million people died because of AMR in 2019 (Murray et al., 2022). Many antibiotics that have been used in the clinic for decades are losing their efficacy, especially against Gram-negative bacteria (Willyard, 2017). The WHO has published a list of AMR organisms which desperately need new therapies (WHO, 2021). Notably, the most critical priority pathogens are all Gram-negative bacteria (Figure 1.1). Infections caused by Gram-negative pathogens are identified to be much harder to treat compared to Gram-positive organisms, because of their very high intrinsic drug resistance of Gram-negatives (Arzanlou et al., 2017).

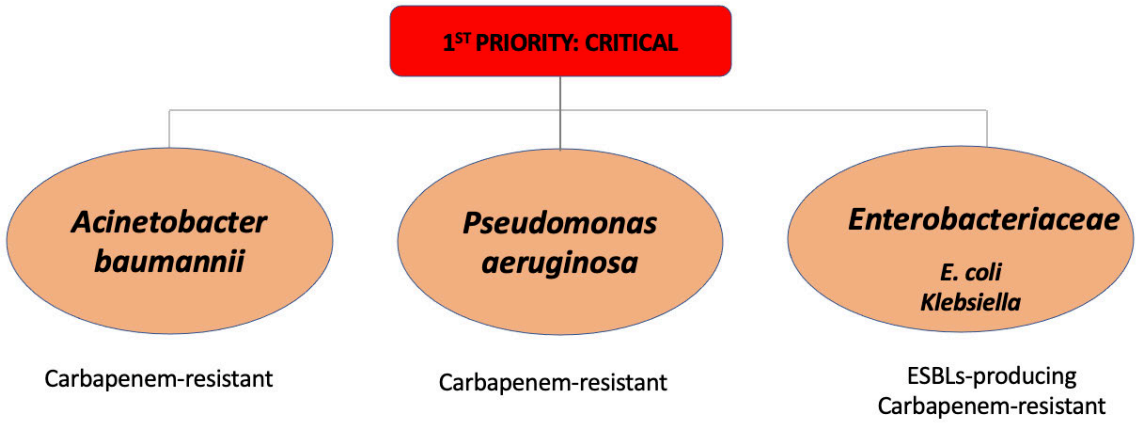


Figure 1.1 The priority pathogens in most urgent need for antimicrobial development according to the WHO (WHO, 2017).

While AMR is a naturally occurring process, several factors have driven and accelerated the development of AMR. Major factors include the overuse of antibiotics in health care settings, the abuse of antibiotics in agriculture leading to the fast development of multidrug-resistant organisms in animals and the environment and the overuse of antiseptics and biocides which can result in resistance against these compounds and cross-resistance to antibiotics (Venter et al., 2017).

New antimicrobials are desperately needed due to the rapidly increasing rate of resistance development (Venter, 2019). At the same time there has been a sharp decrease in antibacterial drug discovery (Al-Tawfiq et al., 2021). Due to the large investment needed for new drug discovery but the low financial returns on antimicrobials for pharmaceutical companies, many companies have abandoned their antimicrobial development programmes (Klug et al., 2021; Venter, 2019). This has resulted in a paucity of new antimicrobials at a time when they are desperately needed. Most newly developed antibiotics are for Gram-positive infections, with antibiotics against high priority pathogens such as multi-drug-resistant *Pseudomonas aeruginosa*, and carbapenem-resistant *Enterobacteriaceae* in severe shortage (Al-Tawfiq et al., 2021). As indicated above, the WHO identified the organisms for which there is an urgent need to develop new antimicrobials with Gram-negative organisms as a critical priority at the top of this list (WHO, 2017).

This current research project aims to address the lack of antimicrobial drug development against critical level priority pathogens. Specifically, it focusses on the identification of compounds that could inhibit bacterial drug efflux pumps and so restore the activity of antimicrobials against multidrug resistant Gram-negative pathogens.

1.2 The health and economic burden of AMR

The spread of AMR is a threat to humans worldwide and an urgent issue which requires global, coordinated action plans to address (Prestinaci et al., 2015; WHO, 2021). From the O'Neill report, it was estimated that the number of deaths associated with AMR will dramatically increase over time from 700,000 to 10 million per year by 2050 unless urgent action is taken

(O'Neill, 2016). If this threat is not managed, the spread of AMR could make many common bacterial infections untreatable.

Recent predictive statistical modelling has estimated that 4.95 million deaths were associated with bacterial AMR globally in 2019, including 1.27 million deaths directly attributable to resistance (Murray et al., 2022). The six leading pathogens for deaths associated with resistance are *Escherichia coli, Staphylococcus aureus, Klebsiella pneumoniae, Streptococcus pneumoniae, Acinetobacter baumannii,* and *Pseudomonas aeruginosa* (WHO, 2017). They were responsible for 0.93 million deaths directly attributable to resistance and 3.57 million deaths associated with AMR in 2019 (Murray et al., 2022). AMR is a leading cause of death globally, with the highest burdens occurring in low-resource settings (Rudd et al., 2018).

The cost of AMR to national economies is significant as it affects productivity of patients or their caregivers through prolonged hospital stays, longer time off work, reduced quality of life, greater likelihood of death due to inadequate or delayed treatment and increased burden on family of infected patients. AMR results in increased costs such as those for private insurance coverage, disease surveillance (Smith & Coast, 2012) as well as the need for more expensive and intensive care. It was also estimated that the highest likelihood of death was from respiratory infections (ceftazidime-resistant *P. aeruginosa*) and bloodstream infections, both leading to high hospital expenses and premature death costs in Australia (Wozniak et al., 2022). Additionally, treatment failure caused by AMR contributes to increased costs of care associated with additional investigations such as laboratory tests and X-ray examinations, additional or alternative treatments, often much more expensive than drugs used to treat infections caused by sensitive organisms and additional side effects from more toxic treatments, which have to be managed (Imai et al., 2022).

1.3 The antibiotic pipeline is running dry

Even though antimicrobial resistant infections are becoming a major threat to global health, the clinical pipeline of new antimicrobials is running dry. In 2019, the WHO identified 32 antibiotics in clinical development addressing the WHO list of priority pathogens, however,

only six were classified as innovative (Venter, 2019; WHO, 2021). Antibiotic shortages are now affecting countries worldwide and especially in health systems.

Due to AMR, there are a very limited number of antibiotics to treat infections caused by high priority organisms such as multidrug-resistant *P. aeruginosa,* and carbapenem-resistant *Enterobacteriaceae* (Al-Tawfiq et al., 2021). New antimicrobial agents are urgently needed for the top priority organisms as classified by the WHO. Indeed, we need new models and ways to develop antibiotics if we do not want to slip into a post-antibiotic era (Piddock et al., 2022; Venter et al., 2017).

1.4 Reversing resistance as an alternative option for antibiotic development

The trends in antibiotic development and the continued emergence of resistance suggested that the standard pharmaceutical and economic model will be far away from sufficient to address the lack of new antibiotics. Approaches that could allow the reversal of resistance could therefore be an alternative option for antimicrobial development (Venter, 2019). It has been suggested that 'the existing classes of antibiotics are probably the best we will ever have' (Cormican & Vellinga, 2012). Hence developing strategies to save these precious antibiotics by reversing resistance to them could be an ideal option for antimicrobial development.

The remainder of this review of literature will focus on the mechanisms of AMR and how these may be reversed through the inhibition of bacterial efflux pumps.

1.5 Antimicrobial resistance and mechanisms

1.5.1 Antimicrobial resistance

Naturally produced antibiotics are thought to have first appeared over 40 million years ago, suggesting that resistance also evolved in a similar era (Wilson, 2014). Accordingly, AMR is a natural phenomenon rather than a modern trend. AMR has been a noteworthy clinical issue since the first mass introduction of penicillin into clinical use in the 1940s (Gaynes, 2017; Powers, 2004). However, the recent extensive use and abuse of antimicrobials by humans has created strong selective pressure upon bacteria (Murray et al., 2022; Sartelli et al., 2020)

which has driven a rapid increase in the rate of resistance development. In addition to AMR, multidrug resistance (MDR) has also evolved where microorganisms become resistant to antibiotics in three or more classes of antimicrobials (Magiorakos et al., 2012; Venter et al., 2017).

1.5.2 General mechanisms of resistance

To survive exposure to cytotoxic chemicals, bacteria have developed different mechanisms of resistance. Briefly, resistance to antibiotics can be mediated by five primary mechanisms (Figure 1.2): 1) efflux pumps that expel cytotoxic agents out of the cell thereby reducing their on-target levels to sub toxic concentrations; 2) inactivating enzymes that alter the chemical structure of antibiotics, e.g. β-lactamases; 3) decreasing the membrane permeability to limit the amount of the toxic agent entering into the cell; 4) target modification whereby bacteria alter the drug target to prevent binding of the antibiotic; and 5) alternative enzyme production which allows bacteria to rescue a crucial metabolic pathway targeted by antibiotics (Wilson, 2014). These resistance mechanisms can be intrinsic (already existing in the wild-type organism) or acquired either through mutations or horizontal gene transfer (Arzanlou et al., 2017; Wilson, 2014). Due to their major role in MDR in Gram-negative bacteria, efflux pumps will be the focus of this review.

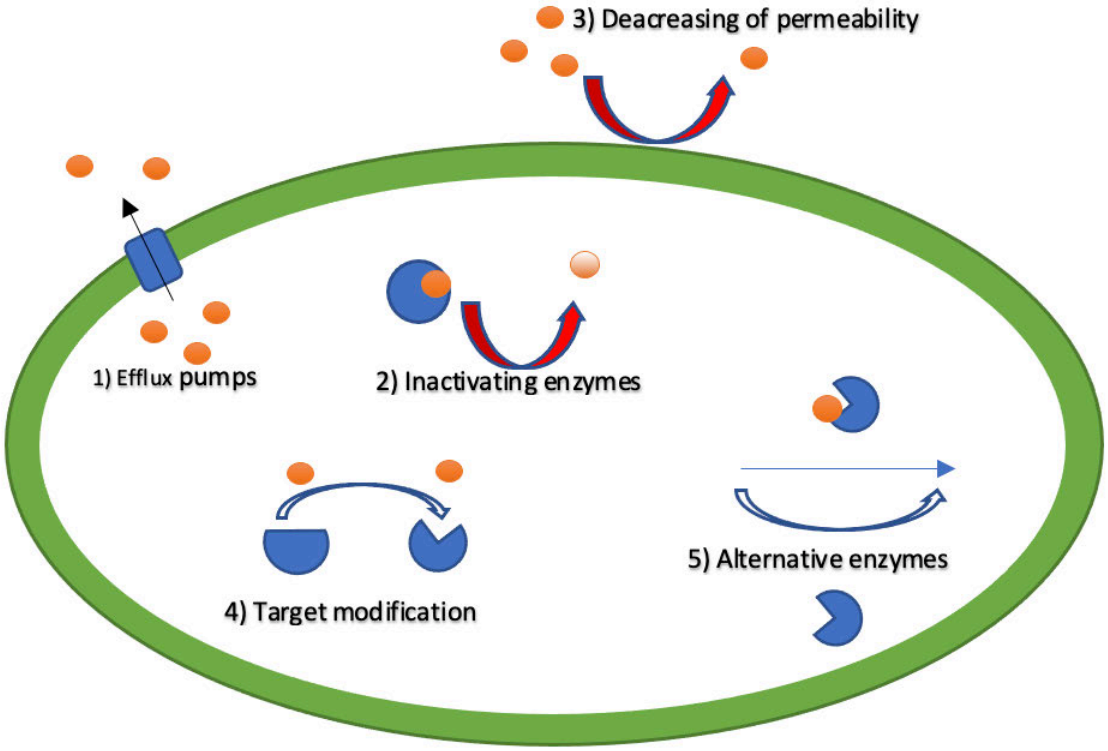


Figure 1.2 Mechanisms of bacterial resistance.

1) Active efflux, where drug efflux pumps could expel the drugs from inside bacterial cells thereby lowering their concentrations to sub-toxic levels; 2) bacterial inactivation enzymes could alter the chemical structures of antimicrobials to render them inactive; 3) decreased permeability of bacterial membranes could limit the amount of antimicrobial agents entering the cells; 4) target modification involves alteration to the drug target to prohibit the binding of antimicrobial thereby reducing its effectiveness; and 5) alternative enzyme production could allow bacteria to rescue a crucial metabolic pathway targeted by antibiotics.

1.5.3 Gram-negative bacteria and AMR

Infections caused by Gram-negative pathogens are generally harder to treat compared to Gram-positive bacteria because these organisms possess high intrinsic drug resistance, (Arzanlou et al., 2017). This intrinsic drug resistance is primarily due to the presence of i) both inner and outer cell membranes which work together as a formidable permeability barrier,

and ii) a variety of multidrug efflux pumps that expel antibiotics from the cell (Kobylka et al., 2020; Lamut et al., 2019; Venter et al., 2015). The expression of efflux pumps can be upregulated in the presence of antimicrobials to confer resistance to multiple classes of antibiotics (Lomovskaya et al., 1999; Van Bambeke et al., 2000). Our lab has previously identified that AMR is driven by hyperexpression of the drug efflux pumps from the case study of *P. aeruginosa* isolates from environmental hotspots (Amsalu et al., 2020). In addition, bacteria can acquire new resistance mechanisms by horizontal gene transfer including drug efflux pump gene that is transferred on a specific plasmid (Sun et al., 2019). Hence, AMR is the consequence of both acquired and intrinsic mechanisms of resistance (Arzanlou et al., 2017).

1.6 Bacterial Drug Efflux Pumps

Amongst the adaptive responses listed above that facilitate resistance, drug efflux is potentially the most rapid and efficient resistance mechanism when bacteria are first exposed to toxic antibiotics (Blair et al., 2015; Du et al., 2018; Nichols et al., 2011). Drug efflux pumps expel hazardous agents, consequently lowering their concentration inside cells to sub-lethal levels (Nikaido & Pagès, 2012; Piddock, 2006a; Poole, 2004; Venter et al., 2015). Drug efflux pumps expel a variety of structurally distinct classes of antimicrobials, and export biocides (Amsalu et al., 2020), thereby facilitating acquisition of the MDR phenotype (Piddock, 2006a; Poole, 2004; Venter et al., 2015). In addition, efflux pumps are also responsible for transporting bacterial substances necessary for pathogenesis, including quorum sensing chemical messages and components of biofilms. Hence, in addition to their role in AMR, efflux pumps also play a critical role in virulence and biofilm formation (Alav et al., 2018; Fernando & Kumar, 2013; Padilla et al., 2010; Pérez-Varela et al., 2019; Soto, 2013).

There are six different families of bacterial efflux proteins. These include the ATP-binding cassette (ABC) superfamily, which directly use ATP as the energy source to drive transportation (Du et al., 2018), the small MDR family, the major facilitator superfamily (MFS), the multidrug and toxin extrusion (MATE) family, the resistance–nodulation–cell division

(RND) superfamily (summarized in Figure 1.3), and the proteobacterial antimicrobial compound efflux (PACE) family (Hassan et al., 2018). Due to their broad substrate specificity (Nikaido & Pagès, 2012), the overexpression of these efflux pumps results in the decreasing susceptibility of pathogens to a variety of antibacterial compounds and biocides (Piddock, 2006a; Sjuts et al., 2016). Of most relevance to this project are RND transporters that are widely present in Gram-negative bacteria as they are the drug efflux pumps responsible for clinical MDR (Davin-Regli et al., 2021; Piddock, 2006a) and biocide tolerance (Amsalu et al., 2020; Dong et al., 2022; Meyer et al., 2022; Nikaido & Pagès, 2012).

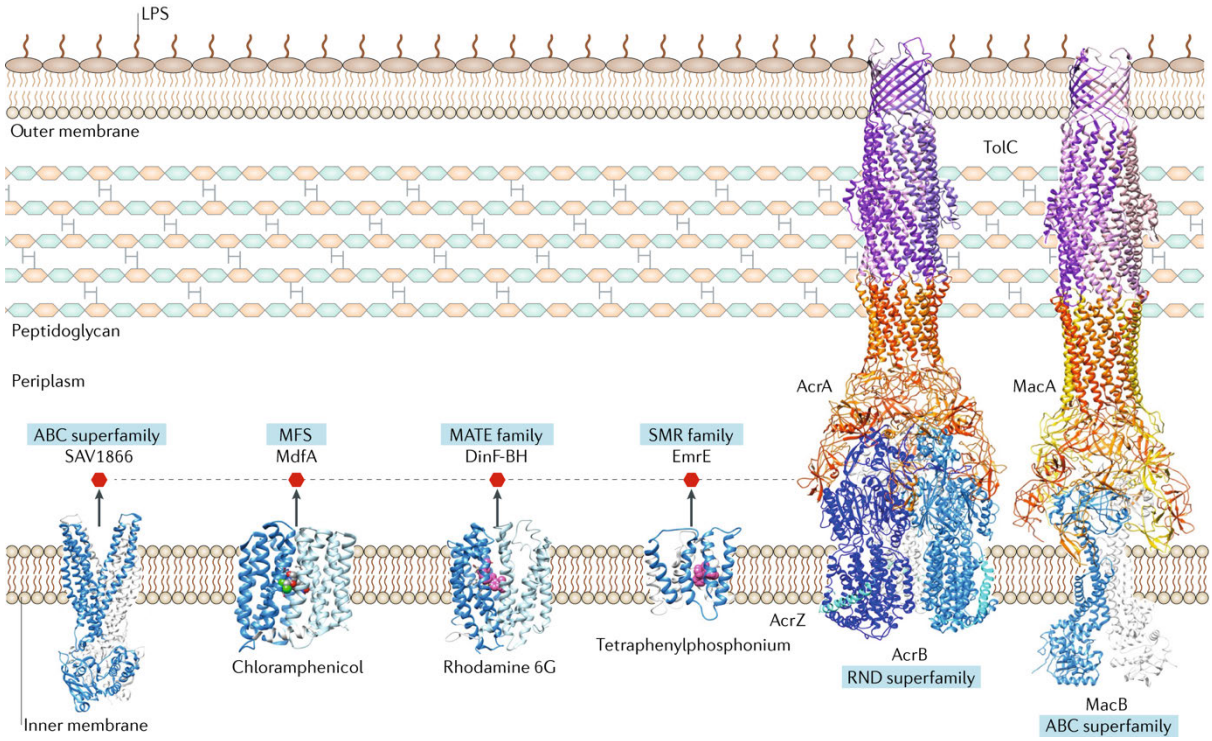


Figure 1.3 The typical structures of multidrug transporters and representative tripartite assemblies (Du et al., 2018) (SAV1866, MdFA, DinF-BH, EmrE, AcrAB-TolC, and MacAB are examples of efflux pumps in these families). Permission has been obtained for the use of this figure.

1.6.1 Role of efflux pumps in virulence

In addition to conferring multidrug resistance, efflux pumps are also involved in virulence (Alcalde-Rico et al., 2016). During the process of an infection, a bacterial pathogen must be able to survive the anti-infective defence mechanisms conducted in order to colonise the host. These defence mechanisms include the production of a variety of antimicrobial agents such as fatty acids, peptides or even detergents such as bile salts many of which are substrates of drug efflux pumps (Fernando & Kumar, 2013; Thanassi et al., 1997).

Several previous studies demonstrated that bacteria lacking efflux pumps displayed a substantial reduction in virulence or were even completely attenuated and unable to infect the host (Sifri et al., 2006). Different MDR efflux pumps can extrude a large variety of agents, including quorum sensing molecules that are involved in the regulation of the expression of virulence determinants (Alcalde-Rico et al., 2018). Drug efflux pumps can also directly export virulence factors (Schroeder et al., 2017). Consequently, drug efflux pumps are important determinants of bacterial virulence (Alvarez-Ortega et al., 2013; Martinez et al., 2009; Piddock, 2006b). Inhibition of efflux pumps could therefore be an important way to prevent infection by MDR Gram-negative bacteria.

1.6.2 Role of efflux pumps in biofilm formation and resistance

Efflux pumps are also responsible for transporting bacterial substances necessary for biofilm formation such as quorum sensing molecules. Hence, in addition to their role in AMR, efflux pumps also play an important role in biofilm formation (Alav et al., 2018; Dawan et al., 2022; Soto, 2013).

Deletion of efflux pumps has been shown to affect bacterial biofilms through actions including: i) inhibition of biofilm formation by bacteria such as *E. coli* and *Klebsiella pneumoniae* by reducing the transport of substances needed for the synthesis of biofilm structures (Tang et al., 2020) and ii) disruption of bacterial communication by inhibition of quorum sensing (Brackman et al., 2011; Kvist et al., 2008). It was revealed that quorum sensing plays a crucial role in biofilm growth, and may also enhance biofilm thicknesses and robustness (Rosenau et al., 2010; Tielen et al., 2013; Tielen et al., 2010). Biofilms favour the persistence of pathogens

during chronic infections as well as act as a source of bacterial dissemination(Cepas & Soto, 2020). (Schroeder et al., 2017). Bacteria in biofilms can be up to 1000 times more resistant to antimicrobials compared to planktonic cells (Taylor et al., 2014; Brackman & Coenye, 2016).

Consequently, the inhibition of biofilm formation through inhibition of efflux pumps has been proposed as a promising way to control of infections caused by MDR Gram-negative pathogens.

1.6.3 RND type drug efflux pumps of Gram-negative bacteria

The RND efflux pumps present in Gram-negative bacteria are an important family of membrane transport proteins (Colclough et al., 2020). They make a major contribution to MDR and, consequently, have the most clinical significance (Blair et al., 2014; Contreras-Gómez et al., 2022). The most extensively researched tripartite drug efflux complexes are the AcrA-AcrB-TolC and MexA-MexB-OprM transporters from *Escherichia coli* and *Pseudomonas aeruginosa,* respectively (Venter et al., 2015). The RND family of efflux pumps contain a tripartite structure consisting of an inner membrane protein that is the RND protein, an outer membrane protein, and a periplasmic membrane fusion protein which connects the two membrane embedded proteins (Figure 1.4) (Alav et al., 2021; Du et al., 2014).

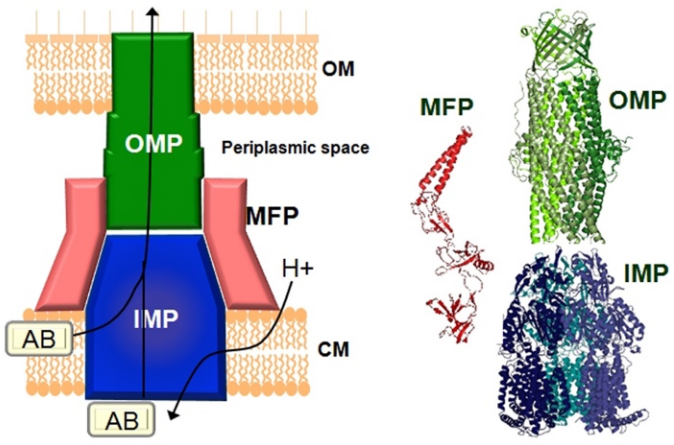


Figure 1.4 Schematic representation of a tripartite drug efflux pump (Venter et al., 2015).

The complex consists of three proteins including an inner membrane protein (IMP), an outer-membrane protein (OMP), and a bridging protein of the other two proteins, the periplasmic membrane fusion protein (MFP).

In *E. coli* the inner membrane protein is AcrB, the outer membrane protein is TolC and the periplasmic adapter is AcrA. AcrAB-TolC is highly conserved in the *Enterobacteriaceae* family (Venter et al., 2015). These proteins possess high homology with MexB, OprM and MexA from *P. aeruginosa* and MexB can even substitute for AcrB to from a functional complex (Du et al., 2018; Krishnamoorthy et al., 2008; Welch et al., 2010). A previous study has shown that MexB has 89% similarity with AcrB, OprM has 35% similarity with TolC, and MexA has 71% similarity with AcrA (Piddock, 2006a).

1.6.4 Molecular mechanism of drug efflux by RND-type drug efflux pumps

Our understanding of the mechanism of substrate binding and translocation in RND efflux pumps has been greatly assisted by structural biology. The AcrAB-TolC RND-type efflux pump uses the proton motive force (p.m.f) to power a peristaltic mechanism that moves substrates through the AcrB subunit and into the TolC channel (Nikaido & Takatsuka, 2009). In the AcrAB-TolC tripartite complex, AcrB determines the substrate specificity and actively exports a large variety of structurally different drugs and toxic agents using the p.m.f. (Murakami et al., 2006).

The protomers of the AcrB trimer have different conformations when actively connected with substrates: the loose (L), tight (T) and open (O) states (Murakami et al., 2006; Seeger et al., 2006). Briefly, substrates are introduced in the L protomer, move further into the drug-binding pocket in the T protomer and then are extruded into a funnel-shaped ‘canyon’ in the docking domain in the O protomer (Seeger et al., 2006).

Structural biology has also assisted in finding inhibitors of these efflux pumps. The discovery of different channels and binding pockets in AcrB has helped us to understand the different drug pathways in efflux pumps (Du et al., 2018).

Substrates first enter the AcrB subunit through one of three possible channels, either from the lipid envelope or from the periplasm (Du et al., 2018; Opperman et al., 2014), and a

postulated third channel which leads directly to the distal binding pocket (DBP) (Zwama et al., 2018). Regardless of the entry mechanism, substrates then move into a shared proximal binding pocket before they are transported further into the AcrB protein. Substrates are next moved into a DBP after first passing via a 'switch loop' that separates the two pockets (Figure 1.5) (Eicher et al., 2012; Nakashima et al., 2011). Substrates finally leave this site and are transported into the TolC channel for expulsion from the cell.

An important discovery was the identification of a 'hydrophobic trap' that resides next to the distal binding pocket (Aron & Opperman, 2018; Opperman & Nguyen, 2015). Some small molecules that bind into this site can completely inhibit the activity of the entire AcrAB-TolC machinery (Alenazy, 2022). Several co-crystal structures of efflux pump inhibitors (EPIs) bound into the hydrophobic trap have now been reported (Sjuts et al., 2016).

Our understanding of the molecular mechanism of drug transport and efflux inhibition can be used as a basis for the discovery of potent EPIs.

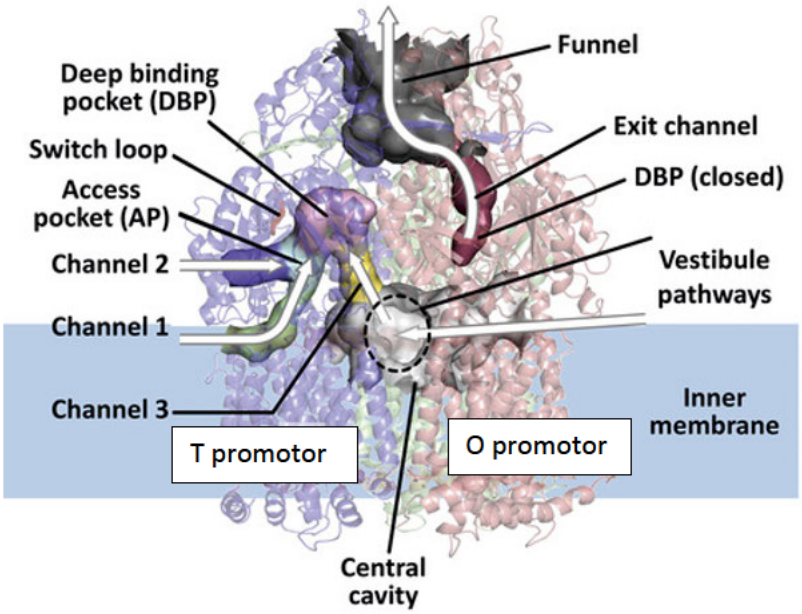


Figure 1.5 Drug pathways in AcrB (Kobylka et al., 2020).

Channel 1: in the periplasmic entry pathway substrates are transported from the proximal binding pocket (PBP) in the L protomer and pass through the 'Switch loop', towards the DBP (Kobylka et al., 2020). The short switch loop is located between the two pockets of AcrB is a possible regulator of drug entry into the DBP. Channel 2: the pathway directly leads substrates from the periplasm (outer leaflet of the inner membrane) to the proximal binding pocket. Higher-molecular-mass drugs such as erythromycin, tend to locate to an entry pocket in L protomer, while smaller drugs such as minocycline and doxorubicin, favour a deep binding pocket within the T protomer. Pump inhibitors, such as the compound ABI-PP enter more deeply into the hydrophobic trap in the T protomer (Du et al., 2018). Channel 3: in the postulated pathway the substrates directly move into the DBP (Zwama et al., 2018).

1.6.5 The inhibition of efflux pumps

Due to the clinical importance of multidrug efflux pumps, such as AcrAB-TolC the discovery of EPIs is a promising approach to reverse MDR and extend the lifetime of precious antibiotics already in wide use (Alenazy, 2022; Sharma et al., 2021; Sionov & Steinberg, 2022; Venter, 2019; Venter et al., 2015; Y. Wang et al., 2016). Most Gram-negative bacteria have closely related AcrB homologues, such as MexB from *P. aeruginosa*, thus the discovery of EPIs with a broad spectrum of activity against Gram-negative bacteria is possible.

So far, most studies have focused on the RND-type inner membrane proteins as described in section 1.5, however, inhibitors of the membrane adapter protein, AcrA has also been described (Abdali et al., 2017).

Small molecule EPIs may have further beneficial effects, such as inhibiting biofilm formation and quorum sensing (described in 1.6.1). Hence, promising EPIs with activity against resistant pathogens will: (i) restore the efficacy of antibiotics where resistance has arisen, (ii) reduce the development of drug-resistant clinical pathogens and prolong the lifetime of antimicrobials, (iii) inhibit the ability of the pathogens to infect their host, and (iv) prevent the development of highly antimicrobial resistant biofilms (Venter et al., 2015). Despite the obvious potential of inhibiting microbial drug efflux pumps, there are currently no EPIs in clinical use. Development of clinically useful inhibitors has been limited by cytotoxicity and

other issues such as the permeability barrier of the Gram-negative outer membrane (Compagne et al., 2023; Venter, 2019).

1.7 Representative EPIs of Gram-negative bacteria identified so far

Phe-Arg-β-naphthylamide (PAβN) was the first RND-type efflux protein inhibitor to be identified (Lomovskaya et al., 2001) (Figure 1.6 a). It was identified by screening for levofloxacin synergists against antimicrobial resistant *P. aeruginosa*. Due to its cytotoxicity, PAβN failed to enter clinical trials (Lomovskaya & Bostian, 2006). However, PAβN often serves as a control in assays that test synergistic antibiotic combinations (Lomovskaya et al., 2001; Orhan et al., 2005; Venter et al., 2015).

The most potent EPIs described so far are the pyranopyridine series of compounds developed by Microbiotix (Opperman et al., 2014) such as MBX2319 (Figure 1.6 b), and derivatives thereof. The MBX2319 was identified from a screen of 183,400 compounds with a cell-based reporter assay that looked for synergism with ciprofloxacin (Opperman et al., 2014). Molecular dynamic simulations were then used to characterise the potential interaction of MBX compounds with AcrB (Vargiu et al., 2014). It was also revealed these compounds interact with the hydrophobic trap and that the compound with the highest affinity was MBX2319 (Sjuts et al., 2016; Vargiu et al., 2014) (Figure 1.6 b).

MBX2319 strongly reduced the minimum inhibitory concentrations (MICs) of fluoroquinolones (ciprofloxacin and levofloxacin), β-lactams (piperacillin, cloxacillin, oxacillin, carbenicillin), chloramphenicol, erythromycin and linezolid from 2 to 8 folds against *E. coli* (Opperman et al., 2014). MBX2319 did not disrupt the bacterial outer and inner membranes, however, it was shown to have weak cytotoxicity in HeLa cells possibly due to its poor aqueous solubility (Opperman et al., 2014). The Pos group subsequently cloned the soluble periplasmic domain of AcrB (AcrBper) to simplify X-ray crystallography and solved the structures of several MBX compounds bound to AcrBper (Sjuts et al., 2016). Chemical optimisation delivered derivatives with increased efficacy, such as MBX3135 (Sjuts et al., 2016), MBX2366, and MBX4055 (Butler et al., 2022). Our group has combined structural features of MBX2319 with

a 2-napthamide derivative identified from a previous screen (Wang, Mowla, Ji, Guo, Lopes, et al., 2018) to yield a new pharmacophore for potential development as EPIs (Gu et al., 2020).

TXA compounds such as TXA09155 (Figure 1.6 d) are compounds being developed by Taxis Pharmaceuticals to help treat MDR *P. aeruginosa* infections (Compagne et al., 2023). TXA09155 is an indole carboxamide derived from another EPI called TXA01182 which was discovered through the screening of various heterocyclic carboxamide compounds (Yuan et al., 2022). It has been shown to inhibit the efflux of various antibiotics, including fluoroquinolones, tetracyclines, and β-lactams in *P. aeruginosa*.

The pyridopyrimidine ABI-PP (Figure 1.6 c) is another noteworthy AcrAB and MexAB specific EPI that has also been co-crystallized with both *E. coli* AcrB and *P. aeruginosa* MexB (Nakashima et al., 2013). There are many other reports in the literature of other EPIs (Marshall et al., 2020), including natural products, semi-synthetic derivatives of existing EPIs and fully synthetic EPIs (reviewed by (AlMatar et al., 2021; Compagne et al., 2023; Grimsey & Piddock, 2019; Seukep et al., 2019; Wang et al., 2016).

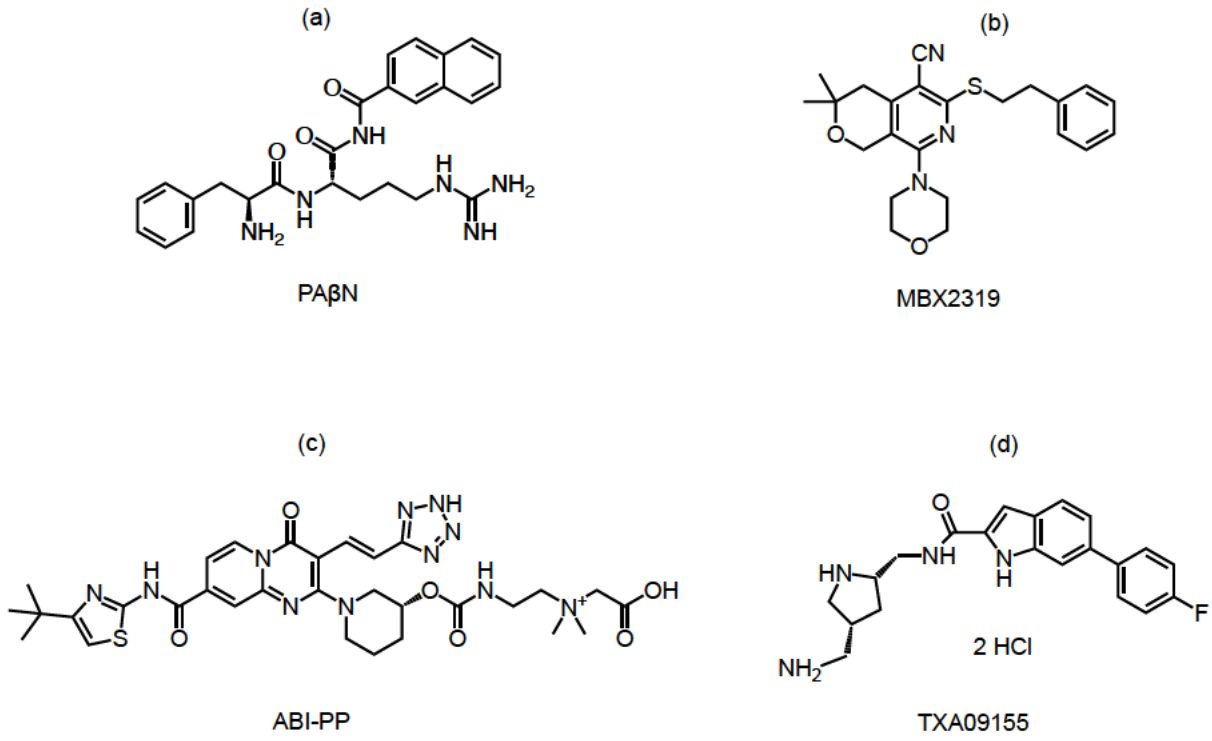


Figure 1.6 Chemical structures of a) PAβN, b) MBX2319 and c) ABI-PP.

Various approaches have been employed to discover new EPIs. One approach is the use of activity guided fractionation assays used to isolate bioactive compounds from natural extracts (Malviya et al., 2017). One example is artesunate isolated from the Chinese herb *Artemisia annua* that was found to increase the efficacy of β-lactam antibiotics against *E. coli* by inhibiting AcrB from the AcrAB-TolC efflux pump. The checkboard assays showed that artesunate acted synergistically with various β-lactam antibiotics (fractional inhibitory concentration (FIC)< 0.5), significantly inhibited the bacterial growth from 3 to 24 h, increased accumulation of daunorubicin and down-regulated AcrB mRNA expression of *E. coli* ATCC 35218 in a dose-dependent manner (Li et al., 2011; Y. Wang et al., 2016).

High-throughput and *in silico* approaches are other strategies employed and have both been used to discover new EPIs from large chemical libraries (Komura et al., 2005; Pisoni, 2021 PhD thesis, A combined *in silico* and microbiological approach for the identification of novel efflux pump inhibitors against AcrAB-TolC, University of South Australia). These compounds can serve as lead compounds for further development (as described below). Our group has successfully performed pioneering studies to identity phytochemical EPIs for the AcrB-TolC efflux pump using *in silico* screening (Ohene-Agyei et al., 2014). Plumbagin (Figure 1.7) from *Plumbago indica*, shikonin (Figure 1.7) from *Lithospermum erythrorhizon* and NDGA (Figure 1.7) were all identified using this method (Ohene-Agyei et al., 2014). Our group also employed *in silico* screening of a library of FDA approved drugs for repurposing as putative efflux pump inhibitors (Pisoni, 2021 PhD thesis, A combined *in silico* and microbiological approach for the identification of novel efflux pump inhibitors against AcrAB-TolC, University of South Australia). Seventeen compounds were selected for further testing. Of these, ivacaftor was the most promising compound as it showed partial efflux inhibition at 100 mM and full inhibition at 200 mM in the Nile Red efflux assay. It had no off-target effects on the outer membrane and did not affect the cells with an efflux pump deletion (Pisoni, 2021 PhD thesis, A combined *in silico* and microbiological approach for the identification of novel efflux pump inhibitors against AcrAB-TolC, University of South Australia). This compound was able to reverse the resistance of minocycline and chloramphenicol at concentrations as low as 2 µg/mL in the presence of a membrane permeabiliser (Liu, 2022 Masters thesis, Inhibitors of bacterial efflux pumps and their effect on antimicrobial resistance, biofilm formation and

virulence, University of Adelaide; Pisoni, 2021 PhD thesis, A combined *in silico* and microbiological approach for the identification of novel efflux pump inhibitors against AcrAB-TolC, University of South Australia).

Another useful approach to the discovery of new EPIs is rational drug design that exploits structural biology data to chemically optimise lead compounds. For instance, the compound A3 (Figure 1.7) was designed based upon the plumbagin and shikonin structures and in concert with crystal structures of AcrB. Compound A3 enhances the antibacterial activity of erythromycin, chloramphenicol, and tetraphenyl-phosphonium against MDR strains of *E. coli* (Wang et al., 2017). Compound A3 served as a promising hit compound due to its antibiotic sensitisation and low cytotoxicity, and subsequent analysis of its target effect indicated that it specifically acts on AcrB (Wang et al., 2017). Further development of A3 yielded the 5-methoxy-2,3-naphthalimide series (Figure 1.7) which are excellent lead compounds that broadly synergise with antimicrobials, reducing by more than 4-fold the minimal inhibitory concentration (MIC) of antibiotics erythromycin, chloramphenicol, and nalidixic acid (Jin et al., 2019). Our group has similarly commenced development of NDGA and identified new, potent EPIs such as the 2H, benzo[h]chromene class of inhibitors (Figure 1.7). These structures all represent valuable new agents to potentially combat MDR.

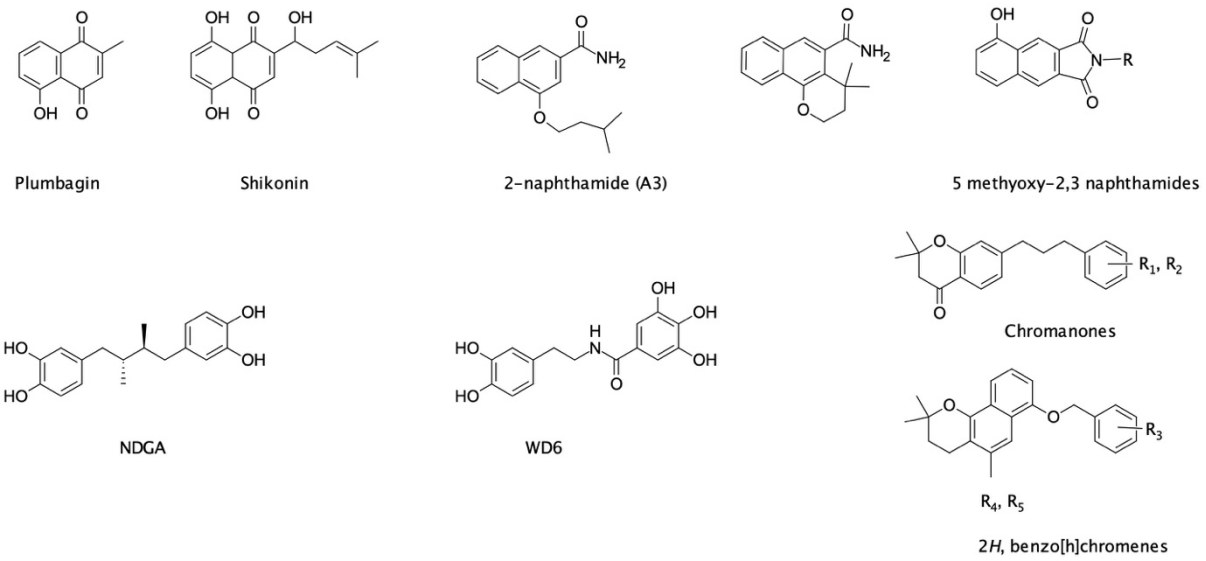


Figure 1.7 Structure of example phytochemicals and synthetic drugs investigated as EPIs.

1.8 Tools for studying efflux pump inhibitors

Despite the critical importance of efflux pumps in bacterial pathogenesis and MDR, there are currently still no EPIs in clinical development that target RND-type transporters. The most concerning problem currently in the discovery of EPIs with clinical potential is the non-specific damage to the bacterial membranes, which is also often the cause of cytotoxicity to mammalian cells (Venter et al., 2015) and a lack of efficacy due to the inability to breach the outer membrane barrier of Gram-negatives. Based upon our understanding of how EPIs block the transport of drugs out of the cells (Schweizer, 2012), there is now an opportunity to discover and develop new EPIs that restore the activity of some of our most precious antibiotics. Our approach for the discovery and further development of EPIs is summarised in Figure 1.8.

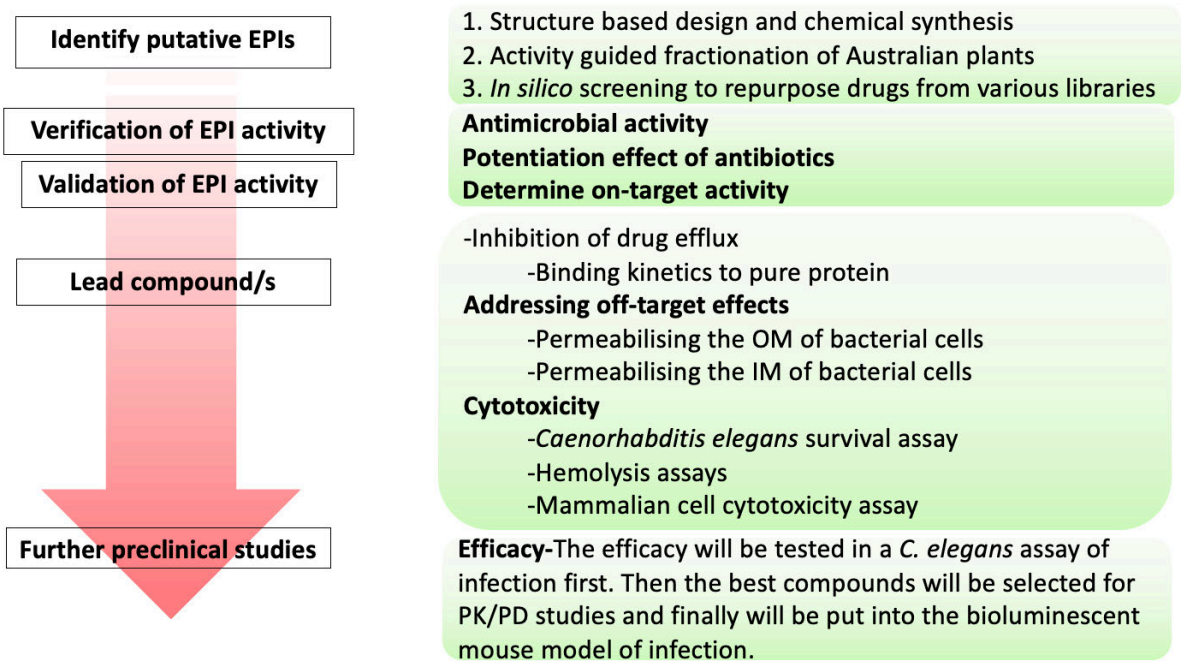


Figure 1.8 Workflow for efflux pump inhibitor development

This project aims to find and characterise compounds which could be qualified as EPIs, satisfying the following criteria (Lomovskaya et al., 2001; Venter et al., 2015).

(a) It must enhance the activity of antibiotics in resistant strains that express a drug efflux pump.

(b) It should not affect sensitive strains lacking the drug efflux pumps.

(c) It must not reduce the MIC of antibiotics which are not substrates of the transporter.

(d) It must increase of the level of accumulation and decrease the level of extrusion of compounds acting as substrates of the efflux pump.

(e) It must not act non-specifically on the bacterial outer membrane.

(f) It must not act non-specifically on the proton gradient across the inner membrane.

The above criteria can be assessed with well-developed methods as outlined below.

(a) Measuring the synergism: The ability of the compounds to potentiate antibiotics is best studied using checkerboard assays (Chai et al., 2022; Gu et al., 2020; Guo et al., 2023; Lomovskaya et al., 2001; Orhan et al., 2005; Wang et al., 2021). The MIC of the antibiotic is evaluated in the presence of a range of different concentrations of the compound.

(b) Ensuring the compound has no effect on strains which lack the drug efflux pump: An effective way to identify this is to perform checkerboard assays on a sensitive strain with a genomic deletion of the inner membrane protein. Consequently, the compound should have no reduction on the MIC of the sensitive strain.

(c) Use a non-substrate: Another way to establish that compounds do not act non-specifically is to measure the effect of the test compound on tobramycin, an antibiotic which is not transported by the MexAB-OprM drug efflux pump from *P. aeruginosa* (details described in Chapter 4). Any reduction in the MIC of tobramycin by a compound would indicate an indirect effect on the efflux pump, which means some other effect such as permeabilisation of membranes by that compound.

(d) Inhibition of substrate transport: The ability of a potential EPI to inhibit substrate transport in a drug efflux pump can be measured by performing substrate accumulation assays or by

measuring substrate efflux in the absence/presence of the putative EPI. Many fluorescent substrates for AcrB undergo a change in fluorescence when bound to DNA/membrane lipids. They can be used to measure the efflux activity of drug transporters. Fluorescent compounds that can be used to measure drug accumulation are Hoechst 33342 (Iyer et al., 2015), berberine, ethidium bromide, TMA-DPH [1-(4-trimethylammoniumphenyl)-6-phenyl-1,3,5-hexatriene-p-toluenesulfonate],N- phenylnaphthylamine (NMP) (Cha et al., 2014; Lomovskaya et al., 2001; Ohene-Agyei et al., 2012); whereas measurement of drug efflux or inhibition of efflux by a test compound can be measured by the Nile Red efflux assay which is compatible even with highly coloured or fluorescent compounds (Bohnert et al., 2010).

(e) Testing of outer membrane permeabilisation: The most effective technique to measure outer membrane permeabilisation is the nitrocefin hydrolysis method. The rate at which nitrocefin travels through the outer membrane is the rate limiting step for the hydrolysis, the effect of test compounds on this rate can be monitored spectroscopically (Lomovskaya et al., 2001).

(f) Testing of inner membrane permeabilisation: To evaluate the integrity of the bacterial inner membrane, the p.m.f in *E. coli* can be measured by performing a simple fluorescence assay utilising the fluorescent membrane potential probe 3,3'-diethyloxacarbocyanine iodide ($DIOC_2(3)$) (Iyer et al., 2015; Phetsang et al., 2016; Venter et al., 2003).

1.9 Studying mechanism of action of EPIs: Kinetic analysis of EPIs binding to AcrB

The tools for studying EPIs described in section 1.5 confirm an on-target activity of an EPI with the inner membrane protein (e.g. AcrB in *E. coli* and MexB in *P. aeruginosa*) and not through off-target effects such as membrane permeabilisation. The binding of EPIs to transporters can also be directly measured with techniques such as surface plasmon resonance (Polyak et al., 2020). In addition, this technique could yield information about the binding affinity of the inhibitor to the efflux protein. EPIs are required to bind with higher affinity than the substrates to exert an effect (Opperman & Nguyen, 2015). Our lab has previously standardised and optimised surface plasmon resonance (SPR) to determine the binding kinetics of substrates and inhibitors to AcrB that allowed for correction of the non-specific

binding of hydrophobic drugs and inhibitors to the large lipophilic integral membrane parts of AcrB (Mowla et al., 2018b; Polyak et al., 2020). SPR is a very powerful biophysical tool for drug identification. This method allows real time monitoring of the binding events and directly measurement of affinity and kinetic constants of biomolecular interactions (Puiu & Bala, 2016). The main advantage of this method compared with other techniques is that it does not require labelling (e.g. fluorescence or radioactive) to analyse molecules. Moreover, this method overcomes other difficulties such as the need for a large amount of pure proteins in other techniques such as the isothermal titration calorimetry assay (Nakashima et al., 2013), which is particularly valuable for membrane-proteins such as AcrB and MexB. The method is also adaptable to a high throughput format.

1.10 Research goal and aims

This goal of this project is to discover and characterise the activity of small molecule inhibitors of RND efflux pumps in Gram-negative bacteria to reverse antimicrobial resistance.

Inhibition of efflux pumps by EPIs provides a promising way to battle MDR through (i) restoring the efficacy of antibiotics where resistance has arisen, (ii) reducing the development of drug-resistant clinical pathogens and prolonging the lifetime of antimicrobials, (iii) inhibiting the ability of the pathogens to infect their host, and (iv) preventing the development of highly antimicrobial resistant biofilms (Venter et al., 2015).

The specific aims of this research were:

(i) Evaluation of the EPI activity of a series of synthetic compounds based on a benzochromene and flavonoid pharmacore to act as AcrB inhibitors.

(ii) Evaluation of ivacaftor as a repurposed inhibitor of the MexB drug efflux protein from *P. aeruginosa*.

CHAPTER 2 General Materials and Methods

2.1 General Materials

2.1.1 General Materials, Growth Medium and Antimicrobial Agents

General chemical reagents including salts and buffers (analytical purity grade), antibiotics, dimethyl sulfoxide (DMSO), ethylenediaminetetraacetic acid (EDTA), and polymyxin B nonapeptide (PMBN), were acquired from Sigma-Aldrich (St Louis, MO). Dodecyl-B-D-maltoside (DDM) was purchased from Carbosynth (Switzerland) and fluorescent substrates including 3,3'-diethyloxacarbocyanine iodide ($DiOC_2$ (3)) and Nile Red were obtained from Molecular Probes (USA). The sensor chips (CM5) used for surface plasmon resonance (SPR) were sourced from Bio-Strategy laboratory products (GE Healthcare, USA). Ivacaftor was obtained from SelleckChem (Boston, USA).

Microbiological growth media including Mueller-Hinton Broth and Agar were purchased from ThermoFisher (USA), Luria-Bertani (LB) Broth was purchased from Difco (Franklin Lakes, New Jersey). Bacteriological agar was obtained from Oxoid® (Adelaide, Australia). All media were autoclaved for 15 minutes at 121°C for sterilisation.

The origins of additional reagents used in assays are listed in specific protocols described below.

2.1.2 Synthetic compounds and repurposed drug tested as efflux pump inhibitors, and antimicrobial agents

Synthetic compounds including 3,4-dihydro-2H-benzo[h]chromen-5-yl)(morpholino)methanone derivatives (G0-G20, H1-H7, and Y1-Y7), and 4H-chromen-4-one (flavonoid) derivatives (S1-S4) were chemically synthesised in the laboratory of our collaborator, Professor Shutao Ma, Department of Medicinal Chemistry, School of Pharmaceutical Sciences, Shandong University, Jinan, P.R. China. The synthesis, structural characterisation and purity analysis (all the synthetic compounds with the purity of 95 %) conducted in the Ma laboratory are described in the accepted paper given in Chapter 3.

Repurposed drug ivacaftor, antibiotics, and membrane permeabilisers are listed in Table 2.1.

Table 2.1 A list of synthetic compounds, antimicrobial agents, membrane permeabilisers, and their abbreviations and supplier.

Compounds	**Abbreviations**	**Supplier**
Ivacaftor	IVA	Sigma Aldrich (St Louis, USA)
Erythromycin	ERY	Sigma Aldrich (St Louis, USA)
Levofloxacin	LEV	Sigma Aldrich (St Louis, USA)
Minocycline	MIN	Sigma Aldrich (St Louis, USA)
Tobramycin	TOB	Sigma Aldrich (St Louis, USA)
Ethylenediamine tetra acetic acid	EDTA	Sigma Aldrich (St Louis, USA)
Colistin	COL	Sigma Aldrich (St Louis, USA)
Polymyxin B nonapeptide	PMBN	Sigma Aldrich (St Louis, USA)
Phe-Arg-β-naphthylamide	PAβN	Sigma Aldrich (St Louis, USA)
Tetracycline	TET	Sigma Aldrich (St Louis, USA)
Meropenem	MER	Sigma Aldrich (St Louis, USA)
Chloramphenicol	CHL	Sigma Aldrich (St Louis, USA)
Oxacillin	OXA	Sigma Aldrich (St Louis, USA)
Novobiocin	NOV	Sigma Aldrich (St Louis, USA)
Tetraphenylphosphonium chloride	TPP	Sigma Aldrich (St Louis, USA)

2.1.3 Preparation of compounds, antimicrobials, and membrane permeabilisers

Solid compounds including synthetic compounds, ivacaftor, antimicrobials and membrane permeabilisers were weighed into Eppendorf tubes. Solvents including DMSO, ethanol, or MilliQ water were added to make a solution. Compound solutions were vortexed and visually observed to make sure all solid materials were dissolved. If undissolved, solutions were placed on a shaker at 37°C for 30 minutes. DMSO was the ideal solvent for sample preparation, and

the final concentration of DMSO in the biological assays were less than 4 % v/v and were confirmed to have no antimicrobial activity against the bacterial strains used in this study.

2.2 General Microbiology

2.2.1 Growth media and buffers for incubation

LB broth media and MH broth media were used for general bacterial growth. MH or LB agar plates were prepared by adding 1.2 % w/v technical agar into MH or LB broth prior to autoclaving. LB + kanamycin agar plates were prepared from autoclaved LB agar to which 25 mg/mL of kanamycin was added.

2.2.2 Preparation and storage of stock cultures of bacteria

Bacterial strains were grown overnight on LB agar or LB + Kanamycin agar, then a single colony was inoculated into 10 mL LB medium or 10 mL LB medium containing 25 mg/mL of kanamycin in a 50 mL centrifuge tube. The incubation was shaken vigorously at 37°C overnight until the OD600 reached OD 1. Then 0.5 mL of the culture was removed and transferred to a cryovial, 0.5 mL 50% glycerol was added, well-mixed and immediately stored at -80°C.

2.2.3 Inoculation of a culture from the frozen stock

A few microliters of the frozen stock (kept on ice) were scraped from the surface using a sterile cotton applicator stick and streaked on an agar plate (containing appropriate antibiotic(s) when necessary). The remainder was returned to the -80°C freezer immediately.

2.2.4 Bacterial strains used for assays

The *Escherichia coli* (*E. coli*) and *Pseudomonas aeruginosa* (*P. aeruginosa*) strains used in the experiments are listed in Table 2.2 and Table 2.3.

Table 2.2 Descriptions and sources of *E. coli* strains used.

***E. coli* strains**	**Description**	**Reference / Source**
BW 25113	Wild type of *E. coli* with constitutive expression of functional AcrAB-TolC pump	Venter lab stock
BW 25113 (DE3) ΔAcrB	Drug sensitive *E. coli* BW25113 strain with a deletion in genomic *acrB*	Venter lab stock
BW 25113 (DE3) ΔAcrB (pAcrB)	An expression strain that contains a knockout of the *acrB* gene and AcrB overexpression induced by transforming the *acrB* coding plasmid (kanamycin resistant)	Venter lab stock
C41 (DE3)	*E. coli* C41 (DE3) strain used for the expression of toxic membrane proteins	Venter lab stock

Table 2.3 Descriptions and sources of *P. aeruginosa* strains used.

***Pseudomonas* strain**	**Description**	**Reference / Source**
PAM 1020	Wild type of *P. aeruginosa* PA01	A kind gift of Dr Olga Lomovskaya, (Lomovskaya et al., 2001).
PAM 1032	*P. aeruginosa* with MexAB-OprM (overexpressed due to a *nalB* mutation)	
PAM 1626	*P. aeruginosa* lacking the *mexAB-oprM*, *mexEF-oprN*, and *mexCD-oprJ* genes	

2.3 Functional assays

2.3.1 Antimicrobial activity assay

Antimicrobial assays were performed to confirm the compounds tested as efflux pump inhibitors (EPIs) had no undesirable antimicrobial activities against *E. coli* or *P. aeruginosa* or other Gram-negative bacteria (Guo et al., 2023). Antimicrobial sensitivity assays were performed using standard broth dilution assays, as recommended by the European Committee on Antimicrobial Susceptibility Testing according to International Standard ISO 20776-1 (ISO, 2019). Briefly, a two-fold dilution series of each test compound into fresh bacterial growth media was performed in 96 well microtiter trays. Log phase bacteria were then seeded into each well (5×10^5 CFU/well) before growing for 18 h at 37°C. The optical density of each well was measured using a plate reader (BioTek, Potton Bedfordshire, UK) at 630 nm (OD_{630}) at 0 h and 18 h. The minimal inhibitory concentration (MIC) was determined as the lowest concentration of antibiotic needed that completely prevent the bacterial growth as detected by no increase in OD_{630} after 18 h. All MIC determinations were repeated at least three times in independent experiments in the presence of 2 % v/v DMSO (at this concentration of DMSO had no effect on bacterial growth).

2.3.2 Checkerboard titration assay

The checkerboard titration assay was used as the primary screening assay to determine the ability of selected compounds to function as EPIs by increasing the susceptibility of Gram-negative organisms to certain antibiotics (Guo et al., 2023; Venter et al., 2015). These assays were performed using 96-well plates with antimicrobials serially diluted vertically down the plate (seven 2-fold serial dilutions) and test compounds serially diluted horizontally across the plate (five 2-fold dilutions) (Wang et al., 2021; Yoshida et al., 2007). A bacterial inoculum 5×10^5 CFU/well was added and the plates were incubated at 37 ^{o}C for 18 h under aerobic conditions (used for *E. coli* BW 25113 (wild type) and BW 25113 (DE3) ΔAcrB (efflux pump deleted strain), PAM 1020 (wild type), PAM 1032 (efflux pump overexpressed strain), and PAM1626 (efflux pump deleted strain)). In assays using compounds which showed high absorbance at time zero, the presence or absence of bacterial growth at 18h was confirmed

with the use of resazurin. In this method, 10 µL of 0.01% w/v resazurin was added in each well and the plate was incubated at 37 ^{o}C for 30 min while shaking. A pink color was indicative of metabolically active cells while a blue colour indicated no growth of the organism (Costa et al., 2021). PAβN was used as a known EPI control.

The compounds which potentiated the effect of an antimicrobial (reduced the MIC) against testing strains expressing the efflux pump were then tested in the checkerboard assay against the testing strains with a deletion of the efflux pump to determine whether the compounds did not synergise with antimicrobials in an efflux pump deleted mutant. All assays were repeated at least twice.

Additional checkerboard assays were also performed on wild-type *E. coli* BW25113 in the presence of membrane permeabiliser colistin (0.5 µg/mL), or on PAM 1020 and PAM 1032 in the presence of membrane permeabilisers including colistin (0.5 µg/mL), and PMBN (0.96 µg/mL). At these concentrations, permeabilisers would permeabilise the outer membrane of *E. coli* and *P. aeruginosa*, allowing compounds to enter the cells more readily (Nguyen et al., 2021). All assays were repeated at least twice.

2.3.3 Nile red efflux assay

The Nile red efflux assay was performed to examine whether the compounds inhibited efflux of the fluorescent efflux pump substrate Nile Red (Bohnert et al., 2010; Guo et al., 2023; Ohene-Agyei et al., 2014; Venter et al., 2015). Nile Red is fluorescent when it accumulates inside the cell but non-fluorescent in the aqueous media.

E. coli BW 25113 (DE3) ΔAcrB propagating the *acrB* expressing plasmid, pAcrB, or *P. aeruginosa* with *mexAB-oprM* overexpressed (PAM 1032), were used in the assay.

Overnight cultures of the required bacterial strain were incubated in LB broth in the presence of 25 µg/mL kanamycin and incubated with shaking at 37°C for 14 to 16 hours until the OD660 reached a plateau. The cells were harvested by centrifugation at 4000 g for 10 min at room temperature and were then washed three times by centrifugation followed by re-suspending the cells in 50 mM potassium phosphate buffer (pH 7.0) containing 1 mM $MgCl_2$. The cells

were then resuspended in the same buffer to an OD_{660} of 1.0 after which cells were allowed to rest for 15 min at room temperature. Aliquots (2 mL) were then transferred to 15-mL conical centrifugation tubes and the ionophore carbonyl cyanide m-chlorophenylhydrazone (CCCP) was added at a final concentration of 10 mM to de-energise the cells. After 15 min, the test compound (putative EPI) was added to the desired final concentration and Nile Red was added to a final concentration of 10 μM after another 15 min. The cell suspension was incubated on a shaker (140 rpm at 37°C) for 3 h. The cells were left at room temperature for 60 min and then centrifuged for 5 min at 3000 g. The supernatant was discarded, and droplets of it clinging to the tube wall were thoroughly removed with absorbent tissues. Subsequently, the cells were resuspended in 0.2 mL assay buffer (20 mM of pH 7.0 potassium phosphate buffer containing 1 mM $MgCl_2$) and were immediately transferred to a quartz cuvette containing 1.8 mL of assay buffer. The fluorescence signal was measured in a fluorimeter (LS 55B, PerkinElmer) with excitation at 552 nm and emission at 636 nm. Excitation and emission slit widths were 10 and 5 nm, respectively. The fluorescence of the cell suspension was followed for 100 s, after which Nile Red efflux was triggered by rapid energisation with 50 mM glucose. Fluorescence was monitored for another 200 s. PAβN was used as a known EPI control in the assay. All assays were repeated at least twice for each compound and concentration.

2.3.4 Nitrocefin assay

The nitrocefin hydrolysis assay was performed to determine if the compounds disrupt the bacterial outer membranes as described previously (Gu et al., 2020; Guo et al., 2023). Briefly, *E. coli* BW25113 cells with constitutive expression of chromosomal β-lactamase were grown in LB broth, then harvested and washed in 50 mM potassium phosphate buffer. The cells were subsequently resuspended in the same buffer and aliquoted in a 96-well plate (flat bottom, Corning Incorporated-Life Science) at an OD_{660} of 0.5. The cell suspension was treated with 10 μM CCCP and the compounds were added to a final concentration of 32 μg/mL. The reaction was started by the addition of nitrocefin (32 mg/L final concentration) (each compound has at least two replicates). Immediately thereafter, hydrolysis of nitrocefin was

monitored by measurement of the increase in absorbance at 490 nm over 20 min (EnSpire, Multimode plate reader, Perkin Elmer). A set of duplicate wells for each compound without the addition of nitrocefin was also monitored over the same time-period to exclude the intrinsic absorbance.

The rates of nitrocefin hydrolysis in the presence of compounds were compared to the rate of a) untreated cells with the vehicle control (DMSO) only; and b) cells treated with the known outer membrane permeabiliser polymyxin B nonapeptide (PMBN). All assays were repeated at least twice for each compound and concentration.

2.3.5 $DiOC_2$(3) assay

The membrane gradient assay was performed using an adaptation of a method described previously (Guo et al., 2023; Venter et al., 2003; Wang et al., 2021) to determine effects of compounds on the bacterial inner membrane.

A 0.1-mL portion of an overnight culture (grown at37°C with shaking at 140 rpm) of *E. coli* BW25113 was added to 50 mL LB broth in an Erlenmeyer flask and grown on a shaker (140 rpm; 37°C) to an OD_{660} of 0.5 (approx. 2-3 h). The culture was then centrifuged at 4000 g for 10 min at room temperature. The pellet was re-suspended in the assay buffer (50 mM potassium phosphate buffer pH 7.0). After another centrifugation and resuspension step, the cells were treated with 2.5 mM K-EDTA and 1% v/v ethanol and incubated at 37°C for 15 min to permeabilise the outer membrane. The cells were harvested by centrifugation (4000 rpm, 10 min, 4°C) and then resuspended in the assay buffer to an OD_{660} of 5. The cells were kept on ice for subsequent experimentation.

The cell suspension (0.2 mL) was transferred to a quartz cuvette containing 1.8 mL of assay buffer at room temperature. The fluorescence was measured in a fluorimeter (LS 55B, PerkinElmer) with excitation and emission wavelengths of 488 nm and 613 nm, respectively and excitation and emission slit widths of 10 and 5 nm, respectively. The fluorescence of the cell suspension was followed for 60 s, before $DiOC_2$ (3) solution was added at a final concentration of 10 μM. After the fluorescence reached a plateau, the cells were energised

by the addition of 0.5% w/v glucose. The fluorescence was monitored until a steady state was reached again before the proton motive force was disrupted by the addition of the ionophore CCCP (10 μM). To measure the effect of test compounds (putative EPIs) on the gradient, the compounds were added to the cell in the cuvette at the desired concentration and incubated with shaking for 10 min before taking the fluorescence reading was commenced. All assays were repeated at least twice for each compound and concentration.

2.3.6 *In vivo* cytotoxicity assay

Evaluation of the toxicity of experimental compounds using the nematode species *Caenorhabditis elegans* (*C. elegans*) is inexpensive and less time-consuming, compared to mammalian models, and may be used prior to screening in more complex animal models (Guo et al., 2023; Tampakakis et al., 2008).

In this study, the maintenance and synchronisation of *C. elegans* nematodes was performed as described previously (Chai et al., 2022; Chai et al., 2020; Tampakakis et al., 2008). Briefly, the nematodes were grown on Nematode Growth Medium agar (1 mM $CaCl_2$, 1 mM $MgSO_4$, 25 mM KPO_4 and 5mg/mL cholesterol, mixed with 0.3% NaCl, 1.2% technical agar and 0.25% peptone) that was seeded with a lawn of *E. coli* OP50. This study was performed using equivalent aged nematodes generated from synchronisation. At the synchronisation step, the nematodes were washed with 0.9 % w/v NaCl from the plates and then treated with a mixture of 10 % w/v sodium hypochlorite solution and 4N NaOH anhydrous in a limited time; then the mixture was vortexed, centrifuged and rinsed with 0.9 % w/v NaCl for three times; then the pellet (containing the nematode eggs) was washed with 0.9 % w/v NaCl and transferred onto the NGM agar plates and incubated at 25°C for 4 days. After this, the nematodes were killed, and their eggs were exposed to grow on the plates to an adult age. The synchronised nematodes were then harvested in Nematode Growth Medium broth (composed of 95% M9 buffer and 5% brain heart infusion broth, supplemented with 10 μg/mL cholesterol), the density of nematodes was adjusted to approximately 25 nematodes per 25 μL. The number of nematodes was counted under a light microscope at 40× and 100× magnification. The putative EPI test compounds were evaluated for their toxicity at 128 μg/mL and were added

to 96-well-plates in the presence of 2% v/v DMSO. Untreated nematodes in the presence of 2% DMSO were used as healthy, positive controls. Additional wells containing 50 μg/mL ampicillin and 2% v/v DMSO were also set as healthy controls to show the survival rate when nematodes were fed with a known antibiotic with low toxicity. Each well was loaded with 25 μL of the test solution and 25 μL of nematodes and 50 μL medium. The nematodes were then incubated at 25˚C and observed for up to 72 h. The number of alive/dead nematodes was counted every 24 h. The percentage of surviving nematodes was calculated every 24 h for 72 h in total. Statistical analysis was performed using two-way ANOVA using Prism (GraphPad Prism 9). All assays were repeated at least twice for each compound and concentration.

2.4 Protein techniques

2.4.1 Preparation of inside out vesicles (ISOVs)

Chemically competent *E. coli* cells were used to produce strains for expression of desired proteins by transformation of recombinant plasmids (pAcrB, pMexB and pGalP) into the cells. Since protein levels significantly varied, and expression was often reduced after storage of the transformed strains at -80°C. Therefore, for these experimental cells were always freshly transformed with plasmids before use. A single transformant was inoculated and grown overnight at 37 °C in LB Broth with 25 μg/mL kanamycin. The cultures were incubated at 18°C until an OD660 reached around 0.3 before gene transcription was induced with 0.5 mM isopropyl β-D-1- thiogalactopyranoside (IPTG). Growth was continued with shaking at 200 rpm overnight to allow expression of the target protein.

The cells were harvested by centrifugation (15 min, 6500 g, 4°C) and resuspended in 0.1M potassium phosphate (pH 7.0). DNAse (10μg/mL) and 10 mM $MgSO_4$ was added, and the suspension incubated for 15 minutes at room temperature. It was then passed twice through a cell disruptor (Constant Systems with Thermoflex Temperature control) at 20 KPsi to break the intact cells into ISOVs. ISOVs were incubated at room temperature for 15 min to allow the DNAse to act. A low-speed spin (10 min, 10,000 g, 4°C) was then carried out to remove the cell debris (pellet), and the supernatant was subjected to a high-speed spin using a 50.2 Ti

rotor (40,000 g, 40 minutes, 4°C) to collect the vesicles. The pellet was resuspended in 50 mM potassium phosphate buffer pH7.0 containing 10% glycerol. Aliquots of 1 mL each were snap frozen and immediately stored in at -80° C.

2.4.2 Determination of protein concentration

The BioRad DC Protein Assay was used to determine the concentrations of protein in ISOVs. This colorimetric assay is based on the formation of a complex between copper and peptide bonds, reducing copper to a monovalent ion. The absorbance at 750nm (A_{750}) was measured, and protein concentrations determined by reading off a standard curve constructed using a set of bovine serum albumin (BSA) standards (0 to 1.5 mg/mL).

2.4.3 Purification of His-tagged proteins

The proteins (AcrB, MexB and GalP) used were His-tagged and therefore the metal binding technique of protein purification was employed. Ni^{2+}–nitrilotriacetate (Ni-NTA) resin was used to select for the exposed histidine residues at the terminal of recombinant proteins as the Ni in the resin interacts with the imidazole side chain of histidine.

The ISOVs prepared from cells expressing required proteins were allowed to solubilise for 1 hour at room temperature while gently shaking. Unsolubilised protein was then removed by ultracentrifugation at 4°C (40000 rpm, 1 h). Ni-NTA resin was equilibrated by washing twice with ice-cold MilliQ water (sedimentation by gravitation). The resin was resuspended in a small volume of wash buffer A (Table 2.4 and Table 2.5) and kept on ice. The supernatant from the ultracentrifugation was then added to the Ni-NTA resin and the protein was allowed to bind to the resin by gentle shaking on the shaker for 1 hour at 4°C. The resin was then transferred into a 2 mL polystyrene mini-column (BioRad laboratories) and the unbound fraction was then allowed to drain away. Then the resin was washed with 60 resin volumes of wash buffers. After that, five resin volumes of elution buffer were added to displace the His-tagged protein from the resin. The first 0.5 resin volume of eluant was discarded. And then the next 3 to 4 resin volumes of eluant were collected as the purified His-tagged protein. A simplified illustration of this method can be seen in Figure 2.1.

Table 2.4 Components of buffers for purifying His-tagged AcrB and MexB

Solubilisation buffer		**Wash buffer A**		**Wash buffer B**		**Elution buffer**	
Tris-HCl (pH 8)	20 mM	Tris (pH 8)	20 mM	K-HEPES (pH 8)	20 mM	Tris (pH 8)	20 mM
Glycerol	10 %	Glycerol	10 %	Glycerol	10 %	Glycerol	10 %
NaCl DDM	0.3 M	NaCl	0.3 M	NaCl	0.3 mM	NaCl	0.3 M
Imidazole	1.5 %	DDM	0.05 %	DDM	0.05 %	DDM	1.5 %
(pH 8.0)	10 mM	Imidazole (pH 8.0)	30 mM	Imidazole (pH 8.0)	50 mM	Imidazole (pH 8.0)	400 mM

Buffers were made up to volume with MilliQ water.

Table 2.5 Components of buffers for purifying His-tagged GalP

Solubilisation buffer		**Wash buffer**		**Elution buffer**	
K-HEPES (pH 7.5)	20 mM	K-HEPES (pH 7.5)	10 mM	K-HEPES (pH 7.5)	20 mM
Glycerol	20 %	Glycerol	10 %	Glycerol	5 %
NaCl	0.3 M	NaCl	0.1 M	NaCl	0.3 mM
DDM	1 %	DDM	0.05 %	DDM	0.05 %
Imidazole (pH 8.0)	20 mM	Imidazole (pH 8.0)	20 mM	Imidazole (pH 8.0)	200 mM

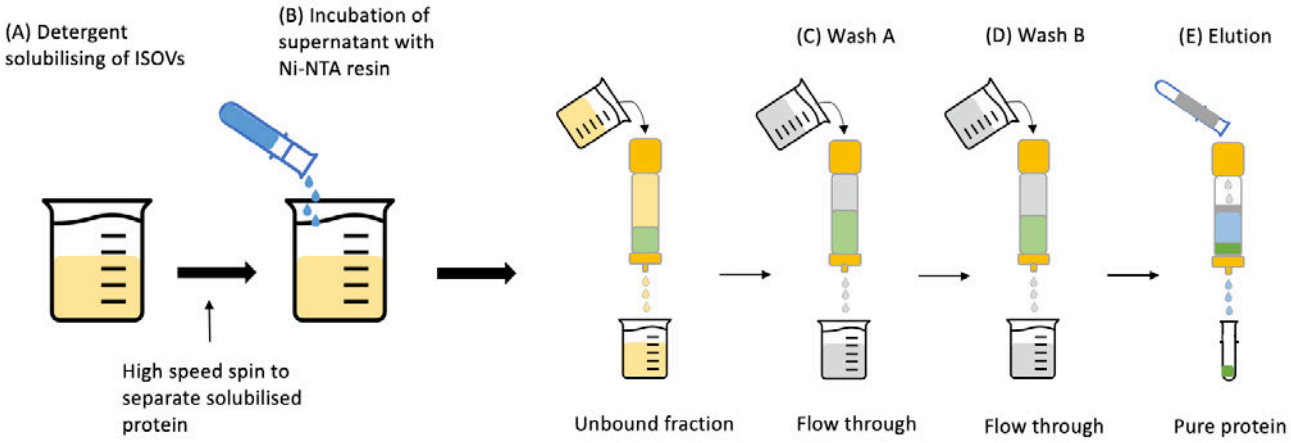


Figure 2.1 Process for the purification of His-tagged proteins

Buffers were made up to volume with MilliQ water.

2.4.4 SDS-PAGE

The expression of the protein in ISOVs and efficiency of protein purification was monitored by SDS-PAGE analysis. Acrylamide gels (10%) were normally used and were prepared using the ingredients described in Table 2.6.

Table 2.6 The components of the solutions used for the SDS-PAGE gel

Stock solution	**Separating gel (10mL of a 10% solution)**	**Stacking gel (5mL of a 5% solution)**
40% acrylamide/Bis mix (37.5:1)	3.75 mL	0.625 mL
1.5 M Tris	3.75 mL (pH 8.8)	1.25 mL (pH 6.8)
10% SDS	150 mL	50 mL
H_2O	7.2 mL	3 mL
10% ammonium persulphate	75 mL	25 mL
TEMED	23 mL	5 mL

The gels were run at 150 V constantly for 150-180 minutes. After completion of the electrophoresis procedure the gel was incubated in staining solution for 1hr at room temperature after it was de-stained. The gels were photographed under the UV light. Buffers and solutions and their components used in the electrophoresis are listed in Table 2.7.

Table 2.7 Buffers and solutions used in SDS-PAGE

Running buffer		**Staining solution**		**De-stain solution**	
Trisma base	15.1 g	Acetic Acid	100 mL	Acetic Acid	70 mL
SDS	5 g	Methanol	400 mL	Methanol	50 mL
Glycine	93.8 g	Coomassie Brilliant		H_2O to	1 L
H_2O to	1 L	Blue-R 250	1 g		
		H_2O to	1 L		

2.5 Surface plasmon resonance

After successful purification of proteins, the binding kinetics of inhibitors were measured by using a surface plasmon resonance (SPR) assay (Mowla et al., 2018b). In this study, SPR was performed in a Biacore S200 biosensor system using covalent immobilisation of proteins on a CM5 sensor chip to characterize binding interactions. Experiments were carried out by modification of methods described in the Biacore assay handbook and Tikhonova and Zugrskaya (Tikhonova & Zgurskaya, 2013), and based on the optimization from our group (Mowla et al., 2018b; Polyak et al., 2020). The method is described in the following sections.

2.5.1 Buffers and reagents

Table 2.8 describes the buffers, solvents and reagents used in the SPR assay.

Table 2.8 Buffers, solvents and reagents used in different stages of SPR

Reagent	**Ingredients**
Surface activating agent	EDC+NHS 1:1 mix (mixed just prior to use) *
Running Buffer A for immobilisation	1.05 PBS + 0.05% Tween 20 (1.05 PBS-P)
Immobilisation Buffer	10 mM Na-Acetate pH 4.5
Deactivating agent	50 mM Tris pH 7.4**
Running buffer B for binding studies	1.05 PBS-P +5% DMSO
Stock solutions for solvent correction	S1: 1.05 PBS-P+ 4.5% DMSO, S2: 1.05 PBS-P+ 5.8% DMSO
Solvent for analytes	Running Buffer B

*N-hydroxysuccinimide (NHS) and 1-ethyl-3-(3-dimethylamino) propyl carbodiimide (EDC) at 1:1 ratio mix was used to activate the surface by modification of the carboxymethyl groups to N- hydroxysuccinimide esters.

**Deactivation of unreacted NHS-esters was using 50 mM Tris pH 7.4.

2.5.2 Preparation of the ligand

Purified His-tagged AcrB was transferred into running buffer A (Table 2.7) by passing through 100 kDa molecular sieve (Thermofisher Scientific) at 1000 rpm for 1 min each time until the imidazole concentration was down to below 10 mM. MexB and GalP was prepared the same way.

2.5.3 Immobilisation of protein

The proteins were transferred to immobilisation buffer (Table 2.7) at a concentration of 2.9 mg/mL, 1.9 mg/mL, and 2.2 mg/mL for AcrB, MexB and GalP respectively (the concentration difference between AcrB, MexB and GalP for use to achieve similar R.U. was determined after several tests). The proteins were then immobilised onto CM5 surface (AcrB on flow cell 2, MexB on flow cell 3 and GalP on flow cell 4) according to the following steps.

1. The surfaces were activated by using a mixture of EDC-NHS (1:1) for 15 min at a flow rate of 10 µL/min.

2. Proteins were injected for 2100 seconds (AcrB to flowcell 2, MexB to flowcell 3, and GalP to flowcell 4) at a flow rate of 10 µL/min.

3. After the desired R.U. was achieved (minimum 10,000 required), remaining groups were blocked with Tris pH 7.4 injecting for 5 min at a flow rate of 30 µL/min

4. The control cell (flow cell 1) received the same treatment except they were treated with only immobilisation buffer instead of the proteins.

2.5.4 Determination of kinetic (equilibrium dissociation) constants

To accurately measure the kinetic parameters of low molecular weight inhibitors to AcrB and MexB, the change in R.U. for each concentration was plotted against concentrations of inhibitor. Each value of R.U. was corrected in three steps. (1) Background noise was corrected by subtracting the R.U. value achieved for the control flow cell (Blank) without protein treated with the same concentrations of compounds. (2) The solvent error during each injection (details described in the following paragraph) was corrected by the solvent correction wizard designed by Biacore. (3) To correction for non-specific binding interactions and obtain specific binding responses for AcrB and MexB for the R.U. values of GalP was subtracted from those of AcrB and MexB. These R.U. values, which are obvious indicators of binding quantity of analytes to AcrB and MexB, were then plotted against concentrations from where affinity constants were determined by fitting the data with a one site specific (non-linear regression) hyperbola in GraphPad prism 9.

Performing solvent correction

The inhibitors studied in this experiment were soluble in DMSO. To study the kinetic behaviour of these analytes, running buffer B (running buffer A containing 5% v/v DMSO) was used to continuing flow over the flow cells while the sample solutions for analysis were prepared in such a way that the DMSO concentration was maintained at 5% v/v. It is to be

noted that, the 5% v/v DMSO concentration was able to keep all the analytes in solution and was decided upon after a trial to use several different concentrations. Through this process could be avoided a large signal difference that created by the difference in refractive indices of solvents. However, there is always the risk of the DMSO concentration being varied slightly between different samples. The effect of these variations is usually very small in terms of absolute response. However, it still significant in kinetic studies where minor differences in response units which could potentially contribute to wrong interpretation of data. To avoid this problem, the solvent correction wizard designed in Biacore S200 by GE healthcare was used. Solvent correction is used to adjust the difference in bulk response. Baseline before and after injection is not affected by DMSO variation.

Solvent correction stock solutions with 4.5% v/v and 5.8% v/v DMSO were prepared following GE Healthcare Life Sciences' instructions (Buffer and sample preparation for direct binding assay in 5% v/v DMSO) according to Table 2.9.

Table 2.9 Solvent correction stock solutions

	4.5 % DMSO	**5.8 % DMSO**
1.05 PBS-P	9.5 mL	9.5 mL
100 % DMSO	0.45 mL	0.58 mL
Final volume	10 mL	10 mL

Using the 4.5% and 5.8% DMSO stock solutions, a series of aliquots for the solvent correction curve were prepared, according to Table 2.10 (volumes given in µL).

Table 2.10 Preparation of solvent correction working solutions

Buffer vial	1	2	3	4	5	6	7	8
4.5 % DMSO	0	200	400	600	800	1000	1200	1400
5.8 % DMSO	1400	1200	1000	800	600	400	200	0

For the assay, the system was first primed with running buffer B and was allowed to run five start-up cycles with solvent correction solutions over control and active surfaces. BiaCore

S200 control software was used to create a solvent correction curve from the response of the reference flow cell and the reference-subtracted response. The wizard subtracted the solvent error from the reference corrected sensogram and the correct binding response at each injection was achieved (for example if the mismatch between the sample and running buffer produces a bulk displacement of -150 R.U. in the reference flow-cell, the corresponding solvent error will be +5 in the reference-subtracted sensogram).

Preparation of analytes

Serial dilutions of inhibitors were prepared in running buffer B in such a way that

the DMSO concentration was 5% v/v. To achieve this, the following process was followed.

- Sample stock (for example 10 mM) was made in 100% DMSO from which 50 µL (20 times dilution) was transferred and mixed with 950 µL of running buffer A to achieve a concentration of 500 µM.
- To prepare a series of concentrations, serial dilution from this were made in running buffer B as illustrated in Figure 2.2.

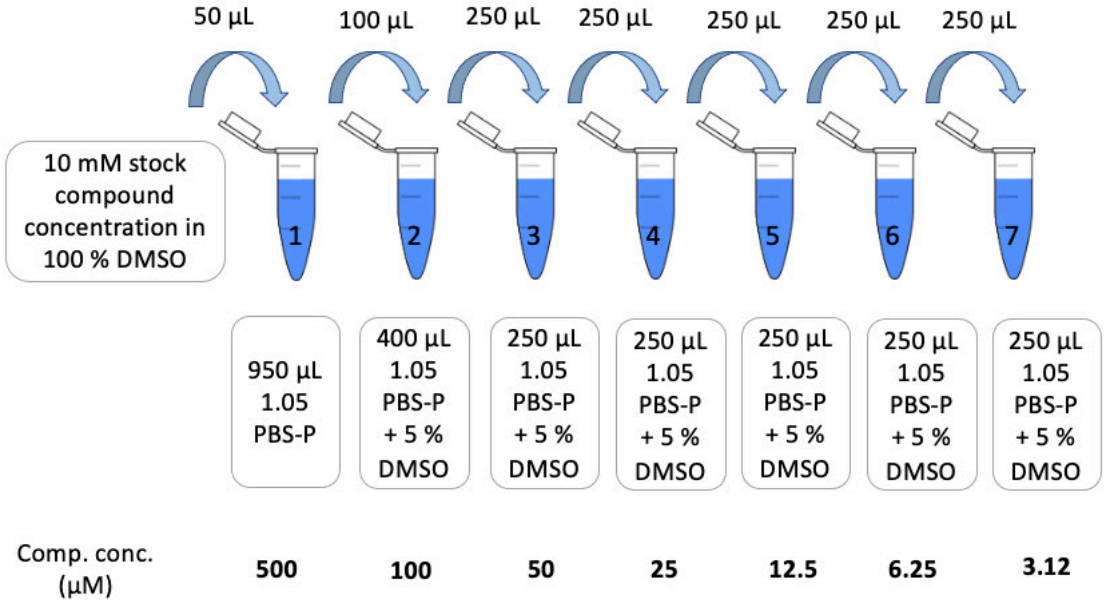


Figure 2.2 Preparation of serial dilution of compounds

Assay set-up

Standard 96-well plates were used for analytes, where 11 compounds could be studied at 8 serial concentrations along the vertical line. Eleven solvent correction working solutions were placed in the instrument in the designated (by the wizard) areas of reagent rack (Figure 2.3).

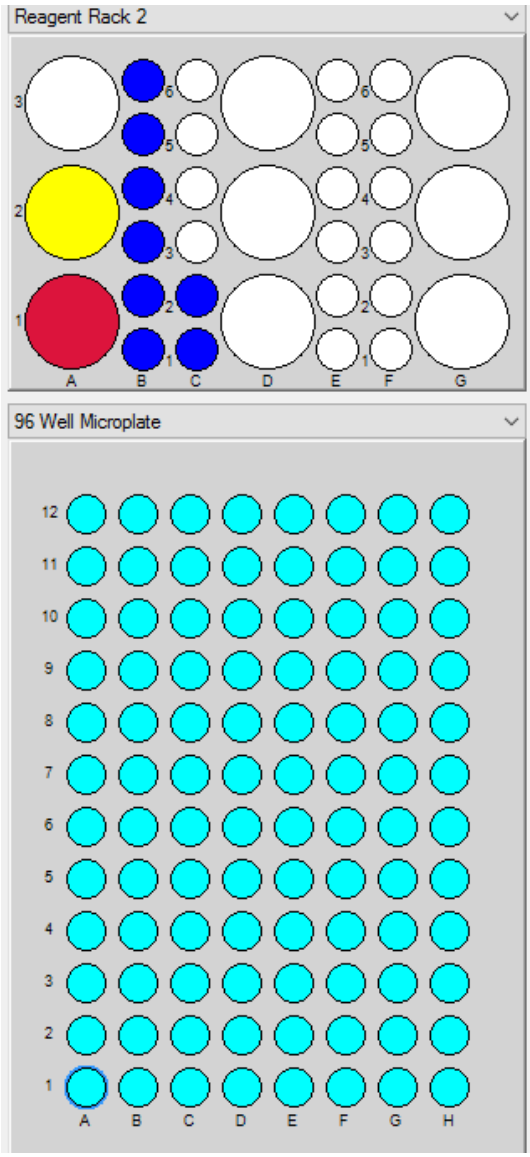


Figure 2.3 Reagent rack 2 attached to 96-well plate used in Biacore S200.

A1 (big red circle) contained running buffer B, A2 (big yellow circle) contained 50% DMSO, B1-B6 and C1-C2 (small dark blue circles) contained solvent correction working solutions serially. The 96-well plate contained analytes at different concentrations.

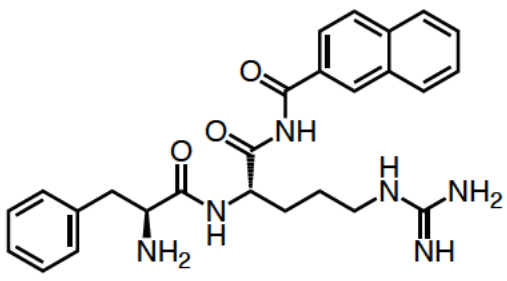
The run started with five start up cycles with the solvent correction solutions over control and active surfaces which was repeated after 60 cycles of analyte injection. Analytes were injected through all the flow cells, under continuous flow. The association and dissociation times were then set at 60 s and 120 s respectively. A solution of 50% v/v DMSO was then used for washing the sensor chips. When the analyte binds to the ligand, the change or increase in refractive index resulting in the interaction could be viewed as R.U. versus time (a sensorgram).

CHAPTER 3 Design and Synthesis of Benzochromene and Flavonoid Derivatives as AcrB Inhibitors for the Reversal of Bacterial Multidrug Resistance

3.1. Introduction

Antibiotic resistance poses an urgent and increasing threat to human health in the 21st century. In Gram-negative pathogens, drug efflux pumps such as AcrAB-TolC complex enable resistance to multiple classes of antibiotics and are the systems preliminarily responsible for intrinsic and acquired multidrug resistance (MDR) (Du et al., 2014; Piddock, 2006a; Zhang et al., 2000). We need to develop antibiotics that can treat resistant pathogens. An efficient way to protract the antibiotic efficiency or to potentiate the antibiotics activity against drug-resistant pathogens is to block drug efflux pumps by efflux pump inhibitors (Abreu et al., 2012; Kourtesi et al., 2013; Lomovskaya & Bostian, 2006; Lomovskaya et al., 2001; Ruggerone et al., 2013; Venter, 2019). The AcrB inner membrane protein from the *Escherichia coli (E. coli*) AcrAB-TolC efflux pump is an important target for the discovery and development of new efflux pump inhibitors (EPIs) (Ohene-Agyei et al., 2014) (as described in Chapter 1). Hence many laboratories, as well as ours, are focusing on the study of potential AcrB inhibitors in the prototypical bacteria *E. coli*.

The first identified and premium standard efflux pump inhibitor (EPI) against RND efflux pumps of Gram-negative bacteria, Phe-Arg-β-naphthylamide (PAβN) (Venter et al., 2015) (Figure 3.1), was found by screening for compounds that could synergy with levofloxacin against antimicrobial resistant *P. aeruginosa*. Due to its cytotoxicity, PAβN failed to enter clinical trials (Venter et al., 2015). However, it remains an important positive control for use in such assays for EPI activity including checkerboard, Nile Red efflux, and binding assays.

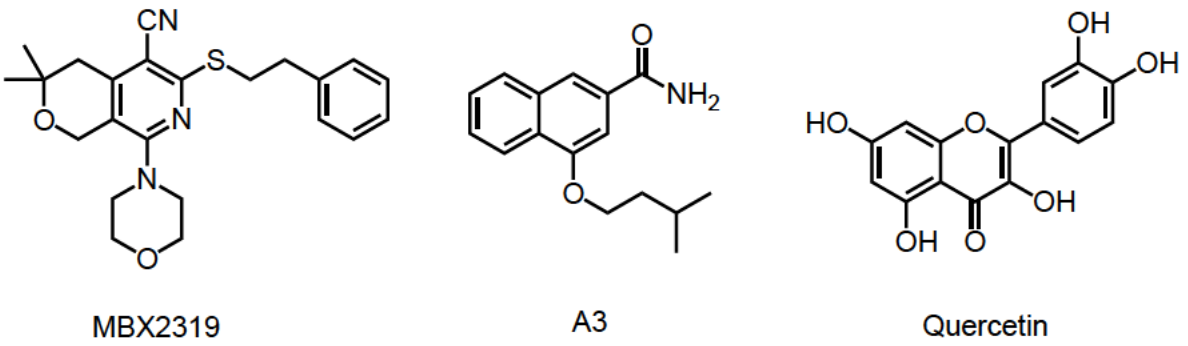


PAβN

Figure 3.1 Chemical structure of PAβN

This Chapter describes the testing of four series of compounds as potential inhibitors of AcrB in *E coli*. These compounds were designed and synthesised by our collaborators at Shandong University, Jinan, China. In total 39 compounds were tested including 3 series of benzo[h]chromene derivatives and one series of flavonoid derivatives (structures are listed in Appendix 1). The benzochromene derivatives (designated as series G, H and Y) were design based on MBX 2319 and A3. As described in Chapter 1.4, MBX2319 (Figure 3.2) was confirmed as a potent EPI by Opperman and his group (Opperman et al., 2014), showing specific efflux inhibitory activity against AcrAB-TolC in *E. coli*, with neither outer and inner membrane disruption nor cytotoxicity in mammalian cells and high potency compared to the known EPI PAβN (Opperman et al., 2014). The compound A3 (Figure 3.2) was developed by our collaborators at Shandong University and previously reported as an EPI by our group (Wang et al., 2017). Compound A3 was designed based on the natural compound, shikonin which is an inhibitor of AcrB (Mowla et al., 2018a; T. Ohene-Agyei et al., 2014; Wang, Mowla, Ji, Guo, De Barros Lopes, et al., 2018) enhancing the antibacterial activity of multiple antibiotics against multidrug resistant *E. coli* expressing AcrB (Mowla et al., 2018b; Ohene-Agyei et al., 2014)

The flavonoid derivatives (designated as the S series) were designed based on the natural compound quercetin (Figure 3.2) a known antimicrobial agent which was reported to inhibit efflux activity in AcrB overexpressing carbapenem-resistant *E. coli* and *K. pneumoniae* in a previous study (Pal & Tripathi, 2020). It was also shown to have high binding affinity based on *in silico* modelling compared to PAβN in previous study in our lab (Ohene-Agyei et al., 2014).



MBX2319 A3 Quercetin

Figure 3.2 Structures of compounds MBX2319, A3, and quercetin.

All these compounds were evaluated as potential AcrB inhibitors against antibiotic-resistant Gram-negative *E. coli*, including the ability to potentiate the activity of antibiotics and to inhibit Nile Red efflux. The off-target effects of the selected compounds, including membrane disruption, were also investigated and cytoxicity assays were conducted.

3.2 Design and Synthesis of Benzochromene Derivatives as AcrB Inhibitors for the Reversal of Bacterial Multidrug Resistance

The data presented in 3.2 is included as a manuscript published in *The European Journal of Medicinal Chemistry*. The Supplementary data to this paper is provided at Appendix 2.

Guo T*, Chen Y*, Chen W, Semple SJ, Gua X, Polyak SW, Suna G, Venter H, Ma S (2023) Design and Synthesis of Benzochromene Derivatives as AcrB Inhibitors for the Reversal of Bacterial Multidrug Resistance. *Eur J Med Chem*. 249:115148

*Joint first authors

Statement of contributions: This article resulted from a collaboration between Shandong University, China and the University of South Australia, Australia (China-Australia Centre for Health Sciences Research). Ting Guo, Department of Medicinal Chemistry, School of Pharmaceutical Sciences, Shandong University was primarily responsible for the synthesis and chemical characterisation of the synthetic compounds. Yang Chen, Clinical and Health Sciences, University of South Australia, was primarily responsible for all the biological work and analysis.

University of South Australia

Statement of Authorship

Title of Paper	Design and synthesis of benzochromene derivatives as AcrB inhibitors for the reversal of bacterial multidrug resistance
Publication Status	☑ Published ☐ Accepted for Publication ☐ Submitted for Publication ☐ Unpublished and Unsubmitted work written in manuscript style
Publication Details Relevant reference details	Ting Guo, Yang Chen, Weijin Chen, Susan J. Semple, Xiaotong Gu, Steven W. Polyak, Guanglin Sun, Henrietta Venter, Shutao Ma European Journal of Medicinal Chemistry 249 (2023) 115148

PRINCIPAL AUTHOR

Name of Principal Author (Candidate)	Yang Chen	
Contribution to the Paper Brief description of your work in this publication	Performed biological characterisations of all compounds, including antimicrobial susceptibility assays, efflux assays, bacterial membrane integrity assays and toxicity assays.	
Overall Percentage (%)	40 %	
Certification	This paper reports on original research I conducted during the period of my Higher Degree by Research candidature and is not subject to any obligations or contractual agreements with a third party that would constrain its inclusion in this thesis.	
Signature *Signatures will be redacted by the Library at the time of publication*	[redacted]	Date 02/02/2023

CO-AUTHOR CONTRIBUTIONS

By signing the Statement of Authorship, each author certifies that:

I. the candidate's stated contribution to the publication is accurate (as detailed above);

II. permission is granted for the candidate in include the publication in the thesis; and

III. the sum of all co-author contribution is equal to 100% less the candidate's stated contribution.

Name of Co-Author 1	Ting Guo	
% Contribution to the Paper	40 %	
Signature *Signatures will be redacted by the Library at the time of publication*	[redacted]	Date 02/02/2023
Name of Co-Author 2	Weijin Chen	

University of South Australia

% Contribution to the Paper	2 %	
Signature *Signatures will be redacted by the Library at the time of publication*	[redacted]	Date 02/02/2023
Name of Co-Author 3	Susan J. Semple	
% Contribution to the Paper	2 %	
Signature *Signatures will be redacted by the Library at the time of publication*	[redacted]	Date 02/02/2023
Name of Co-Author 4	Xiaotong Gu	
% Contribution to the Paper	2 %	
Signature *Signatures will be redacted by the Library at the time of publication*	[redacted]	Date 02/02/2023
Name of Co-Author 5	Steven W. Polyak	
% Contribution to the Paper	2 %	
Signature *Signatures will be redacted by the Library at the time of publication*	[redacted]	Date 02/02/2023
Name of Co-Author 6	Guanglin Sun	
% Contribution to the Paper	2 %	
Signature *Signatures will be redacted by the Library at the time of publication*	[redacted]	Date 02/02/2023
Name of Co-Author 7	Henrietta Venter	
% Contribution to the Paper	5 %	
Signature *Signatures will be redacted by the Library at the time of publication*	[redacted]	Date 02/02/2023
Name of Co-Author 8	Shutao Ma	
% Contribution to the Paper	5 %	

University of South Australia

Signature *Signatures will be redacted by the Library at the time of publication*	[redacted]	Date 02/02/2023

European Journal of Medicinal Chemistry 249 (2023) 115148

Contents lists available at ScienceDirect

European Journal of Medicinal Chemistry

journal homepage: www.elsevier.com/locate/ejmech

Research paper

Design and synthesis of benzochromene derivatives as AcrB inhibitors for the reversal of bacterial multidrug resistance

Ting Guo [a,1], Yang Chen [b,1], Weijin Chen [a], Susan J. Semple [c], Xiaotong Gu [a], Steven W. Polyak [b], Guanglin Sun [a], Henrietta Venter [b,**], Shutao Ma [a,*]

[a] Department of Medicinal Chemistry, Key Laboratory of Chemical Biology (Ministry of Education), School of Pharmaceutical Sciences, Cheeloo College of Medicine, Shandong University, 44 West Wenhua Road, Jinan, 250012, China
[b] Health and Biomedical Innovation, Clinical and Health Sciences, University of South Australia, Adelaide, SA, 5000, Australia
[c] Quality Use of Medicines and Pharmacy Research Centre, Clinical and Health Sciences, University of South Australia, Adelaide, SA, 5000, Australia

ARTICLE INFO

Handling Editor: Z Liu

Keywords:
Multidrug resistance
Efflux pump inhibitor
AcrB
Benzo[h]chromene derivatives
Antibacterial sensitizing activity
Inhibition of efflux

ABSTRACT

A series of novel benzo[h]chromene compounds were designed, synthesized and evaluated for their biological activity as AcrB inhibitors. The compounds were assessed for their ability to potentiate the effect of antibiotics. Compounds with antibiotic-potentiating effects were then evaluated for inhibition of Nile Red efflux, and for off-target effects including activity on the outer and inner bacterial membranes and toxicity. Six compounds were identified to reduce the MIC values of at least one of the tested antibiotics by at least 4-fold, and further reduced the MICs in the presence of a membrane permeabilizer. The identified compounds were also able to inhibit Nile Red efflux at concentrations between 50 μM and 200 μM. The compounds did not disrupt the bacterial outer membrane nor display toxicity in a nematode model (*Caenorhabditis elegans*). The 4-methoxyphenoxy)propoxy derivative compound **G6** possessed the most potent antibacterial potentiation with erythromycin by 8-fold even without the presence of a membrane permeabilizer. Furthermore, **H6**, **G6**, **G10** and **G11** completely abolished the Nile Red efflux at a concentration of 50 μM. The 3,4-dihydro-2*H*-benzo[h]chromen-5-yl)(morpholino)methanone core appears to be a promising chemical skeleton to be further studied in the discovery of more putative AcrB inhibitors.

1. Introduction

As one of the most important medical discoveries of the 20th century, antibiotics have revolutionized medical practice with their ability to treat infections caused by pathogenic microorganisms, saving countless lives. Their breakthrough discoveries have made important contributions to the prevention and treatment of human infection diseases [1]. However, due to the widespread use and misuse of antibiotics, the problem of bacterial resistance has become increasingly serious, especially the emergence of multidrug-resistant (MDR) bacteria, that rapidly exhaust the current human effective antibiotic library [2,3]. Therefore, there is an increasing urgency for us to establish measures against bacterial antimicrobial resistance (AMR). One way of acting against AMR is by developing 'resistance breakers' to reverse resistance and restore the activity of antibiotics [4].

One way of reversing resistance is by inhibiting drug efflux pumps. These efflux pumps protect bacteria by actively expelling secondary metabolites or toxic substances from the bacterial cell. They are a major factor in the development of intrinsic resistance to many antibiotics by Gram-negative and Gram-positive bacteria [5]. The substrate range of drug efflux pumps are not limited to antibiotics, but they can also remove dyes, disinfectants [6,7], detergents [8], heavy metals and toxic

Abbreviations: MDR, Multidrug-resistant; AMR, Bacterial antimicrobial resistance; RND, Resistance-nodulation-division; EPIs, Efflux pump inhibitors; PAβN, Phe-Arg-β-naphthylamide; SAR, Structure-activity relationship; MIC, Minimal inhibitory concentration; p.m.f, Proton motive force; ERY, Erythromycin; LEV, Levofloxacin; MIN, Minocycline; CCCP, Carbonyl cyanide m-chlorophenylhydrazone; PMBN, Polymyxin B nonapeptide; TLC, Thin-layer chromatography; ESI, Electron spray ionization.

* Corresponding author.
** Corresponding author.
E-mail addresses: rietie.venter@unisa.edu.au (H. Venter), mashutao@sdu.edu.cn (S. Ma).
[1] These authors contributed equally.

https://doi.org/10.1016/j.ejmech.2023.115148
Received 8 December 2022; Received in revised form 17 January 2023; Accepted 22 January 2023
Available online 25 January 2023
0223-5234/© 2023 Elsevier Masson SAS. All rights reserved.

organic solvents from bacterial cells [9,10]. In addition, these pumps can perform other functions that contribute to enhancing bacterial virulence and biofilm formation, making them an attractive target for inhibition [11–13].

In Gram-negative bacteria, the resistance–nodulation–division (RND) efflux pump system is the most clinically relevant [5,14,15]. One of the most widely studied multidrug efflux systems is the AcrAB-TolC pump in *Escherichia coli*, a tripartite complex that includes: AcrB, an inner membrane transporter that uses proton gradient to drive the efflux process [16,17]; TolC, which is an outer membrane poring extending from the periplasmic space and across the outer membrane [18]; and the periplasmic membrane adapter protein AcrA that links AcrB and TolC and transmit conformational changes from AcrB to TolC [16,19]. AcrB catalyzes drug/H^+ antiport and is the subunit responsible for substrate selection and binding, thus playing an essential role in the efflux mechanism [20]. Crystal structures have revealed that the structural asymmetry of the AcrB protomers adopts a "functional rotation" mechanism in which each of the three monomers constituting the inner membrane transporter cyclically assumes three conformations, referred to as loose, tight, and open (or access, binding, and extrusion, respectively) [21,22]. Only the fully assembled AcrAB-TolC system is able to extrude substrates [15].

Since so many different classes of antibiotics are affected by efflux, one strategy that has emerged to combat drug resistance is to target bacterial efflux pumps with small-molecule efflux pump inhibitors (EPIs) [23–25]. The last decade has seen a surge in the discovery of AcrB inhibitors, and the most promising and well researched AcrB EPIs reported to date are presented in Figure 1. They are the peptidomimetic Phe-Arg-β-naphthylamide (PAβN) [26], the pyridopyrimidinone D13-9001 [27], the pyranopyridine MBX2319 [28], plumbagin [29], the pyridine piperazine BDM73185 [30], representatives of the arylpiperazine NMP [31], and of the catechol derivative NDGA [29] (Fig. 1). Most of them exert their inhibition of efflux pumps by binding to two identified internal substrate (binding) pockets of AcrB protein: the proximal access pocket in the loose protomer and the distal deep binding pocket exclusively present in the tight protomer [32]. Between them, the distal binding pocket has attracted extensive attention because this is predominantly lined by weakly hydrophobic and weakly polar residues, thereby providing to create a versatile and adaptable environment with numerous so-called multifunctional sites [33].

At present, at least two classes of EPIs, pyridopyrimidines and pyranopyridines, have been shown to bind in this hydrophobic pocket (often referred to as the "hydrophobic trap") that is located within the distal substrate-binding site of AcrB [32]. The hydrophobic trap is lined with phenylalanine residues, such as Phe136, Phe178, Phe610, Phe615, Phe617 and Phe628, which can stabilize inhibitors mainly through π-stacking interactions [34]. The most successful class of compounds targeting this pocket is pyranopyridine analogs [28]. Since the disclosure of the first hit compound MBX2319, dozens of pyranopyridine derivatives have been synthesized and identified as AcrB inhibitors. The compound MBX3135 (Fig. 1) is a milestone of these inhibitors with potent synergistic antibacterial activity in combination with levofloxacin and piperacillin against *Escherichia coli* AB1157, which is about an order of magnitude lower than that of previous reported EPIs acting on the AcrAB-TolC efflux pump system [35]. Currently, this series is in the process of lead optimization, and MBX3796 (Fig. 1) and MBX4191 (Fig. 1) represent the latest lead compounds in the optimization process [36,37]. These promising compounds have been patented, but no EPIs have been clinically approved to date, mainly because of the low *in vivo* efficacy, poor pharmacokinetic properties and/or toxicity problems, which indicates that the development of effective inhibitors targeting AcrB for clinical use remains a challenge. New EPIs with novel scaffolds or biological activity would be a welcome addition in the fight against MDR bacteria.

It is well known that the hydrophobic two ring system is a privileged moiety in the design of pyranopyridines, especially for the binding in the hydrophobic pocket of AcrB [28]. The structural feature of the pyranopyridine core makes it possible to form strong hydrophobic interaction with the nearby amino-acid residues, such as Try327 and Met573. In addition, the pyranopyridine core is parallel to the benzene ring of Phe628 side chain, resulting in extensive π-π stacking interaction [34]. A cocrystal structure of MBX3135 bound to AcrB revealed the general structure of the distal hydrophobic pocket binding site of AcrB protein (Fig. 2A). Our previous results further indicated that the bicyclic 2-naphthoamide derivative **A3** (Fig. 2B) which potentiated the antibacterial activity of multiple antibiotics against multidrug resistant *Escherichia coli* (*E. coli*) expressing AcrB is an effective pharmacophore for AcrB inhibitor development [38]. The docking experiments demonstrated

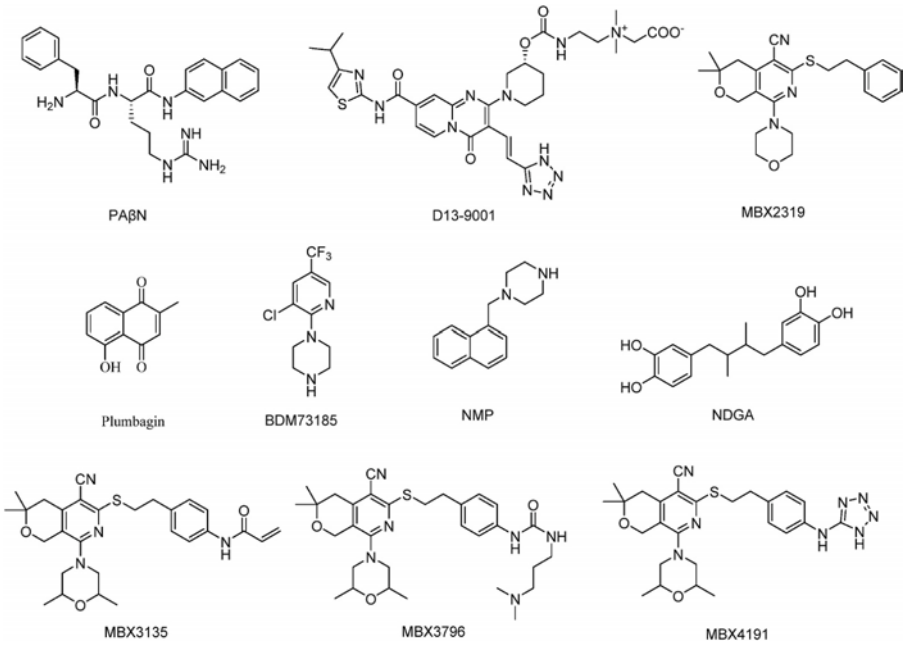


Fig. 1. Chemical structures of some representative promising AcrB inhibitors.

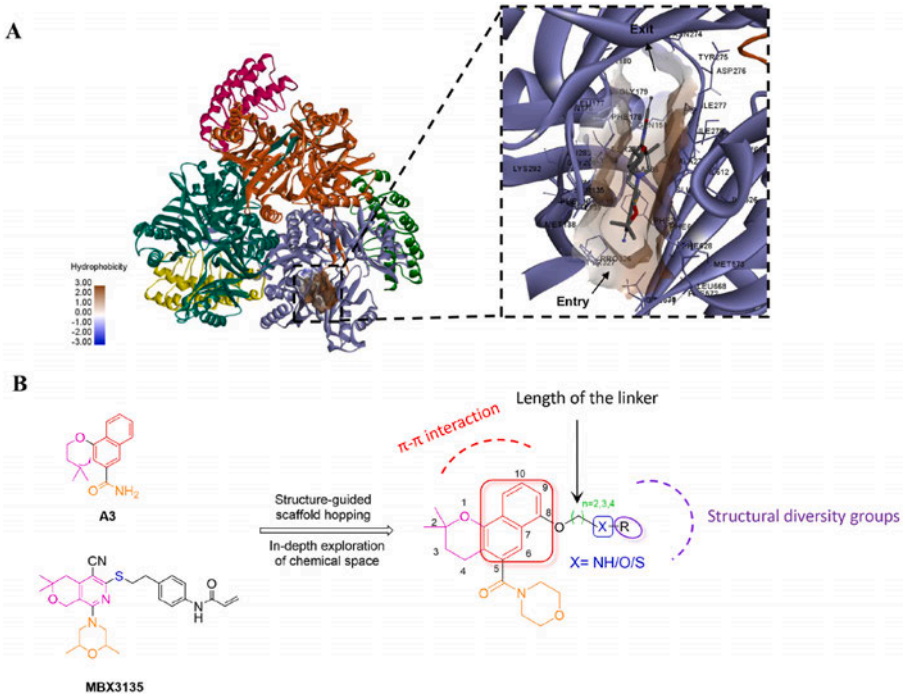


Fig. 2. Design strategy of target compounds. (A) Crystal structure of AcrB in complex with MBX3135 (PDB ID code 5ENR); (B) Schematic illustration of the structure-based design.

that the naphthalene moiety of **A3** was also accommodated in the hydrophobic pocket through a π-π stacking interaction with Phe628. In addition, 2*H*-benzo[h]chromenes (Fig. 2B), the derivatives of **A3** obtained by an integrated molecular design and scaffold hopping strategy, were reported as AcrB inhibitors with excellent reversal of bacterial multidrug resistance [39]. By further docking of this hit compound 2*H*-benzo[h]chromene core with the AcrB protein (PDB: 5ENR), we found that there is still a hydrophilic cavity filled with solvent water molecules at the exit region of the distal binding region that can accommodate additional structurally diverse groups, which provides the potential for AcrB inhibitor improvement.

Based on the above, at the C-5 position of the 2*H*-benzo[h]chromene core, we retained the polar group morpholino that could form hydrogen bonds with resident water to maintain the binding affinity for AcrB. We also tried to extend structurally diverse groups in the side chain to explore the interaction and spatial volume capacity of amino acids in the binding pocket (Fig. 2). In addition, the effect of linker length in the structure-activity relationship (SAR) study has not been systemically investigated. The connecting chains of different chain lengths can also form hydrophobic interactions with the surrounding hydrophobic amino acids to enhance the binding force of the designed small molecule ligands to the AcrB protein. In the present study, we therefore focused on the structural design and advancement at the 8-position of the 2*H*-benzo[h]chromene side chain, and the understanding of the SAR of the synergistic antimicrobial activity targeting AcrB protein. In the molecular design, three series of structurally similar compounds, H, G and Y series (Fig. 2), with different chain lengths and substituent groups at the 8-position of the 2*H*-benzo[h]chromene ring, were synthesized for comparison. The ability of these compounds to potentiate the activity of antibiotics against *E. coli*, to inhibit Nile Red efflux and to target AcrB specifically was systematically evaluated.

2. Results and discussion

2.1. Chemistry

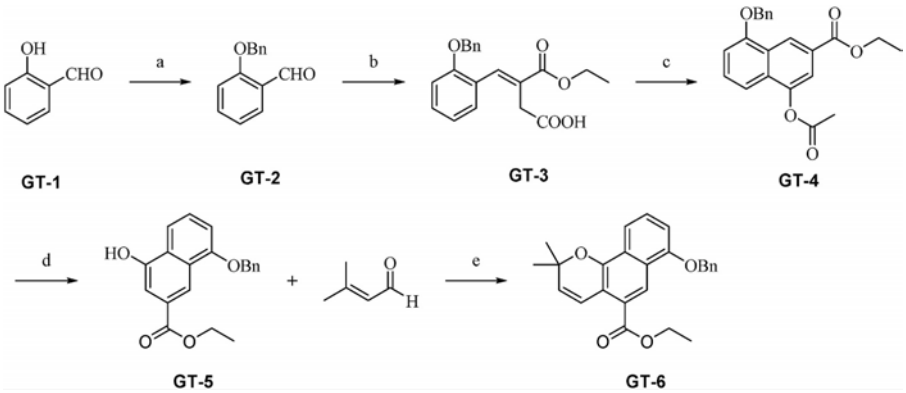
The synthetic route of 2*H*-benzo[h]chromene-5-carboxylate **GT-6** as a key intermediate for the benzo[h]chromene derivatives were described previously [39], as shown in Scheme 1. Commercially obtained ortho-hydroxybenzaldehyde **GT-1** was used as the starting material to react with benzyl bromide to obtain benzyl ether intermediate **GT-2**, and its phenolic hydroxyl group was protected. Then intermediate **GT-3** was obtained by the Stobbe condensation reaction under the action of alkali. In the presence of acetic anhydride and sodium acetate, through high temperature cyclization to obtain intermediate **GT-4**. Under alkaline conditions, **GT-4** was deacetylated to obtain phenol intermediate **GT-5**, which was then catalyzed by phenylboronic acid to react with 3-methyl-2-butenal to form a phenylboronate intermediate by coordinating with boron atom. Then the key intermediate **GT-6** was obtained through an electrocyclization reaction.

The synthetic routes of the benzo[h]chromene derivatives, encompassing the H, G and Y series, are outlined in Scheme 2. **GT-6** was hydrolyzed with NaOH to afford **GT-7**, which was condensed with morphine to obtain intermediate **GT-8**. Under the catalysis of palladium carbon, the benzyl protecting group was removed by hydrogen reduction to obtain the **GT-9**, which was then subjected to nucleophilic substitution reactions with 1,2-dibromoethane, 1,3-dibromopropane and 1,4-dibromobutane to obtain **GT-H**, **GT-G** and **GT-Y**, respectively. The obtained intermediates were subjected to substitution reactions with different nucleophiles to afford H, G and Y series compounds.

2.2. Biological evaluation

2.2.1. Antibacterial activity

The benzo[h]chromene derivatives (H, G and Y series) were evaluated *in vitro* for their antibacterial activity by determining the minimum inhibitory concentration (MIC) against the drug-resistant wild-type *E. coli* BW25113 strain and the antibiotic-sensitive strain with a deletion of the AcrB component of the AcrAB-TolC efflux pump (BW25113 ΔAcrB). This allowed the determination of the concentration of the target compounds that could be added to the tested bacterial strains without producing a direct antibacterial activity in following antimicrobial synergy assays. None of the compounds showed any antibacterial activity against wild-type *E. coli* BW25113 at 512 μg/mL or the



Scheme 1. Synthetic route for key intermediate **GT-6**. Reagents and conditions: (a) Benzyl bromide, potassium carbonate, *N*, *N*-dimethylformamide, r.t., 3 h, N_2 atmosphere; (b) Diethyl succinate, Na, ethanol, reflux, 4 h; (c) Sodium acetate, Acetic anhydride, reflux, 6 h; (d) Potassium carbonate, ethanol, reflux, 6 h; (e) Phenylboronic acid, acetic acid, toluene, reflux, 34 h, N_2 atmosphere.

BW25113 ΔAcrB mutant at 256 μg/mL (see Table S1, Supplementary Data).

2.2.2. Ability to reverse bacterial resistance and structure-activity relationship (SAR) analysis

The ability of the tested compounds to reverse antibiotic resistance conferred by the expression of the AcrAB-TolC efflux pump was then determined with standard checkerboard assays in the presence of a panel of antibiotics along with various concentrations of compounds [4,29,40]. The chosen antibiotics were erythromycin (ERY), levofloxacin (LEV), and minocycline (MIN), which are AcrB substrates [41]. The known EPI PAβN was used as a positive control to demonstrate the potentiation effect with antibiotics of a potent EPI.

Those compounds that reduced the MIC values against wide-type *E. coli* BW25113 expressing AcrB for at least one antimicrobials by 4-fold or more are shown in Table 1. Of the G and H series compounds, **H3**, **H5**, **H6**, **G6**, **G10** and **G11** showed outstanding antibacterial synergism with at least one of the antibiotics (ERY, LEV and MIN). For example, **G6** reduced the MIC value of ERY by 8-fold at 128 μg/mL while **H5** reduced it by 4-fold at a concentration as low as 8 μg/mL, and **G10** reduced the MIC value of ERY by 4-fold at 64 μg/mL while **H3** and **H6** reduced it by 4-fold at 128 μg/mL. Moreover, **G10** reduced the MIC value of MIN by 4-fold at 128 μg/mL, and **G11** reduced the MIC of LEV by 4-fold at a concentration as low as 8 μg/mL which was the minimum concentration tested.

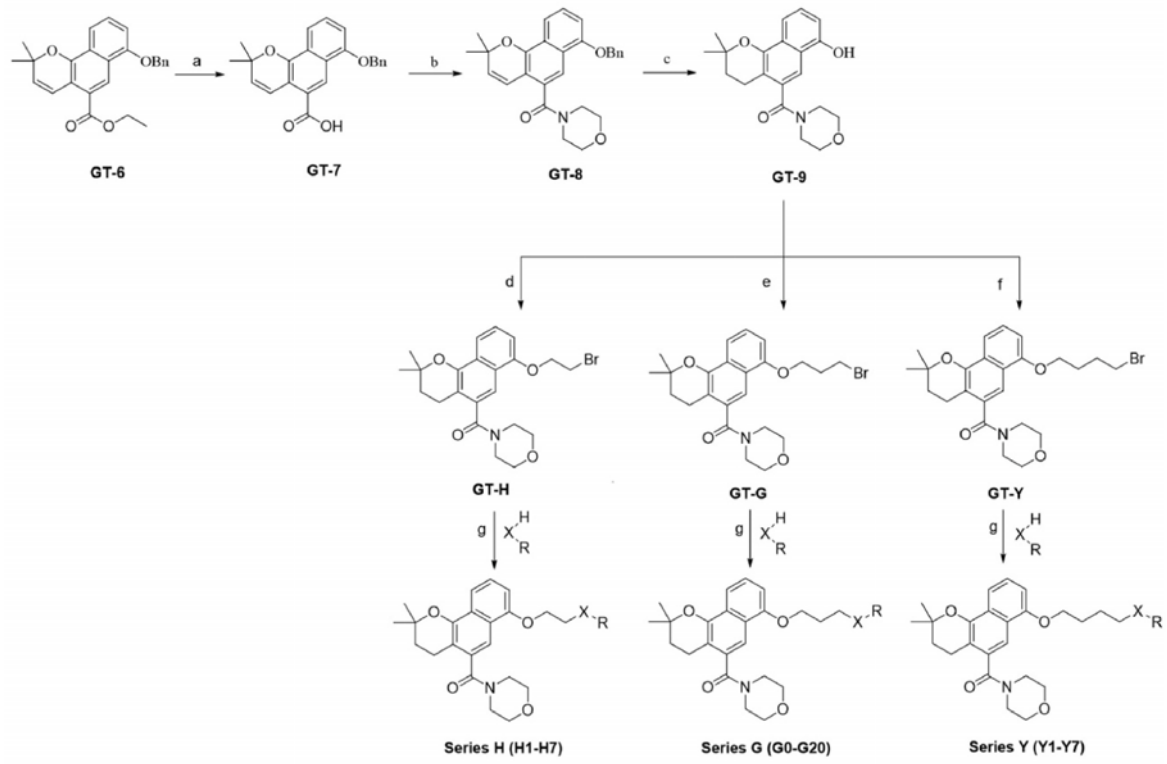
We hypothesized that a possible way to decrease the synergistic concentration of EPIs would be to co-administer them along with a membrane permeabilizing antimicrobial peptide. Colistin, otherwise known as polymyxin E, is cationic lipopeptide that bind to lipopolysaccharide and so permeabilise the outer membrane [4]. Further checkerboard assays were undertaken in the presence of colistin to permeabilise the *E. coli* outer membrane, so that antimicrobial agents could enter the cells more easily. The results in the presence of 0.5 μg/mL colistin are shown in Table 1. Some compounds showed enhanced activity at lower concentrations in the presence of colistin. Notably, compared with synergistic effect in the absence of colistin, the minimum synergistic concentration of **H6** for ERY decreased by 16-fold (from 128 to 8 μg/mL). The minimum synergistic concentration of **G10** for ERY decreased by 4-fold (from 64 to 16 μg/mL), and the MIC value of LEV was reduced by 4-fold at 64 μg/mL. The addition of colistin made **G6** show antibacterial synergism with MIN, and reduced the MIC value of MIN by 4-fold at 64 μg/mL. **H3** reduced the MIC value of ERY by 4-fold at 128 μg/mL. However, in the presence of the colistin, the minimum synergistic concentration of **H5** and **G11** for antibiotics were increased. This paradoxical effect might be due to an Eagle effect of drugs, where more drug kills less [42].

To confirm that the compounds showing antibiotic potentiating activity with the wild-type strain were acting on the efflux pump specifically, their effects on an AcrB efflux pump knockout strain of *E. coli* BW25113 (ΔAcrB) were also tested. In this assay PAβN was used as a negative control to show that a known EPI would not potentiate the effects of the antibiotics in the *E. coli* efflux pump knockout strain. As shown in Table S2, none of those compounds showed effects when this strain was used. This result suggested that the compounds exerted their antibiotic potentiating effects by the inhibition of the AcrB efflux pump.

Based on the observations of antibacterial synergism with antibiotics, the SARs could be summarized in Fig. 3. The 2*H*-benzo[h]chromene core and morpholinoyl group as the pharmacophores played a major role in antibacterial synergism. As for the influence of the linker at the 8-position of the 2*H*-benzo[h]chromene core on the synergetic activity, no significant difference was observed between these compounds with O- or S-substitution. The linker with NH-substitution between the benzo[h]chromene core and the side chain produced inactive compounds. The optimal length that connected the benzo[h]chromene core to the substituent of the side chain was two or three carbons, which was evident by comparing series Y to series H and series G. It may be due to the increase in the number of carbon atoms, which increases the distance between the substituent on the side chain and the binding site of AcrB, resulting in an inability to bind well to the binding site and loss of its activity. In addition, substituents on the side chain had a dramatic effect on the antibacterial synergism. In comparison with the benzo[h]chromeme core side chain substituted with aromatic heterocyclic or alkyl group, the introduction of substituted phenyl and phenylpiperazine could retain the synergism activity. When the number of carbon atoms between the core and the side chain of benzo[h]chromene was two (H series), the introduction of nitro group at the *para*-position of the terminal benzene ring was favorable. When the carbon atom number was three (G series), the introduction of carboxyl group at *meta*-position, methoxy and amino group at the *para*-position of the terminal benzene ring would be beneficial for synergetic effect. In short, these findings have provided new insight for further investigation of AcrB inhibitors.

2.2.3. Nile Red efflux inhibitory activity

Nile Red efflux assays were performed to assess the ability of compounds to inhibit the transport of an efflux substrate through AcrB [29,43,44]. Nile Red is a known substrate of AcrB which is weakly fluorescent in an aqueous environment but strongly fluorescent in non-polar environments, such as DNA and the cell membrane. Thus, the accumulation of Nile Red in bacterial cells followed by a reduction in fluorescence after the addition of glucose can be used to show substrate expulsion via the efflux pump from the inside of the cells to the outside [38]. *E. coli* BW25113 (DE3) ΔAcrB cells containing the pAcrB plasmid that codes for AcrB expression were used in the efflux assays with untreated bacterial cells (negative control) and cells treated with PAβN



compd.	X	R	compd.	X	R	compd.	X	R	compd.	X	R
H1	NH		G2	NH		G11	S		G20	—	
H2	O		G3	NH		G12	—		Y1	NH	
H3	O		G4	NH		G13	—		Y2	O	
H4	S		G5	NH		G14	—		Y3	O	
H5	S		G6	O		G15	—		Y4	S	
H6	—		G7	O		G16	—		Y5	S	
H7	—		G8	O		G17	—		Y6	—	
G0	NH		G9	O		G18	—				
G1	NH		G10	O		G19	—		Y7	—	

Scheme 2. Synthetic route for H, G and Y series. Reagents and conditions: (a) Sodium hydroxide, methanol, H_2O, reflux, 6 h; (b) HBTU, DIPEA, morpholine, acetonitrile, r.t., 2 h; (c) Pd/C catalyst, H_2, ethyl acetate, methanol, r.t., 12 h; (d) Potassium carbonate, 1,2-dibromoethane, acetonitrile, reflux, 12 h; (e) Potassium carbonate, 1,3-dibromopropane, acetonitrile, reflux, 12 h; (f) Potassium carbonate, 1,4-dibromoethane, acetonitrile, reflux, 12 h; (g) Potassium carbonate, *N, N*-dimethylformamide, 80 °C, 6–12 h.

100 μM (positive control).

In the efflux assay, the most potent compounds were able to completely inhibit Nile Red activity to the same level as the bacteria with (+) AcrB + PAβN 100 μM (Fig. 4). The compounds with strong inhibitory activity at the lowest concentration of 50 μM were **H6**, **G6**, **G10**, and **G11**. Besides, **H5** showed complete inhibitory activity at 100 μM, while **H3** showed partial inhibition at 100 μM and complete inhibition at 200 μM. The compounds that were able to inhibit Nile Red efflux, were further investigated for their off-target activities.

2.2.4. The effect of the compounds on the bacterial outer membrane permeability

The Gram-negative bacterial outer membrane is a permeability barrier. Hence, compounds that permeabilise the outer membrane may also synergize non-specifically with antimicrobials [45]. The nitrocefin hydrolysis assay was performed to determine if the compounds disrupted the bacterial outer membranes. Hydrolysis of nitrocefin by β-lactamase produces a coloured agent that can be measured at 486 nm. The rate of nitrocefin hydrolysis is limited by the rate of diffusion across the outer membrane, hence an increased rate of hydrolysis of nitrocefin

Table 1
The effect of benzo[*h*]chromene derivatives (series H and G) with different antimicrobial agents against the wild-type *E. coli* BW25113 (indicated as (+) AcrB) alone and in the presence of 0.5 μg/mL of the membrane permeabilizer colistin.

Compound	Concentration (μg/mL)	MIC (μg/mL)			MIC (μg/mL)		
		ERY*	LEV*	MIN*	ERY* + COL*	LEV*+ COL*	MIN*+ COL*
H3	8	64	0.032	2	8	0.032	1
	16	64	0.032	2	8	0.032	1
	32	64	0.032	2	8	0.032	1
	64	32	0.032	2	8	0.032	0.5
	128	16	0.032	2	4	0.032	0.5
H5	4	N/D	N/D	N/D	8	0.032	1
	8	16	0.016	2	8	0.032	1
	16	16	0.032	2	8	0.032	1
	32	16	0.016	2	4	0.032	0.5
	64	16	0.016	1	4	0.032	0.5
	128	16	0.016	2	N/D	N/D	N/D
H6	0.5	N/D	N/D	N/D	16	0.032	1
	1	N/D	N/D	N/D	16	0.032	0.5
	2	N/D	N/D	N/D	8	0.032	0.5
	4	N/D	N/D	N/D	8	0.032	0.5
	8	32	0.032	2	4	0.032	0.5
	16	32	0.016	2	N/D	N/D	N/D
	32	32	0.016	2	N/D	N/D	N/D
	64	32	0.016	2	N/D	N/D	N/D
	128	16	0.016	1	N/D	N/D	N/D
G6	8	32	0.032	2	16	0.016	0.5
	16	32	0.032	2	16	0.016	0.5
	32	32	0.032	2	16	0.016	0.5
	64	16	0.032	1	16	0.032	0.25
	128	8	0.032	1	8	0.032	0.25
G10	4	N/D	N/D	N/D	8	0.032	0.5
	8	32	0.016	1	8	0.016	0.5
	16	32	0.016	1	4	0.016	0.5
	32	32	0.016	1	4	0.016	0.5
	64	16	0.016	1	4	0.008	0.5
	128	16	0.016	0.5	N/D	N/D	N/D
G11	4	N/D	N/D	N/D	8	0.032	1
	8	64	0.008	2	8	0.032	1
	16	64	0.008	1	8	0.016	1
	32	64	0.008	1	8	0.016	1
	64	64	0.008	1	8	0.008	0.5
	128	64	0.008	1	N/D	N/D	N/D
PAβN (positive control)	8	16	0.016	0.5	N/D		
	16	8	0.008	0.5			
	32	4	0.008	0.5			
	64	2	0.008	0.5			
	128	2	0.001	0.25			
NONE (+) AcrB	0	64	0.032	2	16	0.032	1
NONE (−) AcrB	0	4	0.004	0.25	1	0.004	0.25

*ERY = erythromycin, LEV = levofloxacin, MIN = minocycline, COL = colistin.
Only compounds showing an effect are reported.

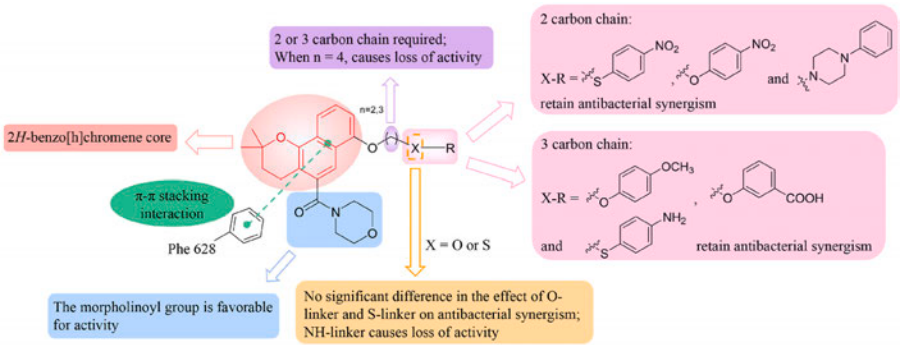


Fig. 3. Summary for SAR study of the target compounds.

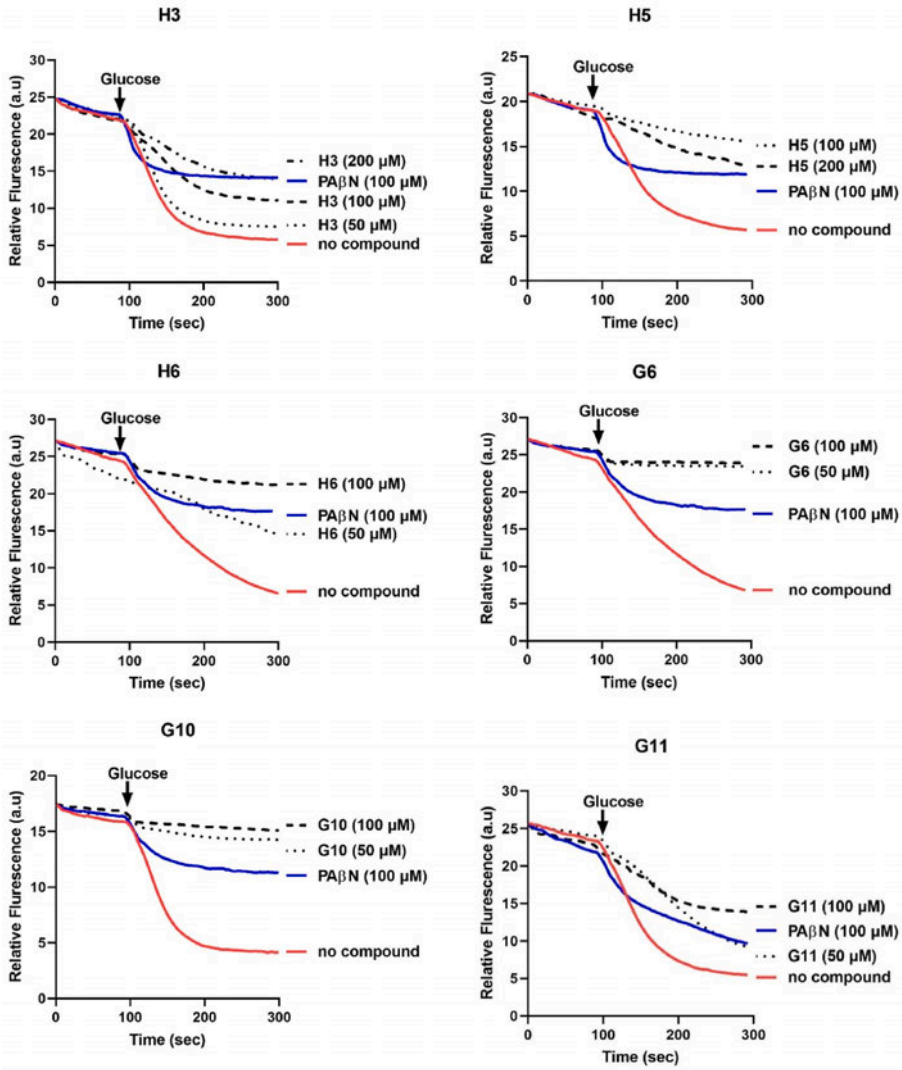


Fig. 4. Inhibition of Nile Red efflux by the compounds. *E. coli* BW25113 (DE3) ΔAcrB cells containing pAcrB plasmid (red line) as the positive control, *E. coli* BW25113 (DE3) ΔAcrB cells containing pAcrB plasmid in the presence of PAβN (100 μM) as known efflux inhibitor control (blue line), and *E. coli* BW25113 (DE3) ΔAcrB cells containing pAcrB plasmid in the presence of different concentrations (50 μM, 100 μM, and 200 μM) of the target compounds (dotted lines) were preloaded with Nile Red before the start of fluorescence measurements. Efflux was triggered at 100 s by adding 0.2% glucose (indicated by the arrow). Representative fluorescent curves are shown for experiments with different batches of cells performed on three different days.

would be indicative of outer membrane permeabilization [29]. When cells were treated with the known membrane disruptor polymyxin B nonapeptide a rapid hydrolysis was observed as expected. In the presence of 128 μg/mL of each of the compounds the, nitrocefin hydrolysis was the same as for untreated cells (Fig. S1). The results suggested that none of the target compounds permeabilised the bacterial outer membrane (Fig. S1).

2.2.5. *The effect of the compounds on the bacterial inner membrane permeability*

RND-type efflux pumps are driven by the proton motive force (p.m.f) to transport substrates across the bacterial inner membrane [46]. The efflux pumps are inactive when the p.m.f is disrupted which can occur if the inner membrane is damaged. Hence the integrity of bacterial inner membranes can be measured by a change of the membrane potential part of the p.m.f using the potentiometric dye $DiOC_2(3)$. This dye shows an increase in fluorescence when the p.m.f is generated by the addition of glucose that can be abolished by the ionophore carbonyl cyanide m-chlorophenylhydrazone (CCCP). If a compound disrupts the inner membrane, thereby stopping the cells from establishing a p.m.f, the fluorescence of $DiOC_2(3)$ will decrease. In this assay, compounds **H3**, **H5**, **H6**, **G6** and **G11** were shown to not disrupt the bacterial inner membrane (Fig. 5). However, **G10** displayed an off-target effect on the bacterial inner membrane so that hardly any membrane potential was established as can been seen from the lack of effect of the membrane disruptor ionophore CCCP.

2.2.6. *Hemolysis assay*

The hemolytic activity of **H3**, **H5**, **H6**, **G6**, **G10** and **G11** at 4, 8, 16, 32, 64, 128 and 256 μg/mL was determined and presented in Fig. 6. The nonionic surfactant, Triton X-100, was used as the positive control [47, 48]. The ability of promising compounds to lyse mice red blood cells was used to evaluate their toxicity toward mammalian cells and the hemolysis rate of Triton X-100 was set as 100%. The measurement results showed that the hemolysis rates of **H3**. **H5**, **H6**, **G6**, **G10** and **G11** were less than 5% hemolysis rate in the concentration range we set (4–256 μg/mL). Therefore, within the concentration range where the target compounds exerted their synergistic effect, it was considered that it does not cause hemolysis of mice red blood cells.

2.2.7. *In vivo toxicity of the compounds against Caenorhabditis elegans*

The toxicity of the compounds was also investigated through a *Caenorhabditis elegans* nematode model [49,50]. Compounds were tested at 128 μg/mL. Nematodes were observed visually using a light microscope to determine the number of living or dead nematodes every 24 h for up to 72 h. The untreated control and ampicillin-treated control indicated approximately 99% survival rate throughout the 72 h period. Nematodes treated with the compounds showed above 90% survival

72

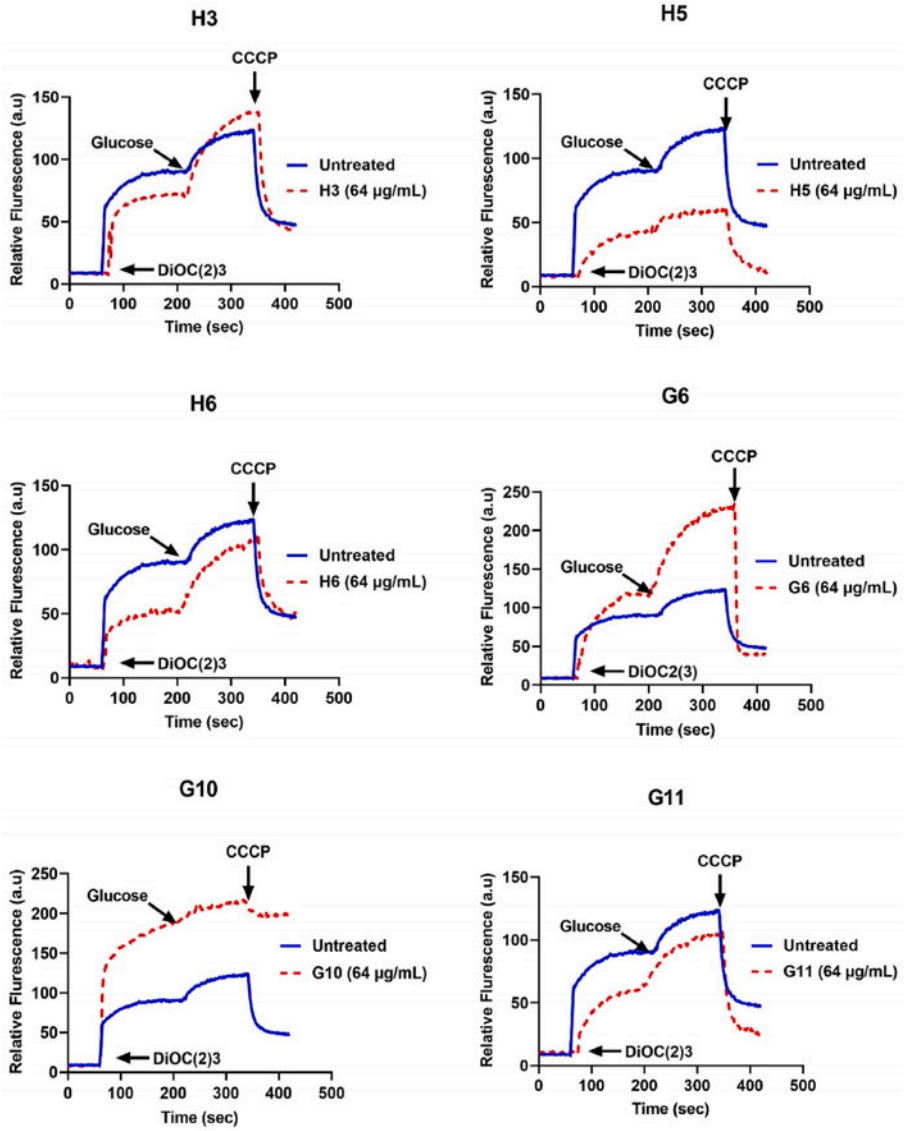


Fig. 5. Effect of the compounds on inner membrane permeabilization. A suspension of *E. coli* BW25113 bacterial suspensions were either left untreated (solid blue line) or exposed to 64 μg/mL compounds (broken red line) for 10 min after which the potentiometric probe, $DiOC_2(3)$ was added, and the fluorescence was monitored until it plateaued. Cells were then re-energized with 0.5% glucose and the establishment of membrane potential (inside negative) was measured as an increase in fluorescence until it plateaued. The membrane potential was then disrupted by the addition of the proton ionophore CCCP, which was observed as a sharp drop in fluorescence intensity. Representative trends are shown from experiments performed on different days.

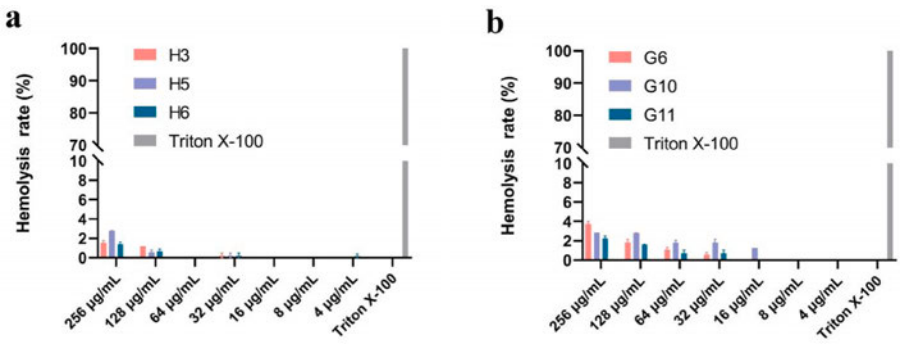


Fig. 6. The hemolysis rate of mice red blood cell induced by (a) **G6**, **G10**, **G11** and (b) **H3**, **H5**, **H6** at different concentrations. 2% Triton X-100 was used as positive control. Values are presented as the mean ± SD; n = 3.

rates across 72 h. A slight reduction in nematode viability compared to the no treatment control was observed for **H5**, **G10** and **G11** at 72 h, however no statistically significant difference was observed between the nematodes treated with the low-toxicity antibiotic ampicillin and these three compounds at 72 h (Fig. 7). This result suggested that the compounds displayed no significant toxicity in *C. elegans*. Notably, compound **G10** which showed bacterial inner membrane disruption (Section 2.2.5) did not cause significant toxicity in the *C. elegans* model.

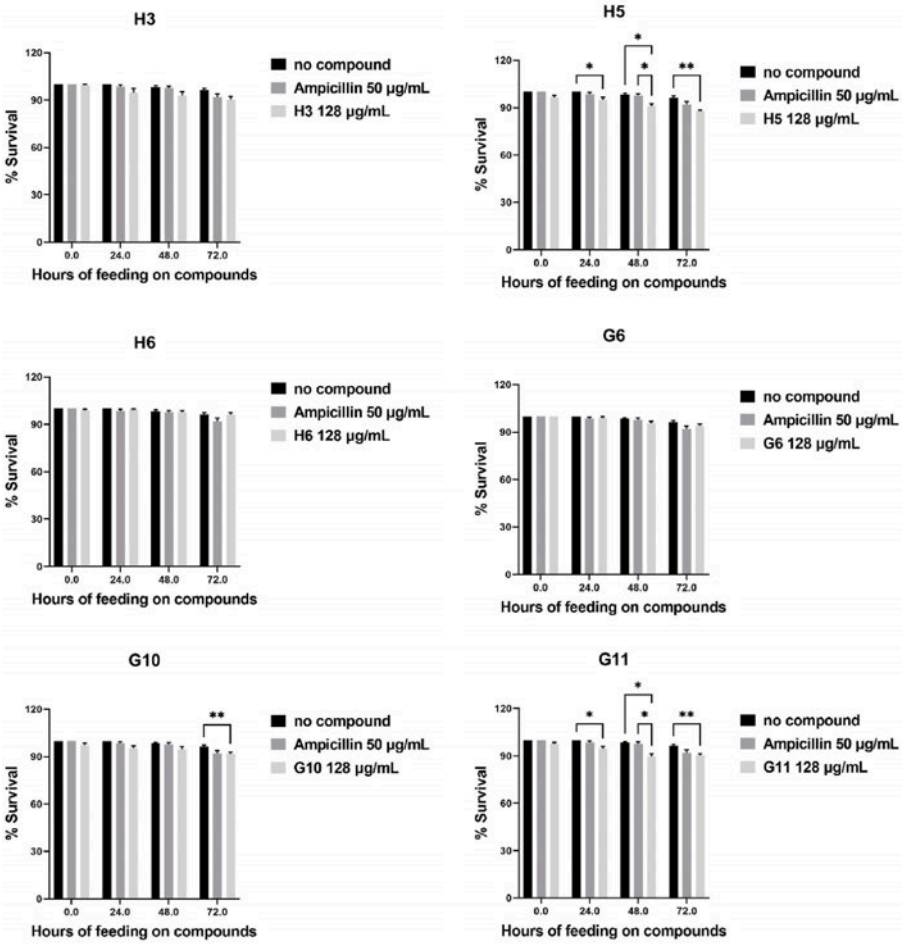


Fig. 7. Effect of the compounds on the survival of *C. elegans* nematodes. Synchronized adult *C. elegans* nematodes were harvested and investigated for toxicity in the presence of 128 μg/mL H and G compounds for 72 h. The nematodes were then counted under a light microscope at 400 × magnification every 24 h up to 72 h. The results are presented in mean percentage of survival ± SEM. Statistical analysis was performed using two-way ANOVA and the asterisks (*) represent statistical significance, and (ns) represents no significance.

2.3. In silico modeling and prediction of G6-AcrB and G10-AcrB binding modes

In addition to the studies of biological activities, we used a reported crystal structure of AcrB (PDB code: 5ENR) for a computational study. **G6** and **G10** both entered the distal hydrophobic pocket (hydrophobic trap) of AcrB and had extensive hydrophobic interaction with the surrounding key amino acid residues Gly136, Val571, Phe628, Val139, Try327, Phe136, Phe178, Val612, Ala279, Phe610, Ile277, Gly179, Phe615 and Ser287.

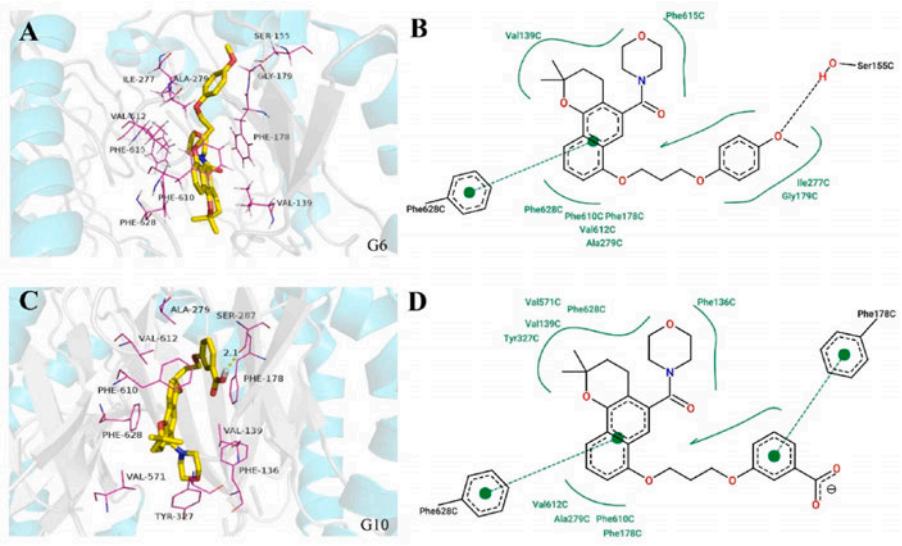


Fig. 8. Binding modes of AcrB (PDB ID code 5ENR). (A) Predicted binding mode of **G6** within active pocket; (B) Predicted interactions between **G6** and amino acids of AcrB; (C) Predicted binding mode of **G10** within active pocket; (D) Predicted interactions between **G10** and amino acids of AcrB.

74

In order to explore the reasons for the significant antibacterial and sensitizing effects of target compounds **G6** and **G10**, we compared and analyzed the docking results of compounds **G6** and **G10** with AcrB protein, respectively, as shown in Fig. 8. The results showed that compound **G6** could interact with Val139, Phe615, Phe628, Phe610, Phe178, Val612, Ala279, Ile277 and Gly279 to form a hydrophobic interaction. The aromatic ring on the benzo[h]chromene core structure formed a π-π stacking interaction with the key amino acid residue Phe628, and the oxygen atom on the methoxy group at the para position of the benzene ring of the outer chain could act as a hydrogen bond acceptor to form a hydrogen bond force with the Ser155 residue at a distance of 1.9 Å. Compound **G10** could form hydrophobic interactions with Val571, Phe628, Val139, Try327, Phe136, Val612, Ala279, Phe610, and Phe178. Similar to compound **G6**, the aromatic ring on the core structure forms π-π stacking interactions with key amino acid residues Phe628 and Phe178, and the carboxyl group on the side chain benzene ring could generate hydrogen bond with Ser287 at a distance of 2.1 Å (the hydrogen bond interaction was not shown in its 2D prediction mode map). The above analysis was consistent with our design idea that the π-π stacking or hydrophobic interaction of Phe628 and Phe178 with the target compound was one of the most important factors for the tight binding of AcrB protein to small molecules. In addition, the benzene ring of the side chain of the benzo[h]chromene core in the **G6** and **G10** structures all extended toward the exit of the binding pocket, and the substituents on the benzene ring could also serve as hydrogen bond donors and acceptors to form an additional hydrogen bond interactions with polar amino acids Ser155 and Ser287, which made the binding to AcrB protein more stable. We speculated that the emergence of this stronger hydrogen-bonding force led to a significant improvement in the drug resistance reversal activity of these two target compounds.

3. Conclusion

Based on the docking studies of the lead compound, thirty-five novel benzo[h]chromene derivatives were rationally designed, synthesized and evaluated for their EPI activity and toxicity. Among them, six compounds (**H3**, **H5**, **H6**, **G6**, **G10** and **G11**) from the H and G series were able to reduce the MIC value of at least one tested antibacterial by 4-fold at sub-MIC concentrations (8–128 μg/mL). The addition of a sub-inhibitory concentration (0.5 μg/mL) of colistin improved the activity of some of the compounds. For example, in the presence of colistin, the minimum synergistic concentration of **H6** for erythromycin decreased by 16-fold (from 128 to 8 μg/mL). This indicated that the benzo[h] chromene derivatives compounds could not easily penetrate the outer membrane of *E. coli*. Subsequently, six compounds with synergetic activity were selected to further assess their ability to inhibit Nile Red efflux and the results revealed that they could completely inhibit Nile red efflux at 50–200 μM. The experimental results on the stability of the inner and outer membrane showed that the compounds with antibacterial sensitizing activity and Nile Red efflux inhibitory activity, had no effect on the permeability of outer membrane and the proton gradient of inner membrane of *E. coli* except for compound **G10** which displayed inner membrane disruption. A low hemolysis rate for all six tested compounds in mouse erythrocytes and low toxicity in a *C. elegans* nematode toxicity model were also demonstrated. Thus, compounds **H3**, **H5**, **H6**, **G6** and **G11** are ideal AcrB inhibitors. Further, in *silico* docking result revealed specific binding mode of compounds. These findings may help in projecting structural analogs with potent EPI activity.

The design of novel EPIs against Gram-negative bacteria is still a great challenge. Many EPIs were discovered earlier, but so far none of them has been used clinically due to the their off-target effect contributing to superfluous toxicity. Disruption and depolarization of the bacterial cell membrane may cause efflux inhibition through a nonspecific effect, leading to the common identification of false-positive EPIs [51]. For instance, PAβN, a well-known EPI, has high specificity for bacterial efflux pump. However, the effect of PAβN is non-specific due to its penetration of the outer membrane of Gram-negative bacteria [52]. Unfortunately, the clinical development of this molecule has been abandoned due to nephrotoxicity [53]. Besides, NMP has been known to reverse the multidrug resistance of *E. coli* overexpressing RND-type efflux pump [31] Nevertheless, this compound is structurally similar to the phenylpiperidine-based SSRI class of antidepressants, it is also likely to be too toxic for use in mammals [54]. In our study, except for **G10**, none of the EPIs at least at test concentration, disturb the membrane function. In addition, with no obvious toxicity in the preliminary *in vitro* model experiments, the EPI discovered in this study seems to have more favorable characteristics than previous ones, suggesting the promising role of the benzo[h]chromene derivatives as adjuvants. Conclusively, the synergism displayed by the benzo[h]chromene derivatives indicates the specificity and true EPI-likeness of the drugs, rather than an outcome of any off-target effects. Nonetheless, these compounds require thorough investigations regarding its pharmacokinetics and pharmacodynamics, although more efforts toward structure–activity relationship study are needed to design suitable candidate drugs. In a word, these new benzo[h]chromene AcrB inhibitors lay a foundation for the research and development of new AcrB inhibitors to reverse bacterial multidrug resistance.

4. Experimental section

4.1. General experimental protocol

All chemicals and reagents were commercially available with no further purification unless otherwise stated. All reactions were monitored by analytical thin-layer chromatography (TLC) using 0.25 mm silica GF254 plates. They were visualized under 254 nm or 365 nm UV light. Chromatographic purifications were carried out using silica gel (200–300 mesh) with gradient elution. ^{1}H NMR and ^{13}C NMR spectra were recorded at 400 MHz or 600 MHz on Bruker Avance, and ^{13}C NMR spectra were recorded at 101 MHz or 151 MHz on Bruker Avance. The following abbreviations are used to denote peak patterns in NMR spectra: singlet (s), doublet (d), triplet (t), quarter (q), multiplet (m), as well as doublet of doublets (dd). All chemical shifts were reported as parts per million (ppm) in the unit relative to the resonance of $CDCl_3$, and DMSO-d_6. Mass and high-resolution mass spectra were obtained on API 4000 and Agilent Q-TOF 6510 by electron spray ionization (ESI) mode. The purity of all target compounds was over 95% as analyzed with an Agilent 1200 Series HPLC system (Agilent, Santa Clara County, USA) equipped with Diamonsil C_{18} column (150 × 4.6 mm, 5 μm) at UV detection of 254 nm. Injection volume is 5 μL, and it was maintained at ambient temperature. The effective chromatogram was obtained using the mobile phase of acetonitrile-water or acetonitrile-0.025 mol/L potassium dihydrogen phosphate buffer and pH value was adjusted to 3 with phosphoric acid at the flow rate of 1.0 mL/min. Melting points were determined by RY-1 melting point apparatus without correction. ^{1}H NMR and ^{13}C NMR spectra of all compounds and their intermediates as well as the HPLC spectra of representative compounds can be referenced in the Supplementary Data.

4.2. Typical procedure for the synthesis of the key intermediate *GT-6*

4.2.1. 2-(Benzyloxy)benzaldehyde *(GT-2)*

The starting material ortho-hydroxybenzaldehyde **GT-1** (5.00 g, 40.97 mmol) was diluted in *N*, *N*-dimethylformamide, to which was added benzyl bromide (7.70 g, 45.30 mmol) and potassium carbonate (11.30 g, 81.76 mmol). The reaction mixture was degassed and protected with dry nitrogen gas. After the reaction solution turned yellow, and the yellow mixture was stirred at room temperature for 3 h. After TLC detection to ensure the complete reaction, the reaction solution was extracted with ethyl acetate/water/saturated salt water. The aqueous phase was removed by liquid separation operation. The combined extracts were washed with water (50 mL × 3) and brine (50 mL). The

organic layer was dried over anhydrous sodium sulfate, filtered and concentrated under reduced pressure to obtain a colorless liquid. The residue was purified via silica gel column chromatography to afford **GT-2** as off-white solid (6.76 g, 77.8%). **GT-2**: ^{1}H NMR (600 MHz, Chloroform-*d*) δ 10.57 (s, 1H), 7.86 (dd, *J* 7.8, 1.8 Hz, 1H), 7.56–7.51 (m, 1H), 7.46–7.39 (m, 4H), 7.38–7.33 (m, 1H), 7.05 (t, *J* 8.4 Hz, 2H), 5.20 (s, 2H). MS (ESI) *m/z* calculated for $C_{14}H_{12}O_2$ $[M + Na]^+$, 235.1, found: 235.3.

4.2.2. (E)-4-(2-(Benzyloxy)phenyl)-3-(ethoxycarbonyl)but-3-enoic acid (GT-3)

Sodium (2.25 g, 98.00 mmol) was dissolved in anhydrous ethanol solution (100 mL), and heated under reflux for 1 h to completely convert it into sodium ethoxide solution. After adding the diethyl succinate (13.87 g, 79.62 mmol) to the reaction solution, the ethanol solution (50 mL) of intermediate **GT-2** (13.00 g, 61.25 mmol) was added dropwise, and the resultant mixture solution was refluxed for 6 h. After the reaction finished, the resulting solution was decompressed to evaporate the solvent. Water (300 mL) was added and then acidified with concentrated hydrochloric acid to pH $<$ 2. The acidified solution was then was extracted with ethyl acetate (100 mL $\times$ 3), and the organic phase was washed three times with saturated brine solution. The organic layer was dried and evaporated under reduced pressure to obtain intermediate **GT-3** as brown oil (14.42 g, 68.8%). The product can be used directly for the next step without purification. **GT-3**: ^{1}H NMR (600 MHz, Chloroform-*d*) δ 8.13 (s, 1H), 7.41 (d, *J* 7.2 Hz, 2H), 7.37 (t, *J* 7.8 Hz, 3H), 7.34–7.29 (m, 4H), 5.13 (s, 2H), 4.29 (q, *J* 7.2 Hz, 2H), 3.49 (s, 2H), 1.34 (t, *J* 7.2 Hz, 3H). MS (ESI) *m/z* calculated for $C_{20}H_{20}O_5$ [M H]$^-$, 339.12, found: 339.48.

4.2.3. Ethyl 4-acetoxy-8-(benzyloxy)-2-naphthoate (GT-4)

The above product **GT-3** (15.00 g, 44.10 mmol) and sodium acetate (3.62 g, 44.10 mmol) were dissolved in acetic anhydride (90.04 g, 882.00 mmol) and reacted under reflux for 6 h. After monitoring the completion of the reaction by TLC, the reaction solvent was concentrated under reduced pressure. Then water (300 mL) was added and followed by extraction with ethyl acetate (100 mL $\times$ 3), washed three times with saturated sodium bicarbonate solution and saturated brine in turn. The combined organic layers were dried on anhydrous magnesium sulfate. The organic phase was concentrated and purified via silica gel column chromatography using petroleum ether-ethyl acetate (8:1) to afford intermediate **GT-4** as yellow solid (12.04 g, 75%). **GT-4**: ^{1}H NMR (400 MHz, Chloroform-*d*) δ 9.02 (s, 1H), 7.85 (d, *J* 1.6 Hz, 1H), 7.51 (t, *J* 6.8 Hz, 3H), 7.46–7.39 (m, 3H), 7.36 (t, *J* 7.2 Hz, 1H), 6.94 (d, *J* 7.6 Hz, 1H), 5.31 (s, 2H), 4.43 (q, *J* 7.2 Hz, 2H), 2.47 (s, 3H), 1.43 (t, *J* 7.2 Hz, 3H). MS (ESI) *m/z* calculated for $C_{22}H_{20}O_5$ $[M + H]^+$, 365.1, found: 365.4.

4.2.4. Ethyl 8-(benzyloxy)-4-hydroxy-2-naphthoate (GT-5)

To a solution of **GT-4** (10.00 g, 27.46 mmol) in ethanol (150 mL), potassium carbonate (5.70 g, 41.19 mmol) was added to it. The mixture was heated and refluxed for 6 h until the reactant was completely dissolved. The reaction solvent was evaporated under reduced pressure, water (200 mL) was added, and the pH was adjusted to 6 with hydrochloric acid. After white solid were precipitated from the reaction system, the resulting mixture was stirred under an ice bath for 1 h. The white solid was filtered, and dried to obtain a crude product. The crude product was purified by silica gel column chromatography using petroleum ether-ethyl acetate (10:1) to afford intermediate **GT-5** as a white solid (7.07 g, 79.9%). **GT-5**: ^{1}H NMR (600 MHz, Chloroform-*d*) δ 8.70 (s, 1H), 7.79 (d, *J* 8.4 Hz, 1H), 7.55–7.50 (m, 3H), 7.48–7.45 (m, 1H), 7.42 (t, *J* 7.2 Hz, 2H), 7.35 (t, *J* 7.2 Hz, 1H), 6.94 (d, *J* 7.8 Hz, 1H), 5.91 (s, 1H), 5.30 (s, 2H), 4.43 (q, *J* 7.2 Hz, 2H), 1.43 (t, *J* 7.2 Hz, 3H). MS (ESI) *m/z* calculated for $C_{20}H_{18}O_4$ [M H]$^-$, 321.1, found: 321.2.

4.2.5. Ethyl 7-(benzyloxy)-2,2-dimethyl-2H-benzo[h]chromene-5-carboxylate (GT-6)

Intermediate **GT-5** (5.00 g, 15.52 mmol) was dissolved in dry toluene (120 mL), and 3-methyl-2-butenal (1.57 g, 18.62 mmol), $PhB(OH)_2$ (2.08 g, 17.07 mmol) were added. The mixture was degassed and protected with dry nitrogen gas, and was heated and refluxed using Dean-Stark trap for 34 h. After the reaction solution was cooled to room temperature, the excess reaction solvent was concentrated under reduced pressure. Then water (200 mL) was added, and the reaction mixture was diluted with ethyl acetate (3 $\times$ 50 mL). The organic layer was washed with saturated sodium bicarbonate solution and saturated brine (3 $\times$ 30 mL), dried over anhydrous magnesium sulfate and then concentrated under reduced pressure. The residue was purified via silica gel column chromatography using petroleum ether-ethyl acetate (100:1) to afford intermediate **GT-6** as yellow solid (3.82 g, 63.3%). **GT-6**: ^{1}H NMR (600 MHz, Chloroform-*d*) δ 8.54 (s, 1H), 7.80 (d, *J* 8.4 Hz, 1H), 7.52 (d, *J* 7.2 Hz, 2H), 7.44–7.38 (m, 3H), 7.35 (t, *J* 7.2 Hz, 1H), 7.32 (d, *J* 10.2 Hz, 1H), 6.87 (d, *J* 7.8 Hz, 1H), 5.74 (d, *J* 9.6 Hz, 1H), 5.28 (s, 2H), 4.41 (q, *J* 7.2 Hz, 2H), 1.52 (s, 6H), 1.43 (t, *J* 7.2 Hz, 3H). MS (ESI) *m/z* calculated for $C_{25}H_{24}O_4$ $[M + H]^+$, 389.18, found: 389.08.

4.3. Typical procedure for the synthesis of the benzo[h]chromene derivatives (H G and Y series)

4.3.1. 7-(Benzyloxy)-2,2-dimethyl-2H-benzo[h]chromene-5-carboxylic acid (GT-7)

To a solution of **GT-6** (4.00 g, 10.30 mmol) in mixed solution (methanol:water 1:1, 50 mL), sodium hydroxide (2.06 g, 51.50 mmol) was added and stirred at 70 °C for 6 h. After the reaction was completed, the methanol was removed under reduced pressure. The resultant mixture was acidified with concentrated hydrochloric acid to adjust the reaction system to pH 6. The resultant precipitate was collected, washed twice with water and dried to obtain **GT-7** as yellow solid (3.15 g, 84.9%). **GT-7**: ^{1}H NMR (600 MHz, Chloroform-*d*) δ 7.76 (d, *J* 8.4 Hz, 1H), 7.61 (s, 1H), 7.32 (t, *J* 7.8 Hz, 1H), 6.78 (d, *J* 7.8 Hz, 1H), 4.15 (t, *J* 6.6 Hz, 2H), 3.90–3.74 (m, 5H), 3.56 (d, *J* 31.8 Hz, 2H), 3.30 (d, *J* 47.4 Hz, 2H), 2.97 (t, *J* 7.2 Hz, 2H), 2.82 (s, 1H), 2.58 (s, 1H), 2.21–2.15 (m, 1H), 2.14–2.06 (m, 2H), 1.88 (d, *J* 6.6 Hz, 2H), 1.40 (s, 6H), 0.49–0.39 (m, 4H). MS (ESI) *m/z* calculated for $C_{23}H_{20}O_4$ [M H]$^-$, 359.13, found: 359.11.

4.3.2. 7-(Benzyloxy)-2,2-dimethyl-2H-benzo[h]chromene-5-yl)(morpholinyl)methanone (GT-8)

To a stirred suspension of **GT-7** (3.50 g, 9.72 mmol) in acetonitrile (50 mL) was added HBTU (3.69 g, 9.72 mmol). The mixture was stirred at room temperature for 0.5 h and then morpholine (0.85 g, 9.72 mmol) and *N, N*-diisopropylethylamine (2.51 g, 19.44 mmol) were added. After the mixture was stirred at room temperature for another 2 h, the reaction solvent was evaporated under reduced pressure. Then water (50 mL) and ethyl acetate were added to the residue and the aqueous phase was separated. The organic layer was washed with saturated brine, dried over anhydrous sodium sulfate and then concentrated under reduced pressure. The residue was purified via silica gel column chromatography using dichloromethane-methanol to afford intermediate **GT-8** as yellow solid (3.08 g, 73.9%). **GT-8**: ^{1}H NMR (600 MHz, Chloroform-*d*) δ 7.81–7.75 (m, 2H), 7.49 (d, *J* 7.2 Hz, 2H), 7.42 (t, *J* 7.2 Hz, 2H), 7.39–7.34 (m, 2H), 6.89 (d, *J* 7.2 Hz, 1H), 6.44 (d, *J* 10.2 Hz, 1H), 5.71 (d, *J* 10.2 Hz, 1H), 5.22 (s, 2H), 3.78–3.88 (m, 4H), 3.56 (s, 2H), 3.29 (s, 2H), 1.52 (s, 6H). MS (ESI) *m/z* calculated for $C_{27}H_{27}NO_4$ $[M + H]^+$, 430.20, found: 430.17.

4.3.3. 7-Hydroxy-2,2-dimethyl-3,4-dihydro-2H-benzo[h]chromene-5-yl)(morpholinyl)methanone (GT-9)

To a solution of **GT-8** (2.50 g, 5.82 mmol) in mixed solution (methanol:ethyl acetate 1:1, 50 mL) was added a catalytic amount of

Pd/C under an atmosphere of hydrogen. The mixture was stirred overnight. The resulting solution was filtered with Celite to remove palladium carbon and washed with dichloromethane-methanol (1:1) solution. All the filtrate was concentrated under reduced pressure to give **GT-9** as off-white solid (1.67 g, 83.9%), which was used for the next step without further purification. **GT-9**: ^{1}H NMR (600 MHz, Chloroform-*d*) δ 7.70 (d, *J* 8.4 Hz, 1H), 7.55 (s, 1H), 7.24–7.19 (m, 1H), 6.75 (d, *J* 7.2 Hz, 1H), 6.44 (s, 1H), 3.90 (s, 1H), 3.84–3.76 (m, 3H), 3.57 (d, *J* 32.4 Hz, 2H), 3.32 (d, *J* 45.6 Hz, 2H), 2.99 (s, 1H), 2.57 (s, 1H), 1.88 (q, *J* 7.2 Hz, 2H), 1.40 (s, 6H). MS (ESI) *m/z* calculated for $C_{20}H_{23}NO_4$ $[M + H]^+$, 342.17, found: 342.17.

*4.3.4. (7-(2-Bromoethoxy)-2,2-dimethyl-3,4-dihydro-2H-benzo[h] chromene-5-yl)(morpholinyl)methanone (**GT-H**)*

To a solution of **GT-9** (0.80 g, 2.34 mmol) in acetonitrile (40 mL), potassium carbonate (0.97 g, 7.02 mmol) and 1,2-dibromoethane (1.76 g, 9.36 mmol) was added. The mixture was refluxed for 10 h. After the reaction came to end, the reaction solution was concentrated under reduced pressure and the residue was purified via silica gel column chromatography using dichloromethane-methanol to afford intermediate **GT-H** as white solid (0.87 g, 83%). **GT-H**: ^{1}H NMR (600 MHz, Chloroform-*d*) δ 7.82 (d, *J* 8.4 Hz, 1H), 7.67 (s, 1H), 7.38–7.32 (m, 1H), 6.80 (d, *J* 7.8 Hz, 1H), 4.44 (d, *J* 25.2 Hz, 2H), 3.94 (s, 1H), 3.83–3.74 (m, 5H), 3.59 (d, *J* 35.4 Hz, 2H), 3.33 (d, *J* 63.0 Hz, 2H), 3.02 (s, 1H), 2.60 (s, 1H), 1.90 (s, 2H), 1.42 (s, 6H). MS (ESI) *m/z* calculated for $C_{22}H_{26}BrNO_4$ $[M + H]^+$, 448.11, found: 448.27.

*4.3.5. (7-(3-Bromopropoxy)-2,2-dimethyl-3,4-dihydro-2H-benzo[h] chromene-5-yl)(morpholinyl)methanone (**GT-G**)*

The synthetic procedures of intermediates **GT-G** were similar to those of **GT-H**. **GT-G**: white solid, yield 85.7%, ^{1}H NMR (600 MHz, Chloroform-*d*) δ 7.79 (d, *J* 9.0 Hz, 1H), 7.59 (s, 1H), 7.39–7.34 (m, 1H), 6.84 (d, *J* 7.8 Hz, 1H), 4.26 (t, *J* 6.0 Hz, 2H), 3.90 (s, 1H), 3.83 (d, *J* 15.0 Hz, 3H), 3.67 (d, *J* 9.0 Hz, 2H), 3.58 (d, *J* 22.2 Hz, 2H), 3.34 (s, 1H), 3.28 (s, 1H), 3.00 (s, 1H), 2.61 (s, 1H), 2.48–2.40 (m, 2H), 1.90 (q, *J* 7.2 Hz, 2H), 1.42 (s, 6H). MS (ESI) *m/z* calculated for $C_{23}H_{28}BrNO_4$ $[M + H]^+$, 462.13, found: 462.05.

*4.3.6. (7-(4-Bromoethoxy)-2,2-dimethyl-3,4-dihydro-2H-benzo[h] chromene-5-yl)(morpholinyl)methanone (**GT-Y**)*

The synthetic procedures of intermediates **GT-Y** were similar to those of **GT-H**. **GT-Y**: white solid, yield 67.4%, ^{1}H NMR (600 MHz, Chloroform-*d*) δ 7.78 (d, *J* 8.4 Hz, 1H), 7.62 (s, 1H), 7.38–7.32 (m, 1H), 6.79 (d, *J* 7.8 Hz, 1H), 4.15 (t, *J* 6.0 Hz, 2H), 3.92 (s, 1H), 3.81 (s, 3H), 3.61 (s, 1H), 3.56–3.50 (m, 3H), 3.32 (d, *J* 52.2 Hz, 2H), 3.01 (s, 1H), 2.61 (s, 1H), 2.17–2.11 (m, 2H), 2.10–2.05 (m, 2H), 1.93–1.86 (m, 2H), 1.42 (s, 6H). MS (ESI) *m/z* calculated for $C_{24}H_{30}BrNO_4$ $[2\ M + Na]^+$, 973.26, found: 973.09.

*4.3.7. General methods for the preparation of the chromanone derivatives **H** series (**H1**–**H7**)*

To a solution of GT-H (0.34 mmol, 1.0 eq) in *N, N*-dimethylformamide (10 mL) were added potassium carbonate (1.02 mmol, 3.0 eq) and structurally diverse substituents (1.02 mmol, 3.0 eq). The solution was refluxed for 6–12 h. After the reaction was completed, the reaction mixture was poured in water (50 mL) and extracted with ethyl acetate, washed three times with saturated brine, dried over anhydrous sodium sulfate and the solvent was removed under reduced pressure. The residue was then purified via silica gel column chromatography using petroleum ether-ethyl acetate or dichloromethane-methanol to afford the desired compounds.

*4.3.7.1. (2,2-Dimethyl-7-(2-(propylamino)ethoxy)-3,4-dihydro-2H-benzo[h]chromen-5-yl)(morpholino)methanone (**H1**).* White solid, yield 57.5%; m.p.98–102 °C, R_f 0.28 (dichloromethane/methanol 20:1 v/v). ^{1}H NMR (600 MHz, Chloroform-d) δ 7.77 (d, *J* 8.4 Hz, 1H), 7.65 (s, 1H), 7.32 (t, *J* 8.4 Hz, 1H), 6.79 (d, *J* 7.8 Hz, 1H), 4.25 (s, 2H), 3.94–3.73 (m, 4H), 3.56 (d, *J* 31.2 Hz, 2H), 3.29 (d, *J* 43.8 Hz, 3H), 3.16 (t, *J* 4.8 Hz, 2H), 2.97 (s, 1H), 2.75 (t, *J* 7.2 Hz, 2H), 2.59 (s, 1H), 1.88 (s, 2H), 1.64–1.56 (m, 2H), 1.41 (s, 6H), 0.93 (t, *J* 7.2 Hz, 3H). ^{13}C NMR (151 MHz, Chloroform-*d*) δ 169.88, 154.30, 149.34, 133.13, 126.80, 125.79, 124.61, 114.30, 111.46, 110.55, 105.68, 74.59, 67.07, 66.86, 51.31, 48.24, 47.41, 41.95, 32.28, 26.71, 22.41, 20.07, 11.50. HRMS (ESI) *m/z* calculated for $C_{25}H_{34}N_2O_4$ $[M + H]^+$, 427.2597, found: 427.2611.

*4.3.7.2. (7-(2-(4-Methoxyphenoxy)ethoxy)-2,2-dimethyl-3,4-dihydro-2H-benzo[h]chromen-5-yl)(morpholino)methanone (**H2**).* White solid, yield 67.3%; m.p.137–140 °C, R_f 0.42 (petroleum ether/ethyl acetate 1:1 v/v). ^{1}H NMR (600 MHz, Chloroform-*d*) δ 7.81 (d, *J* 8.4 Hz, 1H), 7.63 (s, 1H), 7.36 (t, *J* 7.8 Hz, 1H), 6.94–6.90 (m, 2H), 6.88–6.83 (m, 3H), 4.43 (s, 4H), 3.85 (s, 2H), 3.78 (s, 5H), 3.53 (d, *J* 19.8 Hz, 2H), 3.27 (d, *J* 28.8 Hz, 2H), 3.01 (s, 1H), 2.60 (s, 1H), 1.90 (d, *J* 5.4 Hz, 2H), 1.43 (s, 6H). ^{13}C NMR (151 MHz, Chloroform-*d*) δ 169.77, 154.47, 154.23, 152.90, 149.32, 133.17, 126.87, 125.69, 124.81, 115.90, 114.75, 114.52, 111.64, 110.80, 105.95, 74.61, 67.38, 67.27, 66.88, 55.68, 47.42, 41.92, 32.34, 20.13. HRMS (ESI) *m/z* calculated for $C_{29}H_{33}NO_6$ $[M + H]^+$, 492.2386, found: 492.2363.

*4.3.7.3. (2,2-Dimethyl-7-(2-(4-nitrophenoxy)ethoxy)-3,4-dihydro-2H-benzo[h]chromen-5-yl)(morpholino)methanone (**H3**).* White solid, yield 40.9%; m.p.202–205 °C, R_f 0.48 (petroleum ether/ethyl acetate 2:1 v/v). ^{1}H NMR (600 MHz, Chloroform-*d*) δ 8.25–8.19 (m, 2H), 7.84 (d, *J* 9.0 Hz, 1H), 7.58 (s, 1H), 7.37 (t, *J* 7.8 Hz, 1H), 7.06–7.01 (m, 2H), 6.87 (d, *J* 7.8 Hz, 1H), 4.51 (d, *J* 15.0 Hz, 4H), 3.83 (s, 2H), 3.78–3.74 (m, 2H), 3.52 (s, 2H), 3.26 (d, *J* 16.2 Hz, 2H), 2.98 (s, 1H), 2.60 (s, 1H), 1.93–1.87 (m, 2H), 1.42 (s, 6H). ^{13}C NMR (151 MHz, Chloroform-*d*) δ 169.71, 163.61, 154.12, 149.40, 141.91, 133.48, 126.91, 125.86, 125.60, 124.73, 114.95, 114.63, 111.70, 110.48, 106.01, 74.71, 67.22, 66.86, 66.70, 47.37, 41.93, 32.29, 26.73, 20.11. HRMS (ESI) *m/z* calculated for $C_{28}H_{30}N_2O_7$ $[M + H]^+$, 507.2131, found: 507.2148.

*4.3.7.4. (7-(2-((4-Aminophenyl)thio)ethoxy)-2,2-dimethyl-3,4-dihydro-2H-benzo[h]chromen-5-yl)(morpholino)methanone (**H4**).* Light pink solid, yield 70.9%; m.p.144–147 °C, R_f 0.26 (petroleum ether/ethyl acetate 1:1 v/v). ^{1}H NMR (600 MHz, Chloroform-*d*) δ 7.77 (d, *J* 8.4 Hz, 1H), 7.59 (s, 1H), 7.32–7.27 (m, 3H), 6.71 (d, *J* 7.8 Hz, 1H), 6.62–6.56 (m, 2H), 4.23 (t, *J* 6.6 Hz, 2H), 3.90–3.74 (m, 6H), 3.56 (d, *J* 33.6 Hz, 2H), 3.34 (d, *J* 48.0 Hz, 2H), 3.00 (s, 1H), 2.58 (s, 1H), 1.97–1.69 (m, 4H), 1.41 (s, 6H). ^{13}C NMR (151 MHz, Chloroform-*d*) δ 169.85, 154.25, 149.28, 146.46, 134.49, 132.96, 126.82, 125.71, 124.69, 122.15, 115.59, 114.23, 111.60, 110.86, 105.72, 74.58, 67.28, 66.89, 47.46, 41.97, 35.35, 32.32, 20.11. HRMS (ESI) *m/z* calculated for $C_{28}H_{32}N_2O_4S$ $[M + H]^+$, 493.2161, found: 493.2174.

*4.3.7.5. (2,2-Dimethyl-7-(2-((4-nitrophenyl)thio)ethoxy)-3,4-dihydro-2H-benzo[h]chromen-5-yl)(morpholino)methanone (**H5**).* White solid, yield 54.5%; m.p.182–186 °C, R_f 0.28 (petroleum ether/ethyl acetate 2:1 v/v). ^{1}H NMR (600 MHz, Chloroform-*d*) δ 8.15–8.10 (m, 2H), 7.82 (d, *J* 9.0 Hz, 1H), 7.56 (s, 1H), 7.42 (d, *J* 8.4 Hz, 2H), 7.33 (t, *J* 7.8 Hz, 1H), 6.78 (d, *J* 7.8 Hz, 1H), 4.39 (t, *J* 7.2 Hz, 2H), 3.89–3.77 (m, 4H), 3.59–3.51 (m, 4H), 3.28 (d, *J* 27.0 Hz, 2H), 2.99 (s, 1H), 2.60 (s, 1H), 1.90 (d, *J* 6.6 Hz, 2H), 1.42 (s, 6H). ^{13}C NMR (151 MHz, Chloroform-*d*) δ 169.67, 153.85, 149.40, 146.25, 145.52, 133.48, 126.88, 126.79, 125.55, 124.64, 124.00, 114.95, 111.76, 110.44, 105.88, 74.71, 66.90, 66.52, 47.40, 41.96, 32.29, 26.73, 20.11. HRMS (ESI) *m/z* calculated for $C_{28}H_{30}N_2O_6S$ $[M + H]^+$, 523.1921, found: 523.1903.

*4.3.7.6. (2,2-Dimethyl-7-(2-(4-phenylpiperazin-1-yl)ethoxy)-3,4-dihydro-2H-benzo[h]chromen-5-yl)(morpholino)methanone **(H6)***. White solid, yield 72.8%; m.p.98–101 °C, R_f 0.53 (dichloromethane/methanol 30:1 v/v). ^{1}H NMR (600 MHz, Chloroform-*d*) δ 7.80 (d, *J* 9.0 Hz, 1H), 7.63 (s, 1H), 7.36 (t, *J* 8.4 Hz, 1H), 7.27 (d, *J* 7.2 Hz, 1H), 7.25 (s, 1H), 6.93 (d, *J* 7.8 Hz, 2H), 6.88–6.82 (m, 2H), 4.33 (s, 2H), 3.85 (d, *J* 61.2 Hz, 4H), 3.57 (d, *J* 21.6 Hz, 2H), 3.36–3.22 (m, 6H), 3.03 (s, 3H), 2.84 (s, 4H), 2.61 (s, 1H), 1.90 (d, *J* 9.6 Hz, 2H), 1.43 (s, 6H). ^{13}C NMR (151 MHz, Chloroform-*d*) δ 169.88, 154.45, 151.23, 149.40, 133.15, 129.05, 126.88, 125.80, 124.79, 119.70, 116.06, 114.31, 111.59, 110.68, 105.83, 74.63, 66.94, 66.66, 57.20, 53.65, 49.15, 47.46, 42.00, 32.35, 20.14. HRMS (ESI) *m/z* calculated for $C_{32}H_{39}N_3O_4$ $[M + H]^+$, 530.3019, found: 530.3034.

*4.3.7.7. (2,2-Dimethyl-7-(2-(2-methyl-1H-benzo[d]imidazole-1-yl) ethoxy)-3,4-dihydro-2H-benzo[h]chromen-5-yl)(morpholino)methanone **(H7)***. White solid, yield 61.9%; m.p.219–221 °C, R_f 0.47 (dichloromethane/methanol 30:1 v/v). ^{1}H NMR (600 MHz, Chloroform-*d*) δ 7.79 (d, *J* 8.4 Hz, 1H), 7.71 (d, *J* 6.6 Hz, 1H), 7.43 (d, *J* 6.6 Hz, 1H), 7.33–7.27 (m,3H), 7.25–7.23 (m, 1H), 6.72 (d, *J* 7.2 Hz, 1H), 4.64 (s, 1H), 4.54 (d, *J* 15.6 Hz, 1H), 4.41 (d, *J* 28.2 Hz, 2H), 3.93–3.81 (m, 3H), 3.75 (s, 1H), 3.42 (d, *J* 30.0 Hz, 2H), 3.05 (s, 2H), 2.99 (t, *J* 9.0 Hz, 1H), 2.69 (s, 3H), 2.57–2.52 (m, 1H), 1.90–1.83 (m, 2H), 1.39 (s, 6H). ^{13}C NMR (151 MHz, Chloroform-*d*) δ 169.47, 153.71, 151.45, 149.35, 142.63, 135.40, 133.50, 126.80, 125.41, 124.31, 122.17, 119.15, 115.07, 111.80, 110.21, 109.22, 105.47, 74.69, 66.84, 66.22, 47.25, 43.12, 41.91, 32.24, 20.05, 13.95. HRMS (ESI) *m/z* calculated for $C_{30}H_{33}N_3O_4$ $[M + H]^+$, 500.2549, found: 500.2564.

*4.3.8. General methods for the preparation of the chromanone derivatives **G** series **(G0-G20)***

The preparation method of **G0-G20** is similar to that of **H1–H7**.

*4.3.8.1. (2,2-Dimethyl-7-(3-(propylamino)propoxy)-3,4-dihydro-2H-benzo[h]chromen-5-yl)(morpholino)methanone **(G0)***. White solid, yield 44.3%; m.p.96–99 °C, R_f 0.52 (dichloromethane/methanol 10:1 v/v). ^{1}H NMR (600 MHz, Chloroform-*d*) δ 7.76 (d, *J* 8.4 Hz, 1H), 7.61 (s, 1H), 7.33 (t, *J* 7.8 Hz, 1H), 6.80 (d, *J* 7.8 Hz, 1H), 4.17 (t, *J* 5.4 Hz, 2H), 3.89–3.76 (m, 4H), 3.57 (d, *J* 30.6 Hz, 2H), 3.30 (d, *J* 45.0 Hz, 2H), 3.00 (s, 1H), 2.89 (s, 2H), 2.66–2.56 (m, 3H), 2.13–2.03 (m, 3H), 1.89 (d, *J* 7.2 Hz, 2H), 1.58–1.51 (m, 2H), 1.41 (s, 6H), 0.92 (t, *J* 7.2 Hz, 3H). ^{13}C NMR (151 MHz, Chloroform-*d*) δ 169.88, 154.64, 149.34, 133.02, 126.82, 125.82, 124.71, 113.94, 111.49, 110.65, 105.43, 74.57, 66.91, 66.52, 51.77, 47.44, 46.86, 41.95, 32.34, 29.65, 22.93, 20.12, 11.64. HRMS (ESI) *m/z* calculated for $C_{26}H_{36}N_2O_4$ $[M + H]^+$, 441.2753, found: 441.2768.

*4.3.8.2. (7-(3-((Furan-2-ylmethyl)amino)propoxy)-2,2-dimethyl-3,4-dihydro-2H-benzo[h]chromen-5-yl)(morpholino)methanone **(G1)***. Yellow solid, yield 45.7%; m.p.98–101 °C, R_f 0.25 (dichloromethane/methanol 30:1 v/v). ^{1}H NMR (600 MHz, Chloroform-*d*) δ 7.77 (d, *J* 8.4 Hz, 1H), 7.61 (s, 1H), 7.36–7.30 (m, 2H), 6.80 (d, *J* 7.8 Hz, 1H), 6.31–6.27 (m, 1H), 6.17 (d, *J* 3.0 Hz, 1H), 4.18 (t, *J* 6.0 Hz, 2H), 3.89–3.77 (m, 6H), 3.56 (d, *J* 27.0 Hz, 2H), 3.30 (d, *J* 42.6 Hz, 2H), 3.01 (s, 1H), 2.88 (t, *J* 7.8 Hz, 2H), 2.59 (s, 1H), 2.12–2.05 (m, 2H), 1.98–1.86 (m, 3H), 1.42 (s, 6H). ^{13}C NMR (151 MHz, Chloroform-*d*) δ 169.86, 154.62, 153.72, 149.33, 141.74, 133.00, 126.81, 125.81, 124.70, 113.94, 111.49, 110.64, 110.04, 106.85, 105.44, 74.55, 66.90, 66.39, 47.43, 46.13, 46.03, 41.94, 32.34, 29.65, 20.12. HRMS (ESI) *m/z* calculated for $C_{28}H_{34}N_2O_5$ $[M + H]^+$, 479.2546, found: 479.2531.

*4.3.8.3. (7-(3-((4-Hydroxyphenethyl)amino)propoxy)-2,2-dimethyl-3,4-dihydro-2H-benzo[h]chromen-5-yl)(morpholino)methanone **(G2)***. Yellow solid, yield 51.3%; m.p.108–111 °C, R_f 0.38 (dichloromethane/methanol 10:1 v/v). ^{1}H NMR (600 MHz, Chloroform-*d*) δ 7.77 (d, *J* 8.4 Hz, 1H), 7.56 (s, 1H), 7.33 (t, *J* 8.4 Hz, 1H), 6.94 (d, *J* 7.8 Hz, 2H), 6.76 (d, *J* 7.8 Hz, 1H), 6.65 (d, *J* 8.4 Hz, 2H), 4.11 (s, 2H), 3.81 (d, *J* 38.4 Hz, 5H), 3.55 (d, *J* 37.2 Hz, 3H), 3.29 (d, *J* 45.0 Hz, 2H), 2.98 (s, 1H), 2.93–2.87 (m, 4H), 2.77–2.71 (m, 2H), 2.58 (s, 1H), 2.09 (s, 2H), 1.89 (s, 2H), 1.41 (s, 6H). ^{13}C NMR (151 MHz, Chloroform-*d*) δ 170.23, 155.09, 154.55, 149.41, 132.81, 130.31, 129.56, 126.87, 125.94, 124.66, 115.71, 114.07, 111.44, 110.57, 105.63, 74.66, 66.85, 66.43, 50.81, 47.49, 46.59, 42.07, 34.56, 32.31, 29.14, 20.14. HRMS (ESI) *m/z* calculated for $C_{31}H_{38}N_2O_5$ $[M + H]^+$, 519.2859, found: 519.2845.

*4.3.8.4. (7-(3-(Cyclopropylamino)propoxy)-2,2-dimethyl-3,4-dihydro-2H-benzo[h]chromen-5-yl)(morpholino)methanone **(G3)***. Brown oil, yield 51.3%, R_f 0.52 (dichloromethane/methanol 15:1 v/v). ^{1}H NMR (600 MHz, Chloroform-*d*) δ 7.76 (d, *J* 8.4 Hz, 1H), 7.61 (s, 1H), 7.32 (t, *J* 7.8 Hz, 1H), 6.78 (d, *J* 7.8 Hz, 1H), 4.15 (t, *J* 6.6 Hz, 2H), 3.90–3.74 (m, 5H), 3.56 (d, *J* 31.8 Hz, 2H), 3.30 (d, *J* 47.4 Hz, 2H), 2.97 (t, *J* 7.2 Hz, 2H), 2.82 (s, 1H), 2.58 (s, 1H), 2.21–2.15 (m, 1H), 2.14–2.06 (m, 2H), 1.88 (d, *J* 6.6 Hz, 2H), 1.40 (s, 6H), 0.49–0.39 (m, 4H). ^{13}C NMR (151 MHz, Chloroform-*d*) δ 169.85, 154.56, 149.30, 132.96, 126.76, 125.78, 124.64, 113.91, 111.45, 110.59, 105.41, 74.53, 66.83, 66.45, 47.40, 46.56, 41.92, 32.28, 30.34, 29.26, 20.06, 5.90. HRMS (ESI) *m/z* calculated for $C_{26}H_{34}N_2O_4$ $[M + H]^+$, 439.2597, found: 439.2607.

*4.3.8.5. (7-(3-(Cyclopentylamino)propoxy)-2,2-dimethyl-3,4-dihydro-2H-benzo[h]chromen-5-yl)(morpholino)methanone **(G4)***. Colorless oil, yield 62.7%, R_f 0.54 (dichloromethane/methanol 15:1 v/v). ^{1}H NMR (600 MHz, Chloroform-*d*) δ 7.75 (d, *J* 8.4 Hz, 1H), 7.60 (s, 1H), 7.31 (t, *J* 7.8 Hz, 1H), 6.77 (d, *J* 7.8 Hz, 1H), 4.14 (t, *J* 6.0 Hz, 2H), 3.88–3.71 (m, 4H), 3.54 (d, *J* 31.2 Hz, 2H), 3.28 (d, *J* 43.2 Hz, 2H), 3.13–3.06 (m, 1H), 2.98 (s, 1H), 2.85 (t, *J* 6.0 Hz, 2H), 2.58 (s, 1H), 2.31 (s, 1H), 2.12–2.04 (m, 2H), 1.89–1.81 (m, 4H), 1.69–1.63 (m, 2H), 1.54–1.48 (m, 2H), 1.39 (s, 6H), 1.37–1.31 (m, 2H). ^{13}C NMR (151 MHz, Chloroform-*d*) δ 169.76, 154.54, 149.24, 132.93, 126.71, 125.73, 124.60, 113.84, 111.41, 110.54, 105.34, 74.47, 66.79, 66.50, 59.79, 47.35, 45.53, 41.85, 32.83, 32.24, 29.73, 23.86, 20.02. HRMS (ESI) *m/z* calculated for $C_{28}H_{38}N_2O_4$ $[M + H]^+$, 467.2910, found: 467.2918.

*4.3.8.6. (7-(3-(Cyclohexylamino)propoxy)-2,2-dimethyl-3,4-dihydro-2H-benzo[h]chromen-5-yl)(morpholino)methanone **(G5)***. Brown oil, yield 52.8%; R_f 0.51 (dichloromethane/methanol 15:1 v/v). ^{1}H NMR (600 MHz, Chloroform-*d*) δ 7.76 (d, *J* 8.4 Hz, 1H), 7.60 (s, 1H), 7.32 (t, *J* 8.4 Hz, 1H), 6.78 (d, *J* 7.2 Hz, 1H), 4.16 (t, *J* 6.0 Hz, 2H), 3.87–3.78 (m, 4H), 3.56 (d, *J* 34.2 Hz, 2H), 3.29 (d, *J* 45.6 Hz, 2H), 2.99 (s, 1H), 2.92 (t, *J* 7.2 Hz, 2H), 2.61–2.48 (m, 3H), 2.11 (d, *J* 6.0 Hz, 2H), 1.95–1.86 (m, 4H), 1.75–1.69 (m, 2H), 1.60 (d, *J* 12.6 Hz, 1H), 1.41 (s, 6H), 1.19–1.08 (m, 5H). ^{13}C NMR (151 MHz, Chloroform-*d*) δ 169.84, 154.57, 149.31, 132.99, 126.77, 125.79, 124.65, 113.93, 111.46, 110.60, 105.41, 74.54, 66.86, 66.51, 56.86, 47.42, 43.76, 41.93, 33.05, 32.30, 29.73, 25.92, 24.89, 20.08. HRMS (ESI) *m/z* calculated for $C_{29}H_{40}N_2O_4$ $[M + H]^+$, 481.3066, found: 481.3079.

*4.3.8.7. (7-(3-(4-Methoxyphenoxy)propoxy)-2,2-dimethyl-3,4-dihydro-2H-benzo[h]chromen-5-yl)(morpholino)methanone **(G6)***. White solid, yield 73.8%; m.p.120–123 °C, R_f 0.34 (petroleum ether/ethyl acetate 1:1 v/v). ^{1}H NMR (600 MHz, Chloroform-*d*) δ 7.80 (d, *J* 8.4 Hz, 1H), 7.65 (s, 1H), 7.35 (t, *J* 7.8 Hz, 1H), 6.88–6.80 (m, 5H), 4.30 (t, *J* 6.0 Hz, 2H), 4.21–4.14 (m, 2H), 3.91–3.77 (m, 4H), 3.75 (s, 3H), 3.53 (d, *J* 15.0 Hz, 2H), 3.28 (d, *J* 30.0 Hz, 2H), 3.02 (s, 1H), 2.62 (s, 1H), 2.39–2.32 (m, 2H), 1.93–1.87 (m, 2H), 1.43 (s, 6H). ^{13}C NMR (151 MHz, Chloroform-*d*) δ 169.69, 154.36, 153.77, 152.84, 149.19, 132.92, 126.66, 125.70, 124.54, 115.34, 114.54, 113.89, 111.36, 110.44, 105.37, 74.44, 66.72, 65.13, 64.65, 55.50, 47.25, 41.78, 32.16, 29.25, 19.97. HRMS (ESI) *m/z* calculated for $C_{30}H_{35}NO_6$ $[M + H]^+$, 506.2543,

found: 506.2524.

*4.3.8.8. (7-(3-(2-Aminophenoxy)propoxy)-2,2-dimethyl-3,4-dihydro-2H-benzo[h]chromen-5-yl)(morpholino)methanone (**G7**).* White solid, yield 40.1%; m.p.120–123 °C, R_f 0.44 (dichloromethane/methanol 20:1 v/v). ^{1}H NMR (600 MHz, Chloroform-d) δ 7.79 (d, J 8.4 Hz, 1H), 7.63 (s, 1H), 7.35 (t, *J* 7.8 Hz, 1H), 6.86–6.80 (m, 2H), 6.80–6.76 (m, 1H), 6.73–6.67 (m, 2H), 4.33 (t, *J* 6.0 Hz, 2H), 4.27 (d, *J* 6.0 Hz, 2H), 3.86 (d, *J* 19.2 Hz, 2H), 3.79 (s, 2H), 3.53 (d, *J* 19.2 Hz, 2H), 3.28 (d, *J* 32.4 Hz, 2H), 3.01 (s, 1H), 2.60 (s, 1H), 2.45–2.38 (m, 2H), 1.90 (d, *J* 7.2 Hz, 2H), 1.43 (s, 6H). ^{13}C NMR (151 MHz, Chloroform-*d*) δ 169.85, 154.48, 149.38, 146.36, 136.37, 133.12, 126.84, 125.80, 124.70, 121.36, 118.43, 115.17, 114.16, 110.56, 105.55, 74.60, 66.89, 65.15, 65.00, 47.41, 41.95, 32.34, 29.59, 20.13. HRMS (ESI) *m/z* calculated for $C_{29}H_{34}N_2O_5$ $[M + H]^+$, 491.2546, found: 491.2548.

*4.3.8.9. (7-(3-(4-Chlorophenoxy)propoxy)-2,2-dimethyl-3,4-dihydro-2H-benzo[h]chromen-5-yl)(morpholino)methanone (**G8**).* White solid, yield 47.1%; m.p.106–110 °C, R_f 0.61 (petroleum ether/ethyl acetate 1:1 v/v). ^{1}H NMR (600 MHz, Chloroform-*d*) δ 7.79 (d, *J* 8.4 Hz, 1H), 7.61 (s, 1H), 7.35 (t, *J* 8.4 Hz, 1H), 7.25–7.19 (m, 2H), 6.87–6.81 (m, 3H), 4.30 (t, *J* 6.0 Hz, 2H), 4.19 (s, 2H), 3.86 (d, *J* 25.2 Hz, 2H), 3.79 (s, 2H), 3.54 (s, 2H), 3.28 (d, *J* 25.2 Hz, 2H), 2.99 (s, 1H), 2.60 (s, 1H), 2.40–2.33 (m, 2H), 1.90 (d, *J* 7.2 Hz, 2H), 1.42 (s, 6H). ^{13}C NMR (151 MHz, Chloroform-*d*) δ 169.97, 157.45, 154.44, 149.41, 133.07, 129.28, 126.86, 125.83, 124.70, 116.69, 115.81, 114.19, 111.50, 110.52, 105.58, 74.63, 66.88, 64.98, 64.68, 47.42, 41.99, 32.32, 29.26, 20.12. HRMS (ESI) *m/z* calculated for $C_{29}H_{32}ClNO_5$ $[M + H]^+$, 510.2047, found: 510.2031.

*4.3.8.10. (2,2-Dimethyl-7-(3-(4-nitrophenoxy)propoxy)-3,4-dihydro-2H-benzo[h]chromen-5-yl)(morpholino)methanone (**G9**).* White solid, yield 66.4%; m.p.157–160 °C, R_f 0.47 (dichloromethane/methanol 30:1 v/v). ^{1}H NMR (600 MHz, Chloroform-*d*) δ 8.20–8.14 (m, 2H), 7.79 (d, *J* 8.4 Hz, 1H), 7.60 (s, 1H), 7.35 (t, *J* 8.4 Hz, 1H), 6.99–6.93 (m, 2H), 6.83 (d, *J* 7.8 Hz, 1H), 4.32 (t, *J* 6.0 Hz, 4H), 3.85 (d, *J* 22.2 Hz, 2H), 3.78 (s, 2H), 3.53 (s, 2H), 3.27 (d, *J* 18.0 Hz, 2H), 2.98 (s, 1H), 2.62 (s, 1H), 2.45–2.38 (m, 2H), 1.90 (d, *J* 6.0 Hz, 2H), 1.42 (s, 6H). ^{13}C NMR (151 MHz, Chloroform-*d*) δ 169.82, 163.77, 154.28, 149.40, 141.63, 133.31, 126.84, 125.81, 125.73, 124.66, 114.42, 114.36, 111.53, 110.34, 105.55, 74.66, 66.86, 65.49, 64.37, 47.37, 41.94, 32.28, 29.09, 26.71, 20.09. HRMS (ESI) *m/z* calculated for $C_{29}H_{32}N_2O_7$ $[M + H]^+$, 521.2288, found: 521.2278.

*4.3.8.11. 3-(3-((2,2-Dimethyl-5-(morpholine-4-carbonyl)-3,4-dihydro-2H-benzo[h]chromen-7-yl)oxy)propoxy)benzoic acid (**G10**).* White solid, yield 57.3%; m.p.157–160 °C, R_f 0.50 (dichloromethane/methanol 20:1 v/v). ^{1}H NMR (600 MHz, Chloroform-*d*) δ 7.92 (s, 1H), 7.75 (d, *J* 8.4 Hz, 1H), 7.72 (s, 1H), 7.45 (d, *J* 7.2 Hz, 1H), 7.36–7.30 (m, 2H), 7.14 (t, *J* 7.8 Hz, 1H), 6.94–6.89 (m, 1H), 6.83 (d, *J* 7.8 Hz, 1H), 4.63 (s, 1H), 4.51 (s, 1H), 4.30–4.24 (m, 2H), 3.94 (s, 1H), 3.85–3.78 (m, 3H), 3.60 (d, *J* 22.2 Hz, 2H), 3.33 (d, *J* 42.6 Hz, 2H), 3.02–2.96 (m, 1H), 2.62–2.57 (m, 1H), 2.35 (d, *J* 7.8 Hz, 2H), 1.89 (q, *J* 7.2 Hz, 2H), 1.41 (s, 6H). ^{13}C NMR (151 MHz, Chloroform-*d*) δ 170.76, 166.57, 156.52, 154.35, 149.45, 132.54, 131.04, 129.18, 126.98, 125.96, 124.95, 121.29, 120.62, 116.02, 114.49, 111.26, 110.87, 106.76, 74.71, 66.83, 66.25, 62.68, 47.52, 42.27, 32.28, 28.60, 20.13. HRMS (ESI) *m/z* calculated for $C_{30}H_{33}NO_7$ $[M + H]^+$, 520.2335, found: 520.2318.

*4.3.8.12. (7-(3-((4-Aminophenyl)thio)propoxy)-2,2-dimethyl-3,4-dihydro-2H-benzo[h]chromen-5-yl)(morpholino)methanone (**G11**).* White solid, yield 57.3%; m.p.149–153 °C, R_f 0.52 (dichloromethane/methanol 50:1 v/v). ^{1}H NMR (600 MHz, Chloroform-*d*) δ 7.79 (d, *J* 9.0 Hz, 1H), 7.61 (s, 1H), 7.36 (t, *J* 7.8 Hz, 1H), 7.28 (d, *J* 3.6 Hz, 2H), 6.80 (d, *J* 7.8 Hz, 1H), 6.61 (d, *J* 8.4 Hz, 2H), 4.21 (t, *J* 6.0 Hz, 2H), 3.97–3.69 (m, 6H), 3.57 (d, *J* 19.2 Hz, 2H), 3.32 (d, *J* 42.6 Hz, 2H), 3.03 (t, *J* 6.6 Hz, 3H), 2.62 (s, 1H), 2.16 (t, *J* 6.6 Hz, 2H), 1.92 (d, *J* 6.6 Hz, 2H), 1.44 (s, 6H). ^{13}C NMR (151 MHz, Chloroform-*d*) δ 169.88, 154.54, 149.34, 146.04, 133.86, 132.98, 126.81, 125.82, 124.69, 122.98, 115.59, 113.98, 111.52, 110.67, 105.53, 74.57, 66.90, 66.48, 47.44, 41.96, 33.13, 32.34, 29.09, 20.13. HRMS (ESI) *m/z* calculated for $C_{29}H_{34}N_2O_4S$ $[M + H]^+$, 507.2318, found: 507.2299.

*4.3.8.13. (2,2-Dimethyl-7-(3-morpholinopropoxy)-3,4-dihydro-2H-benzo[h]chromen-5-yl)(morpholino)methanone (**G12**).* White solid, yield 45.2%; m.p.118–120 °C, R_f 0.45 (dichloromethane/methanol 20:1 v/v). ^{1}H NMR (600 MHz, Chloroform-*d*) δ 7.77 (d, *J* 8.4 Hz, 1H), 7.61 (s, 1H), 7.34 (t, *J* 8.4 Hz, 1H), 6.81 (d, *J* 7.8 Hz, 1H), 4.17 (t, *J* 6.0 Hz, 2H), 3.91–3.78 (m, 4H), 3.72 (t, *J* 4.2 Hz, 4H), 3.56 (d, *J* 19.8 Hz, 2H), 3.30 (d, *J* 40.2 Hz, 2H), 2.99 (s, 1H), 2.59 (s, 3H), 2.48 (s, 4H), 2.12–2.04 (m, 2H), 1.89 (d, *J* 6.6 Hz, 2H), 1.41 (s, 6H). ^{13}C NMR (151 MHz, Chloroform-*d*) δ 169.87, 154.62, 149.31, 133.00, 126.80, 125.78, 124.70, 113.92, 111.45, 110.62, 105.43, 74.55, 66.88, 66.86, 66.33, 55.63, 53.73, 47.41, 41.93, 32.31, 26.46, 20.09. HRMS (ESI) *m/z* calculated for $C_{27}H_{36}N_2O_5$ $[M + H]^+$, 469.2702, found: 469.2690.

*4.3.8.14. (2,2-Dimethyl-7-(3-(4-phenylpiperazin-1-yl)propoxy)-3,4-dihydro-2H-benzo[h]chromen-5-yl)(morpholino)methanone (**G13**).* White solid, yield 63.9%; m.p.158–160 °C, R_f 0.47 (dichloromethane/methanol 20:1 v/v). ^{1}H NMR (600 MHz, Chloroform-d) δ 7.78 (d, J 8.4 Hz, 1H), 7.65 (s, 1H), 7.35 (t, *J* 7.8 Hz, 1H), 7.27 (d, *J* 7.2 Hz, 1H), 7.25 (s, 1H), 6.94 (d, *J* 8.4 Hz, 2H), 6.88–6.81 (m, 2H), 4.20 (t, *J* 6.0 Hz, 2H), 3.91–3.77 (m, 4H), 3.58 (d, *J* 24.0 Hz, 2H), 3.32 (d, *J* 42.0 Hz, 2H), 3.23 (t, *J* 4.8 Hz, 4H), 3.01 (s, 1H), 2.66 (t, *J* 4.8 Hz, 7H), 2.17–2.10 (m, 2H), 1.90 (d, *J* 7.2 Hz, 2H), 1.43 (s, 6H). ^{13}C NMR (151 MHz, Chloroform-*d*) δ 169.92, 154.69, 151.31, 149.35, 133.02, 129.01, 126.84, 125.83, 124.75, 119.56, 115.98, 113.94, 111.49, 110.69, 105.48, 74.58, 66.93, 66.48, 55.29, 53.31, 49.12, 47.45, 41.97, 32.35, 26.86, 20.13. HRMS (ESI) *m/z* calculated for $C_{33}H_{41}N_3O_4$ $[M + H]^+$, 544.3175, found: 544.3179.

*4.3.8.15. (7-(3-(1H-Imidazole-1-yl)propoxy)-2,2-dimethyl-3,4-dihydro-2H-benzo[h]chromen-5-yl)(morpholino)methanone (**G14**).* White solid, yield 43.5%; m.p.130–133 °C, R_f 0.45 (dichloromethane/methanol 15:1 v/v). ^{1}H NMR (400 MHz, Chloroform-d) δ 7.80 (d, J 8.4 Hz, 1H), 7.59 (s, 1H), 7.45 (s, 1H), 7.32 (t, J 8.0 Hz, 1H), 7.04 (s, 1H), 6.90 (s, 1H), 6.72 (d, J 7.6 Hz, 1H), 4.28–4.19 (m, 2H), 4.03 (t, J 5.6 Hz, 2H), 3.83 (d, *J* 22.4 Hz, 4H), 3.56 (s, 2H), 3.30 (d, *J* 17.6 Hz, 2H), 3.03–2.94 (m, 1H), 2.65–2.56 (m, 1H), 2.38–2.27 (m, 2H), 1.93–1.86 (m, 4H), 1.42 (s, 6H). ^{13}C NMR (151 MHz, Chloroform-*d*) δ 169.69, 153.85, 149.35, 137.09, 133.34, 129.51, 126.71, 125.66, 124.43, 118.81, 114.42, 111.43, 109.94, 105.44, 74.59, 66.76, 63.92, 47.26, 43.44, 41.82, 32.13, 30.56, 26.62, 19.99. HRMS (ESI) *m/z* calculated for $C_{26}H_{31}N_3O_4$ $[M + H]^+$, 450.2393, found: 450.2399.

*4.3.8.16. (2,2-Dimethyl-7-(3-(2-methyl-1H-imidazole-1-yl)propoxy)-3,4-dihydro-2H-benzo[h]chromen-5-yl)(morpholino)methanone (**G15**).* Brown oil, yield 41.2%; R_f 0.23 (dichloromethane/methanol 30:1 v/v). ^{1}H NMR (400 MHz, Chloroform-*d*) δ 7.81 (d, *J* 8.4 Hz, 1H), 7.61 (s, 1H), 7.33 (t, *J* 8.0 Hz, 1H), 6.90 (s, 1H), 6.80 (s, 1H), 6.74 (d, *J* 7.6 Hz, 1H), 4.16 (t, *J* 6.4 Hz, 2H), 4.04 (t, *J* 5.6 Hz, 2H), 3.84 (d, *J* 24.0 Hz, 4H), 3.57 (s, 2H), 3.31 (d, *J* 13.6 Hz, 2H), 3.00 (d, *J* 17.2 Hz, 1H), 2.61 (d, *J* 16.4 Hz, 1H), 2.33 (s, 3H), 2.32–2.26 (m, 2H), 1.91 (q, *J* 6.4 Hz, 2H), 1.43 (s, 6H). ^{13}C NMR (151 MHz, Chloroform-*d*) δ 169.77, 153.84, 149.43, 144.46, 133.37, 127.33, 126.78, 125.74, 124.47, 118.97, 114.48, 111.51, 110.00, 105.42, 74.67, 66.85, 63.75, 47.34, 42.42, 41.90, 32.20, 30.24, 26.70, 20.06, 12.72. HRMS (ESI) *m/z* calculated for $C_{27}H_{33}N_3O_4$ $[M + H]^+$, 464.2549, found: 464.2554.

*4.3.8.17. (2,2-Dimethyl-7-(3-(4-nitro-1H-imidazole-1-yl)propoxy)-3,4-dihydro-2H-benzo[h]chromen-5-yl)(morpholino)methanone (**G16**).* Light cyan solid, yield 22.4%; m.p.100–103 °C, R_f 0.45 (dichloromethane/methanol 20:1 v/v). ^{1}H NMR (600 MHz, Chloroform-*d*) δ 7.83 (d, *J* 7.2 Hz, 1H), 7.78 (s, 1H), 7.54 (s, 1H), 7.41 (s, 1H), 7.33 (t, *J* 7.8 Hz, 1H), 6.76–6.72 (m, 1H), 4.33 (s, 2H), 4.09 (s, 2H), 3.89–3.75 (m, 4H), 3.57 (d, *J* 16.2 Hz, 2H), 3.29 (d, *J* 22.8 Hz, 2H), 2.97 (d, *J* 19.2 Hz, 1H), 2.62 (d, *J* 17.4 Hz, 1H), 2.40 (d, *J* 6.0 Hz, 2H), 1.90 (s, 2H), 1.42 (s, 6H). ^{13}C NMR (151 MHz, Chloroform-*d*) δ 169.75, 153.62, 149.54, 136.07, 133.77, 126.87, 125.67, 124.48, 119.02, 114.98, 111.63, 109.70, 105.73, 74.79, 66.84, 63.71, 47.34, 45.09, 41.94, 32.23, 22.76, 20.08. HRMS (ESI) *m/z* calculated for $C_{26}H_{30}N_4O_6$ $[M + H]^+$, 495.2244, found: 495.2250.

*4.3.8.18. (2,2-Dimethyl-7-(3-(2-methyl-1H-benzo[d]imidazole-1-yl)propoxy)-3,4-dihydro-2H-benzo[h]chromen-5-yl)(morpholino)methanone (**G17**).* White solid, yield 50.1%; m.p.140–143 °C, R_f 0.49 (dichloromethane/methanol 10:1 v/v). ^{1}H NMR (600 MHz, Chloroform-*d*) δ 7.82 (d, *J* 8.4 Hz, 1H), 7.68 (d, *J* 6.6 Hz, 2H), 7.34–7.27 (m, 2H), 7.21 (t, *J* 7.2 Hz, 1H), 7.15 (t, *J* 8.4 Hz, 1H), 6.69 (d, *J* 7.8 Hz, 1H), 4.43 (t, *J* 6.6 Hz, 2H), 4.03 (t, *J* 5.4 Hz, 2H), 3.89 (s, 2H), 3.81 (s, 2H), 3.57 (d, *J* 18.0 Hz, 2H), 3.32 (d, *J* 27.0 Hz, 2H), 3.02 (d, *J* 17.4 Hz, 1H), 2.62 (d, *J* 13.2 Hz, 1H), 2.53 (s, 3H), 2.44–2.37 (m, 2H), 1.92 (d, *J* 7.2 Hz, 2H), 1.44 (s, 6H). ^{13}C NMR (151 MHz, Chloroform-*d*) δ 169.83, 153.84, 151.47, 149.54, 142.77, 135.00, 133.48, 126.88, 125.77, 124.55, 122.04, 121.85, 119.13, 114.61, 111.64, 110.07, 108.92, 105.56, 74.73, 66.91, 63.98, 47.43, 41.98, 40.31, 32.28, 29.29, 20.13, 13.55. HRMS (ESI) *m/z* calculated for $C_{31}H_{35}N_3O_4$ $[M + H]^+$, 514.2706, found: 514.2692.

*4.3.8.19. (7-(3-(2H-1,2,3-Triazol-2-yl)propoxy)-2,2-dimethyl-3,4-dihydro-2H-benzo[h]chromen-5-yl)(morpholino)methanone (**G18**).* White solid, yield 23.4%; m.p.159–162 °C, R_f 0.55 (dichloromethane/methanol 20:1 v/v). ^{1}H NMR (600 MHz, Chloroform-*d*) δ 7.78 (d, *J* 8.4 Hz, 1H), 7.62 (s, 1H), 7.59 (s, 2H), 7.32 (t, *J* 7.2 Hz, 1H), 6.76 (d, *J* 7.8 Hz, 1H), 4.72 (s, 2H), 4.15 (s, 2H), 3.89–3.80 (m, 4H), 3.59 (d, *J* 41.4 Hz, 2H), 3.32 (d, *J* 52.8 Hz, 2H), 3.01 (s, 1H), 2.61–2.53 (m, 3H), 1.90 (d, *J* 6.6 Hz, 2H), 1.42 (s, 6H). ^{13}C NMR (151 MHz, Chloroform-*d*) δ 169.81, 154.31, 149.34, 134.06, 133.17, 126.82, 125.70, 124.66, 114.30, 111.59, 110.57, 105.58, 74.59, 66.90, 65.04, 51.78, 47.43, 41.95, 32.33, 29.46, 20.12. HRMS (ESI) *m/z* calculated for $C_{25}H_{30}N_4O_4$ $[M + H]^+$, 451.2345, found: 451.2345.

*4.3.8.20. (7-(3-(1H-Tetrazol-1-yl)propoxy)-2,2-dimethyl-3,4-dihydro-2H-benzo[h]chromen-5-yl)(morpholino)methanone (**G19**).* White solid, yield 52.8%; m.p.110–114 °C, R_f 0.52 (dichloromethane/methanol 20:1 v/v). ^{1}H NMR (600 MHz, Chloroform-*d*) δ 8.50 (s, 1H), 7.80 (d, *J* 8.4 Hz, 1H), 7.56 (s, 1H), 7.32 (t, *J* 7.8 Hz, 1H), 6.76 (d, *J* 7.2 Hz, 1H), 4.94 (d, *J* 28.2 Hz, 2H), 4.17 (d, *J* 19.2 Hz, 2H), 3.93–3.78 (m, 4H), 3.59 (d, *J* 40.8 Hz, 2H), 3.32 (d, *J* 53.4 Hz, 2H), 3.00 (s, 1H), 2.65–2.60 (m, 3H), 1.90 (d, *J* 6.0 Hz, 2H), 1.42 (s, 6H). ^{13}C NMR (151 MHz, Chloroform-*d*) δ 169.76, 154.01, 152.84, 149.39, 133.38, 126.83, 125.64, 124.57, 114.61, 111.64, 110.29, 105.60, 74.65, 66.88, 64.50, 50.14, 47.41, 41.95, 32.29, 29.04, 20.10. HRMS (ESI) *m/z* calculated for $C_{24}H_{29}N_5O_4$ $[M + H]^+$, 452.2298, found: 452.2303.

*4.3.8.21. (7-(3-(2H-Tetrazol-2-yl)propoxy)-2,2-dimethyl-3,4-dihydro-2H-benzo[h]chromen-5-yl)(morpholino)methanone (**G20**).* White solid, yield 47.2%; m.p.145–147 °C, R_f 0.44 (dichloromethane/methanol 20:1 v/v). ^{1}H NMR (600 MHz, Chloroform-*d*) δ 8.59 (s, 1H), 7.81 (d, *J* 8.4 Hz, 1H), 7.50 (s, 1H), 7.32 (t, *J* 7.8 Hz, 1H), 6.73 (d, *J* 7.2 Hz, 1H), 4.75–4.67 (m, 2H), 4.10 (d, *J* 25.2 Hz, 2H), 3.88–3.77 (m, 4H), 3.58 (d, *J* 38.4 Hz, 2H), 3.30 (d, *J* 41.4 Hz, 2H), 2.63 (s, 1H), 2.57–2.50 (m, 2H), 1.92–1.88 (m, 2H), 1.42 (s, 6H). ^{13}C NMR (151 MHz, Chloroform-*d*) δ 169.74, 153.72, 149.49, 142.78, 133.69, 126.84, 125.67, 124.48, 114.87, 111.61, 109.86, 105.67, 74.75, 66.84, 64.11, 47.35, 45.32, 41.94, 32.24, 29.30, 20.08. HRMS (ESI) *m/z* calculated for $C_{24}H_{29}N_5O_4$ $[M + H]^+$, 452.2298, found: 452.2306.

*4.3.9. General methods for the preparation of the chromanone derivatives **Y** series (**Y1**–**Y7**)*

The preparation method of **Y1–Y7** is similar to that of **H1–H7**.

*4.3.9.1. (2,2-Dimethyl-7-(4-(propylamino)butoxy)-3,4-dihydro-2H-benzo[h]chromen-5-yl)(morpholino)methanone (**Y1**).* White solid, yield 22.6%; m.p.98–101 °C, R_f 0.21 (dichloromethane/methanol 20:1 v/v). ^{1}H NMR (600 MHz, Chloroform-*d*) δ 7.75 (d, *J* 8.4 Hz, 1H), 7.66 (s, 1H), 7.30 (t, *J* 7.8 Hz, 1H), 6.64 (d, *J* 7.2 Hz, 1H), 3.98 (s, 1H), 3.89–3.84 (m, 3H), 3.79 (s, 1H), 3.72 (s, 1H), 3.63 (s, 1H), 3.49 (s, 1H), 3.37 (s, 1H), 3.24 (s, 1H), 3.01–2.92 (m, 3H), 2.89–2.83 (m, 2H), 2.58 (d, *J* 16.2 Hz, 1H), 2.19–2.13 (m, 1H), 1.98 (t, *J* 12.6 Hz, 1H), 1.90–1.71 (m, 7H), 1.40 (s, 6H), 0.90 (t, *J* 7.2 Hz, 3H). ^{13}C NMR (151 MHz, Chloroform-*d*) δ 169.85, 154.40, 149.27, 133.27, 126.73, 125.85, 124.59, 114.01, 111.40, 110.61, 105.51, 74.57, 67.15, 66.80, 49.76, 47.84, 47.44, 41.98, 32.30, 26.65, 23.46, 20.07, 19.75, 11.20. HRMS (ESI) *m/z* calculated for $C_{27}H_{38}N_2O_4$ $[M + H]^+$, 455.2910, found: 455.2924.

*4.3.9.2. (7-(4-(4-Methoxyphenoxy)butoxy)-2,2-dimethyl-3,4-dihydro-2H-benzo[h]chromen-5-yl)(morpholino)methanone (**Y2**).* White solid, yield 48.3%; m.p.144–149 °C, R_f 0.39 (petroleum/ethyl acetate 2:1 v/v). ^{1}H NMR (600 MHz, Chloroform-*d*) δ 7.78 (d, *J* 8.4 Hz, 1H), 7.65 (s, 1H), 7.35 (t, *J* 7.8 Hz, 1H), 6.87–6.80 (m, 5H), 4.19 (t, *J* 6.6 Hz, 2H), 4.02 (t, *J* 6.0 Hz, 2H), 3.90–3.78 (m, 4H), 3.77 (s, 3H), 3.56 (d, *J* 19.2 Hz, 2H), 3.31 (d, *J* 43.2 Hz, 2H), 3.02 (s, 1H), 2.61 (s, 1H), 2.13–2.06 (m, 2H), 2.05–1.99 (m, 2H), 1.90 (d, *J* 7.2 Hz, 2H), 1.43 (s, 6H). ^{13}C NMR (151 MHz, Chloroform-*d*) δ 169.90, 154.67, 153.86, 153.15, 149.35, 133.00, 126.84, 125.84, 124.76, 115.50, 114.71, 113.92, 111.51, 110.71, 105.43, 74.57, 68.17, 67.79, 66.90, 55.69, 47.44, 41.95, 32.36, 26.24, 26.02, 20.14. HRMS (ESI) *m/z* calculated for $C_{31}H_{37}NO_6$ $[M + H]^+$, 520.2699, found: 520.2714.

*4.3.9.3. (2,2-Dimethyl-7-(4-(4-nitrophenoxy)butoxy)-3,4-dihydro-2H-benzo[h]chromen-5-yl)(morpholino)methanone (**Y3**).* White solid, yield 39.8%; m.p.182–186 °C, R_f 0.35 (petroleum/ethyl acetate 2:1 v/v). ^{1}H NMR (600 MHz, Chloroform-*d*) δ 8.18 (d, *J* 9.6 Hz, 2H), 7.79 (d, *J* 8.4 Hz, 1H), 7.62 (s, 1H), 7.35 (t, *J* 7.8 Hz, 1H), 6.93 (d, *J* 9.0 Hz, 2H), 6.81 (d, *J* 7.8 Hz, 1H), 4.21–4.14 (m, 4H), 3.85 (d, *J* 27.6 Hz, 2H), 3.80–3.75 (m, 2H), 3.56 (s, 2H), 3.29 (d, *J* 30.0 Hz, 2H), 2.99 (s, 1H), 2.62 (s, 1H), 2.10 (t, *J* 3.0 Hz, 4H), 1.90 (d, *J* 6.6 Hz, 2H), 1.42 (s, 6H). ^{13}C NMR (151 MHz, Chloroform-*d*) δ 169.85, 163.90, 154.48, 149.37, 141.49, 133.17, 126.83, 125.81, 125.77, 124.70, 114.35, 114.11, 111.51, 110.48, 105.41, 74.62, 68.35, 67.54, 66.87, 47.39, 41.94, 32.30, 26.72, 25.98, 20.10. HRMS (ESI) *m/z* calculated for $C_{30}H_{34}N_2O_7$ $[M + H]^+$, 535.2444, found: 535.2458.

*4.3.9.4. (7-(4-((4-Aminophenyl)thio)butoxy)-2,2-dimethyl-3,4-dihydro-2H-benzo[h]chromen-5-yl)(morpholino)methanone (**Y4**).* Light yellow solid, yield 62.7%; m.p.162–165 °C, R_f 0.37 (petroleum/ethyl acetate 1:1 v/v). ^{1}H NMR (600 MHz, Chloroform-*d*) δ 7.77 (d, *J* 8.4 Hz, 1H), 7.60 (s, 1H), 7.34 (t, *J* 8.4 Hz, 1H), 7.22 (d, *J* 8.4 Hz, 2H), 6.78 (d, *J* 7.8 Hz, 1H), 6.58 (d, *J* 8.4 Hz, 2H), 4.10 (t, *J* 5.4 Hz, 2H), 3.91–3.72 (m, 6H), 3.57 (d, *J* 30.0 Hz, 2H), 3.31 (d, *J* 51.6 Hz, 1H), 3.02 (s, 1H), 2.85 (t, *J* 6.0 Hz, 2H), 2.60 (s, 1H), 2.05–1.97 (m, 2H), 1.90 (d, *J* 6.0 Hz, 2H), 1.85–1.77 (m, 2H), 1.42 (s, 6H). ^{13}C NMR (151 MHz, Chloroform-*d*) δ 169.91, 154.64, 149.34, 146.02, 133.91, 132.92, 126.83, 125.83, 124.71, 123.06, 115.55, 113.87, 111.54, 110.72, 105.36, 74.57, 67.62, 66.91, 47.47, 41.97, 36.04, 32.36, 28.04, 26.00, 20.14. HRMS (ESI) *m/z* calculated for $C_{30}H_{36}N_2O_4S$ $[M + H]^+$, 521.2474, found: 521.2486.

80

4.3.9.5. (7-(4-((4-Chlorophenyl)thio)butoxy)-2,2-dimethyl-3,4-dihydro-2H-benzo[h]chromen-5-yl)(morpholino)methanone ***(Y5)***. White solid, yield 55.3%; m.p.168–170 °C, R_f 0.73 (petroleum/ethyl acetate 1:2 v/v). ^{1}H NMR (600 MHz, Chloroform-*d*) δ 7.79 (d, *J* 8.4 Hz, 1H), 7.61 (s, 2H), 7.34 (t, *J* 7.8 Hz, 1H), 7.25–7.23 (m, 2H), 7.22–7.19 (m, 2H), 6.78 (d, *J* 7.8 Hz, 1H), 4.13 (t, *J* 6.6 Hz, 2H), 3.86 (d, *J* 35.4 Hz, 2H), 3.79 (s, 2H), 3.55 (d, *J* 19.2 Hz, 2H), 3.29 (d, *J* 38.4 Hz, 2H), 3.00 (t, *J* 7.2 Hz, 3H), 2.61 (s, 1H), 2.08–2.00 (m, 2H), 1.94–1.86 (m, 4H), 1.43 (s, 6H). ^{13}C NMR (151 MHz, Chloroform-*d*) δ 169.87, 154.53, 149.38, 135.09, 133.09, 131.87, 130.49, 128.96, 126.85, 125.80, 124.72, 114.06, 111.59, 110.63, 105.41, 74.62, 67.46, 66.92, 47.44, 41.97, 33.72, 32.35, 28.16, 25.88, 20.14. HRMS (ESI) *m/z* calculated for $C_{30}H_{34}ClNO_4S$ $[M + H]^+$, 540.1975, found: 540.1988.

4.3.9.6. (2,2-Dimethyl-7-(4-(4-phenylpiperazin-1-yl)butoxy)-3,4-dihydro-2H-benzo[h]chromen-5-yl)(morpholino)methanone ***(Y6)***. White solid, yield 68.8%; m.p.125–128 °C, R_f 0.47 (dichloromethane/methanol 20:1 v/v). ^{1}H NMR (600 MHz, Chloroform-*d*) δ 7.77 (d, *J* 8.4 Hz, 1H), 7.64 (s, 1H), 7.34 (t, *J* 7.8 Hz, 1H), 7.25–7.23 (m, 2H), 6.92 (d, *J* 7.8 Hz, 2H), 6.84 (t, *J* 7.8 Hz, 1H), 6.80 (d, *J* 7.8 Hz, 1H), 4.14 (t, *J* 6.0 Hz, 2H), 3.93–3.74 (m, 4H), 3.57 (d, *J* 22.8 Hz, 2H), 3.30 (d, *J* 45.6 Hz, 2H), 3.21 (t, *J* 4.8 Hz, 4H), 3.00 (s, 1H), 2.62 (t, *J* 4.8 Hz, 5H), 2.50 (t, *J* 7.2 Hz, 2H), 1.99–1.93 (m, 2H), 1.89 (d, *J* 6.6 Hz, 2H), 1.83–1.76 (m, 2H), 1.42 (s, 6H). ^{13}C NMR (151 MHz, Chloroform-*d*) δ 169.86, 154.69, 151.27, 149.31, 132.98, 128.96, 126.81, 125.81, 124.75, 119.49, 115.94, 113.85, 111.45, 110.71, 105.40, 74.53, 67.99, 66.88, 58.12, 53.17, 49.02, 47.42, 41.94, 32.32, 27.22, 23.50, 20.10. HRMS (ESI) *m/z* calculated for $C_{34}H_{43}N_3O_4$ $[M + H]^+$, 558.3332, found: 558.3339.

4.3.9.7. (2,2-Dimethyl-7-(4-(2-methyl-1H-benzo[d]imidazole-1-yl) butoxy)-3,4-dihydro-2H-benzo[h]chromen-5-yl)(morpholino)methanone ***(Y7)***. White solid, yield 43.6%; m.p.156–160 °C, R_f 0.52 (dichloromethane/methanol 20:1 v/v). ^{1}H NMR (600 MHz, Chloroform-*d*) δ 7.79 (d, *J* 8.4 Hz, 1H), 7.69 (d, *J* 7.8 Hz, 1H), 7.57 (s, 1H), 7.33 (t, *J* 7.8 Hz, 1H), 7.29–7.26 (m, 1H), 7.23–7.19 (m, 2H), 6.76 (d, *J* 7.8 Hz, 1H), 4.22 (t, *J* 7.2 Hz, 2H), 4.11 (t, *J* 6.0 Hz, 2H), 3.81 (d, *J* 45.6 Hz, 4H), 3.49 (s, 2H), 3.24 (d, *J* 17.4 Hz, 2H), 2.99 (s, 1H), 2.62 (s, 4H), 2.12–2.04 (m, 2H), 1.97–1.88 (m, 4H), 1.42 (s, 6H). ^{13}C NMR (151 MHz, Chloroform-*d*) δ 169.81, 154.37, 151.20, 149.41, 142.59, 135.03, 133.27, 126.85, 125.75, 124.67, 122.03, 121.79, 119.10, 114.29, 111.55, 110.35, 108.99, 105.52, 74.64, 67.41, 66.85, 47.36, 43.48, 41.94, 32.31, 26.73, 26.64, 20.11, 13.84. HRMS (ESI) *m/z* calculated for $C_{32}H_{37}N_3O_4$ $[M + H]^+$, 528.2862, found: 528.2875.

4.4. Antimicrobial assays

Antimicrobial assays were performed to assess if the chosen compounds have any antimicrobial activity against *E. coli*. Antimicrobial sensitivity assays were performed using standard broth dilution assays, as recommended by the European Committee on Antimicrobial Susceptibility Testing according to International Standard ISO 20776-1 [55]. Briefly, a two-fold dilution series of each test compound into fresh bacterial growth media was performed in 96 well microtiter trays. Log phase bacteria were then seeded into each well (5×10^5 CFU/well) before growing for 18 h at 37 °C. The optical density of each well was then measured using a plate reader (BioTek, Potton Bedfordshire, UK) at 630 nm (OD_{630}) at 0 h and 18 h. The MIC was determined as the lowest concentration of antibiotic needed that completely prevent the bacterial growth as detected by no increase in OD_{630} after 18 h. All MIC determinations were repeated at least three times on different days with different batches of cells in the presence of 2% DMSO (at this concentration of DMSO had no effect on bacterial growth).

4.5. Checkerboard titration assay

The checkerboard titration assay was used as the primary screening assay to determine the ability of selected compounds to function as EPIs by increasing the susceptibility of Gram-negative organisms to certain antibiotics [15]. These assays were performed using 96-well plates with antimicrobials serially diluted vertically down the plate (seven 2-fold serial dilutions) and test compounds were serially diluted horizontally across the plate (five 2-fold dilutions) [39,56]. A bacterial inoculum 5×10^5 CFU/well was added and the plates were incubated at 37 °C for 18 h under aerobic conditions. In assays using compounds which showed high absorbance at time zero, the presence or absence of bacterial growth at 18 h was confirmed with the use of resazurin. In this method, 10 μL of 0.01% resazurin was added in each well and the plate was incubated at 37 °C for 30 min while shaking. A pink color was indicative of metabolically active cells while a blue colour indicated no growth of the organism. PAβN was used as a known EPI control.

The compounds which reduced the MIC of the antimicrobials against *E. coli* BW25113 were then tested for in the checkerboard assay against *E. coli* strain BW25113 with a deletion of the *acrB* gene (ΔAcrB) to ascertain that the compounds do not synergize with antibiotics against an efflux deleted mutant.

Additional checkerboard assays were also performed on wild-type *E. coli* BW25113 in the presence of a sub-MIC concentration of colistin (0.5 μg/mL). At this concentration, colistin would permeabilise the outer membrane of *E. coli*, allowing compounds to enter the cells more readily [57].

4.6. Nile red efflux assay

The Nile red efflux assay was performed to examine whether the compounds inhibited efflux of the fluorescent efflux pump substrate Nile Red [15,29,43]. Nile Red is fluorescent when it accumulates inside the cell but non-fluorescent in the aqueous media.

E. coli BW 25113 (DE3) ΔAcrB propagating the AcrB expressing plasmid, pAcrB, was used in the assay.

An overnight culture of the required *E. coli* strain was incubated in LB broth in the presence of 25 μg/mL kanamycin and incubated with shaking at 37 °C for 14–16 h until the OD_{660} reached a plateau. The cells were harvested by centrifugation at 4000 g for 10 min at room temperature and were then washed three times by re-suspending the cells in 50 mM potassium phosphate buffer (pH 7.0) containing 1 mM $MgCl_2$. The cells were then resuspended in the same buffer to an OD_{660} of 1.0 after which cells were allowed to rest for 15 min at room temperature. Aliquots (2 mL) were then transferred to 15-mL conical centrifugation tubes and CCCP was added to a final concentration of 10 mM to de-energise the cells. After 15 min, the compound was added to the desired final concentration and Nile Red was added to a final concentration of 10 μM after another 15 min. The cell suspension was incubated on a shaker (140 rpm at 37 °C) for 3 h. The cells were left at room temperature for 60 min and then centrifuged for 5 min at 3000 g. The supernatant was discarded, and droplets of it clinging to the tube wall were thoroughly removed with absorbent tissues. Subsequently, the cells were resuspended in 0.2 mL assay buffer (20 mM of pH 7.0 potassium phosphate buffer containing 1 mM $MgCl_2$) and was immediately transferred to a quartz cuvette containing 1.8 mL of assay buffer. The fluorescence signal was measured in a fluorimeter (LS 55B, PerkinElmer) with excitation at 552 nm and emission at 636 nm. Excitation and emission slit widths were 10 and 5 nm, respectively. The fluorescence of the cell suspension was followed for 100 s, after which Nile Red efflux was triggered by rapid energisation with 50 mM glucose. Fluorescence was monitored for another 200 s.

4.7. Nitrocefin uptake assay

The nitrocefin hydrolysis assay was performed to determine if the

compounds disrupt the bacterial outer membranes as described previously [58]. Briefly, *E. coli* BW25113 cells with constitutive expression of chromosomal β-lactamase were grown in LB broth, then harvested and washed in 50 mM potassium phosphate buffer. The cells were subsequently resuspended in the same buffer and aliquoted in a 96-well plate (flat bottom, Corning Incoporated-Life Science) at an OD_{660} of 0.5. The cell suspension was treated with 10 μM CCCP and the compounds were added to a final concentration of 128 μg/mL. The reaction was started by the addition of nitrocefin (32 μg/mL final concentration). Immediately thereafter, hydrolysis of nitrocefin was monitored by measurement of the increase in absorbance at 490 nm over 20 min (EnSpire, Multimode plate reader, PerkinElmer). A set of duplicate wells for each compound without the addition of nitrocefin was also monitored over the same time period to exclude the intrinsic absorbance.

The rates of nitrocefin hydrolysis in the presence of compounds were compared to the rate of a) untreated cells with the vehicle control (DMSO) only; and b) cells treated with the known outer membrane permeabilizer Polymyxin B nonapeptide (PMBN).

4.8. $DiOC_2(3)$ assay

The membrane gradient assay was performed using an adaptation of a method described previously [39,59] to determine effects of compounds on the bacterial inner membrane.

A 0.1-mL portion of an overnight culture (grown at 37 °C with shaking at 140 rpm) of *E. coli* BW25113 was added to 50 mL LB broth in an Erlenmeyer flask and grown on a shaker (140 rpm; 37 °C) to an OD_{660} of 0.5 (approx. 2–3 h). The culture was then centrifuged at 4000 g for 10 min at room temperature. The pellet was re-suspended in the assay buffer (50 mM potassium phosphate buffer pH 7.0). After another centrifugation and resuspension step, the cells were treated with 2.5 mM K-EDTA and 1% ethanol and incubated at 37 °C for 15 min to permeabilise the outer membrane. The cells were harvested by centrifugation (4000 rpm, 10 min, 4 °C) and then resuspended in the assay buffer to an OD_{660} of 5. The cells were kept on ice for subsequent experimentation.

The cell suspension (0.2 mL) was transferred to a quartz cuvette containing 1.8 mL of assay buffer at room temperature. The fluorescence was measured in a fluorimeter (LS 55B, PerkinElmer) with excitation and emission wavelengths of 488 nm and 613 nm respectively and excitation and emission slit widths of 10 and 5 nm respectively. The fluorescence of the cell suspension was followed for 60 s, before $DiOC_2(3)$ solution was added at a final concentration of 10 μM. After the fluorescence reached a plateau, the cells were energized by the addition of 0.5% glucose. The fluorescence was monitored until a steady state was reached again before the proton motive force was disrupted by the addition of the ionophore CCCP (10 μM). To measure the effect of test compounds (putative EPIs) on the gradient, the compounds were added to the cell in the cuvette at the desired concentration and incubated with shaking for 10 min before taking the fluorescence reading was commenced.

4.9. Hemolysis assay

Hemolysis activity of **H3**, **H5**, **H6**, **G6**, **G10** and **G11** were determined using fresh isolated mice red blood cells. Fresh isolated mice red blood cells were washed with PBS buffer three times and prepared as 5% PBS solution. The test compounds and controls were diluted with PBS buffer by two-fold serial dilution, incubated with 5% red blood cells (1:1) at 37 °C for 1 h, and then centrifuged at 1500 r/min for 10 min. The supernatants (30 μL) were transformed to a 96-well microplate with PBS buffer (70 μL) in each well, and absorbance of all wells at 540 nm was recorded by a microplate reader. The PBS buffer was used as negative control, while 2% Triton X-100 was used as positive control. Tests were conducted in triplicate. The percentage of hemolysis was calculated as follows: Hemolysis $(Abs_{sample}\text{-}Abs_{PBS})/(Abs_{Positive}\text{-}Abs_{PBS}) \times 100\%$ [60].

4.10. Caenorhabditis elegans survival assay

Evaluation of the toxicity of putative EPIs using *C. elegans* is inexpensive and less time-consuming, compared to mammalian models. The maintenance and synchronisation of *C. elegans* nematodes was performed as we have described before [50,61,62]. Briefly, the nematodes were grown on Nematode Growth Medium agar (1 mM $CaCl_2$, 1 mM $MgSO_4$, 25 mM KPO_4 and 5 mg/mL cholesterol, mixed with 0.3% NaCl, 1.2% technical agar and 0.25% peptone) that was seeded with a lawn of *E. coli* OP50. This study was using equivalent aged nematodes generated from synchronized nematodes. The nematodes were then harvested in Nematode Growth Medium broth (composed of 95% M9 buffer and 5% brain heart infusion broth, supplemented with 10 μg/mL cholesterol), the density of nematodes was adjusted to approximately 25 nematodes per 25 μL. The number of nematodes was counted under a light microscope at 40 × and 100 × magnification. The compounds were evaluated for their toxicity at 128 μg/mL and were added to 96-well-plates in the presence of 2% DMSO. Untreated nematodes in the presence of 2% DMSO were used as healthy, positive control. Additional wells containing 50 μg/mL ampicillin and 2% DMSO were also set as healthy controls to show the survival rate when nematodes were fed with a known antibiotic with low toxicity. Each well was loaded with 25 μL of the test solution and 25 μL of nematodes and 50 μL medium. The nematodes were then incubated at 25 °C and observed for up to 72 h. The number of alive/dead nematodes was counted every 24 h. The percentage of surviving nematodes was calculated every 24 h for 72 h in total. Statistical analysis was performed using two-way ANOVA of Prism (GraphPad Prism 9).

4.11. Computational analysis of compound binding

The molecular docking was performed using Sybyl-X-2.1. The crystal structure of AcrB (PDB ID code 5ENR) was downloaded from the PDB database. Water molecules and co-crystal ligand MBX3135 were removed while docking. The structure of test compounds was sketched in Chembio2D and converted to 3D while energy was minimized based on the Tripos force field in Sybyl-X-2.1. Surflex-Dock module was used for molecular docking. The compound and AcrB protein interaction were scored according to the Total-Score scoring function. The larger was the Total-Score value, the better were the matching and binding effect of the compound and the protein. With a Total-Score >5 as the threshold, PyMol was used to visually inspected and analyzed the best docking results.

Declaration of competing interest

The authors declare that they have no known competing financial interests or personal relationships that could have appeared to influence the work reported in this paper.

Data availability

Data will be made available on request.

Acknowledgements

This work was supported financially by National Natural Science Foundation of China (81973179), National Health and Medical Research Council of Australia (GN1147538), and Key Project of Major Project of New and Old Kinetic Energy Conversion of Shandong Province in 2020.

Appendix A. Supplementary data

Supplementary data to this article can be found online at https://doi.

org/10.1016/j.ejmech.2023.115148.

References

[1] B. Ribeiro da Cunha, L.P. Fonseca, C.R.C. Calado, Antibiotic discovery: where have we come from, where do we go? Antibiotics 8 (2019) 45.
[2] E.C. Bragginton, L.J.V. Piddock, UK and European Union public and charitable funding from 2008 to 2013 for bacteriology and antibiotic research in the UK: an observational study, Lancet Infect. Dis. 14 (2014) 857–868.
[3] M. Hamad, F. Al-Marzooq, G. Orive, T.H. Al-Tel, Superbugs but no drugs: steps in averting a post-antibiotic era, Drug Discov. Today 24 (2019) 2225–2228.
[4] H. Venter, Reversing resistance to counter antimicrobial resistance in the World Health Organisation's critical priority of most dangerous pathogens, Biosci. Rep. 39 (2019).
[5] M. Arzanlou, Wern C. Chai, H. Venter, Intrinsic, adaptive and acquired antimicrobial resistance in Gram-negative bacteria, Essays Biochem. 61 (2017) 49–59.
[6] A. Amsalu, S.A. Sapula, M. De Barros Lopes, B.J. Hart, A.H. Nguyen, B. Drigo, J. Turnidge, L.E. Leong, H. Venter, Efflux pump-driven antibiotic and biocide cross-resistance in Pseudomonas aeruginosa isolated from different ecological niches: a case study in the development of multidrug resistance in environmental hotspots, Microorganisms 8 (2020) 1647.
[7] M.E. Wand, E.M. Darby, J.M.A. Blair, J.M. Sutton, Contribution of the efflux pump AcrAB-TolC to the tolerance of chlorhexidine and other biocides in Klebsiella spp, J. Med. Microbiol. 71 (2022).
[8] H.I. Zgurskaya, H. Nikaido, Multidrug resistance mechanisms: drug efflux across two membranes, Mol. Microbiol. 37 (2000) 219–225.
[9] D.H. Nies, Efflux-mediated heavy metal resistance in prokaryotes, FEMS Microbiol. Rev. 27 (2003) 313–339.
[10] J.L. Ramos, E. Duque, M.T. Gallegos, P. Godoy, M.I. Ramos-Gonzalez, A. Rojas, W. Teran, A. Segura, Mechanisms of solvent tolerance in gram-negative bacteria, Annu. Rev. Microbiol. 56 (2002) 743–768.
[11] J.M.A. Blair, M.A. Webber, A.J. Baylay, D.O. Ogbolu, L.J.V. Piddock, Molecular mechanisms of antibiotic resistance, Nat. Rev. Microbiol. 13 (2015) 42–51.
[12] J.M.A. Blair, G.E. Richmond, L.J.V. Piddock, Multidrug efflux pumps in Gram-negative bacteria and their role in antibiotic resistance, Future Microbiol. 9 (2014) 1165–1177.
[13] X. Wang-Kan, J.M.A. Blair, B. Chirullo, J. Betts, R.M.L. Ragione, A. Ivens, V. Ricci, T.J. Opperman, L.J.V. Piddock, Lack of AcrB efflux function confers loss of virulence on *Salmonella enterica* serovar typhimurium, mBio 8 (2017) e00968, 00917.
[14] M.A.S. Moreira, E.C. de Souza, C.A. de Moraes, Multidrug efflux systems in gram-negative bacteria, Braz. J. Microbiol. 35 (2004) 19–28.
[15] H. Venter, R. Mowla, T. Ohene-Agyei, S. Ma, RND-Type drug efflux pumps from gram-negative bacteria: molecular mechanism and inhibition, Front. Microbiol. 6 (2015) 377.
[16] D. Du, Z. Wang, N.R. James, J.E. Voss, E. Klimont, T. Ohene-Agyei, H. Venter, W. Chiu, B.F. Luisi, Structure of the AcrAB–TolC multidrug efflux pump, Nature 509 (2014) 512–515.
[17] L. Daury, F. Orange, J.-C. Taveau, A. Verchère, L. Monlezun, C. Gounou, R.K. R. Marreddy, M. Picard, I. Broutin, K.M. Pos, O. Lambert, Tripartite assembly of RND multidrug efflux pumps, Nat. Commun. 7 (2016), 10731.
[18] V. Koronakis, A. Sharff, E. Koronakis, B. Luisi, C. Hughes, Crystal structure of the bacterial membrane protein TolC central to multidrug efflux and protein export, Nature 405 (2000) 914–919.
[19] A.J. Hazel, N. Abdali, I.V. Leus, J.M. Parks, J.C. Smith, H.I. Zgurskaya, J. C. Gumbart, Conformational dynamics of AcrA govern multidrug efflux pump assembly, ACS Infect. Dis. 5 (2019) 1926–1935.
[20] X.Z. Li, H. Nikaido, Efflux-mediated drug resistance in bacteria, Drugs 64 (2004) 159–204.
[21] S. Murakami, R. Nakashima, E. Yamashita, T. Matsumoto, A. Yamaguchi, Crystal structures of a multidrug transporter reveal a functionally rotating mechanism, Nature 443 (2006) 173–179.
[22] H.-K. Tam, W.E. Foong, C. Oswald, A. Herrmann, H. Zeng, K.M. Pos, Allosteric drug transport mechanism of multidrug transporter AcrB, Nat. Commun. 12 (2021) 3889.
[23] E. Kapp, S.F. Malan, J. Joubert, S.L. Sampson, Small molecule efflux pump inhibitors in Mycobacterium tuberculosis: a rational drug design perspective, Mini-Rev. Med. Chem. 18 (2018) 72–86.
[24] Y. Wang, H. Venter, S. Ma, Efflux pump inhibitors: a novel approach to combat efflux-mediated drug resistance in bacteria, Curr. Drug Targets 17 (2016) 702–719.
[25] V. Thakur, A. Uniyal, V. Tiwari, A comprehensive review on pharmacology of efflux pumps and their inhibitors in antibiotic resistance, Eur. J. Pharmacol. 903 (2021), 174151.
[26] T.E. Renau, R. Leger, E.M. Flamme, J. Sangalang, M.W. She, R. Yen, C.L. Gannon, D. Griffith, S. Chamberland, O. Lomovskaya, S.J. Hecker, V.J. Lee, T. Ohta, K. Nakayama, Inhibitors of efflux pumps in Pseudomonas aeruginosa potentiate the activity of the fluoroquinolone antibacterial levofloxacin, J. Med. Chem. 42 (1999) 4928–4931.
[27] K.I. Yoshida, K. Nakayama, M. Obtsuka, N. Kuru, Y. Yokomizo, A. Sakamoto, M. Takemura, K. Hoshino, H. Kanda, H. Nitanai, K. Namba, K. Yoshida, Y. Imamura, J.Z. Zhang, V.J. Lee, W.J. Watkins, MexAB-OprM specific efflux pump inhibitors in Pseudomonas aeruginosa. Part 7: highly soluble and in vivo active quaternary ammonium analogue D13-9001, a potential preclinical candidate, Bioorg. Med. Chem. 15 (2007) 7087–7097.
[28] T.J. Opperman, S.M. Kwasny, H.S. Kim, S.T. Nguyen, C. Houseweart, S. D'Souza, G. C. Walker, N.P. Peet, H. Nikaido, T.L. Bowlin, Characterization of a novel pyranopyridine inhibitor of the AcrAB efflux pump of Escherichia coli, Antimicrob. Agents Chemother. 58 (2014) 722–733.
[29] T. Ohene-Agyei, R. Mowla, T. Rahman, H. Venter, Phytochemicals increase the antibacterial activity of antibiotics by acting on a drug efflux pump, Microbiologyopen 3 (2014) 885–896.
[30] C. Plé, H.-K. Tam, A. Vieira Da Cruz, N. Compagne, J.-C. Jiménez-Castellanos, R. T. Müller, E. Pradel, W.E. Foong, G. Malloci, A. Ballée, M.A. Kirchner, P. Moshfegh, A. Herledan, A. Herrmann, B. Deprez, N. Willand, A.V. Vargiu, K.M. Pos, M. Flipo, R.C. Hartkoorn, Pyridylpiperazine-based allosteric inhibitors of RND-type multidrug efflux pumps, Nat. Commun. 13 (2022) 115.
[31] H.A. Bohnert, W.V. Kern, Selected arylpiperazines are capable of reversing multidrug resistance in Escherichia coli overexpressing RND efflux pumps, Antimicrob. Agents Chemother. 49 (2005) 849–852.
[32] D. Du, X. Wang-Kan, A. Neuberger, H.W. van Veen, K.M. Pos, L.J.V. Piddock, B. F. Luisi, Multidrug efflux pumps: structure, function and regulation, Nat. Rev. Microbiol. 16 (2018) 523–539.
[33] J. Kobylka, M.S. Kuth, R.T. Müller, E.R. Geertsma, K.M. Pos, AcrB: a mean, keen, drug efflux machine, Ann. N. Y. Acad. Sci. 1459 (2020) 38–68.
[34] H. Sjuts, A.V. Vargiu, S.M. Kwasny, S.T. Nguyen, H.S. Kim, X.Y. Ding, A.R. Ornik, P. Ruggerone, T.L. Bowlin, H. Nikaido, K.M. Pos, T.J. Opperman, Molecular basis for inhibition of AcrB multidrug efflux pump by novel and powerful pyranopyridine derivatives, P. Natl.Acad. Sci.USA. 113 (2016) 3509–3514.
[35] S.T. Nguyen, S.M. Kwasny, X.Y. Ding, S.C. Cardinale, C.T. McCarthy, H.S. Kim, H. Nikaido, N.P. Peet, J.D. Williams, T.L. Bowlin, T.J. Opperman, Structure-activity relationships of a novel pyranopyridine series of Gram-negative bacterial efflux pump inhibitors, Bioorg. Med. Chem. 23 (2015) 2024–2034.
[36] Z. Aron, T.J. Opperman, Optimization of a novel series of pyranopyridine RND efflux pump inhibitors, Curr. Opin. Microbiol. 33 (2016) 1–6.
[37] D.T. Moir, T.J. Opperman, Z.D. Aron, T.L. Bowlin, Adjunctive therapy for multidrug-resistant bacterial infections: type III secretion system and efflux inhibitors, Drug Discov. Today 26 (2021) 2173–2181.
[38] Y. Wang, R. Mowla, L. Guo, A.D. Ogunniyi, T. Rahman, M.A. De Barros Lopes, S. Ma, H. Venter, Evaluation of a series of 2-napthamide derivatives as inhibitors of the drug efflux pump AcrB for the reversal of antimicrobial resistance, Bioorg.Med. Chem. Lett. 27 (2017) 733–739.
[39] Y. Wang, R. Alenazy, X. Gu, S.W. Polyak, P. Zhang, M.J. Sykes, N. Zhang, H. Venter, S. Ma, Design and structural optimization of novel 2H-benzo[h]chromene derivatives that target AcrB and reverse bacterial multidrug resistance, Eur. J. Med. Chem. 213 (2021), 113049.
[40] O. Lomovskaya, M.S. Warren, A. Lee, J. Galazzo, R. Fronko, M. Lee, J. Blais, D. Cho, S. Chamberland, T. Renau, Identification and characterization of inhibitors of multidrug resistance efflux pumps in Pseudomonas aeruginosa: novel agents for combination therapy, Antimicrob. Agents Chemother. 45 (2001) 105–116.
[41] R. Mowla, Y. Wang, S. Ma, H. Venter, Kinetic analysis of the inhibition of the drug efflux protein AcrB using surface plasmon resonance, Biochim. Biophys. Acta Biomembr. 1860 (2018) 878–886.
[42] M.-L. Wu, J. Tan, T. Dick, Eagle effect in nonreplicating persister mycobacteria, Antimicrob. Agents Chemother. 59 (2015) 7786–7789.
[43] J.A. Bohnert, B. Karamian, H. Nikaido, Optimized Nile Red efflux assay of AcrAB-TolC multidrug efflux system shows competition between substrates, Antimicrob. Agents Chemother. 54 (2010) 3770–3775.
[44] C. Jin, R. Alenazy, Y. Wang, R. Mowla, Y. Qin, J.Q.E. Tan, N.D. Modi, X. Gu, S. W. Polyak, H. Venter, Design, synthesis and evaluation of a series of 5-methoxy-2, 3-naphthalimide derivatives as AcrB inhibitors for the reversal of bacterial resistance, Bioorg. Med. Chem. Lett 29 (2019) 882–889.
[45] T.J. Opperman, S.T. Nguyen, Recent advances toward a molecular mechanism of efflux pump inhibition, Front. Microbiol. 6 (2015) 421.
[46] L. Amaral, A. Martins, G. Spengler, J. Molnar, Efflux pumps of Gram-negative bacteria: what they do, how they do it, with what and how to deal with them, Front. Pharmacol. (2014) 168.
[47] N. Zhang, D. Song, W. Chen, S. Zhang, P. Zhang, N. Zhang, S. Ma, Modification of 5-methylphenanthridium from benzothiazoles to indoles as potent FtsZ inhibitors: broadening the antibacterial spectrum toward vancomycin-resistant enterococci, Eur. J. Med. Chem. 224 (2021), 113723.
[48] D. Song, N. Zhang, P. Zhang, N. Zhang, W. Chen, L. Zhang, T. Guo, X. Gu, S. Ma, Design, synthesis and evaluation of novel 9-arylalkyl-10-methylacridinium derivatives as highly potent FtsZ-targeting antibacterial agents, Eur. J. Med. Chem. 221 (2021), 113480.
[49] P.R. Hunt, The C. elegans model in toxicity testing, J. Appl. Toxicol. 37 (2017) 50–59.
[50] W.C. Chai, J.J. Whittall, D. Song, S.W. Polyak, A.D. Ogunniyi, Y. Wang, F. Bi, S. Ma, S.J. Semple, H. Venter, Antimicrobial action and reversal of resistance in MRSA by difluorobenzamide derivatives targeted at FtsZ, Antibiotics 9 (2020) 873.
[51] D. Machado, L. Fernandes, S.S. Costa, R. Cannalire, G. Manfroni, O. Tabarrini, I. Couto, S. Sabatini, M. Viveiros, Mode of action of the 2-phenylquinoline efflux inhibitor PQQ4R against Escherichia coli, PeerJ 5 (2017) e3168.
[52] R.P. Lamers, J.F. Cavallari, L.L. Burrows, The efflux inhibitor phenylalanine-arginine beta-naphthylamide (PAbetaN) permeabilizes the outer membrane of gram-negative bacteria, PLoS One 8 (2013), e60666.
[53] W.J. Watkins, Y. Landaverry, R. Léger, R. Litman, T.E. Renau, N. Williams, R. Yen, J.Z. Zhang, S. Chamberland, D. Madsen, D. Griffith, V. Tembe, K. Huie, M. N. Dudley, The relationship between physicochemical properties, in vitro activity and pharmacokinetic profiles of analogues of diamine-Containing efflux pump inhibitors, Bioorg.Med.Chem. Lett. 13 (2003) 4241–4244.

83

[54] A. Lamut, L. Peterlin Mašič, D. Kikelj, T. Tomašič, Efflux pump inhibitors of clinically relevant multidrug resistant bacteria, Med. Res. Rev. 39 (2019) 2460–2504.
[55] I. Iso, 20776-1: 2019 (en) Susceptibility testing of infectious agents and evaluation of performance of antimicrobial susceptibility test devices–Part 1: Broth micro-dilution reference method for testing the in vitro activity of antimicrobial agents against rapidly growing aerobic bacteria involved in infectious diseases, International Organization for Standardization, Geneva (Switzerland), 2019, p. 20776, 20771.
[56] K.-i. Yoshida, K. Nakayama, M. Ohtsuka, N. Kuru, Y. Yokomizo, A. Sakamoto, M. Takemura, K. Hoshino, H. Kanda, H. Nitanai, MexAB-OprM specific efflux pump inhibitors in Pseudomonas aeruginosa. Part 7: highly soluble and in vivo active quaternary ammonium analogue D13-9001, a potential preclinical candidate, Bioorg. Med. Chem. 15 (2007) 7087–7097.
[57] H.T. Nguyen, H. Venter, T. Veltman, R. Williams, L.A. O'Donovan, C.C. Russell, A. McCluskey, S.W. Page, A.D. Ogunniyi, D.J. Trott, In vitro synergistic activity of NCL195 in combination with colistin against Gram-negative bacterial pathogens, Int. J. Antimicrob. Agents 57 (2021), 106323.
[58] X. Gu, L.A. Pisoni, Y. Wang, D. Song, M.J. Sykes, Y. Qin, S.J. Semple, S.W. Polyak, H. Venter, S. Ma, Design and synthesis of novel 4-substituted quinazoline-2-carboxamide derivatives targeting AcrB to reverse the bacterial multidrug resistance, Bioorg. Chem. 105 (2020), 104394.
[59] H. Venter, R.A. Shilling, S. Velamakanni, L. Balakrishnan, H.W. Van Veen, An ABC transporter with a secondary-active multidrug translocator domain, Nature 426 (2003) 866–870.
[60] S. Lin, J.-J. Koh, T.T. Aung, W.L.W. Sin, F. Lim, L. Wang, R. Lakshminarayanan, L. Zhou, D.T.H. Tan, D. Cao, R.W. Beuerman, L. Ren, S. Liu, Semisynthetic flavone-derived antimicrobials with therapeutic potential against methicillin-resistant Staphylococcus aureus (MRSA), J. Med. Chem. 60 (2017) 6152–6165.
[61] E. Tampakakis, I. Okoli, E. Mylonakis, A C. elegans-based, whole animal, in vivo screen for the identification of antifungal compounds, Nat. Protoc. 3 (2008) 1925–1931.
[62] W.C. Chai, J.J. Whittall, S.W. Polyak, K. Foo, X. Li, C.J. Dutschke, A.D. Ogunniyi, S. Ma, M.J. Sykes, S.J. Semple, Cinnamaldehyde Derivatives Act as Antimicrobial Agents against Acinetobacter Baumannii through the Inhibition of Cell Division, 2022.

3.3 Design and Synthesis of Flavonoid Derivatives as AcrB Inhibitors for the Reversal of Bacterial Multidrug Resistance

3.3.1 On-target effect of compound S4

In this study, four flavonoid derivatives (Appendix 1 Figure A.2) were evaluated *in vitro* for their antibacterial activity by through measuring the minimum inhibitory concentration (MIC) against the drug-resistant wild-type *E. coli* BW25113 strain and the antibiotic-sensitive strain with a deletion of the AcrB component of the AcrAB-TolC efflux pump (BW25113 ΔAcrB). Compound S4 displayed marginal antibacterial activity with an MIC of 256 μg/mL against wild-type *E. coli* BW 25113.

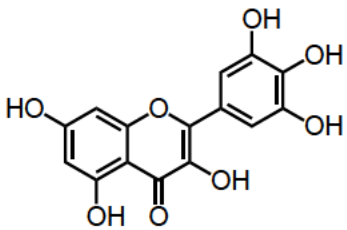
Compound S4 was also the only compound in the flavonoid series, that showed some potentiation activity. It reduced the MIC value of ERY by 2-fold at 128 μg/mL, and MIN by 2-fold at 64 μg/mL (Table 3.1).

Further checkerboard assays were then conducted in the presence of colistin to permeabilise the *E. coli* outer membrane, to allow antimicrobial agents entering the cells more easily. S4 reduced the MIC values of ERY and MIN by 2 folds only at 128 μg/mL (Table 3.1).

To determine if compound S4 had activity with the wild-type strain through action on the efflux pump specifically, the effects on efflux pump knockout strain of *E. coli* BW25113 were also tested. PAβN was used as a negative control to show that an EPI would not potentiate the effects of the antibiotics in the *E. coli* efflux pump knockout strain. Compound S4 lowered the MIC values of MIN by 4-fold at 128 μg/mL in the knockout strain (Table 3.2). This result suggested that compound S4 might have activities other than efflux inhibition. In the efflux inhibition assay, S4 did not inhibit Nile Red efflux at the highest concentration tested of 200 μM (Figure 3.3).

Table 3.1 The effect of flavonoid derivative(S4[#]) with different antimicrobial agents against the wild-type *E. coli* BW25113 alone and in the presence of membrane permeabiliser colistin.

Results are from assays performed in duplicate on at least two different days with different batches of cells.

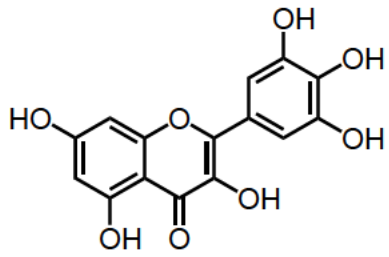
	Concentration (μg/mL)	MIC (μg/mL)					
		ERY*	**LEV***	**MIN***	**ERY* +COL***	**LEV* +COL***	**MIN* +COL***
S4	0	64	0.063	2	16	0.032	1
	8	64	0.063	2	16	0.032	1
	16	64	0.063	2	16	0.032	1
	32	64	0.063	2	16	0.032	1
	64	64	0.063	1	16	0.032	1
	128	32	0.063	1	8	0.032	0.5

*ERY = erythromycin, LEV = levofloxacin, MIN = minocycline, COL = colistin

#S4 is the only compound from the S series that showed an effect

Table 3.2 The effect of flavonoid derivative S4 with different antimicrobial agents against the drug sensitive *E. coli* BW25113 strain with a deletion in genomic *acrB* (*E. coli* BW25113 ΔAcrB).

Results are from assays performed in duplicate on at least two different days with different batches of cells.

Compound	Concentration (μg/mL)	MIC (μg/mL)		
		ERY*	LEV*	MIN*
S4	0	4	0.0063	0.25
	8	4	0.0063	0.125
	16	4	0.0063	0.125
	32	4	0.0063	0.125
	64	4	0.0063	0.125
	128	4	0.0063	0.0625

*ERY = erythromycin, LEV = levofloxacin, MIN = minocycline

#S4 is the only compound from the S series that showed an effect

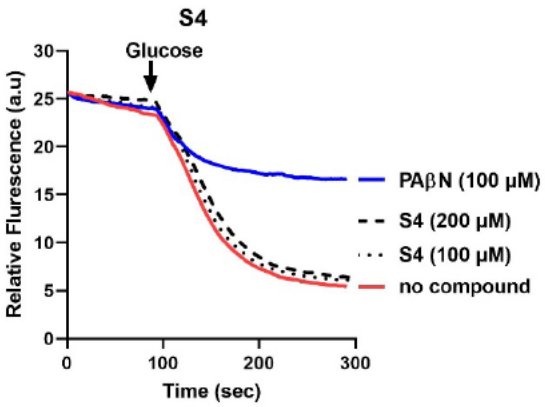


Figure 3.3 Compound S4 was not able to inhibit Nile Red efflux.

E. coli BW25113 (DE3) ΔAcrB cells containing pAcrB plasmid (red line) with no compound (efflux positive control), *E. coli* BW25113 (DE3) ΔAcrB cells containing pAcrB plasmid in the presence of PAβN (100 μM) as known inhibitor (efflux-negative control, blue line), and *E. coli* BW25113 (DE3) ΔAcrB cells containing pAcrB plasmid in the presence of different concentrations (100 μM, and 200 μM) of the target compounds (dotted lines) were preloaded with Nile Red before the start of fluorescence measurements. Efflux was triggered at 100 seconds by the addition of 0.2% glucose (indicated by the arrow). Representative fluorescent curves are shown for experiments with different batches of cells performed on three different days.

3.3.2 Off-target effects of compound S4

In the nitrocefin hydrolysis assay, the hydrolysis rate in the presence of S4 was much faster than that observed for the untreated cells, even though it was not as fast as for cells treated with the known membrane disruptor polymyxin B nonapeptide. This result suggested that S4 permeabilised the outer membrane at the maximum tested concentration of 128 μg/mL (Fig 3.4).

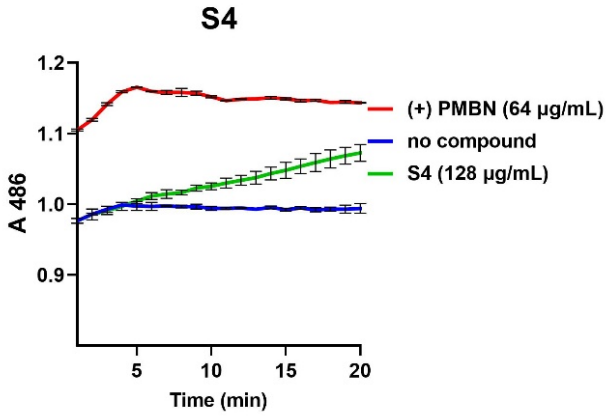


Figure 3.4 S4 permeabilised the bacterial outer membrane.

E. coli BW25113 wild-type cells were treated with 10 µM CCCP to inhibit the efflux of nitrocefin. Nitrocefin was added to the cells that received no compound (blue lines) or were treated with the outer membrane permeabiliser polymyxin B nonapeptide (PMBN, red lines) as the positive control or the test compounds at 128 µg/mL (green lines). Nitrocefin hydrolysis by the periplasmic β-lactamase was observed as an increase in A486. PMBN as positive control that permeabilise the outer membrane shows a fast initial rate of nitrocefin hydrolysis in comparison with the untreated cells. Representative traces are shown from experiments done on different days.

Unfortunately, S4 could not be tested for its effect on the inner membrane permeability because it has an intense yellow colour, which was found to quench the fluorescence of the potentiometric dye $DiOC_2(3)$, and thus, interfered with the assay.

Despite the off-target effects of compound S4 on the bacterial outer membrane, this compound did not show toxicity at 128 µg/mL on the *Caenorhabditis elegans* nematodes (Figure 3.5).

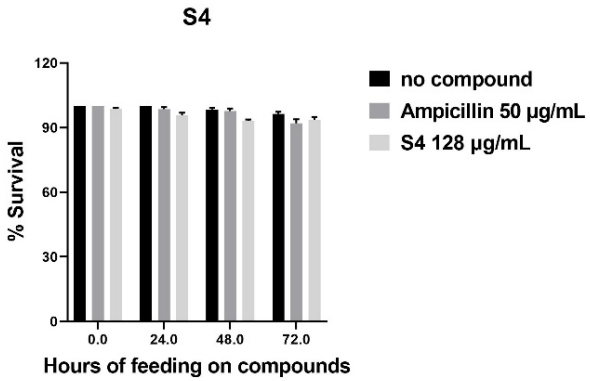


Figure 3.5 Effect of compound S4 on survival of *C. elegans* nematodes.

Synchronised adult *C. elegans* nematodes were harvested and investigated for toxicity in the presence of 128 μg/mL compounds S4 for 72 h. The nematodes were then to be counted under a light microscope at 400× magnification for up to 72 h every 24 h. The results are presented as nematodes survival curves of the percentage of alive nematodes. The results are presented in mean percentage of survival ± SEM. Statistical analysis was performed using two-way ANOVA and the asterisks (*) represent statistical significance, and (ns) represents no significance.

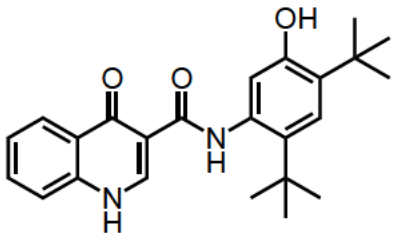
3.3.3 Conclusion

In conclusion, only compound S4 of flavonoid derivatives potentiated with ERY and MIN in the presence of membrane permeabiliser colistin. However, it lowered the MIC value of MIN against efflux pump knockout strain and was not able to inhibit Nile Red efflux at highest concentration tested. In addition, it also affected the bacterial outer membrane, but was not toxic on *C. elegans*. These results suggested that compound S4 might have activities other than efflux inhibition.

CHAPTER 4 Evaluation of Ivacaftor as MexB efflux pump inhibitor

4.1 Introduction

In the search for new therapeutic options to combat disease, a possible strategy is to find new uses for drugs that have already been approved for clinical use. The use of the drugs for a new purpose outside the scope of their original medical indication is called 'repurposing' (Pushpakom et al., 2019). In the search for new EPIs, our laboratory has examined the potential of repurposing existing drugs. A previous PhD study in our laboratory involved screening a database of Food and Drug Administration (FDA) -approved compounds for potential AcrB inhibitors using an *in-silico* approach (Pisoni, 2021 PhD thesis, A combined *in silico* and microbiological approach for the identification of novel efflux pump inhibitors against AcrAB-TolC, University of South Australia). In this study, a combined structure and ligand-based model was developed to screen compounds based on their structural similarities to known inhibitors of AcrB, as well as their *in silico* docking in various crystal structures of the AcrB protein. The highest scoring compounds were then subjected to *in vitro* testing to determine if they displayed inhibition of the AcrB efflux pump in *Escherichia coli*. In this study it was found that ivacaftor (Figure 4.1) was a drug which fulfilled all criteria required of a good EPI. Ivacaftor scored highly in the *in-silico* screening, and when tested *in vitro* it showed potentiation with the antibiotic substrates erythromycin and chloramphenicol against wild-type *E. coli* but did not show potentiation against an AcrB knock-out strain; it inhibited the efflux of Nile red in *E. coli* cells in a dose dependent manner; and did not have any effect on the *E. coli* bacterial outer membrane (OM).



Ivacaftor

Figure 4.1 Structure of ivacaftor

Ivacaftor is used in the treatment of the genetically inherited disease cystic fibrosis (CF). It is a potentiator of the cystic fibrosis transmembrane conductance regulator (CFTR) protein (Eckford et al., 2012; Rowe et al., 2014) which is a chloride channel found in epithelial cells. CF is caused by mutations in this CFTR gene that renders it defective and results in the build-up of thick mucus throughout the body, including in the respiratory tract (Goss & Burns, 2007). Ivacaftor is a potentiator in CFTR with a G551D mutation (~80% of CF patients) (S. M. Rowe et al., 2014). By improving the function of the CFTR protein ivacaftor helps to reduce the build-up of thick mucus in the lungs as well as improving other symptoms (O'Sullivan & Flume, 2009).

Chronic bacterial infection with *Pseudomonas aeruginosa* and other pathogens is the predominant cause of mortality in people suffering from cystic fibrosis (Bhagirath et al., 2016). These organisms are intrinsically resistant to multiple classes of antibiotics and can form impenetrable bacterial biofilms; hence very few treatment options remain (Bhagirath et al., 2016). It has been shown that ivacaftor can greatly improve clinical outcomes for people with CF, including lowering rates of infection caused by CF pathogens such as *P. aeruginosa* (Frost et al., 2019).

Drug efflux pumps are a main contributor to intrinsic drug resistance in pathogens such as *P. aeruginosa* (Arzanlou et al., 2017) They have also been shown to play a role in bacterial biofilm formation (Amaral et al., 2014; Baugh et al., 2014) and are needed to establish an infection (Colclough et al., 2020). Therefore, we hypothesised that ivacaftor has another role in CF, namely inhibition of non-specific drug efflux pumps and that this could contribute to the reduction in infection observed for people treated with ivacaftor (Davis et al., 2012). MexAB-

OprM is the main contributor to drug efflux in *P. aeruginosa* isolates (Masuda et al., 2000). As described in Chapter 1, MexB in *P. aeruginosa* shares 87 % sequence homology with AcrB and could even functionally substitute for AcrB in an AcrB-deleted strain (Krishnamoorthy et al., 2008; Piddock, 2006a; Welch et al., 2010). Tripartite efflux pump assemblies such as the AcrAB-TolC complex from *E. coli* and MexAB-OprM from *P. aeruginosa* are responsible for multi-drug resistance in Gram-negative bacteria (Arzanlou et al., 2017; Poole, 2007). Among these complexes, the inner membrane protein (IMP) is the key component responsible for drug recognition and binding (Eicher et al., 2009; Ohene-Agyei et al., 2012; Pos, 2009). Hence the compounds, which can directly block the drug binding with AcrB or MexB by binding with high affinity could be promising efflux pump inhibitors (EPIs) (Venter et al., 2015).

In this chapter the ability of ivacaftor to inhibit the MexB efflux protein from *P. aeruginosa* was investigated. At first, the binding affinity of inner membrane MexB with ivacaftor was tested using surface plasmon resonance (SPR). Our laboratory has previously optimised this method for measuring drug binding to AcrB (Mowla et al., 2018b). SPR is a very powerful biophysical tool for drug discovery. It allows the real time monitoring of binding actions and could directly determine the affinity and kinetic constants of biomolecular interactions (Puiu & Bala, 2016; Tikhonova & Zgurskaya, 2013). In addition, the galactose permease protein GalP, which is also an integral sugar binding protein of similar hydrophobicity to AcrB, was also used in the SPR study to as a control for non-specific binding (Mowla et al., 2018b; A. Welch et al., 2010). In the study described in this chapter, the AcrB, MexB and GalP proteins were purified, and the binding affinity of various potential inhibitors of AcrB and MexB was determined using SPR (Mowla et al., 2018b). Subsequently, the ability of ivacaftor to reverse resistance to antibiotics and to inhibit Nile Red efflux was investigated.

4.2 Results and discussion

4.2.1 Determining the kinetics of ivacaftor binding to MexB using Surface Plasmon Resonance (SPR)

4.2.1.1 The purification of inner membrane proteins

The plasmids pAcrB, pMexB and pGalP harbouring the His-tagged genes of AcrB, MexB and GalP respectively were transformed into competent cells of the *E. coli* expression strain C41 (DE3) to overexpress AcrB, MexB and GalP for purification.

The proteins were purified by Ni-NTA resin affinity chromatography by exploiting the His-tags at their C-terminals. The concentrations of purified His-tagged proteins were determined using the Bio-Rad DC protein assay. Notably, AcrB, MexB and GalP could be purified to yields of around 2 -3 mg of pure protein per litre of culture. The purity of the proteins was then confirmed with SDS-PAGE using a 10% acrylamide gel with the results shown in Figure 4.2. GalP runs at a MW lower than the calculated molecular weight (Figure 4.2). However, integral membrane proteins often run anomalously on SDS–PAGE because of different detergent binding and improper unfolding (Seyedmohammad et al., 2016; Ward et al., 1999).

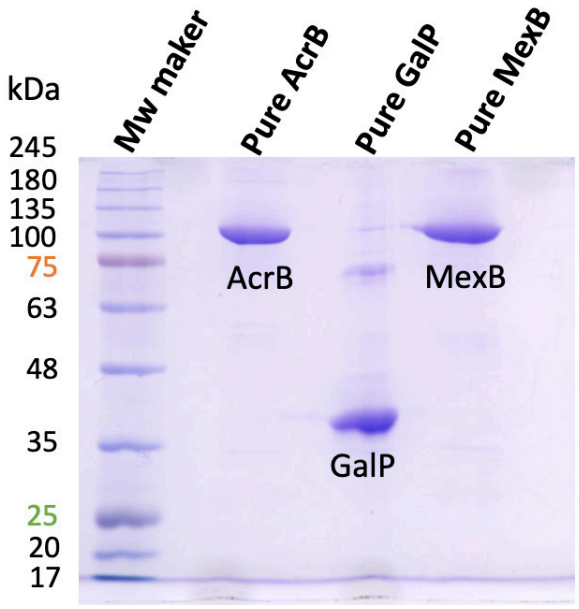


Figure 4.2 SDS-PAGE analysis of purified protein AcrB, GalP and MexB (each lane was loaded with 5 μg pure protein).

A 245 kDa GangNam pre-stained protein ladder (Lane 1) was used for evaluation. The purified AcrB protein (Lane 2), GalP protein (Lane 3) and MexB protein (Lane 4) were separated on a 10% acrylamide gel. SDS-PAGE was carried out at 150 V for 3 h. Proteins were visualised with Coomassie Brilliant Blue upon completion of electrophoresis. Purified AcrB (MW=112 kDa), GalP (MW=50.98 kDa) and MexB (MW=112.8 kDa) are indicated in text.

4.2.1.2 Immobilisation of proteins

Proteins were immobilised to the dextran matrix of a CM5 chip by amine coupling (Section 2.5) before the interaction of analytes to the protein surface was analysed after successful immobilisation of ligand to the chip surface. Integral membrane proteins such as AcrB and MexB have a large hydrophobic surface onto which lipophilic drugs can interact and bind in many ways in addition to binding to the target site. This non-specific binding forms a substantial part of the total binding response in integral membrane proteins. Therefore, it is necessary to correct for non- specific binding to determine the kinetic parameters for protein-substrate interaction. Due to the plasticity in the AcrB/MexB binding sites it is not possible to

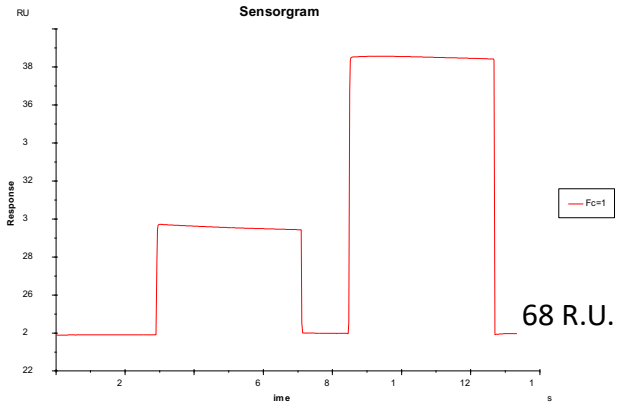
construct a mutant that does not bind substrates at all (Bohnert et al., 2008). Therefore, the sugar transporter GalP was also immobilised and used as a control for non-specific binding as it has a similar hydrophobicity as AcrB and MexB (Mowla et al., 2018b; Polyak et al., 2020). To obtain specific binding of inhibitors to MexB/AcrB and to correct for non-specific binding, R.U. values of GalP were manually subtracted from those of AcrB.

For analytes with strong binding, the surface has to be regenerated each time by using an appropriate regenerating agent. However, for interactions involving AcrB-substrates/inhibitors showed there was quick dissociation with the analytes washing off completely, therefore no regeneration was necessary. Indeed, the association and dissociation were both very fast, occurring literally within 30 seconds, which made the calculation of Kd for each interaction impossible for each injection. For this reason, a series of concentrations for each analyte was used as suggested previously by the group of Zgurskaya (Tikhonova et al., 2011).

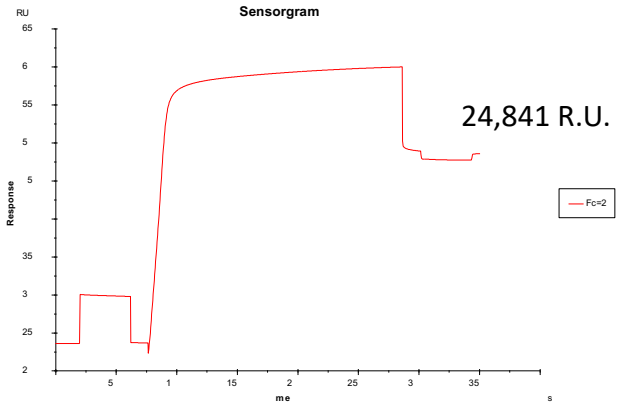
The data were then fitted with a one binding site hyperbola (GraphPad Prism 9) and the respective Kd values were calculated.

The total amount of protein immobilised to the chip surface was calculated from the R.U. achieved after immobilisation. Figure 4.3 shows representative sensograms of successful immobilisation of AcrB, MexB and GalP on the sensor surfaces.

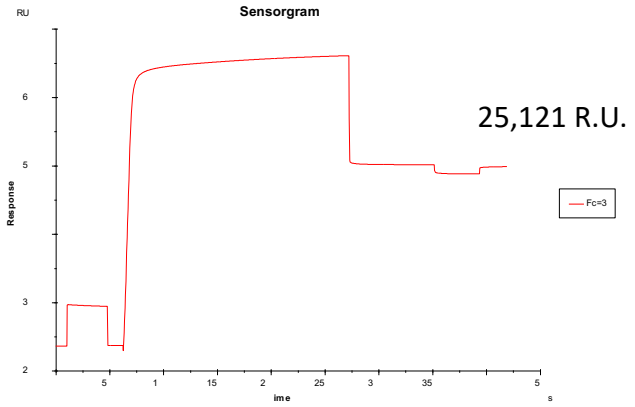
(A) Blank



(B) AcrB



(C) MexB



(D) GalP

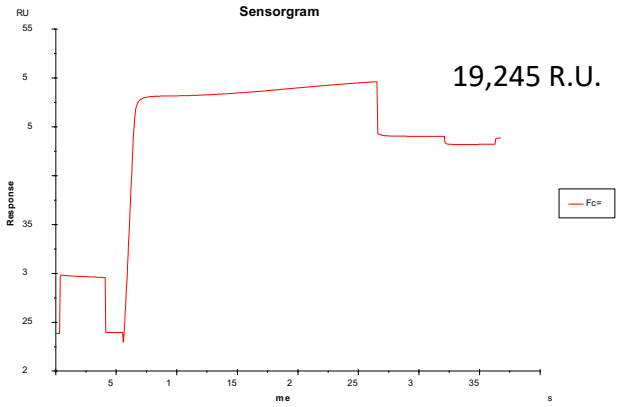


Figure 4.3 Immobilisation of (A) Blank (B) AcrB (C) MexB and (D) GalP on the CM5 chip surface.

The CM5 chip surface was activated by 15 µL/min injection of NHS/EDC mix for 15 mins after which proteins were injected at a flow rate of 10 µL/min. A control group of immobilisation buffer without any proteins (A Blank) was injected for 1250 seconds to achieve 68 R.U. AcrB (B) was injected for 2600 seconds to achieve 24,841 R.U. MexB (C) was injected for 2600 seconds to achieve 25,121 R.U. GalP (D) injection was stopped after at same time point to achieve 19,245 R.U. The remaining esters were blocked with Tris buffer pH 7.4 for 5 mins at 10 µL/min. A change in the response signal by 1,000 R.U. is equivalent to the change in a surface concentration of 1 ng protein/mm^2 or approximately 6–10 mg/mL in a bulk protein concentration (Biacore Assay Handbook), the concentrations of AcrB, MexB and GalP coupled to the chip surface were 50 µg/mL.

4.2.1.3 Binding affinity of PAβN and ivacaftor determined by SPR

For PAβN, binding affinity to AcrB was 56.32 µM (r^2=0.9999) (Figure 4.4 A), and to MexB it was 31.75 µM (r^2=0.9993) (Figure 4.4 B). The Kd obtained for ivacaftor binding with MexB was 39.64 µM (r^2=0.9985) (Figure 4.4 C). The results showed PAβN has similar binding affinity for AcrB and MexB. The binding of ivacaftor against AcrB could not be determined (results not shown) while the interaction of ivacaftor to MexB showed a similar Kd to that of PAβN, however as the reaction did not reach equilibrium, a substantial amount of non-specific binding might still have been observed. This resulted in a very high upper limit for the Kd value of ivacaftor binding to MexB, similar to that described before for SPR of ligands to AcrB in the absence of correction for non-specific binding (Tikhonova et al., 2011).

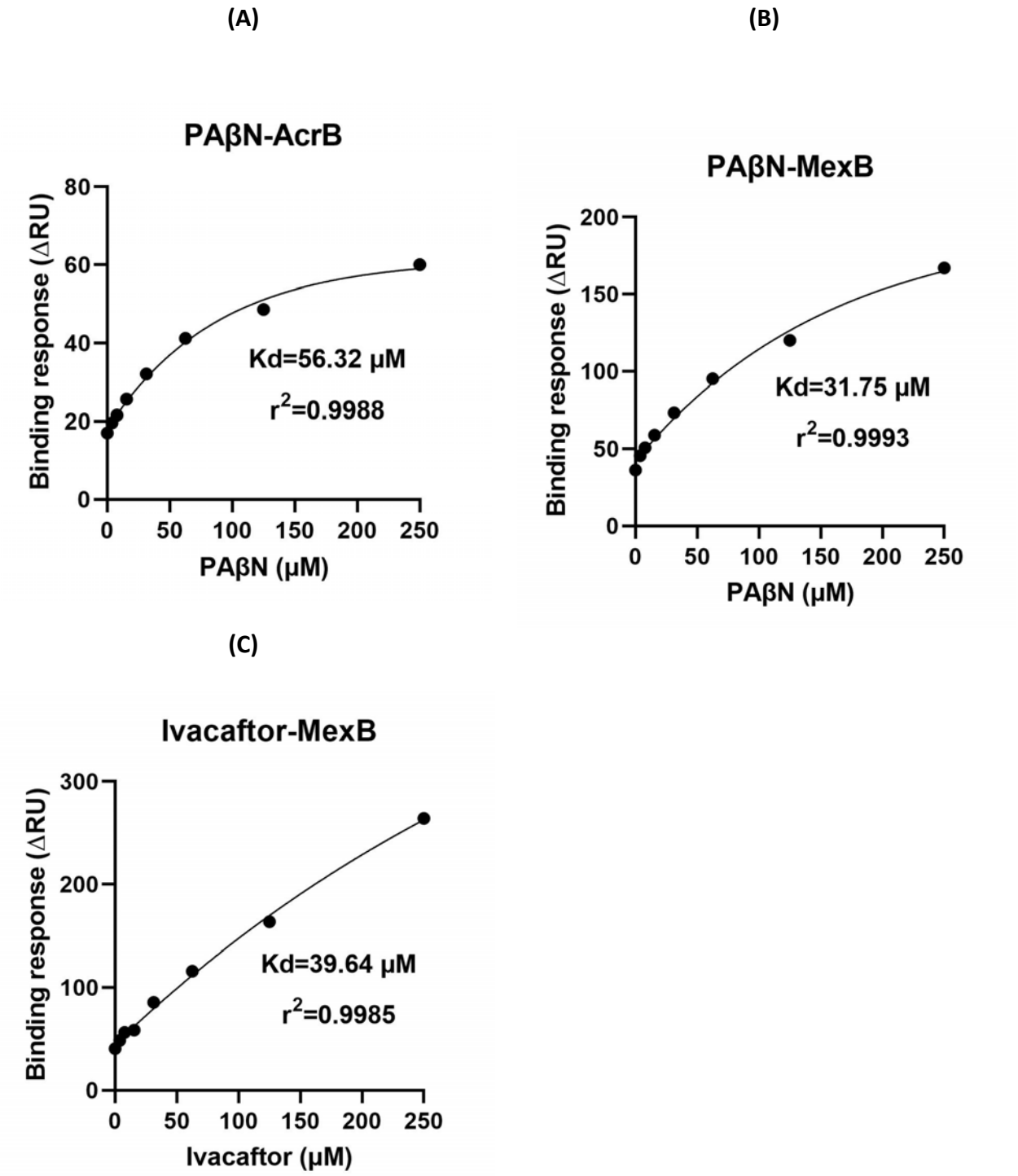


Figure 4.4 Kinetics of binding of PAβN and ivacaftor to purified AcrB and MexB using SPR.

The signals obtained for the specific binding of PAβN to AcrB (A) and MexB (B) and of ivacaftor to to MexB (C) were plotted against the concentrations of the compounds used. Data were analysed by fitting into a one-site specific binding hyperbola to obtain K_d. Results are representative of three independent experiments repeated on at least three different days with different batches of purified protein.

This project was the first to apply SPR techniques to study the effects of ivacaftor on MexB and provided evidence of a direct interaction between MexB and ivacaftor.

4.2.2 Antibacterial activity

The potential antibacterial activity of ivacaftor was assessed by determining its minimum inhibitory concentration (MIC) against the wild-type drug resistant strain of *P. aeruginosa* (PAM 1020), the antibiotic sensitive strain of *P. aeruginosa* lacking the *mexAB-oprM, mexEF-oprN* and *mexCD-oprJ* genes (PAM 1626), and the *P. aeruginosa* strain with that overexpresses the MexAB-OprM efflux pump (PAM 1032). This allowed the determination of the concentration of ivacaftor that could be added to the bacterial strains without producing a direct antibacterial activity in subsequent antimicrobial synergy assays. Ivacaftor showed no antibacterial activity against any of the three strains at the maximum tested concentration of 128 μg/mL.

4.2.3 Ability to reverse drug resistance

4.2.3.1 Three antibiotics were recognised as MexB substrates and one antibiotic as non-substrate

The ability of the compounds to recover the antibiotic activity conferred by the expression of the MexAB-OprM efflux pump was then determined with standard checkerboard assays in the presence of selective antibiotics along with various concentrations of ivacaftor (Lomovskaya et al., 2001; Ohene-Agyei et al., 2014). At first, the antimicrobial sensitivity of a

panel antibiotics was determined for PAM 1020, PAM 1032 and PAM 1626 to find out the best substrates of MexAB-OprM efflux pump. Based upon these results (Table 4.1), large variations between the three strains were identified for erythromycin (ERY), levofloxacin (LEV), and minocycline (MIN), which indicated these three antibiotics were efflux pump substrates. Tetracycline and meropenem were also considered for synergy testing however due to time limitations only three antimicrobials were used for synergy testing. In addition, these three chosen antimicrobials were given priority because they were used in the study described in Chapter 3. This allowed a more direct comparison of the activities on both MexB and AcrB using the same three antimicrobials. By contrast, minimal MIC differences (2-fold or none) between the three strains were found for tobramycin (TOB), which suggested that TOB was not a substrate for the efflux pump and could be used as a non-substrate control. Therefore, any effective (more than 2-fold) reduction of the MIC in TOB would indicate that the compound does not act specifically on the MexB efflux pump but acts by other mechanisms of action such as membrane permeabilisation.

Table 4.1 MICs for a panel of antibiotics against *P. aeruginosa* PAM 1020 (*P. aeruginosa* wild type), PAM 1032 (*P. aeruginosa* with MexAB-OprM overexpressed) and PAM 1626 (*P. aeruginosa* lacking the *mexAB-oprM, mexEF-oprN* and *mexCD-oprJ* genes).

Results are from assays performed in duplicate on at least two different days with different batches of cells.

Antibiotics	MIC (μg/mL)		
	PAM 1020 (WT)	PAM 1032 (MexAB-OprM Overexpressed)	PAM 1626 (Efflux pump Knockout)
Erythromycin	128	256	16
Levofloxacin	1	4	0.031
Minocycline	64	128	0.5
Tobramycin	1	1	0.5
Tetracycline	32	128	1
Meropenem	1	4	0.125
Chloramphenicol	128	512	256
Oxacillin	>512	>512	256
Novobiocin	>512	>512	128
Tetraphenylphosphonium chloride (TPP)	>512	>512	256

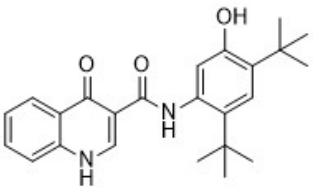
4.2.3.2 Potentiation of antibiotics by ivacaftor in *P. aeruginosa*

Ivacaftor was tested for antibiotic potentiating effects with ERY, LEV, and MIN against the wild-type *P. aeruginosa* (PAM 1020) and the efflux pump overexpressed *P. aeruginosa* (PAM 1032) to evaluate the ability to reverse antimicrobial resistance using standard checkerboard

assays (Lomovskaya et al., 2001; Ohene-Agyei et al., 2014). Checkerboard assays with the non-substrate tobramycin were conducted to show the specificity. The known EPI, PAβN, was also included as a positive control to demonstrate the potentiation effect with antibiotics. Despite the SPR results showing ivacaftor binding to MexB, ivacaftor was not able to synergise with erythromycin, levofloxacin or minocycline in either *P. aeruginosa* WT (PAM 1020; Table 4.2) or the *P. aeruginosa* that overexpresses MexAB-OprM (PAM 1032, Table 4.3). Since ivacaftor was able to inhibit resistance and efflux in AcrB (Pisoni, 2021 PhD thesis, A combined *in silico* and microbiological approach for the identification of novel efflux pump inhibitors against AcrAB-TolC, University of South Australia) and was shown to bind to the purified MexB protein, a reasonable explanation for this result could be that ivacaftor is not able to penetrate through the outer membrane of *P. aeruginosa* as has been described for many other compounds (Krishnamoorthy et al., 2017; Leus et al., 2023; López et al., 2020; Nikaido & Vaara, 1985). To investigate this hypothesis, the effect of ivacaftor on efflux pump driven antimicrobial resistance in *P. aeruginosa* was investigated in the presence of membrane permeabilisers.

Table 4.2 The minimum inhibitory concentration for ERY, LEV, MIN, and TOB against the wild-type *P. aeruginosa* (PAM 1020) at different concentrations of ivacaftor and EPI control PAβN.

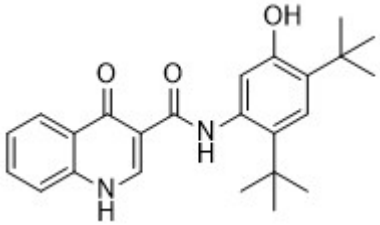
Results are from assays performed in duplicate on at least two different days with different batches of cells.

	Concentration (mg/mL)	MIC (mg/mL)			
		ERY*	**LEV***	**MIN***	**TOB***
Ivacaftor	0	128	1	64	1
	8	128	1	64	1
	16	128	1	64	1
	32	128	1	64	1
	64	128	1	64	1
	128	128	1	64	1
PAβN	0	128	1	64	1
(Positive control)	8	32	0.5	16	1
	16	16	0.25	16	1
	32	8	0.25	16	1
	64	4	0.25	16	1
	128	4	0.06	8	1

*ERY = erythromycin, LEV = levofloxacin, MIN = minocycline, TOB = tobramycin

Table 4.3 The minimum inhibitory concentration for ERY, LEV, MIN, and TOB against the efflux pump overexpressed strain of *P. aeruginosa* (PAM 1032) at different concentrations of test ivacaftor and EPI control PAβN.

Results are from assays performed in duplicate on at least two different days with different batches of cells.

	Concentration (mg/mL)	MIC (mg/mL)			
		ERY*	**LEV***	**MIN***	**TOB***
Ivacaftor	0	256	4	128	1
	8	256	4	128	1
	16	256	4	128	1
	32	256	4	128	1
	64	256	4	128	1
	128	256	4	128	1
PAβN	0	256	4	128	1
(Positive control)	8	64	2	32	1
	16	64	2	16	1
	32	32	1	16	1
	64	16	0.25	16	1
	128	8	0.13	8	1

*ERY = erythromycin, LEV = levofloxacin, MIN = minocycline, TOB = tobramycin

4.2.3.3 Potentiation of antibiotics by ivacaftor against *P. aeruginosa* in the presence of membrane permeabilisers colistin, and PMBN.

To investigate the hypothesis that the outer membrane of *P. aeruginosa* serves as a barrier for ivacaftor penetration the checkerboard assays were repeated in the presence of the outer membrane permeabilisers colistin or polymyxin B nonapeptide (PMBN) at sub-MIC concentrations as we have done before (Nguyen et al., 2021; Pi et al., 2020; Pi et al., 2022). At first the MIC values for each of the three permeabilisers were determined. As expected from the mechanism of action of these three compounds, the MIC values were not influenced

by the absence or presence of a drug efflux pump and all three the test strains had the same MIC values of 2 μg/mL each for colistin and PMBN (Table 4.4).

Table 4.4 The minimum inhibitory concentration for colistin, and PMBN against PAM 1020, PAM 1032, and PAM 1626.

Results are from assays performed in duplicate on at least three different days with different batches of cells.

Membrane permeabiliser	Minimum inhibitory concentration (MIC)		
	PAM 1020 (Wild type)	PAM 1032 (MexAB-OprM overexpressed)	PAM 1626 (Efflux pumps deleted)
Colistin	2 μg/mL	2 μg/mL	2 μg/mL
PMBN	2 μg/mL	2 μg/mL	2 μg/mL

The potential for synergy between colistin or PMBN and ivacaftor was investigated with checkerboard assays. Both outer membrane permeabilisers synergised with ivacaftor to bestow antimicrobial activity on ivacaftor (Table 4.5).

Table 4.5 The MIC values for ivacaftor in the presence of colistin or PMBN.

	Minimum inhibitory concentration (MIC) in μg/mL					FIC
	Single compounds			Combinations		
	Colistin	**PMBN**	**Ivacaftor**	**Colistin : Iva**	**PMBN : Iva**	
PAM 1020 (Wild-type)	2	2	>128	1 : 2	1 : 8	0.5*
PAM 1032 (MexAB-OprM overexpressed)	2	2	>128	1 : 2	1 : 8	0.5*

FIC, fractional inhibitory concentration index. * synergistic, FIC ≦ 0.5; additive or partially synergistic, 0.5 < FIC ≦ 1; indifferent, 1 < FIC ≦ 4; and antagonistic, FIC >4.

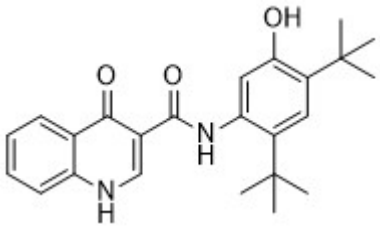
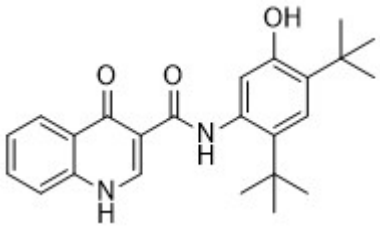
Colistin and PMBN were then used in addition to ivacaftor in the checkerboard assays against PAM 1020 (wild type strain) and PAM 1032 (efflux pump overexpressed strain) respectively. Ivacaftor was able to potentiate the activity of all the three tested antibiotics at low concentrations in the presence of the outer membrane permeabilisers. Significantly, there is a dramatic increase in ivacaftor efficacy with reduction in MIC values already being observed at ivacaftor concentrations as low as 0.5 μg/mL and synergy being observed at ivacaftor concentrations of 2 μg/mL. The most dramatic activity was found in the presence of PMBN. In the presence of 1 μg/mL PMBN, ivacaftor reduced the MIC value of ERY by 8-fold at 4 μg/mL against PAM 1032 (MexAB-OprM overexpressed). It also obtained a reduction of 4-fold at 8 μg/mL for all the three antibiotics (ERY, LEV and MIN) against PAM 1020 (Wild-type) strain. Ivacaftor also achieved good synergism in the presence of 0.5 μg/mL colistin. Notably, in this combination, ivacaftor reduced the MIC value for ERY at 4μg/mL, and for LEV and MIN by 8-fold at 4 μg/mL against PAM 1020 (Wild-type) strain. It also reduced the MIC for ERY by

4-fold at 2 μg/mL, for LEV by 8-fold at 4 μg/mL, and for MIN by 4-fold at 4 μg/mL against PAM 1032 (MexAB-OprM overexpressed).

Table 4.6 The minimum inhibitory concentration for ERY, LEV, MIN, and TOB against the wild-type *P. aeruginosa* (PAM 1020) at different concentrations of ivacaftor in the presence of 0.5 μg/mL colistin.

Results are from assays performed in duplicate on at least three different days with different batches of cells.

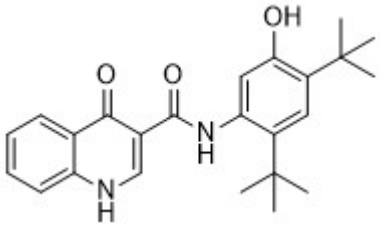
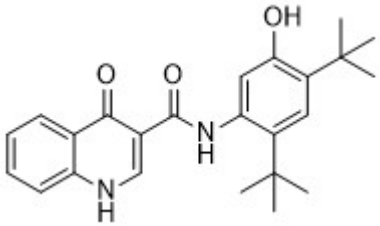
*ERY = erythromycin, LEV = levofloxacin, MIN = minocycline, TOB = tobramycin

	Concentration (mg/mL)	MIC (mg/mL)			
		ERY	**LEV**	**MIN**	**TOB**
Against PAM 1020					
Ivacaftor 	0	64	1	8	0. 25
	0.5	64	1	4	0.25
	1	64	0.5	4	0. 25
	2	32	0.5	4	0. 25
	4	16	0.125	1	-
Against PAM 1032 (MexAB-OprM overexpressing)					
Ivacaftor 	0	128	4	16	0. 25
	0.5	128	2	8	0.25
	1	64	2	8	0. 25
	2	32	1	8	0. 25
	4	-	0.5	4	-

*ERY = erythromycin, LEV = levofloxacin, MIN = minocycline, TOB = tobramycin. - indicates not tested.

Table 4.7 The minimum inhibitory concentration for ERY, LEV, MIN, and TOB against the wild-type *P. aeruginosa* (PAM 1020) the efflux pump overexpressed strain of *P. aeruginosa* (PAM 1032) at different concentrations of ivacaftor in the presence of 1 μg/mL PMBN.

Results are from assays performed in duplicate on at least three different days with different batches of cells.

Compound	Concentration (μg/mL)	MIC (μg/mL)			
		ERY	**LEV**	**MIN**	**TOB**
Against PAM 1020					
Ivacaftor 	0	2	0.0312	1	2
	1	1	0.0312	1	2
	2	1	0.0156	1	2
	4	1	0.0156	0.5	2
	8	0.5	0.007	0.25	2
Against PAM 1032					
Ivacaftor 	0	8	0.125	2	2
	1	4	0.063	1	2
	2	4	0.063	1	2
	4	4	0.063	1	2
	8	2	0.031	1	2
	16	1	0.031	0.5	2

*ERY = erythromycin, LEV = levofloxacin, MIN = minocycline, TOB = tobramycin

In the agreement with these results, the combination of antibiotics/ivacaftor/outer membrane permeabilisers was strongly synergistic (a 4-fold reduction or greater was considered as a synergistic effect). It demonstrated that ivacaftor caused a dramatic sensitization of strain PAM 1020 and PAM 1032 to ERY, LEV and MIN in the presence of sub-MIC amounts of colistin or PMBN.

4.2.4 Nile Red efflux

Nile Red efflux assays were then performed to determine the effects of ivacaftor to inhibit the transport of an efflux substrate through MexB. Nile Red is a known substrate of AcrB. It is weakly fluorescent in the aqueous solution but strongly fluorescent in non-polar environments, such as DNA and the cell membrane (Bohnert et al., 2010; Ohene-Agyei et al., 2014). Thus, the reduction of Nile Red fluorescence can be observed as an indication of expulsion of the substrate from the inside of the cells to the outside (Wang et al., 2017). As MexB shares a high similarity to AcrB in structure and function, our hypothesis was that the Nile Red efflux assay could also be used in the measurement of MexB inhibition. The efflux pump MexAB-OprM overexpressed *P. aeruginosa* (PAM 1032) strain was used in the Nile Red efflux assays. Cells were preloaded with Nile Red and the drop in fluorescence after the energisation of cells by glucose addition was measured. The ability of the ivacaftor to inhibit Nile Red efflux was measured by the relative fluorescence, compared to PAM 1032 cells in the presence of the established RND-type efflux pump inhibitor, PAβN. In the efflux assay, ivacaftor was tested at 100 μM and 200 μM and PAβN at 100 μM. Ivacaftor at 200 μM was able to abolish Nile Red efflux activity (Figure 4.5). This was comparable with a previous study in our lab, where ivacaftor showed partial inhibition at 100 μM and full inhibition at 200 μM for AcrB in *E. coli* (Pisoni, 2021 PhD thesis, A combined *in silico* and microbiological approach for the identification of novel efflux pump inhibitors against AcrAB-TolC, University of South Australia). Although the effect of the known inhibitor control PAβN at this concentration was not as clear as what is typically seen with AcrB in the Nile Red assay (Gu et al., 2020), this assay had not previously been conducted with MexB and could be further optimised in future studies with different concentrations of PAβN.

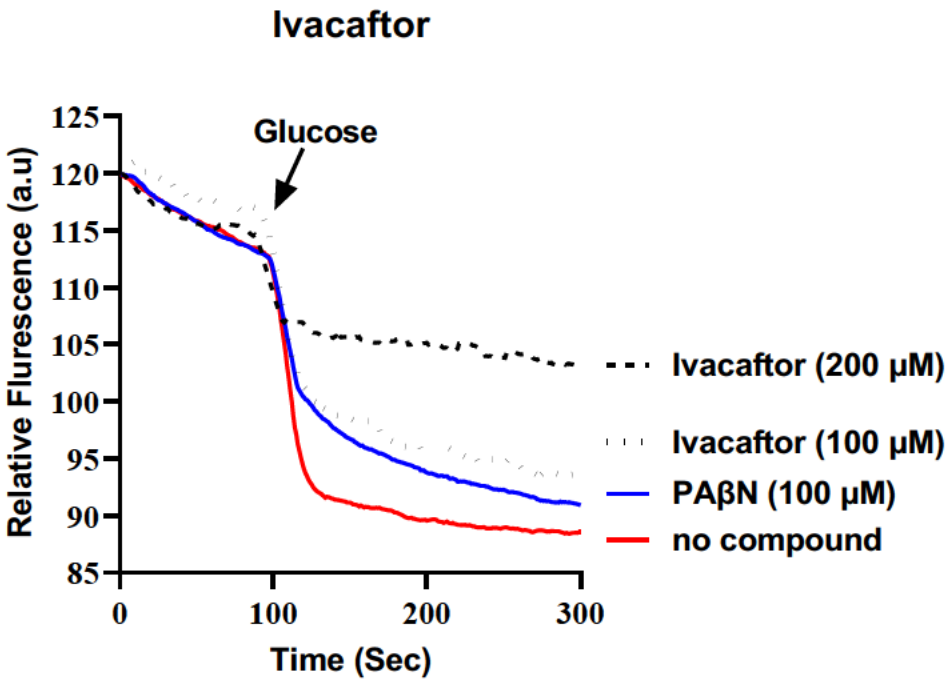


Figure 4.5 Inhibition of Nile Red efflux by ivacaftor.

The efflux pump MexAB-OprM overexpressing *P. aeruginosa* (PAM 1032) cells without any compound (red line), or in the presence of PAβN (100 μM) as known inhibitor control (blue line), or different concentrations (100 μM and 200 μM) of ivacaftor (dotted lines) were preloaded with Nile Red (10 μM) before the start of fluorescence measurements. Efflux was then triggered at 100 seconds by the adding of 0.2 % glucose (indicated by the arrow). Representative fluorescent curves are shown for experiments with different batches of cells performed on three different days.

4.3 Conclusion

Ivacaftor has been identified as AcrB inhibitor in a previous study in our laboratory. It showed potentiation with the ERY and chloramphenicol (CAM) against wild-type *E. coli*, and also inhibited the Nile Red efflux at 200 μM (Pisoni, 2021 PhD thesis, A combined *in silico* and microbiological approach for the identification of novel efflux pump inhibitors against AcrAB-TolC, University of South Australia). It is an approved drug that used clinically for CF treatment. When used clinically it has been shown to reduce the rates of infections in CF patients caused

by *P. aeruginosa*. Therefore, we hypothesised that ivacaftor has the potential to be putative MexB inhibitor and investigated the hypothesis. In the investigation, we wanted to identify the activities of ivacaftor to act as a MexB inhibitor, and to find out whether ivacaftor's effect on efflux pumps could also contribute to combatting infection in CF patients. As a result, in the presence of outer membrane permeabilisers colistin or PMBN, ivacaftor was able to enhance the activity of all three tested antibiotics (ERY, LEV, and MIN) (at least 4-fold reduction of their MICs) against both wild type and MexAB-OprM overexpressed strains of *P. aeruginosa* at a low concentration of 4 μg/mL ivacaftor (10.2 μM). This activity is comparable to other EPIs in current development where the inhibitors with the highest efficacy are reported to fully potentiate antimicrobial activity at 3 μM (Sjuts et al., 2016).

An explanation of why ivacaftor failed to potentiate the antibiotics alone against *P. aeruginosa* is the low membrane permeability of the *P. aeruginosa* outer membrane (Hancock & Brinkman, 2002). Hence the ability of ivacaftor to synergise with antibiotics was achieved by the addition of either colistin or PMBN. These classic membrane permeabilisers, weaken the permeability of the outer membrane by binding with the lipopolysaccharides (LPS) of the outer membrane (Vaara et al., 1983). We were also able to show inhibition of substrate efflux by ivacaftor as ivacaftor at 200 μM was able to completely inhibit the efflux of Nile Red. To conclude, these findings suggest that ivacaftor could be acting as a MexB inhibitor to reduce the efflux pump driven antibiotic resistance in *P. aeruginosa*. Since efflux pumps also play a role in biofilm formation and virulence, ivacaftor also has the potential to reduce biofilm formation and regulate the excretion of virulence thereby reducing infection in CF patients. Hence the effect of ivacaftor on biofilm formation and virulence could also be an important target to investigate in future studies.

CHAPTER 5 General Discussion, Conclusions and Future Directions

5.1 Introduction

Antimicrobial resistance (AMR) has been identified as one of the biggest threats to modern medicine and public health (Murray et al., 2022). New approaches to combat drug resistant bacteria and address the shortage of new antimicrobials are desperately needed, particularly for Gram-negative bacteria. As described in Chapter 1, the drug efflux pumps present in bacterial pathogens have been proposed as promising drug targets for the control of infections caused by multidrug resistant bacteria.

Bacterial drug efflux pumps play a crucial role in multidrug resistance (MDR), biofilm formation and virulence. Drug efflux pumps expel a variety of structurally distinct classes of antimicrobials, as well as biocides reducing their concentration inside bacterial cells to sub-lethal levels (Nikaido & Pagès, 2012; Piddock, 2006a; Poole, 2004; Venter et al., 2015). (Webber & Piddock, 2003), thereby facilitating bacteria to acquire an MDR phenotype (Piddock, 2006a; Poole, 2004; Venter et al., 2015). Additionally, they are responsible for transporting bacterial substances necessary for pathogenesis, including the quorum sensing chemical messages and components of biofilms. Therefore, they also play a critical role in virulence (Fernando & Kumar, 2013).

This thesis details the identification and evaluation of compounds as inhibitors of RND efflux pumps in Gram-negative bacteria including the AcrAB-TolC efflux pump in *E. coli* and MexAB-OprM efflux pump in *Pseudomonas*. These microorganisms are amongst the most critical in terms of the need for new antimicrobial drugs and compounds to tackle multidrug resistance (WHO 2017). In this project the inner membrane protein, AcrB of AcrAB-TolC and MexB of MexAB-OprM were targeted for the discovery and development of putative inhibitors for the bacterial drug efflux pumps. Many of the previously studied efflux pump inhibitors (EPIs) have failed to enter clinical use due to non-specific effects and toxicity (Compagne et al., 2023). The issues with previously identified EPIs include mammalian cell toxicity for PAβN (Lomovskaya et al., 2006), off-target effects for NMP (Bolla et al., 2011), and a limited range of *in vivo* potency for the MBX derivatives (Opperman et al., 2018) and D13-9001 (Yoshida et al., 2007). Since off-target activity and cytotoxicity are some of the issues hampering further

progression of EPIs, these issues were addressed in this thesis. Off-target activity was investigated by testing the outer- and inner membrane permeability. In this project, an *in vivo Caenorhabditis elegans* nematode survival model was used to investigate the toxicity of compounds in a cheap and time-efficient way prior to testing in more complex mammalian animal models. The determination of *in vivo* efficacy would be the next step using a nematode model of infection (Kirienko et al., 2014). For example, *C. elegans* can be infected with *P. aeruginosa* and the ability of compounds to promote the survival of infected worms can be assessed (Dharmalingam et al., 2012; Sebastián et al., 2019). This could identify the most promising candidate compounds to investigate further in mouse models of infection such as the a luminescent model our group has used previously to assess the *in vivo* activity of new antimicrobial compounds (Nguyen et al., 2021; Nguyen et al., 2022; Pi et al., 2020; Pi et al., 2021). This model uses recombinant luciferase-expressing strains of bacteria to monitor the bacterial burden data in individual mice using a biophotonic imaging system (Ogunniyi et al., 2018).

5.2 Synthetic efflux pump inhibitors

In Chapter 3 the biological activities of a series of benzo[h]chromene and flavonoid derivatives are reported that were designed and synthesised by our collaborators from Shandong University, China. These compounds were based on the novel EPIs MBX 2319 and A3 as well as the natural antimicrobial compound quercetin. Thirty-nine benzo[h]chromene and flavonoid derivatives were firstly evaluated for their efficacy as AcrB inhibitors. Six of the benzo[h]chromene derivates (G6, G10, G11, H3, H5 and H6) were identified as potential EPIs owing to their antibacterial sensitising activity against *E. coli*, leading to a 2 to 32 fold reduction in the MIC values of at least one of the antibiotics tested (erythromycin (ERY), levofloxacin (LEV) and minocycline (MIN)). They also displayed strong inhibition of Nile Red efflux (Guo et al., 2023). These compounds did not have off-target effects such as outer membrane disruption or permeabilisation of the inner membrane (with the exception of compound G10). None of the six compounds displayed toxicity in the *C. elegans* (in vivo toxicity model).

In terms of the structure activity relationships for the benzo[h]chromene derivatives, the results suggested that the R group structure of the 4-methoxyphenoxypropoxy (in G6) and 4-aminophenyl (in G11) were important for more potent EPI activity. Another EPI called A3, which has been previously published by our group, is the compound from which the G and H series compounds in this study were developed (Wang et al., 2017). Compound A3 produced an 8-fold reduction of the MIC value of erythromycin at 512 μg/mL in a previous study (Wang et al., 2016), while the best performing compound G6 resulted in an 8-fold reduction of the MIC value of erythromycin at a lower concentration of 128 μg/mL. Furthermore, G6 caused a 16-fold reduction in the MIC value of erythromycin in the presence of the membrane permeabiliser colistin. At 50 μM Compound G6 was more active in inhibiting Nile Red efflux compared to the parent compound A3 (A3 could partially inhibit Nile Red efflux at 50 μM and fully inhibit efflux at 100 μM) (Wang et al., 2016). In this current study the *C. elegans* model was used to test the compounds for *in vivo* toxicity. Previous studies examining A3 used mammalian cell lines to examine *in vitro* cytotoxicity, but no *in vivo* toxicity testing had previously been undertaken on A3 or any of its derivatives. In summary, G6 seems to have better efficacy and at lower concentrations compared to A3. In future studies, modifications to the R side chain of G6 could be made to further optimise the EPI activity.

The effects on bacterial inner membrane permeability were examined for the six most active compounds. A compound that exhibits effects on inner membrane permeability is not desirable as it may also be harmful to mammalian cells. For example, polymyxin B and colistin are compounds that are known to act on the inner membrane of Gram-negative bacteria but can also affect the permeability of mammalian cells which at least in part explains why they have considerable potential to produce nephrotoxicity when used clinically (Gai et al., 2019). Daptomycin is an example of an antibiotic which targets the cytoplasmic membrane of Gram-positives it is used clinically but can produce toxicity to skeletal muscle cells (Yamada et al., 2020). Amongst the six active compounds only compound G10 was found to have an off-target effect on the bacterial inner membrane. It is noteworthy, however, that compound G10 was not toxic to *C. elegans* at the tested concentration. Another issue with compounds that disrupt bacterial inner membranes is that the proton motive force (p.m.f) can be easily disrupted by such compounds (Venter et al., 2015). The p.m.f is an electrochemical gradient

of protons, generated across the membrane (Nicholls, 1974). If the membrane is disrupted, then the gradient will also be disrupted. The function of RND efflux pumps is also driven by the p.m.f (Venter et al., 2015). Hence a compound like G10 that has inner membrane disruption, may also inhibit the efflux pump in a non-specific manner.

One of the flavonoid derivatives, compound S4, had activity in terms of potentiating the activity of erythromycin and minocycline against *E. coli*. However, it was also found to have effects on the bacterial membrane and to exhibit some intrinsic antibacterial activity. Therefore, this suggested that the activity of S4 was not a specific effect on the AcrB efflux pump.

Significantly the 3,4-dihydro-2H-benzo[h]chromen-5-yl)(morpholino)methanone core of benzo[h]chromene derivatives appears to be a promising and novel chemical skeleton for the further pursuit of new AcrB inhibitors without off-target effects *in vitro* or cytotoxicity. Further series of compounds based on the best performing compounds identified in this study should be developed in the future with a focus on enhanced interactions with the AcrB binding site and the hydrophobic trap to increase EPI potency. The improved activity found with some of the compounds in the presence of the membrane permeabiliser colistin suggests that the bacterial outer membrane may be a barrier to the entry of these compounds into the bacterial cell. In future studies, there is the possibility to investigate the employment of Hergenrother's 'eNTRy' rules (Muñoz & Hergenrother, 2021) to chemically alter the best compounds so that they can penetrate the outer membrane of Gram-negatives more easily. These rules are based on studies showing that small molecules that contain an 'ionisable Nitrogen, have low Three-dimensionality, and are Rigid' are more likely to accumulate in *E. coli* cells (Muñoz & Hergenrother, 2021).

One of the limitations of this study is the aqueous solubility of the compounds. Some small molecule compounds that can bind to the 'hydrophobic trap' next to the distal binding pocket in AcrB can completely inhibit the efflux pump (Du et al., 2018; Sjuts et al., 2016). However, this tends to lead to the discovery of hydrophobic compounds with low aqueous solubility. Therefore, our future studies also need to focus on the solubility aspects of these compounds, as well as the biological efficacy of the compounds. For example, the Opperman group has

made chemical modifications to increase aqueous solubility of MBX efflux pump inhibitors (Aron & Opperman, 2016).

AcrB has a very broad substrate recognition profile and constitutive expression of AcrB renders the bacteria resistant to many antibiotic classes (Venter et al., 2015). Moreover, orthologues of this pump are present in many other Gram-negative bacteria, for example MexB in *P. aeruginosa* that shares 86% amino acid sequence identity with AcrB (Piddock, 2006a; A. Welch et al., 2010). Therefore, EPIs developed against AcrB have the potential to be effective in other Gram-negative organisms too. Hence, it is worth extending the evaluation of the six benzo[h]chromene compounds identified as AcrB inhibitors to MexB and RND efflux pumps from other Gram-negative bacteria.

5.3 Repurposed efflux pump inhibitor, ivacaftor

In Chapter 4, the investigation into ivacaftor as a potential inhibitor of the MexB efflux pump from the MexAB-OprM complex in *P. aeruginosa* was reported. Ivacaftor is a transmembrane conductance protein potentiator that is clinically used to treat the majority of cystic fibrosis (CF) patients (Bhagirath et al., 2016). In a previous study in our laboratory docking and ligand models to screen for AcrB inhibitors were developed using known AcrB substrates and inhibitors from the literature (Pisoni, 2021 PhD thesis, A combined *in silico* and microbiological approach for the identification of novel efflux pump inhibitors against AcrAB-TolC, University of South Australia). A total of 23 compounds were then selected using these *in silico* models by screening a database of 1391 FDA-approved drugs. The 23 selected compounds were used for *in vitro* assays with ivacaftor found to be the only drug that fulfilled all *in vitro* testing criteria required of a good EPI in *E. coli* (Pisoni, 2021 PhD thesis, A combined *in silico* and microbiological approach for the identification of novel efflux pump inhibitors against AcrAB-TolC, University of South Australia). Ivacaftor showed potentiation with the antibiotic substrates erythromycin and chloramphenicol against wild-type *E. coli* but did not show potentiation of erythromycin against the AcrB knock-out strain. It inhibited the efflux of Nile Red in a dose dependent manner; and did not have any effect on the *E. coli* bacterial outer membrane (Pisoni, 2021 PhD thesis, A combined *in silico* and microbiological approach

for the identification of novel efflux pump inhibitors against AcrAB-TolC, University of South Australia). The findings of this previous study were interesting given that clinical use of ivacaftor has been associated with reduced infection rates with important CF pathogens including *P. aeruginosa* (Frost et al., 2019). This led to the hypothesis that ivacaftor may also be an inhibitor of the MexB efflux pump in *P. aeruginosa.*

In this study, the inner membrane protein MexB was purified and then applied using an SPR technique to examine the direct binding of ivacaftor. It was found that the compound ivacaftor could bind with MexB protein with a similar Kd to that of PAβN. However, as the reaction did not reach equilibrium, a substantial amount of non-specific binding might still have been observed. This resulted in a very high upper limit for the Kd value of ivacaftor binding to MexB, similar to that described before for SPR of ligands to AcrB in the absence of correction for non-specific binding (Tikhonova et al., 2011).

There were many difficulties encountered in measuring the binding to this efflux protein. Inner membrane proteins are not stable and very easily lose their activity when extracted from their native environment (Seddon et al., 2004). Immobilisation processes can denature the proteins (Sigal et al., 1996). If the analysis of the protein in the SPR instrument at room temperature takes too long, this can also lead to the protein becoming unstable (Mowla et al., 2018b; Polyak et al., 2020).

Checkerboard assays were also undertaken to examine whether the ivacaftor could potentiate the effects of antibiotics in *P. aeruginosa* strains that express and overexpress the MexAB-OprM efflux pump. Although ivacaftor was not found to potentiate the tested antibiotics when used alone, it did greatly enhance the activity of all the three antibiotics tested (ERY, LEV and MIN) against both wild type and MexAB-OprM overexpressed strains of *P. aeruginosa* in the presence of a membrane permeabiliser polymyxin B nonapeptide (PMBN), with 4 to 8 folds MIC reductions. The most encouraging result was the 8-fold reduction of the MIC of ERY at a low concentration of 4 μg/mL against PAM 1032 (MexAB-OprM overexpressed). A reduction of 4-fold at 8 μg/mL for all the three antibiotics (ERY, LEV and MIN) against PAM 1020 (wild-type) strain was also observed. The potentiation of ivacaftor in the presence of colistin was also found. There were 4 to 8 folds reductions for all three tested

antibiotics against both wild type and efflux pump overexpressed strains. Prior studies have identified that *P. aeruginosa* possesses a lower outer membrane permeability than *E. coli,* being 2 to 100 times less permeable than *E. coli* because of its selective porins (Breidenstein et al., 2011; Ferrer-Espada et al., 2019). This may explain why ivacaftor was previously observed to potentiate antibiotic activity in *E. coli* without any membrane permeabiliser but demonstrated no activity in *P. aeruginosa*. However, in the presence of the outer membrane permeabilisers PMBN and colistin, ivacaftor was much more effective Colistin is used clinically in people with cystic fibrosis despite its potential for toxicities such as nephrotoxicity and neurotoxicity due to the limited antibiotics available to treat MDR *P. aeruginosa* strains that are prevalent in this patient population (Taccetti et al., 2021). Colistin is often used as an inhaled antibiotic treatment via a nebuliser which can deliver a relatively high concentration of the drug directly to the lungs (Taccetti et al., 2021).

In addition to its antibiotic potentiating effects, ivacaftor was able to completely inhibit Nile Red efflux in *P. aeruginosa* at a concentration of 200 μM. Toxicity assessments for ivacaftor were not undertaken as it is a drug already in clinical use. Therefore, ivacaftor could be a promising EPI for MexB.

The antibiotic potentiating effects of ivacaftor may not be the only explanation for the reduction in infection rates observed in CF patients treated with the drug. Through its effects on the CFTR ion channel it improves mucus hydration and increases mucus clearance from the airway (Donaldson et al., 2018). This would also make the lung environment less favourable for *P aeruginosa* infection. We hypothesise that other activities of ivacaftor may also contribute to this reduction in infection rates in patients. Since efflux pumps are also responsible for transporting bacterial substances necessary for pathogenesis, including quorum sensing compounds and components of biofilms, efflux pumps also play a critical role in virulence and biofilm formation (Fernando & Kumar, 2013). Hence, through inhibition of RND efflux pumps ivacaftor also has the potential to reduce biofilm formation and regulate the excretion of virulence factors (Venter et al., 2015), thereby reducing the infection in CF patients. Patients with CF who have chronic infections often have highly organised bacterial biofilms (Mann & Wozniak, 2012; Römling & Balsalobre, 2012), in their lungs. Such impenetrable biofilms have high resistance against antibiotics and host immunity

(Thanabalasuriar et al., 2019). Therefore, the effects of ivacaftor on *P. aeruginosa* biofilms are an important potential target to examine further. To investigate this hypothesis, our lab has recently undertaken biofilm formation analysis studies on different *P. aeruginosa* strains, and found that the EPI PAβN can reduce biofilm formation by the efflux pump overexpressing strain of *P. aeruginosa* (Liu, 2022 Masters thesis, Inhibitors of bacterial efflux pumps and their effect on antimicrobial resistance, biofilm formation and virulence, University of Adelaide). Hence, evaluation of ivacaftor on the inhibition of bacterial biofilm formation and virulence will be an important future direction for this research.

In other studies the nematode *C. elegans* has been successfully employed as an alternative method to evaluate virulence mechanisms of a variety of bacterial pathogens including *P. aeruginosa* (Brackman et al., 2011; Powell & Ausubel, 2008; Richter et al., 2017; Sifri et al., 2006). In these studies, the nematodes were infected with the chosen bacterial strains and then treated with antibiotics or combinations of drugs as an antimicrobial therapy to investigate the effects. Therefore, a similar model could be used to assess the ability of ivacaftor to treat nematodes infected with *P. aeruginosa* and other antimicrobial resistant Gram-negative pathogens.

5.4 Conclusion

If strategies to tackle AMR are not developed, it has been predicted as a major cause of death by 2050 (O'Neill, 2016). Already in 2019, there were nearly 5 million people who died due to AMR (Murray et al., 2022). Efforts are urgently needed to discover new antimicrobial therapies in order to introduce new drugs into clinical use (Murray et al., 2022). Rapidly increasing rates of AMR are causing a huge burden on public health systems and economies worldwide. There is still a shortage of new antimicrobials for infections caused by Gram-negative organisms including the most critical priority pathogens according to the WHO (WHO, 2017). To tackle this issue, the reversal of AMR could be an alternative option for antibiotic development. Inhibition of bacterial efflux pumps is one promising strategy to restore the activity of antimicrobial agents against multidrug resistant Gram-negative pathogens. Although many efflux pump inhibitors that target RND-type efflux pumps have been identified

so far, none of them have progressed to clinical use. The main reasons for this are cell toxicity, off-target issues, and limited range of *in vivo* potency.

This study investigated both novel synthetic compounds with a new pharmacophore and a clinically used drug as inhibitors of RND pumps in Gram-negative pathogens to combat the emerging AMR. This study has contributed to identifying the 3,4-dihydro-2*H*-benzo[h]chromen-5-yl)(morpholino)methanone core structure as a promising chemical skeleton for the further development of new AcrB inhibitors and potentially inhibitors of other RND pumps. Moreover, the clinically used CF drug ivacaftor has been shown for the first time to bind to the MexB efflux pump protein of *P. aeruginosa*, to greatly enhance antibiotic activity against a multidrug resistant *P. aeruginosa* strain in the presence of bacterial membrane permeabilisers, and to inhibit the efflux of Nile Red in a *P. aeruginosa* strain that overexpresses MexAB-OprM. This compound therefore warrants further study as a putative EPI which could circumvent the issues of toxicity seen with many other EPIs as it is already in clinical use.

References

Abdali, N., et al. (2017). Reviving antibiotics: efflux pump inhibitors that interact with AcrA, a membrane fusion protein of the AcrAB-TolC multidrug efflux pump. *ACS infectious diseases, 3*(1), 89-98.

Abreu, A. C., et al. (2012). Plants as sources of new antimicrobials and resistance-modifying agents. *Natural product reports, 29*(9), 1007-1021.

Al-Tawfiq, J. A., et al. (2021). Antibiotics in the pipeline: a literature review (2017–2020). *Infection*, 1-12.

Alav, I., et al. (2021). Structure, assembly, and function of tripartite efflux and type 1 secretion systems in gram-negative bacteria. *Chemical reviews, 121*(9), 5479-5596.

Alav, I., et al. (2018). Role of bacterial efflux pumps in biofilm formation. *Journal of antimicrobial chemotherapy, 73*(8), 2003-2020.

Alcalde-Rico, M., et al. (2016). Multidrug efflux pumps at the crossroad between antibiotic resistance and bacterial virulence. *Frontiers in microbiology, 7*, 1483.

Alcalde-Rico, M., et al. (2018). Role of the multidrug resistance efflux pump MexCD-OprJ in the Pseudomonas aeruginosa quorum sensing response. *Frontiers in microbiology, 9*, 2752.

Alenazy, R. (2022). Drug Efflux Pump Inhibitors: A Promising Approach to Counter Multidrug Resistance in Gram-Negative Pathogens by Targeting AcrB Protein from AcrAB-TolC Multidrug Efflux Pump from Escherichia coli. *Biology, 11*(9), 1328.

AlMatar, M., et al. (2021). Efflux pump inhibitors: new updates. *Pharmacological Reports, 73*(1), 1-16.

Alvarez-Ortega, C., et al. (2013). RND multidrug efflux pumps: what are they good for? *Frontiers in microbiology, 4*, 7.

Amaral, L., et al. (2014). Efflux pumps of Gram-negative bacteria: what they do, how they do it, with what and how to deal with them. *Frontiers in pharmacology*, 168.

Amsalu, A., et al. (2020). Efflux pump-driven antibiotic and biocide cross-resistance in Pseudomonas aeruginosa isolated from different ecological niches: a case study in the development of multidrug resistance in environmental hotspots. *Microorganisms, 8*(11), 1647.

Aron, Z., & Opperman, T. J. (2016). Optimization of a novel series of pyranopyridine RND efflux pump inhibitors. *Current opinion in microbiology, 33*, 1-6.

Aron, Z., & Opperman, T. J. (2018). The hydrophobic trap—the Achilles heel of RND efflux pumps. *Research in microbiology, 169*(7-8), 393-400.

Arzanlou, M., et al. (2017). Intrinsic, adaptive and acquired antimicrobial resistance in Gram-negative bacteria. *Essays in biochemistry, 61*(1), 49-59.

Baugh, S., et al. (2014). Inhibition of multidrug efflux as a strategy to prevent biofilm formation. *Journal of antimicrobial chemotherapy, 69*(3), 673-681.

Bhagirath, A. Y., et al. (2016). Cystic fibrosis lung environment and Pseudomonas aeruginosa infection. *BMC pulmonary medicine, 16*(1), 1-22.

Blair, J. M., et al. (2014). Multidrug efflux pumps in Gram-negative bacteria and their role in antibiotic resistance. *Future Microbiol, 9*(10), 1165-1177. doi:10.2217/fmb.14.66

Blair, J. M., et al. (2015). Molecular mechanisms of antibiotic resistance. *Nature Reviews Microbiology, 13*(1), 42-51.

Bohnert, et al. (2010). Optimized Nile Red efflux assay of AcrAB-TolC multidrug efflux system shows competition between substrates. *Antimicrobial agents and chemotherapy, 54*(9), 3770-3775.

Bohnert, et al. (2008). Site-directed mutagenesis reveals putative substrate binding residues in the Escherichia coli RND efflux pump AcrB. *Journal of bacteriology, 190*(24), 8225-8229.

Bolla, J.-M., et al. (2011). Strategies for bypassing the membrane barrier in multidrug resistant Gram-negative bacteria. *FEBS letters, 585*(11), 1682-1690.

Brackman, G., et al. (2011). Quorum sensing inhibitors increase the susceptibility of bacterial biofilms to antibiotics in vitro and in vivo. *Antimicrobial agents and chemotherapy, 55*(6), 2655-2661.

Breidenstein, E. B., et al. (2011). Pseudomonas aeruginosa: all roads lead to resistance. *Trends in microbiology, 19*(8), 419-426.

Butler, M. M., et al. (2022). Optimized pyridazinone nutrient channel inhibitors are potent and specific antimalarial leads. *Molecular Pharmacology, 102*(3), 172-182.

Cepas, V., & Soto, S. M. (2020). Relationship between virulence and resistance among gram-negative bacteria. *Antibiotics, 9*(10), 719.

Cha, H.-j., et al. (2014). Switch-loop flexibility affects transport of large drugs by the promiscuous AcrB multidrug efflux transporter. *Antimicrobial agents and chemotherapy, 58*(8), 4767-4772.

Chai, W. C., et al. (2022). Cinnamaldehyde derivatives act as antimicrobial agents against Acinetobacter baumannii through the inhibition of cell division. *Frontiers in microbiology*.

Chai, W. C., et al. (2020). Antimicrobial action and reversal of resistance in MRSA by difluorobenzamide derivatives targeted at FtsZ. *Antibiotics, 9*(12), 873.

Colclough, A. L., et al. (2020). RND efflux pumps in Gram-negative bacteria; regulation, structure and role in antibiotic resistance. *Future Microbiology, 15*(2), 143-157.

Compagne, N., et al. (2023). Update on the Discovery of Efflux Pump Inhibitors against Critical Priority Gram-Negative Bacteria. *Antibiotics, 12*(1), 180.

Contreras-Gómez, M. J., et al. (2022). Role of the multi-drug efflux systems on the baseline susceptibility to ceftazidime/avibactam and ceftolozane/tazobactam in clinical isolates of non-carbapenemase-producing carbapenem-resistant Pseudomonas aeruginosa. *Frontiers in pharmacology, 13*.

Cormican, M., & Vellinga, A. (2012). Existing classes of antibiotics are probably the best we will ever have. *Bmj, 344*.

Costa, P., et al. (2021). Application of the Resazurin Cell Viability Assay to Monitor Escherichia coli and Salmonella Typhimurium Inactivation Mediated by Phages. *Antibiotics, 10*(8), 974.

Davin-Regli, A., et al. (2021). Clinical Status of Efflux Resistance Mechanisms in Gram-Negative Bacteria. *Antibiotics, 10*(9), 1117.

Davis, P. B., et al. (2012). Ivacaftor. *Nature reviews Drug discovery, 11*(5), 349-351.

Dawan, J., et al. (2022). Role of efflux pump-mediated antibiotic resistance in quorum sensing-regulated biofilm formation by Salmonella Typhimurium. *Pathogens, 11*(2), 147.

Dharmalingam, K., et al. (2012). Swietenia macrophylla extract promotes the ability of Caenorhabditis elegans to survive Pseudomonas aeruginosa infection. *Journal of ethnopharmacology, 139*(2), 657-663.

Donaldson, S. H., et al. (2018). Effect of ivacaftor on mucociliary clearance and clinical outcomes in cystic fibrosis patients with G551D-CFTR. *JCI insight, 3*(24).

Dong, N., et al. (2022). Distribution and spread of the mobilised RND efflux pump gene cluster tmexCD-toprJ in clinical Gram-negative bacteria: a molecular epidemiological study. *The Lancet Microbe, 3*(11), e846-e856.

Du, et al. (2018). Multidrug efflux pumps: structure, function and regulation. *Nature Reviews Microbiology, 16*(9), 523-539.

Du, D., et al. (2014). Structure of the AcrAB-TolC multidrug efflux pump. *Nature, 509*(7501), 512-515. doi:10.1038/nature13205

Eckford, P. D., et al. (2012). Cystic Fibrosis Transmembrane Conductance Regulator (CFTR) Potentiator VX-770 (Ivacaftor) Opens the Defective Channel Gate of Mutant CFTR in a

Phosphorylation-dependent but ATP-independent Manner* ♦. *Journal of Biological Chemistry, 287*(44), 36639-36649.
Eicher, T., et al. (2012). Transport of drugs by the multidrug transporter AcrB involves an access and a deep binding pocket that are separated by a switch-loop. *Proceedings of the National Academy of Sciences, 109*(15), 5687-5692.
Fernando, D. M., & Kumar, A. (2013). Resistance-nodulation-division multidrug efflux pumps in gram-negative bacteria: role in virulence. *Antibiotics, 2*(1), 163-181.
Ferrer-Espada, R., et al. (2019). A permeability-increasing drug synergizes with bacterial efflux pump inhibitors and restores susceptibility to antibiotics in multi-drug resistant Pseudomonas aeruginosa strains. *Scientific reports, 9*(1), 1-12.
Frost, F. J., et al. (2019). Ivacaftor is associated with reduced lung infection by key cystic fibrosis pathogens. A cohort study using national registry data. *Annals of the American Thoracic Society, 16*(11), 1375-1382.
Gai, Z., et al. (2019). Molecular mechanisms of colistin-induced nephrotoxicity. *Molecules, 24*(3), 653.
Gaynes, R. (2017). The discovery of penicillin—new insights after more than 75 years of clinical use. *Emerging Infectious Diseases, 23*(5), 849.
Goss, C. H., & Burns, J. L. (2007). Exacerbations in cystic fibrosis· 1: Epidemiology and pathogenesis. *Thorax, 62*(4), 360-367.
Grimsey, E. M., & Piddock, L. J. (2019). Do phenothiazines possess antimicrobial and efflux inhibitory properties? *FEMS microbiology reviews, 43*(6), 577-590.
Gu, X., et al. (2020). Design and synthesis of novel 4-substituted quinazoline-2-carboxamide derivatives targeting AcrB to reverse the bacterial multidrug resistance. *Bioorganic Chemistry, 105*, 104394.
Guo, T., et al. (2023). Design and synthesis of benzochromene derivatives as AcrB inhibitors for the reversal of bacterial multidrug resistance. *European journal of medicinal chemistry*, 115148.
Hancock, R. E., & Brinkman, F. S. (2002). Function of Pseudomonas porins in uptake and efflux. *Annual review of microbiology, 56*(1), 17-38.
Hassan, K. A., et al. (2018). Pacing across the membrane: the novel PACE family of efflux pumps is widespread in Gram-negative pathogens. *Research in microbiology, 169*(7-8), 450-454.
Imai, S., et al. (2022). Economic and clinical burden from carbapenem-resistant bacterial infections and factors contributing: a retrospective study using electronic medical records in Japan. *BMC Infectious Diseases, 22*(1), 1-11.
ISO, I. (2019). 20776-1: 2019 (en) Susceptibility testing of infectious agents and evaluation of performance of antimicrobial susceptibility test devices–Part 1: Broth micro-dilution reference method for testing the in vitro activity of antimicrobial agents against rapidly growing aerobic bacteria involved in infectious diseases. *Geneva (Switzerland): International Organization for Standardization*, 20776-20771.
Iyer, R., et al. (2015). A fluorescent microplate assay quantifies bacterial efflux and demonstrates two distinct compound binding sites in AcrB. *Antimicrobial agents and chemotherapy, 59*(4), 2388-2397.
Jin, C., et al. (2019). Design, synthesis and evaluation of a series of 5-methoxy-2, 3-naphthalimide derivatives as AcrB inhibitors for the reversal of bacterial resistance. *Bioorganic & medicinal chemistry letters, 29*(7), 882-889.
Kirienko, N., et al. (2014). Pseudomonas methods and protocols.
Klug, D. M., et al. (2021). There is no market for new antibiotics: this allows an open approach to research and development. *Wellcome Open Research, 6*.
Kobylka, J., et al. (2020). AcrB: a mean, keen, drug efflux machine. *Ann N Y Acad Sci, 1459*(1), 38-68. doi:10.1111/nyas.14239

Komura, H., et al. (2005). [High throughput screening of pharmacokinetics and metabolism in drug discovery (III)--investigation on in- silico model for membrane permeability and CYP1A2 inhibition]. *Yakugaku Zasshi, 125*(1), 141-147. doi:10.1248/yakushi.125.141

Kourtesi, C., et al. (2013). Suppl 1: microbial efflux systems and inhibitors: approaches to drug discovery and the challenge of clinical implementation. *The open microbiology journal, 7*, 34.

Krishnamoorthy, G., et al. (2017). Synergy between active efflux and outer membrane diffusion defines rules of antibiotic permeation into Gram-negative bacteria. *MBio, 8*(5), e01172-01117.

Krishnamoorthy, G., et al. (2008). Fitting periplasmic membrane fusion proteins to inner membrane transporters: mutations that enable Escherichia coli AcrA to function with Pseudomonas aeruginosa MexB. *Journal of bacteriology, 190*(2), 691-698.

Kvist, M., et al. (2008). Inactivation of efflux pumps abolishes bacterial biofilm formation. *Applied and environmental microbiology, 74*(23), 7376-7382.

Lamut, A., et al. (2019). Efflux pump inhibitors of clinically relevant multidrug resistant bacteria. *Medicinal Research Reviews, 39*(6), 2460-2504.

Leus, I. V., et al. (2023). Functional Diversity of Gram-Negative Permeability Barriers Reflected in Antibacterial Activities and Intracellular Accumulation of Antibiotics. *Antimicrobial agents and chemotherapy*, e01377-01322.

Li, B., et al. (2011). Artesunate enhances the antibacterial effect of β-lactam antibiotics against Escherichia coli by increasing antibiotic accumulation via inhibition of the multidrug efflux pump system AcrAB-TolC. *Journal of antimicrobial chemotherapy, 66*(4), 769-777.

Liu, S. (2022 Masters thesis, Inhibitors of bacterial efflux pumps and their effect on antimicrobial resistance, biofilm formation and virulence, University of Adelaide). Inhibitors of bacterial efflux pumps and their effect on antimicrobial resistance, biofilm formation and virulence.

Lomovskaya, et al. (2006). Practical applications and feasibility of efflux pump inhibitors in the clinic—a vision for applied use. *Biochemical pharmacology, 71*(7), 910-918.

Lomovskaya, O., & Bostian, K. A. (2006). Practical applications and feasibility of efflux pump inhibitors in the clinic—a vision for applied use. *Biochemical pharmacology, 71*(7), 910-918.

Lomovskaya, O., et al. (1999). Use of a genetic approach to evaluate the consequences of inhibition of efflux pumps in Pseudomonas aeruginosa. *Antimicrob Agents Chemother, 43*(6), 1340-1346. doi:10.1128/aac.43.6.1340

Lomovskaya, O., et al. (2001). Identification and characterization of inhibitors of multidrug resistance efflux pumps in Pseudomonas aeruginosa: novel agents for combination therapy. *Antimicrobial agents and chemotherapy, 45*(1), 105-116.

López, C. A., et al. (2020). Molecular characterization of the outer membrane of Pseudomonas aeruginosa. *Biochimica et Biophysica Acta (BBA)-Biomembranes, 1862*(3), 183151.

Magiorakos, A.-P., et al. (2012). Multidrug-resistant, extensively drug-resistant and pandrug-resistant bacteria: an international expert proposal for interim standard definitions for acquired resistance. *Clinical Microbiology and Infection, 18*(3), 268-281.

Malviya, et al. (2017). Bioassay guided fractionation-an emerging technique influence the isolation, identification and characterization of lead phytomolecules. *Hosp. Pharm, 2*(5).

Mann, E. E., & Wozniak, D. J. (2012). Pseudomonas biofilm matrix composition and niche biology. *FEMS microbiology reviews, 36*(4), 893-916.

Marshall, R. L., et al. (2020). New multidrug efflux inhibitors for Gram-negative bacteria. *MBio, 11*(4), e01340-01320.

Martinez, J. L., et al. (2009). Functional role of bacterial multidrug efflux pumps in microbial natural ecosystems. *FEMS microbiology reviews, 33*(2), 430-449.

Masuda, N., et al. (2000). Substrate specificities of MexAB-OprM, MexCD-OprJ, and MexXY-oprM efflux pumps in Pseudomonas aeruginosa. *Antimicrobial agents and chemotherapy, 44*(12), 3322-3327.

Meyer, C., et al. (2022). Contribution of RND-Type Efflux Pumps in Reduced Susceptibility to Biocides in Acinetobacter baumannii. *Antibiotics, 11*(11), 1635.

Mowla, R., et al. (2018a). Kinetic analysis of the inhibition of the drug efflux protein AcrB using surface plasmon resonance. *Biochimica et Biophysica Acta (BBA) - Biomembranes, 1860*(4), 878-886. doi:https://doi.org/10.1016/j.bbamem.2017.08.024

Mowla, R., et al. (2018b). Kinetic analysis of the inhibition of the drug efflux protein AcrB using surface plasmon resonance. *Biochimica et Biophysica Acta (BBA)-Biomembranes, 1860*(4), 878-886.

Muñoz, K. A., & Hergenrother, P. J. (2021). Facilitating compound entry as a means to discover antibiotics for gram-negative bacteria. *Accounts of chemical research, 54*(6), 1322-1333.

Murakami, S., et al. (2006). Crystal structures of a multidrug transporter reveal a functionally rotating mechanism. *Nature, 443*(7108), 173-179.

Murray, C. J., et al. (2022). Global burden of bacterial antimicrobial resistance in 2019: a systematic analysis. *The Lancet, 399*(10325), 629-655.

Nakashima, R., et al. (2013). Structural basis for the inhibition of bacterial multidrug exporters. *Nature, 500*(7460), 102-106.

Nakashima, R., et al. (2011). Structures of the multidrug exporter AcrB reveal a proximal multisite drug-binding pocket. *Nature, 480*(7378), 565-569.

Nguyen, H. T., et al. (2021). In vitro synergistic activity of NCL195 in combination with colistin against Gram-negative bacterial pathogens. *International journal of antimicrobial agents, 57*(5), 106323.

Nguyen, H. T., et al. (2022). Impact of a novel anticoccidial analogue on systemic staphylococcus aureus infection in a bioluminescent mouse model. *Antibiotics, 11*(1), 65.

Nicholls, D. G. (1974). The influence of respiration and ATP hydrolysis on the proton-electrochemical gradient across the inner membrane of rat-liver mitochondria as determined by ion distribution. *European Journal of Biochemistry, 50*(1), 305-315.

Nichols, R. J., et al. (2011). Phenotypic landscape of a bacterial cell. *Cell, 144*(1), 143-156.

Nikaido, H., & Pagès, J.-M. (2012). Broad-specificity efflux pumps and their role in multidrug resistance of Gram-negative bacteria. *FEMS microbiology reviews, 36*(2), 340-363.

Nikaido, H., & Takatsuka, Y. (2009). Mechanisms of RND multidrug efflux pumps. *Biochimica et Biophysica Acta (BBA)- Proteins and Proteomics*.

Nikaido, H., & Vaara, M. (1985). Molecular basis of bacterial outer membrane permeability. *Microbiological reviews, 49*(1), 1-32.

O'Neill, J. (2016). Tackling drug-resistant infections globally: final report and recommendations.

O'Sullivan, B. P., & Flume, P. (2009). *The clinical approach to lung disease in patients with cystic fibrosis.* Paper presented at the Seminars in respiratory and critical care medicine.

Ogunniyi, A. D., et al. (2018). Bioluminescent murine models of bacterial sepsis and scald wound infections for antimicrobial efficacy testing. *PloS one, 13*(7), e0200195.

Ohene-Agyei, et al. (2014). Phytochemicals increase the antibacterial activity of antibiotics by acting on a drug efflux pump. *Microbiologyopen, 3*(6), 885-896. doi:10.1002/mbo3.212

Ohene-Agyei, T., et al. (2012). Mutations in MexB that affect the efflux of antibiotics with cytoplasmic targets. *FEMS microbiology letters, 333*(1), 20-27.

Ohene-Agyei, T., et al. (2014). Phytochemicals increase the antibacterial activity of antibiotics by acting on a drug efflux pump. *Open Microbiol., 3*(6), 885-896. doi:10.1002/mbo3.212

Opperman, et al. (2014). Characterization of a novel pyranopyridine inhibitor of the AcrAB efflux pump of Escherichia coli. *Antimicrobial agents and chemotherapy, 58*(2), 722-733.

Opperman, T., et al. (2018). In Vivo Proof of Principle for MBX-4191, A Pyranopyridine Efflux Pump Inhibitor. *Poster, 564*.

Opperman, T. J., & Nguyen, S. T. (2015). Recent advances toward a molecular mechanism of efflux pump inhibition. *Frontiers in microbiology, 6*, 421.

Orhan, G., et al. (2005). Synergy tests by E test and checkerboard methods of antimicrobial combinations against Brucella melitensis. *Journal of clinical microbiology, 43*(1), 140-143.

Padilla, E., et al. (2010). Klebsiella pneumoniae AcrAB efflux pump contributes to antimicrobial resistance and virulence. *Antimicrobial agents and chemotherapy, 54*(1), 177-183.

Pal, A., & Tripathi, A. (2020). Quercetin inhibits carbapenemase and efflux pump activities among carbapenem-resistant Gram-negative bacteria. *Apmis, 128*(3), 251-259.

Pérez-Varela, M., et al. (2019). Roles of efflux pumps from different superfamilies in the surface-associated motility and virulence of Acinetobacter baumannii ATCC 17978. *Antimicrobial agents and chemotherapy, 63*(3), e02190-02118.

Phetsang, W., et al. (2016). Fluorescent trimethoprim conjugate probes to assess drug accumulation in wild type and mutant Escherichia coli. *ACS infectious diseases, 2*(10), 688-701.

Pi, H., et al. (2020). In vitro activity of robenidine analog NCL195 in combination with outer membrane permeabilizers against Gram-negative bacterial pathogens and impact on systemic Gram-positive bacterial infection in mice. *Frontiers in microbiology, 11*, 1556.

Pi, H., et al. (2021). Repurposing of the fasciolicide triclabendazole to treat infections caused by staphylococcus spp. and vancomycin-resistant enterococci. *Microorganisms, 9*(8), 1697.

Pi, H., et al. (2022). In Vitro Activity of Robenidine Analogues NCL259 and NCL265 against Gram-Negative Pathogens. *Antibiotics, 11*(10), 1301.

Piddock, L. J., et al. (2022). A Nonprofit Drug Development Model Is Part of the Antimicrobial Resistance (AMR) Solution. *Clinical Infectious Diseases, 74*(10), 1866-1871.

Piddock, L. J. V. (2006a). Clinically relevant chromosomally encoded multidrug resistance efflux pumps in bacteria. *Clinical microbiology reviews, 19*(2), 382-402.

Piddock, L. J. V. (2006b). Multidrug-resistance efflux pumps? not just for resistance. *Nature Reviews Microbiology, 4*(8), 629-636.

Pisoni, L. A. (2021 PhD thesis, A combined *in silico* and microbiological approach for the identification of novel efflux pump inhibitors against AcrAB-TolC, University of South Australia). *A combined in silico and microbiological approach for the identification of novel efflux pump inhibitors against AcrAB-TolC.* (PhD). Universith of South Australia, PhD thesis.

Polyak, S. W., et al. (2020). Measuring Small Molecule Binding to Escherichia coli AcrB by Surface Plasmon Resonance. In *Targeting Enzymes for Pharmaceutical Development* (pp. 119-130): Springer.

Poole, K. (2004). Efflux-mediated multiresistance in Gram-negative bacteria. *Clinical Microbiology and Infection, 10*(1), 12-26.

Poole, K. (2007). Efflux pumps as antimicrobial resistance mechanisms. *Annals of medicine, 39*(3), 162-176.

Powell, J. R., & Ausubel, F. M. (2008). Models of Caenorhabditis elegans infection by bacterial and fungal pathogens. In *Innate immunity* (pp. 403-427): Springer.

Powers, J. (2004). Antimicrobial drug development–the past, the present, and the future. *Clinical Microbiology and Infection, 10*, 23-31.

Prestinaci, F., et al. (2015). Antimicrobial resistance: a global multifaceted phenomenon. *Pathogens and global health, 109*(7), 309-318.

Puiu, M., & Bala, C. (2016). SPR and SPR imaging: Recent trends in developing nanodevices for detection and real-time monitoring of biomolecular events. *Sensors, 16*(6), 870.

Pushpakom, S., et al. (2019). Drug repurposing: progress, challenges and recommendations. *Nature reviews Drug discovery, 18*(1), 41-58.

Richter, K., et al. (2017). Taking the silver bullet colloidal silver particles for the topical treatment of biofilm-related infections. *ACS applied materials & interfaces, 9*(26), 21631-21638.
Römling, U., & Balsalobre, C. (2012). Biofilm infections, their resilience to therapy and innovative treatment strategies. *Journal of internal medicine, 272*(6), 541-561.
Rosenau, F., et al. (2010). Lipase LipC affects motility, biofilm formation and rhamnolipid production in Pseudomonas aeruginosa. *FEMS microbiology letters, 309*(1), 25-34.
Rowe, et al. (2014). Validation of Kepler's multiple planet candidates. III. Light curve analysis and announcement of hundreds of new multi-planet systems. *The Astrophysical Journal, 784*(1), 45.
Rowe, S. M., et al. (2014). Clinical mechanism of the cystic fibrosis transmembrane conductance regulator potentiator ivacaftor in G551D-mediated cystic fibrosis. *American journal of respiratory and critical care medicine, 190*(2), 175-184.
Rudd, K. E., et al. (2018). The global burden of sepsis: barriers and potential solutions. *Critical Care, 22*(1), 1-11.
Ruggerone, P., et al. (2013). RND efflux pumps: structural information translated into function and inhibition mechanisms. *Current topics in medicinal chemistry, 13*(24), 3079-3100.
Sartelli, M., et al. (2020). Antibiotic use in low and middle-income countries and the challenges of antimicrobial resistance in surgery. *Antibiotics, 9*(8), 497.
Schroeder, M., et al. (2017). The complex relationship between virulence and antibiotic resistance. *Genes, 8*(1), 39.
Schweizer, H. P. (2012). Understanding efflux in Gram-negative bacteria: opportunities for drug discovery. *Expert opinion on drug discovery, 7*(7), 633-642.
Sebastián, M., et al. (2019). High growth potential of long-term starved deep ocean opportunistic heterotrophic bacteria. *Frontiers in microbiology*, 760.
Seddon, A. M., et al. (2004). Membrane proteins, lipids and detergents: not just a soap opera. *Biochimica et Biophysica Acta (BBA)-Biomembranes, 1666*(1-2), 105-117.
Seeger, M. A., et al. (2006). Structural asymmetry of AcrB trimer suggests a peristaltic pump mechanism. *Science, 313*(5791), 1295-1298.
Seukep, A. J., et al. (2019). Plant-derived secondary metabolites as the main source of efflux pump inhibitors and methods for identification. *Journal of Pharmaceutical Analysis*.
Seyedmohammad, S., et al. (2016). Structural model of FeoB, the iron transporter from Pseudomonas aeruginosa, predicts a cysteine lined, GTP-gated pore. *Bioscience reports, 36*(2).
Sharma, N., et al. (2021). Antibiotic adjuvants: A promising approach to combat multidrug resistant bacteria. *Current drug targets, 22*(12), 1334-1345.
Sifri, C. D., et al. (2006). Virulence of Staphylococcus aureus small colony variants in the Caenorhabditis elegans infection model. *Infection and immunity, 74*(2), 1091-1096.
Sigal, G. B., et al. (1996). A self-assembled monolayer for the binding and study of histidine-tagged proteins by surface plasmon resonance. *Analytical Chemistry, 68*(3), 490-497.
Sionov, R. V., & Steinberg, D. (2022). Targeting the holy triangle of quorum sensing, biofilm formation, and antibiotic resistance in pathogenic bacteria. *Microorganisms, 10*(6), 1239.
Sjuts, H., et al. (2016). Molecular basis for inhibition of AcrB multidrug efflux pump by novel and powerful pyranopyridine derivatives. *Proceedings of the National Academy of Sciences, 113*(13), 3509-3514.
Smith, R., & Coast, J. (2012). The economic burden of antimicrobial resistance: why it is more serious than current studies suggest.
Soto, S. M. (2013). Role of efflux pumps in the antibiotic resistance of bacteria embedded in a biofilm. *Virulence, 4*(3), 223-229.

Sun, D., et al. (2019). Horizontal gene transfer mediated bacterial antibiotic resistance. In (Vol. 10, pp. 1933): Frontiers Media SA.
Taccetti, G., et al. (2021). Cystic fibrosis: Recent insights into inhaled antibiotic treatment and future perspectives. *Antibiotics, 10*(3), 338.
Tampakakis, E., et al. (2008). A C. elegans-based, whole animal, in vivo screen for the identification of antifungal compounds. *Nature protocols, 3*(12), 1925-1931.
Tang, M., et al. (2020). The role and relationship with efflux pump of biofilm formation in Klebsiella pneumoniae. *Microb Pathog, 147*, 104244. doi:10.1016/j.micpath.2020.104244
Thanabalasuriar, A., et al. (2019). Neutrophil extracellular traps confine Pseudomonas aeruginosa ocular biofilms and restrict brain invasion. *Cell host & microbe, 25*(4), 526-536. e524.
Thanassi, D. G., et al. (1997). Active efflux of bile salts by Escherichia coli. *Journal of bacteriology, 179*(8), 2512-2518.
Tielen, P., et al. (2013). Interaction between extracellular lipase LipA and the polysaccharide alginate of Pseudomonas aeruginosa. *BMC microbiology, 13*(1), 1-12.
Tielen, P., et al. (2010). Extracellular enzymes affect biofilm formation of mucoid Pseudomonas aeruginosa. *Microbiology, 156*(7), 2239-2252.
Tikhonova, E. B., et al. (2011). Sequential mechanism of assembly of multidrug efflux pump AcrAB-TolC. *Chemistry & biology, 18*(4), 454-463.
Tikhonova, E. B., & Zgurskaya, H. I. (2013). Assessment of multidrug efflux assemblies by surface plasmon resonance. In *Bacterial Cell Surfaces* (pp. 133-155): Springer.
Vaara, et al. (1983). Sensitization of Gram-negative bacteria to antibiotics and complement by a nontoxic oligopeptide. *Nature, 303*(5917), 526-528.
Van Bambeke, F., et al. (2000). Antibiotic efflux pumps. *Biochemical pharmacology, 60*(4), 457-470.
Vargiu, A. V., et al. (2014). Molecular mechanism of MBX2319 inhibition of Escherichia coli AcrB multidrug efflux pump and comparison with other inhibitors. *Antimicrobial agents and chemotherapy, 58*(10), 6224-6234.
Venter, H. (2019). Reversing resistance to counter antimicrobial resistance in the World Health Organisation's critical priority of most dangerous pathogens. *Bioscience reports, 39*(4).
Venter, H., et al. (2017). Antimicrobial resistance in healthcare, agriculture and the environment: the biochemistry behind the headlines. *Essays in biochemistry, 61*(1), 1-10.
Venter, H., et al. (2015). RND-type drug efflux pumps from Gram-negative bacteria: molecular mechanism and inhibition. *Front Microbiol, 6*, 377. doi:10.3389/fmicb.2015.00377
Venter, H., et al. (2003). An ABC transporter with a secondary-active multidrug translocator domain. *Nature, 426*(6968), 866-870.
Wang, et al. (2016). Efflux pump inhibitors: a novel approach to combat efflux-mediated drug resistance in bacteria. *Current drug targets, 17*(6), 702-719.
Wang, Y., et al. (2021). Design and structural optimization of novel 2H-benzo [h] chromene derivatives that target AcrB and reverse bacterial multidrug resistance. *European journal of medicinal chemistry, 213*, 113049.
Wang, Y., et al. (2017). Evaluation of a series of 2-napthamide derivatives as inhibitors of the drug efflux pump AcrB for the reversal of antimicrobial resistance. *Bioorg Med Chem Lett, 27*(4), 733-739. doi:10.1016/j.bmcl.2017.01.042
Wang, Y., et al. (2018). Design, synthesis and biological activity evaluation of novel 4-subtituted 2-naphthamide derivatives as AcrB inhibitors. *European Journal of Medicinal Chemistry, 143*, 699-709. doi:https://doi.org/10.1016/j.ejmech.2017.11.102
Wang, Y., et al. (2018). Design, synthesis and biological activity evaluation of novel 4-subtituted 2-naphthamide derivatives as AcrB inhibitors. *European journal of medicinal chemistry, 143*, 699-709.

Wang, Y., et al. (2016). Efflux Pump Inhibitors: A Novel Approach to Combat Efflux-Mediated Drug Resistance in Bacteria. *Curr Drug Targets, 17*(6), 702-719. doi:10.2174/1389450116666151001103948

Ward, A., et al. (1999). Expression of prokaryotic membrane transport proteins in Escherichia coli. *Biochemical Society Transactions, 27*(6), 893-899.

Webber, M., & Piddock, L. (2003). The importance of efflux pumps in bacterial antibiotic resistance. *Journal of antimicrobial chemotherapy, 51*(1), 9-11.

Welch, et al. (2010). Promiscuous partnering and independent activity of MexB, the multidrug transporter protein from Pseudomonas aeruginosa. *Biochemical Journal, 430*(2), 355-364.

Welch, A., et al. (2010). Promiscuous partnering and independent activity of MexB, the multidrug transporter protein from Pseudomonas aeruginosa. *Biochemical Journal, 430*(2), 355-364.

WHO. (2017). *Antibacterial agents in clinical development: an analysis of the antibacterial clinical development pipeline, including tuberculosis*. Retrieved from

WHO. (2021). Antimicrobial Resistance. Retrieved from https://www.who.int/news-room/fact-sheets/detail/antimicrobial-resistance

Willyard, C. (2017). The drug-resistant bacteria that pose the greatest health threats. *Nature News, 543*(7643), 15.

Wilson, D. N. (2014). Ribosome-targeting antibiotics and mechanisms of bacterial resistance. *Nature Reviews Microbiology, 12*(1), 35-48.

Wozniak, T. M., et al. (2022). Disease burden, associated mortality and economic impact of antimicrobial resistant infections in Australia. *The Lancet Regional Health-Western Pacific, 27*, 100521.

Yamada, T., et al. (2020). Evaluation of daptomycin-induced cellular membrane injury in skeletal muscle. *Biological and Pharmaceutical Bulletin, 43*(9), 1338-1345.

Yoshida, K.-i., et al. (2007). MexAB-OprM specific efflux pump inhibitors in Pseudomonas aeruginosa. Part 7: highly soluble and in vivo active quaternary ammonium analogue D13-9001, a potential preclinical candidate. *Bioorganic & medicinal chemistry, 15*(22), 7087-7097.

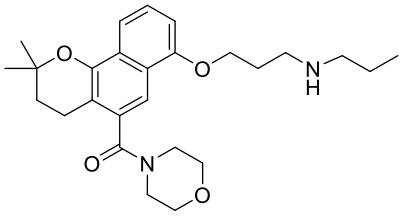
Yuan, Y., et al. (2022). Evaluation of heterocyclic carboxamides as potential efflux pump inhibitors in Pseudomonas aeruginosa. *Antibiotics, 11*(1), 30.

Zhang, L., et al. (2000). Multiple antibiotic resistance in Stenotrophomonas maltophilia: involvement of a multidrug efflux system. *Antimicrobial agents and chemotherapy, 44*(2), 287-293.

Zwama, M., et al. (2018). Multiple entry pathways within the efflux transporter AcrB contribute to multidrug recognition. *Nature Communications, 9*(1), 1-9.

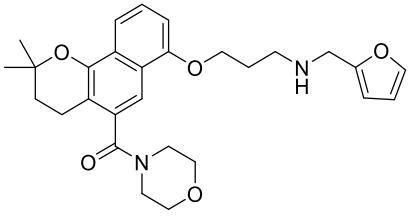
Appendices

Appendix 1. Chapter 3 Names and structures of benzochromene and flavonoid derivatives (39 compounds)



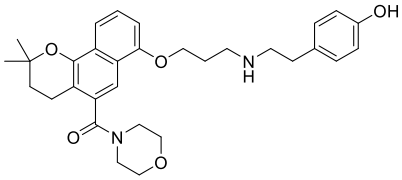
(2,2-dimethyl-7-(3-(propylamino)propoxy)-3,4-dihydro-2H-benzo[h]chromen-5-yl)(morpholino)methanone

G0



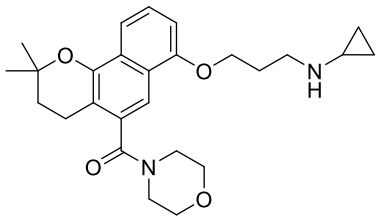
(7-(3-((furan-2-ylmethyl)amino)propoxy)-2,2-dimethyl-3,4-dihydro-2H-benzo[h]chromen-5-yl)(morpholino)methanone

G1



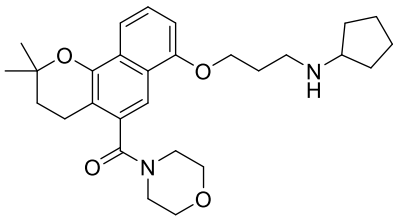
(7-(3-((4-hydroxyphenethyl)amino)propoxy)-2,2-dimethyl-3,4-dihydro-2H-benzo[h]chromen-5-yl)(morpholino)methanone

G2



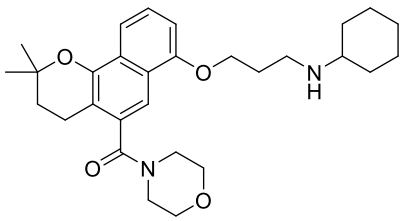
(7-(3-(cyclopropylamino)propoxy)-2,2-dimethyl-3,4-dihydro-2H-benzo[h]chromen-5-yl)(morpholino)methanone

G3



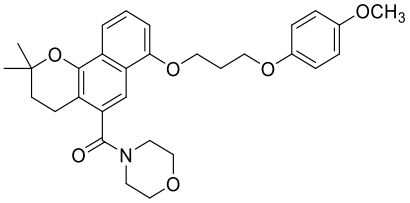
(7-(3-(cyclopentylamino)propoxy)-2,2-dimethyl-3,4-dihydro-2H-benzo[h]chromen-5-yl)(morpholino)methanone

G4



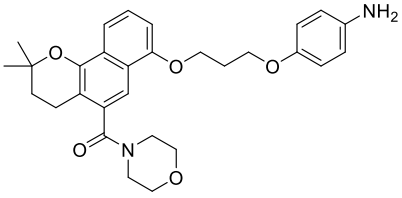
(7-(3-(cyclohexylamino)propoxy)-2,2-dimethyl-3,4-dihydro-2H-benzo[h]chromen-5-yl)(morpholino)methanone

G5



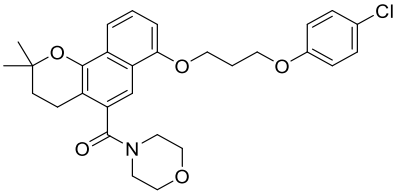
(7-(3-(4-methoxyphenoxy)propoxy)-2,2-dimethyl-3,4-dihydro-2H-benzo[h]chromen-5-yl)(morpholino)methanone

G6



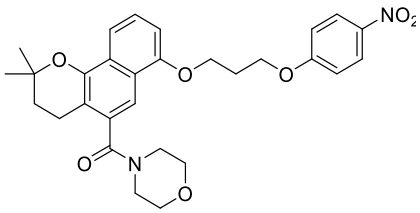
(7-(3-(4-aminophenoxy)propoxy)-2,2-dimethyl-3,4-dihydro-2H-benzo[h]chromen-5-yl)(morpholino)methanone

G7



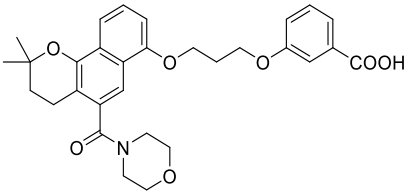
(7-(3-(4-chlorophenoxy)propoxy)-2,2-dimethyl-3,4-dihydro-2H-benzo[h]chromen-5-yl)(morpholino)methanone

G8



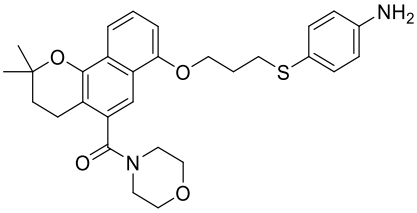
(2,2-dimethyl-7-(3-(4-nitrophenoxy)propoxy)-3,4-dihydro-2H-benzo[h]chromen-5-yl)(morpholino)methanone

G9



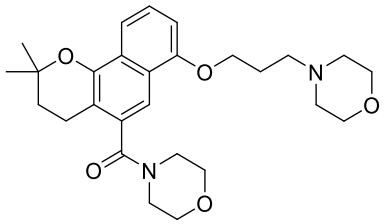
3-(3-((2,2-dimethyl-5-(morpholine-4-carbonyl)-3,4-dihydro-2H-benzo[h]chromen-7-yl)oxy)propoxy)benzoic acid

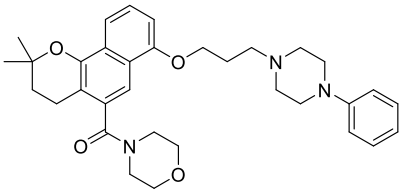
G10

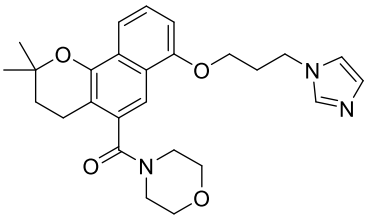


(7-(3-((4-aminophenyl)thio)propoxy)-2,2-dimethyl-3,4-dihydro-2H-benzo[h]chromen-5-yl)(morpholino)methanone

G11







(2,2-dimethyl-7-(3-morpholinopropoxy)-3,4-dihydro-2H-benzo[h]chromen-5-yl)(morpholino)methanone

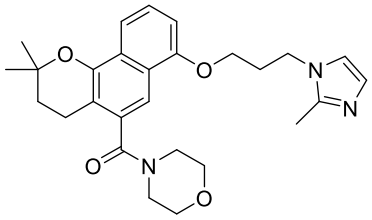
G12

(2,2-dimethyl-7-(3-(4-phenylpiperazin-1-yl)propoxy)-3,4-dihydro-2H-benzo[h]chromen-5-yl)(morpholino)methanone

G13

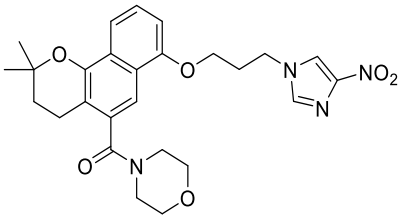
(7-(3-(1H-imidazol-1-yl)propoxy)-2,2-dimethyl-3,4-dihydro-2H-benzo[h]chromen-5-yl)(morpholino)methanone

G14



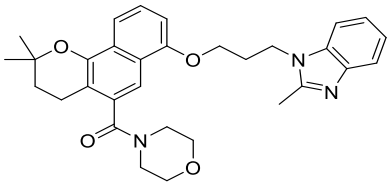
(2,2-dimethyl-7-(3-(2-methyl-1H-imidazol-1-yl)propoxy)-3,4-dihydro-2H-benzo[h]chromen-5-yl)(morpholino)methanone

G15



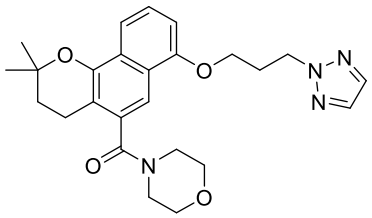
(2,2-dimethyl-7-(3-(4-nitro-1H-imidazol-1-yl)propoxy)-3,4-dihydro-2H-benzo[h]chromen-5-yl)(morpholino)methanone

G16



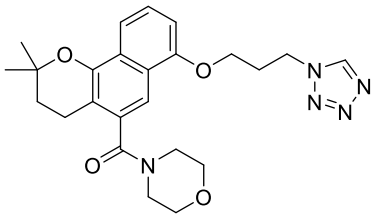
(2,2-dimethyl-7-(3-(2-methyl-1H-benzo[d]imidazol-1-yl)propoxy)-3,4-dihydro-2H-benzo[h]chromen-5-yl)(morpholino)methanone

G17



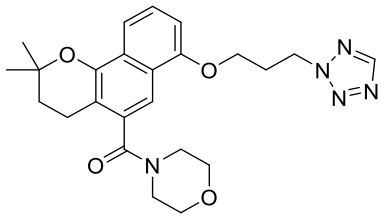
(7-(3-(2H-1,2,3-triazol-2-yl)propoxy)-2,2-dimethyl-3,4-dihydro-2H-benzo[h]chromen-5-yl)(morpholino)methanone

G18



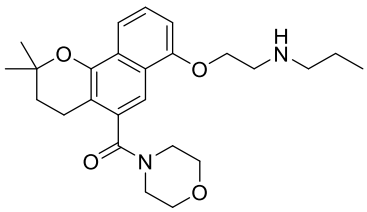
(7-(3-(1H-tetrazol-1-yl)propoxy)-2,2-dimethyl-3,4-dihydro-2H-benzo[h]chromen-5-yl)(morpholino)methanone

G19



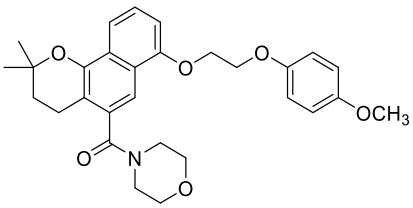
(7-(3-(2H-tetrazol-2-yl)propoxy)-2,2-dimethyl-3,4-dihydro-2H-benzo[h]chromen-5-yl)(morpholino)methanone

G20



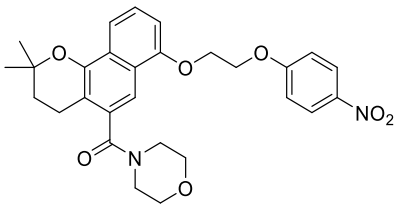
(2,2-dimethyl-7-(2-(propylamino)ethoxy)-3,4-dihydro-2H-benzo[h]chromen-5-yl)(morpholino)methanone

H1



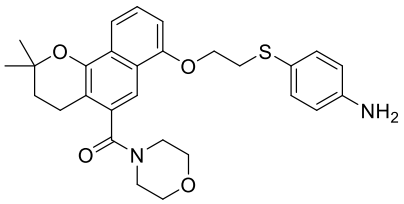
(7-(2-(4-methoxyphenoxy)ethoxy)-2,2-dimethyl-3,4-dihydro-2H-benzo[h]chromen-5-yl)(morpholino)methanone

H2



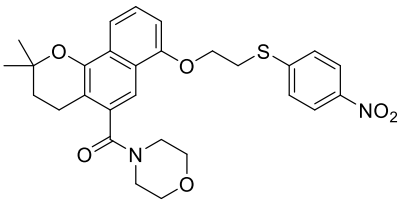
(2,2-dimethyl-7-(2-(4-nitrophenoxy)ethoxy)-3,4-dihydro-2H-benzo[h]chromen-5-yl)(morpholino)methanone

H3



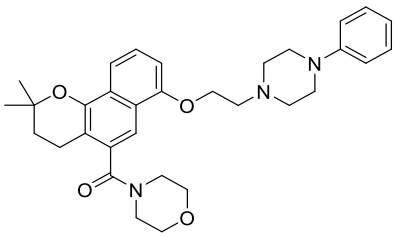
(7-(2-((4-aminophenyl)thio)ethoxy)-2,2-dimethyl-3,4-dihydro-2H-benzo[h]chromen-5-yl)(morpholino)methanone

H4



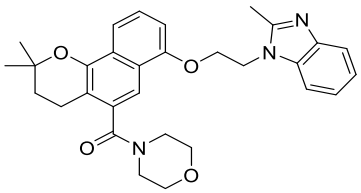
(2,2-dimethyl-7-(2-((4-nitrophenyl)thio)ethoxy)-3,4-dihydro-2H-benzo[h]chromen-5-yl)(morpholino)methanone

H5



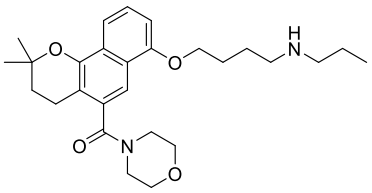
(2,2-dimethyl-7-(2-(4-phenylpiperazin-1-yl)ethoxy)-3,4-dihydro-2H-benzo[h]chromen-5-yl)(morpholino)methanone

H6



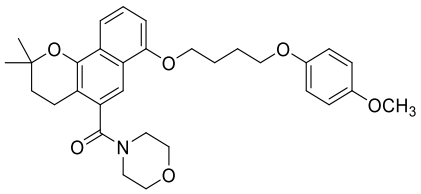
(2,2-dimethyl-7-(2-(2-methyl-1H-benzo[d]imidazol-1-yl)ethoxy)-3,4-dihydro-2H-benzo[h]chromen-5-yl)(morpholino)methanone

H7



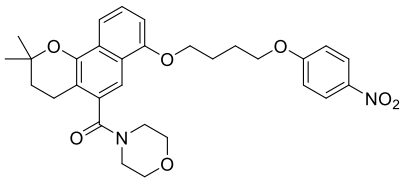
(2,2-dimethyl-7-(4-(propylamino)butoxy)-3,4-dihydro-2H-benzo[h]chromen-5-yl)(morpholino)methanone

Y1



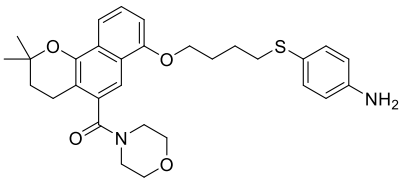
(7-(4-(4-methoxyphenoxy)butoxy)-2,2-dimethyl-3,4-dihydro-2H-benzo[h]chromen-5-yl)(morpholino)methanone

Y2



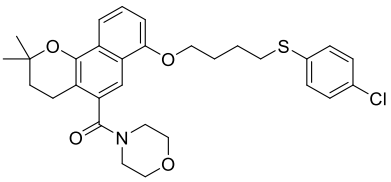
(2,2-dimethyl-7-(4-(4-nitrophenoxy)butoxy)-3,4-dihydro-2H-benzo[h]chromen-5-yl)(morpholino)methanone

Y3



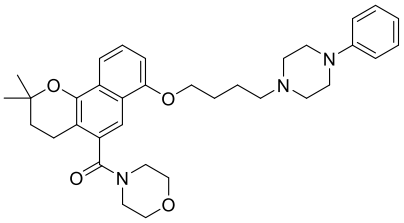
(7-(4-((4-aminophenyl)thio)butoxy)-2,2-dimethyl-3,4-dihydro-2H-benzo[h]chromen-5-yl)(morpholino)methanone

Y4



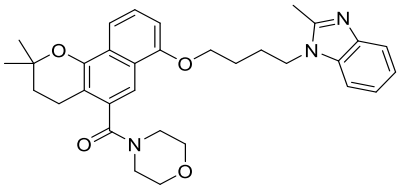
(7-(4-((4-chlorophenyl)thio)butoxy)-2,2-dimethyl-3,4-dihydro-2H-benzo[h]chromen-5-yl)(morpholino)methanone

Y5



(2,2-dimethyl-7-(4-(4-phenylpiperazin-1-yl)butoxy)-3,4-dihydro-2H-benzo[h]chromen-5-yl)(morpholino)methanone

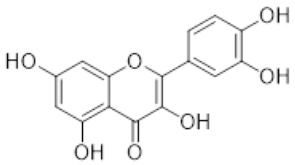
Y6



(2,2-dimethyl-7-(4-(2-methyl-1H-benzo[d]imidazol-1-yl)butoxy)-3,4-dihydro-2H-benzo[h]chromen-5-yl)(morpholino)methanone

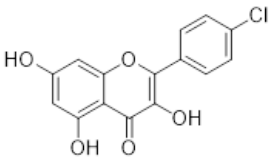
Y7

Figure A.1 Structures of thirty-five benzochromene derivatives.



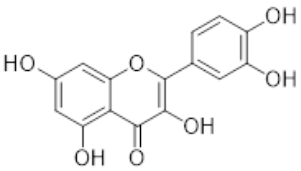
2-(3,4-dihydroxyphenyl)-3,5,7-trihydroxy-4H-chromen-4-one

S1



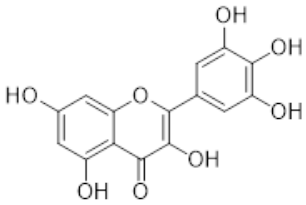
2-(4-chlorophenyl)-3,5,7-trihydroxy-4H-chromen-4-one

S2



2-(3,4-dihydroxyphenyl)-3,5,7-trihydroxy-4H-chromen-4-one

S3



3,5,7-trihydroxy-2-(3,4,5-trihydroxyphenyl)-4H-chromen-4-one

S4

Figure A.2 Structures of four flavonoid derivatives.

Appendix 2. Supplementary of paper in Chapter 3

Table A.1 The inherent antibacterial activities of benzo[*h*]chromene derivatives (series H, G and Y) against wild-type *E. coli* BW25113 and the BW25113 ΔAcrB mutant.

Compound	Strains / MIC (μg/mL)		Compound	Strains / MIC (μg/mL)	
	E. coli BW25113	*E. coli* BW25113 (ΔAcrB)		*E. coli* BW25113	*E. coli* BW25113 (ΔAcrB)
H1	>512	512	G11	>512	>512
H2	>512	>512	G12	>512	256
H3	>512	>512	G13	>512	>512
H4	>512	>512	G14	>512	256
H5	>512	>512	G15	>512	256
H6	>512	>512	G16	>512	>512
H7	>512	>512	G17	>512	>512
G0	>512	256	G18	>512	>512
G1	>512	256	G19	>512	>512
G2	>512	256	G20	>512	>512
G3	>512	256	Y1	>512	256
G4	>512	256	Y2	>512	>512
G5	>512	256	Y3	>512	>512
G6	>512	>512	Y4	>512	>512
G7	>512	>512	Y5	>512	>512
G8	>512	>512	Y6	>512	>512

G9	>512	>512	Y7	>512	>512
G10	>512	>512	PAβN	512	128

Table A.2 The effect of benzo[*h*]chromene derivatives (series H and G) with different antimicrobial agents against the BW25113 ΔAcrB mutant.

Compound	Concentration (μg/mL)	MIC (μg/mL)		
		ERY*	LEV*	MIN*
H3	8	4	0.0063	0.25
	16	4	0.0063	0.25
	32	4	0.0063	0.25
	64	4	0.0063	0.25
	128	4	0.0063	0.25
H5	4	4	0.0063	0.25
	8	4	0.0063	0.25
	16	4	0.0063	0.25
	32	4	0.0063	0.25
	64	4	0.0063	0.25
H6	0.5	4	0.0063	0.25
	1	4	0.0063	0.25
	2	4	0.0063	0.25
	4	4	0.0063	0.25
	8	4	0.0063	0.25
G6	8	4	0.0063	0.25
	16	4	0.0063	0.25
	32	4	0.0063	0.25
	64	4	0.0063	0.25

	128	4	0.0063	0.25
G10	4	4	0.0063	0.25
	8	4	0.0063	0.25
	16	4	0.0063	0.25
	32	4	0.0063	0.25
	64	4	0.0063	0.25
G11	4	4	0.0063	0.25
	8	4	0.0063	0.25
	16	4	0.0063	0.25
	32	4	0.0063	0.25
	64	4	0.0063	0.25
NONE (-) AcrB	0	4	0.0063	0.25

*ERY = erythromycin, LEV = levofloxacin, MIN = minocycline

Only compounds showing an effect are reported.

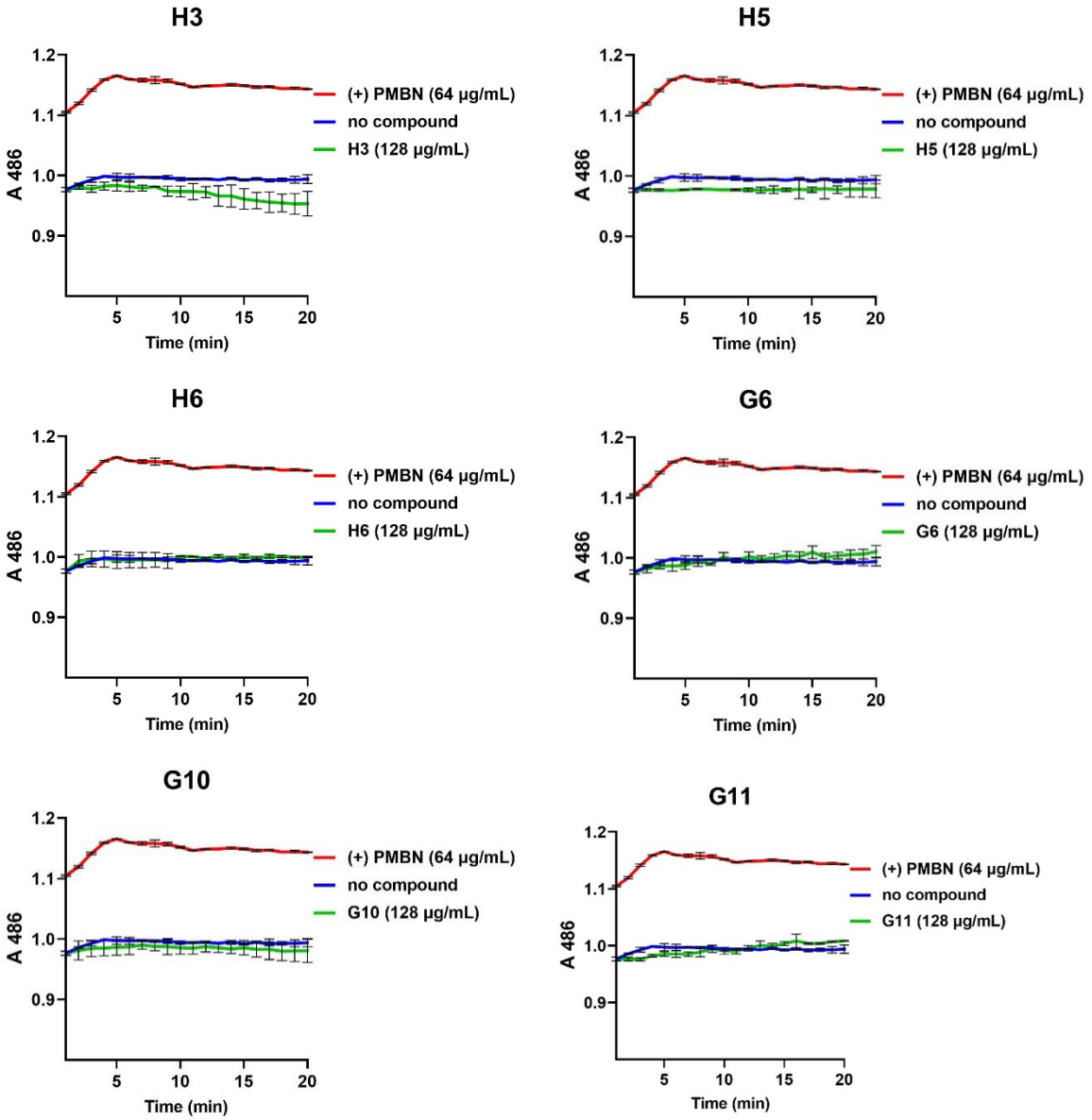
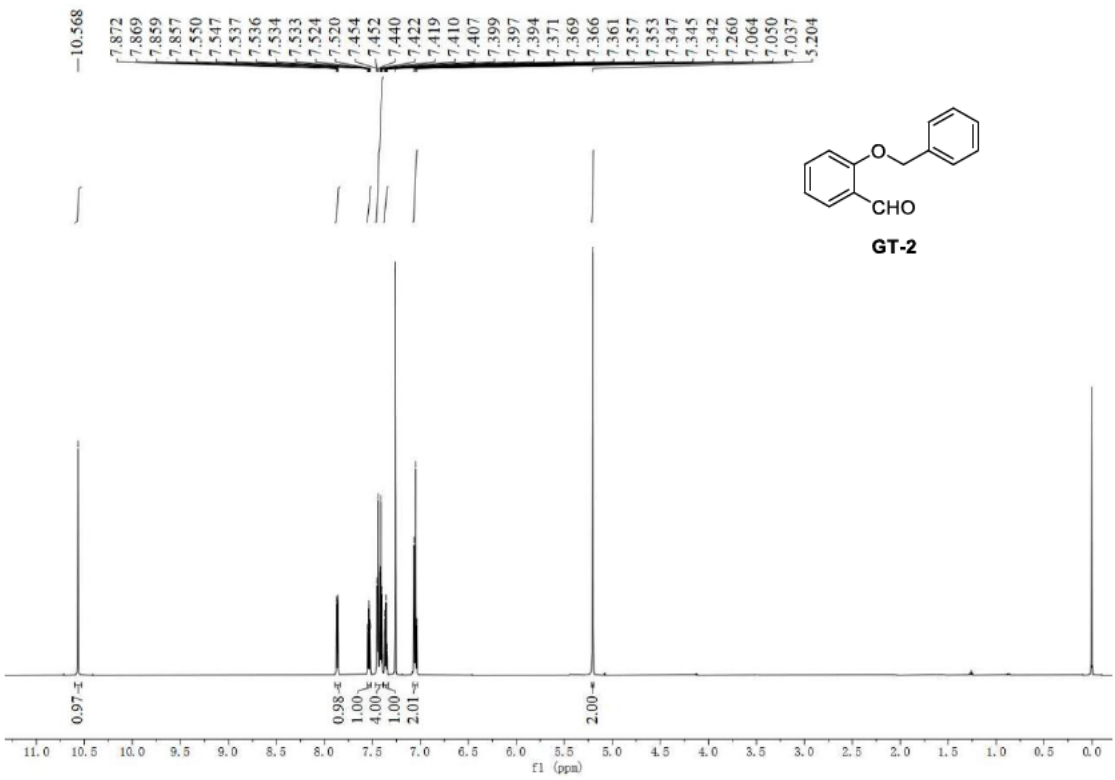


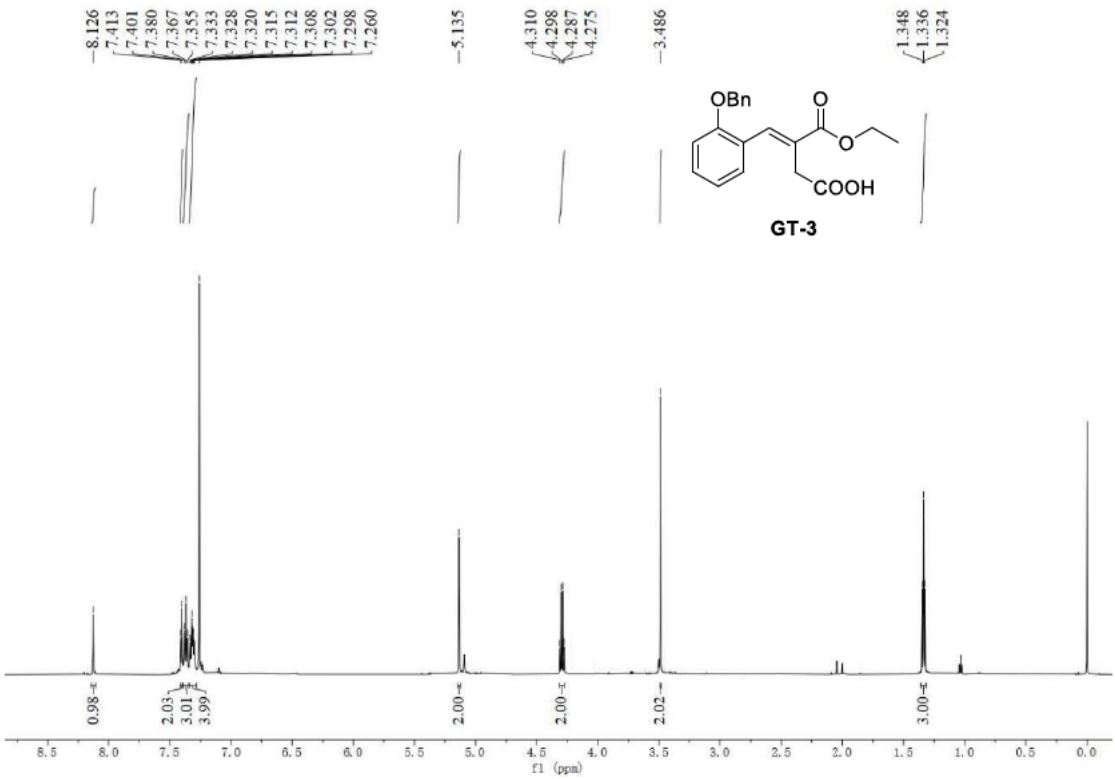
Figure A.3 Effect of the compounds on outer membrane permeabilization. *E. coli* BW25113 wild-type cells were treated with 10 µM CCCP to inhibit the efflux of nitrocefin.

Nitrocefin was added to the cells that received no compound (blue lines) or were treated with the outer membrane permeabilizer polymyxin B nonapeptide (PMBN, red lines) or the test compounds at 128 µg/mL (green lines). Nitrocefin hydrolysis by the periplasmic β-lactamase was observed as an increase in A_{486}. Representative traces are shown from experiments done on different days.

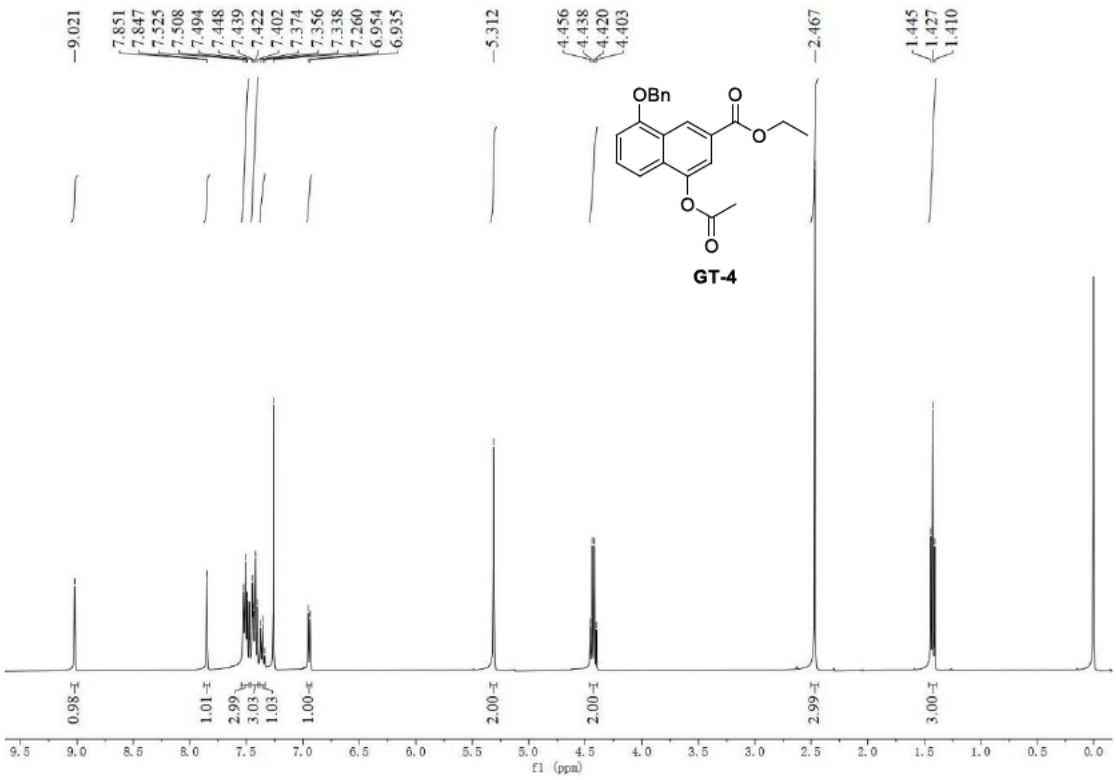
^{1}H-NMR of **GT-2**



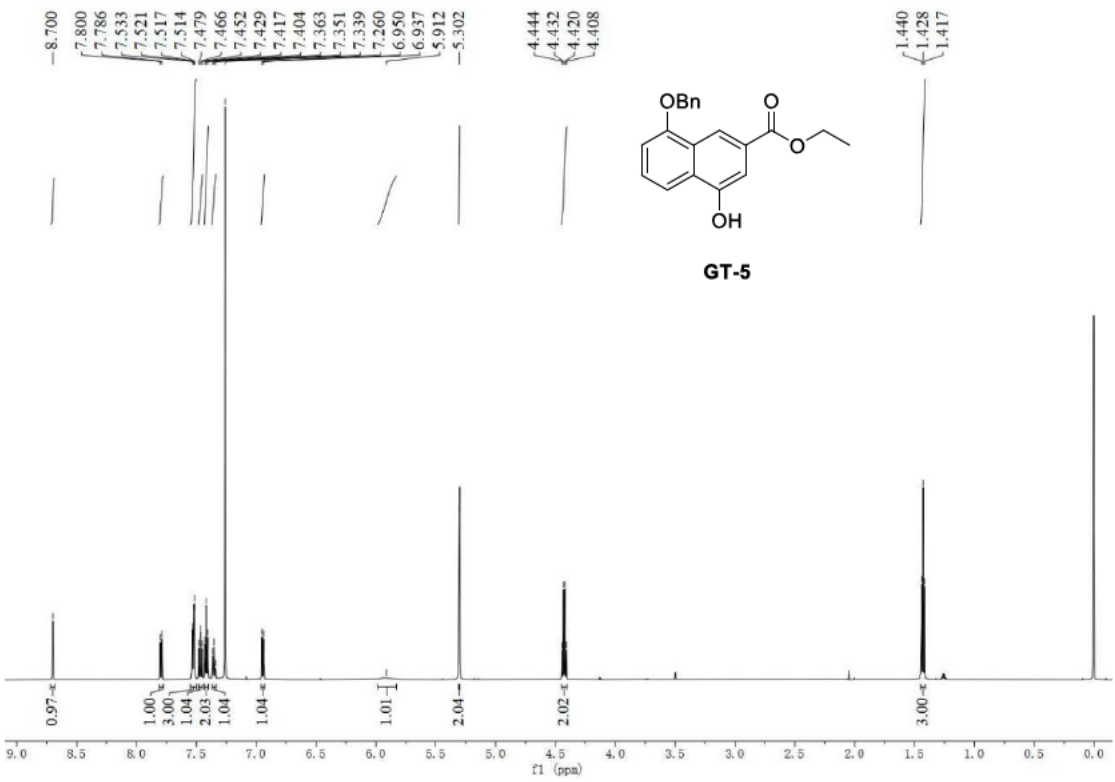
^{1}H-NMR of **GT-3**



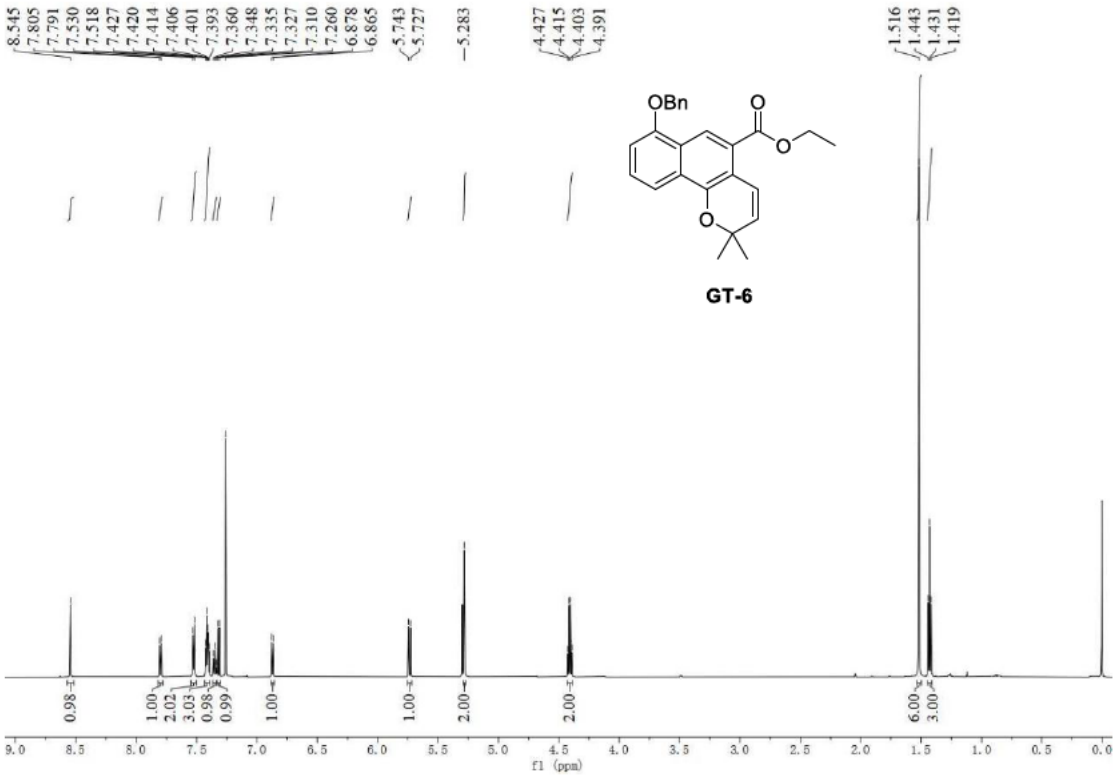
^{1}H-NMR of **GT-4**



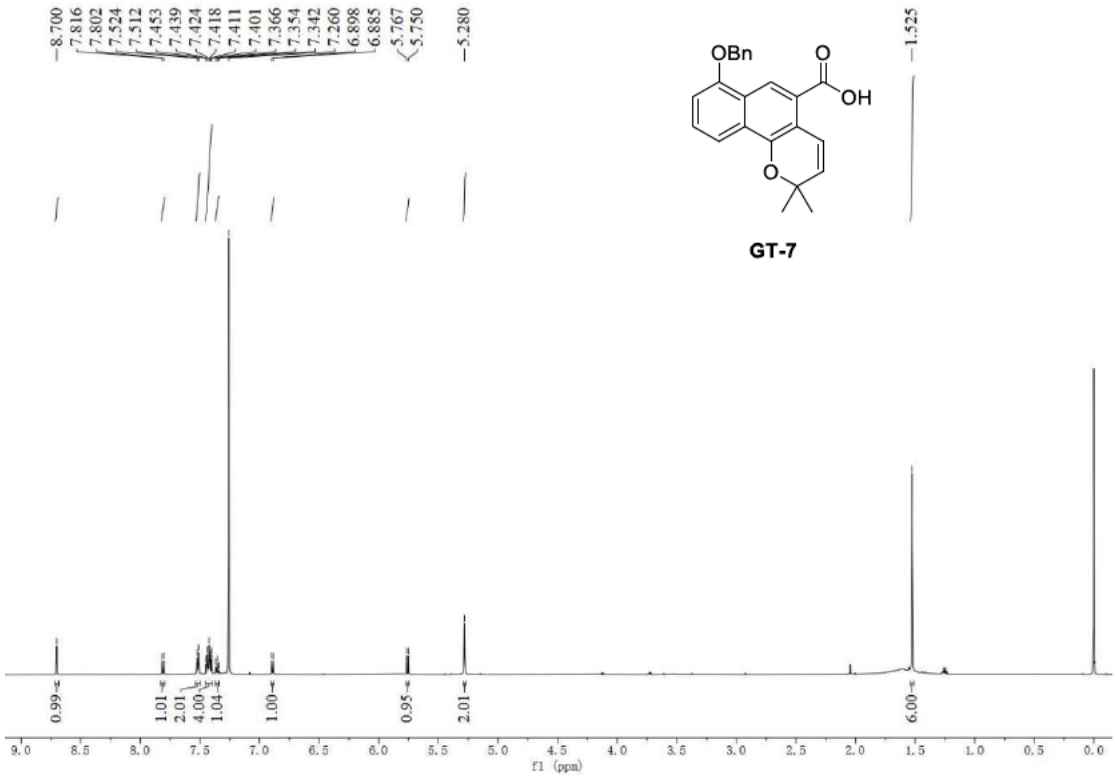
^{1}H-NMR of **GT-5**



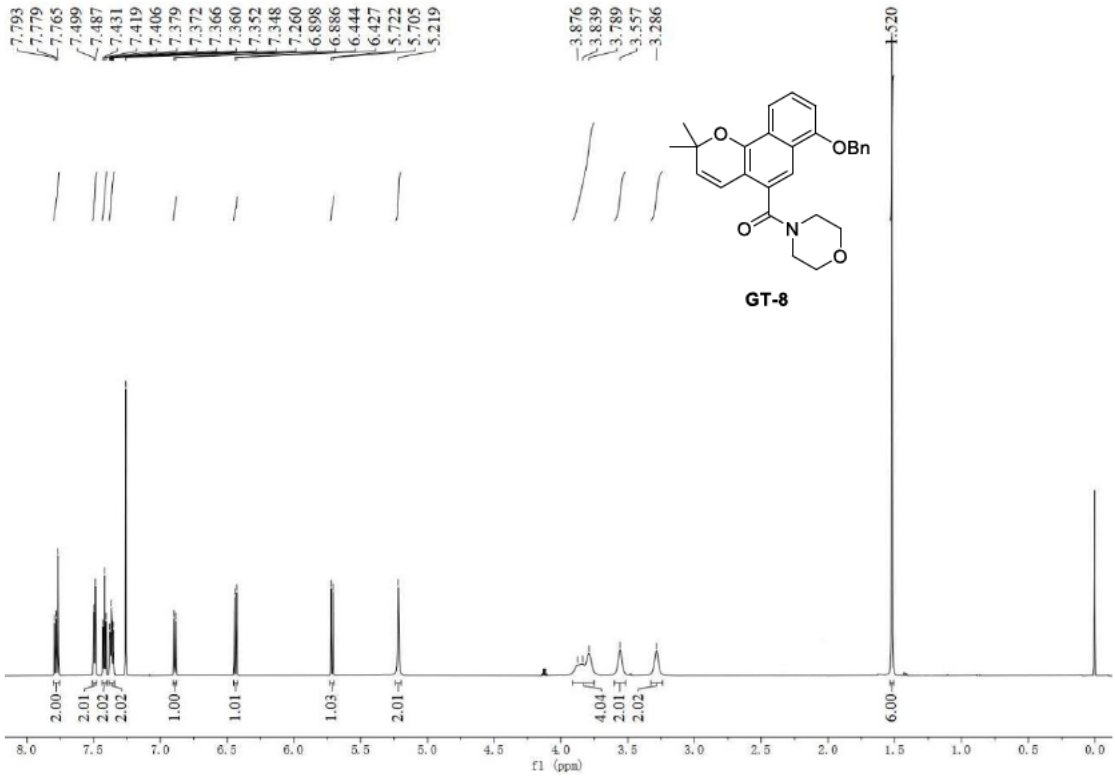
^{1}H-NMR of **GT-6**



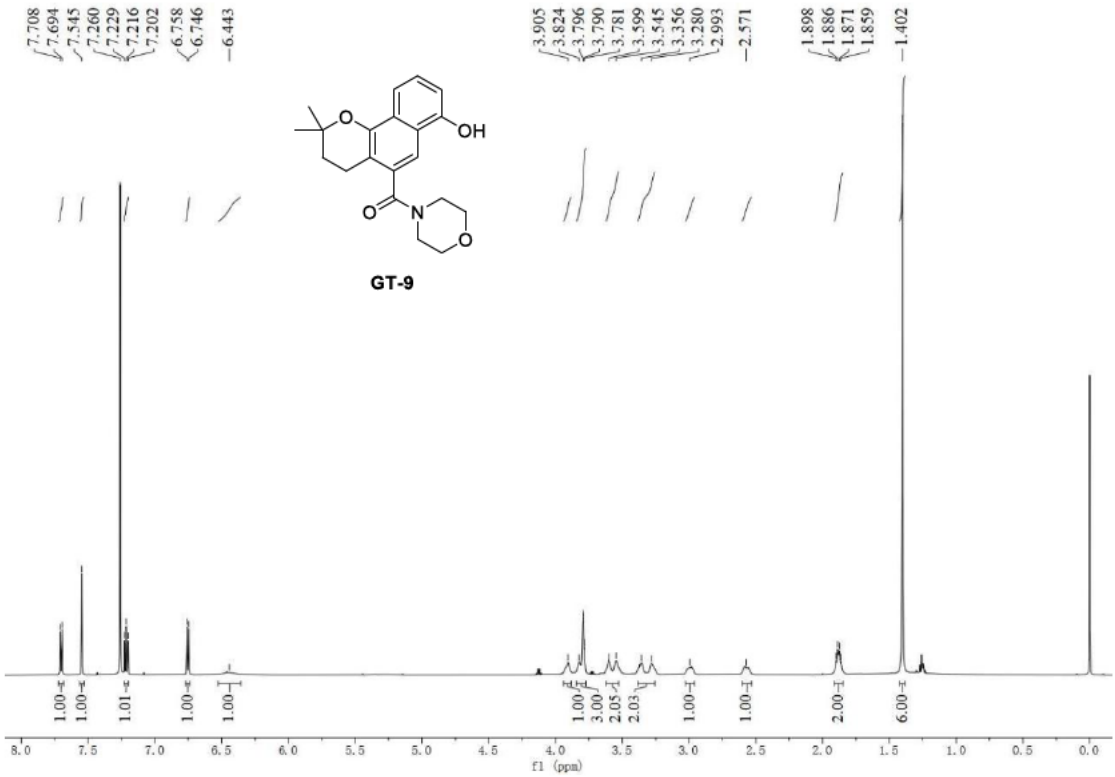
^{1}H-NMR of **GT-7**



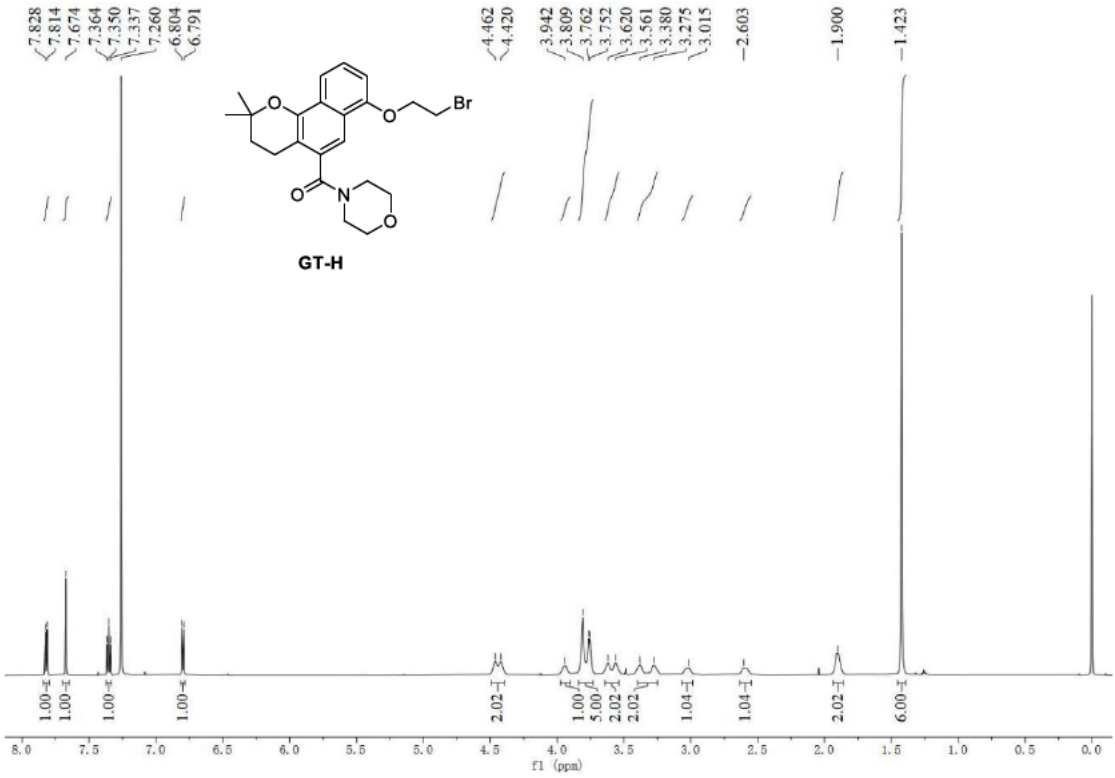
^{1}H-NMR of **GT-8**



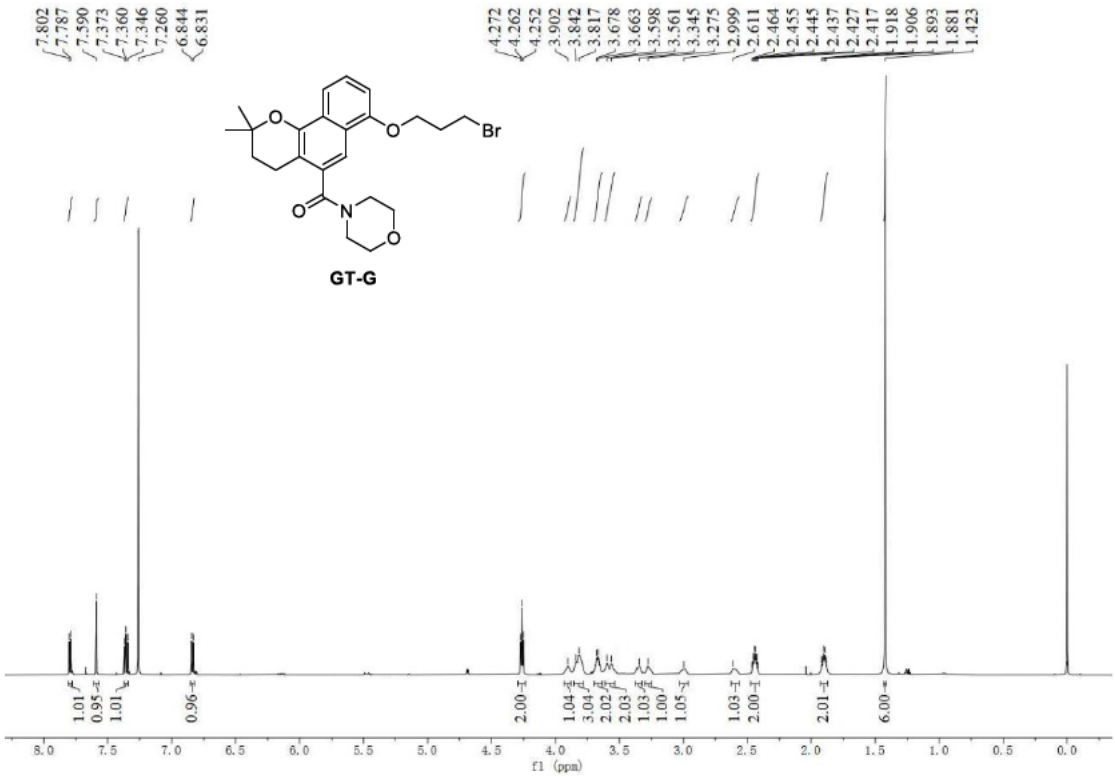
^{1}H-NMR of **GT-9**



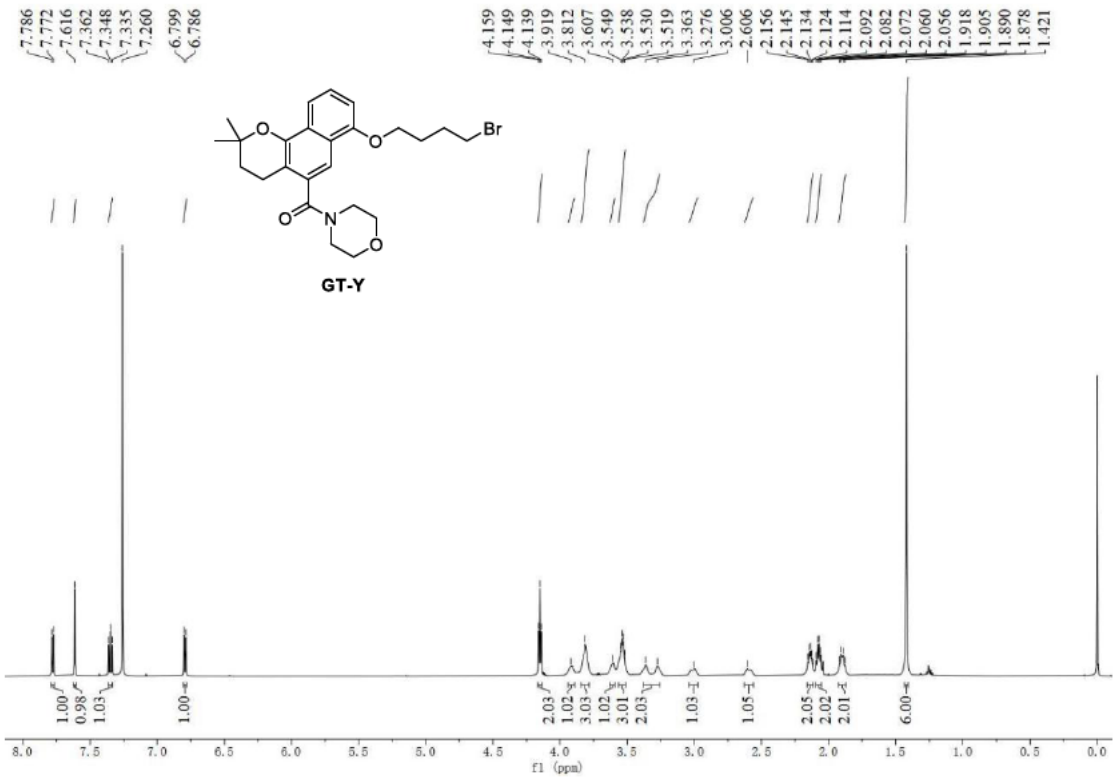
^{1}H-NMR of **GT-H**



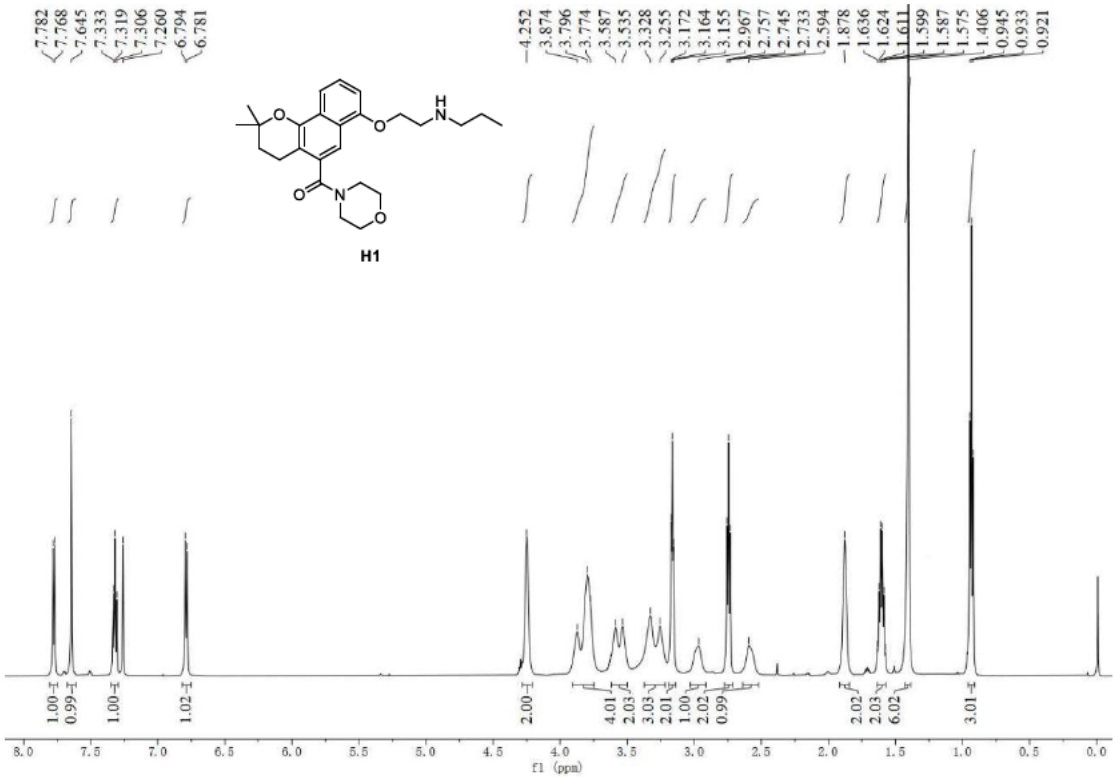
^{1}H-NMR of **GT-G**

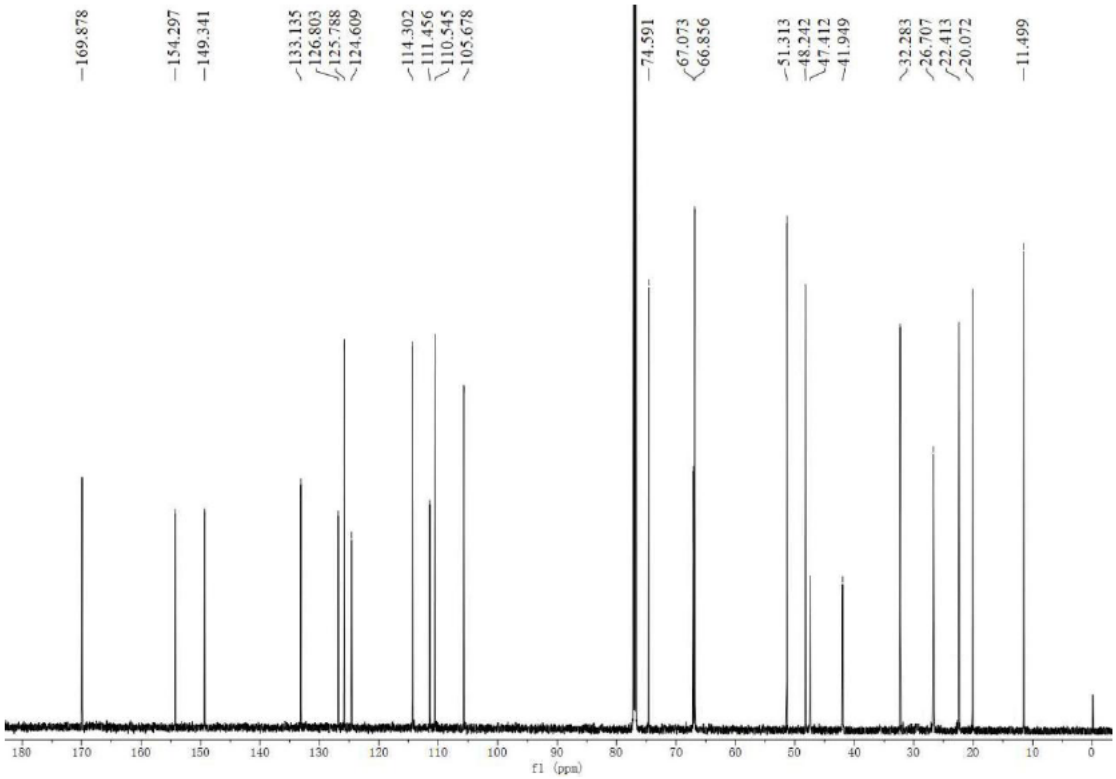


^{1}H-NMR of **GT-Y**

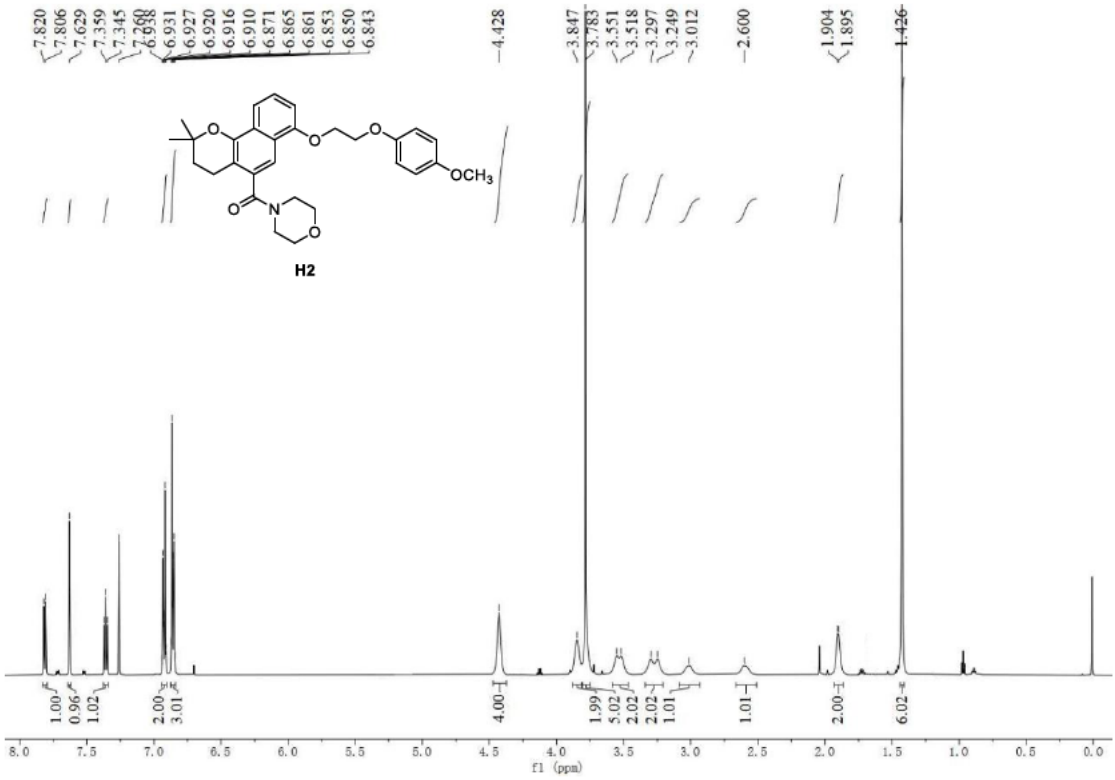

7.786
7.772
7.616
7.362
7.348
7.335
7.260
6.799
6.786
4.159
4.149
4.139
3.919
3.812
3.607
3.549
3.538
3.530
3.519
3.363
3.276
3.006
2.606
2.156
2.145
2.134
2.124
2.114
2.092
2.082
2.072
2.060
2.056
1.918
1.905
1.890
1.878
1.421
Br
O
N
GT-Y
1.00
0.98
1.03
1.00
2.03
1.02
3.03
1.02
3.01
2.03
1.03
1.05
2.05
2.02
2.01
6.00
8.0
7.5
7.0
6.5
6.0
5.5
5.0
4.5
4.0
3.5
3.0
2.5
2.0
1.5
1.0
0.5
0.0
f1 (ppm)

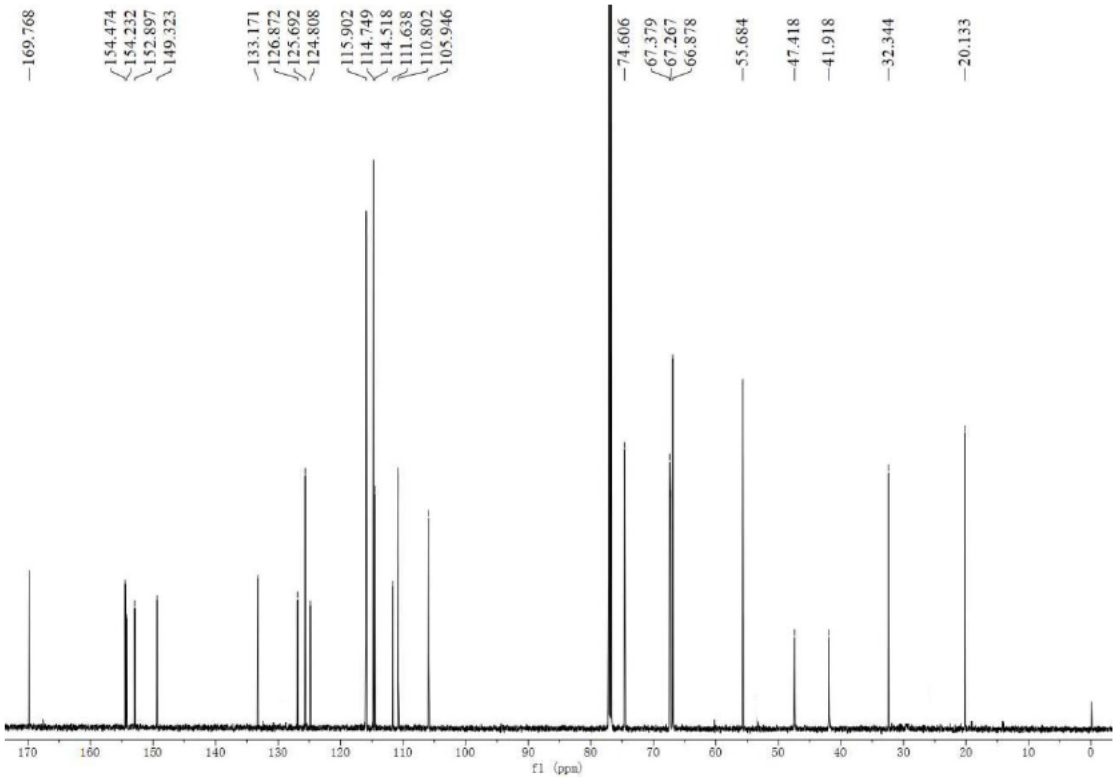
^{1}H-NMR and ^{13}C-NMR of **H1**



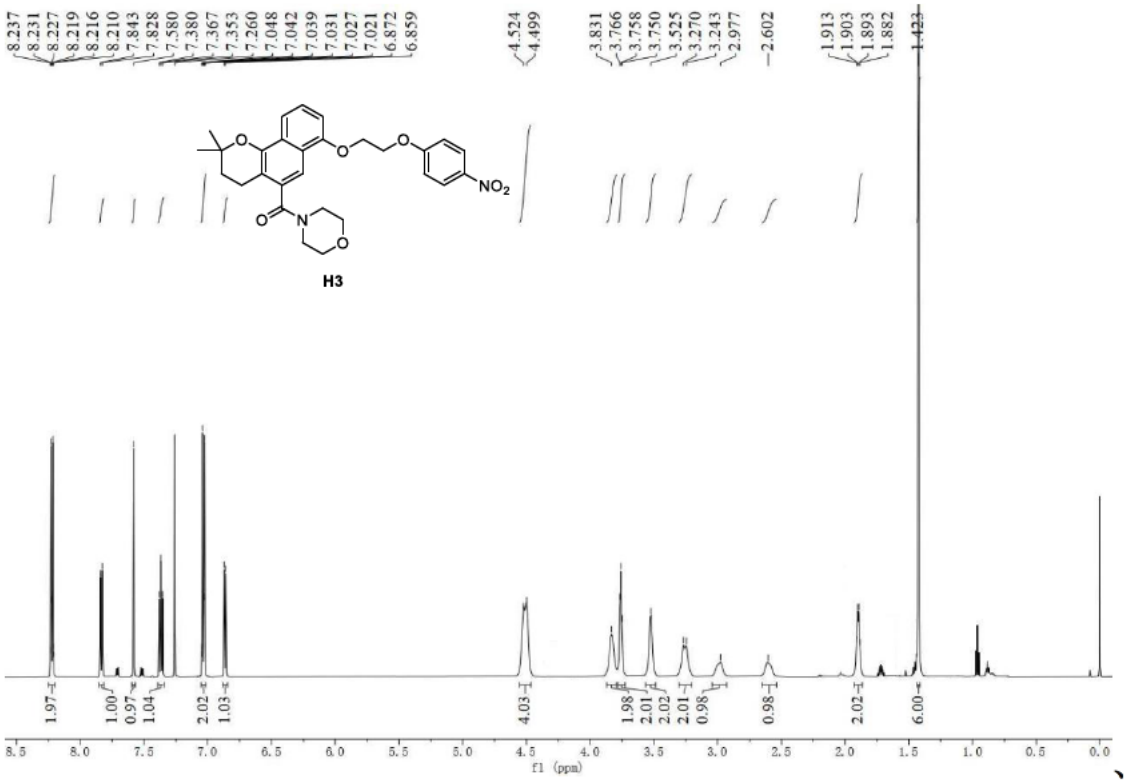


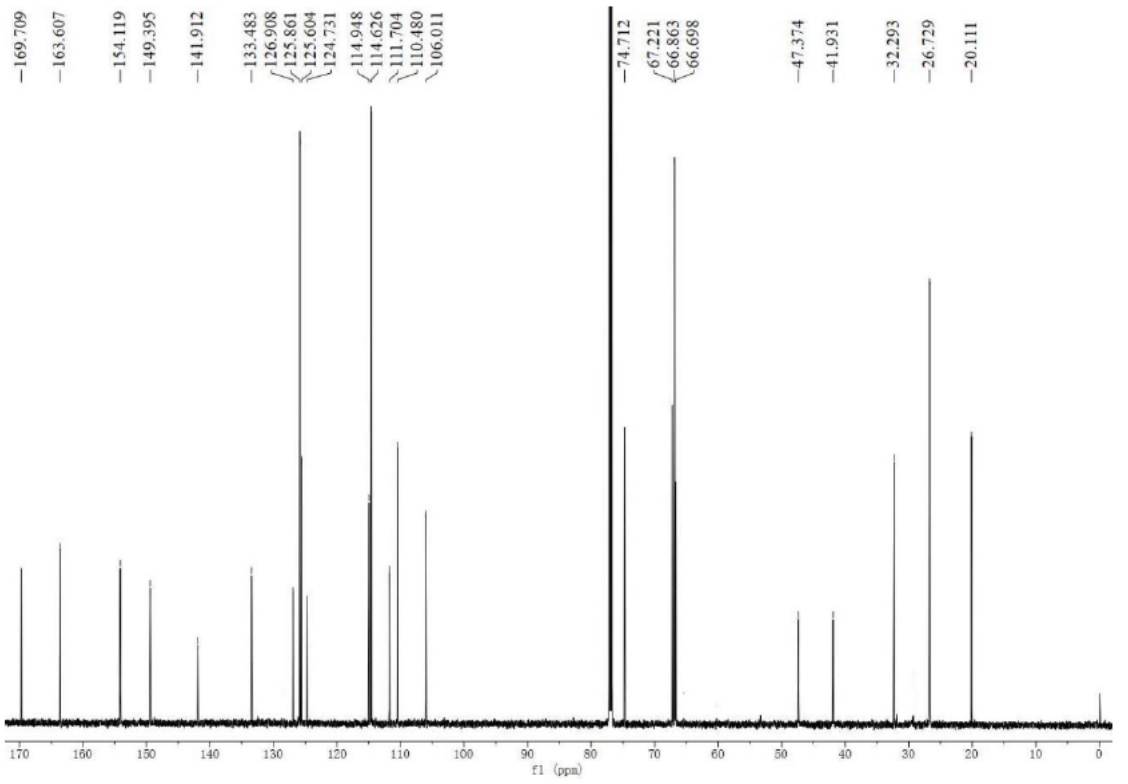
^{1}H-NMR and ^{13}C-NMR of **H2**



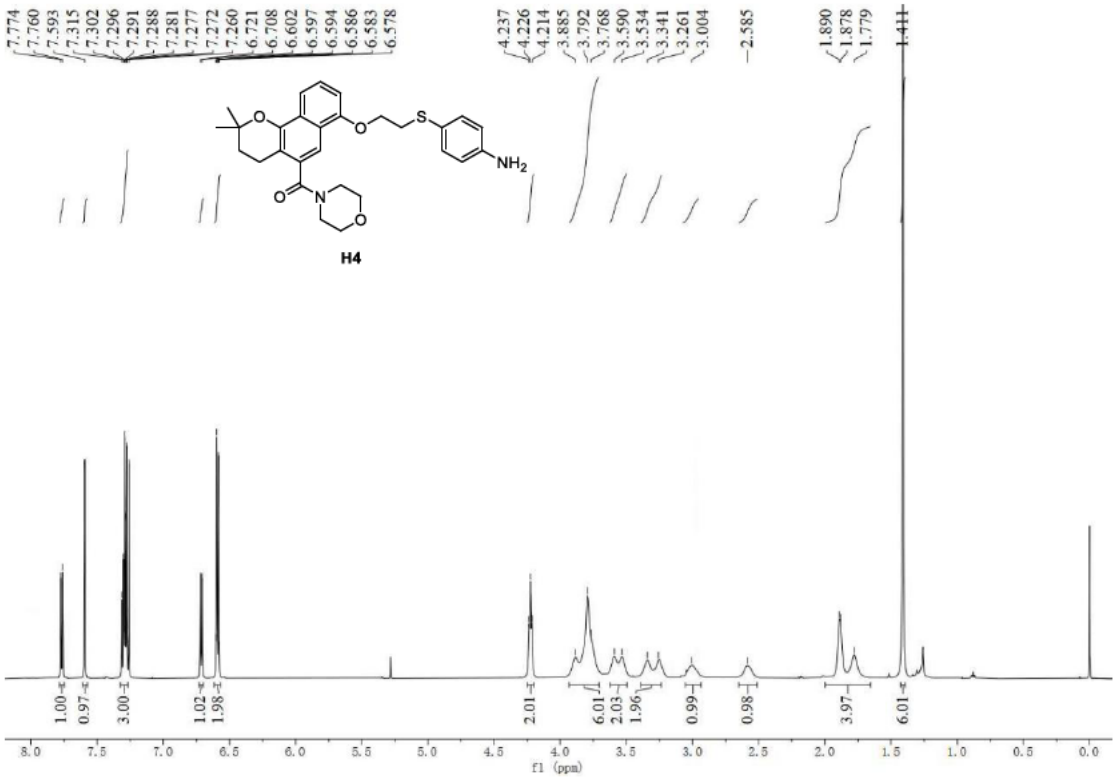


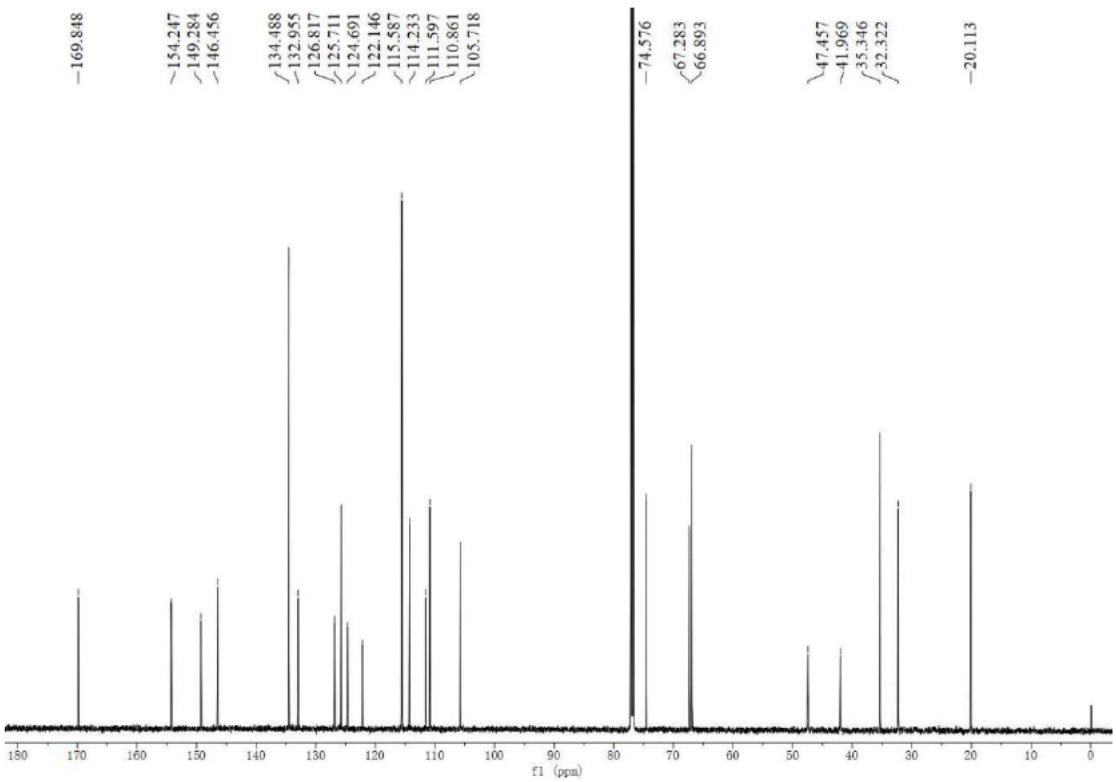
^{1}H-NMR and ^{13}C-NMR of **H3**



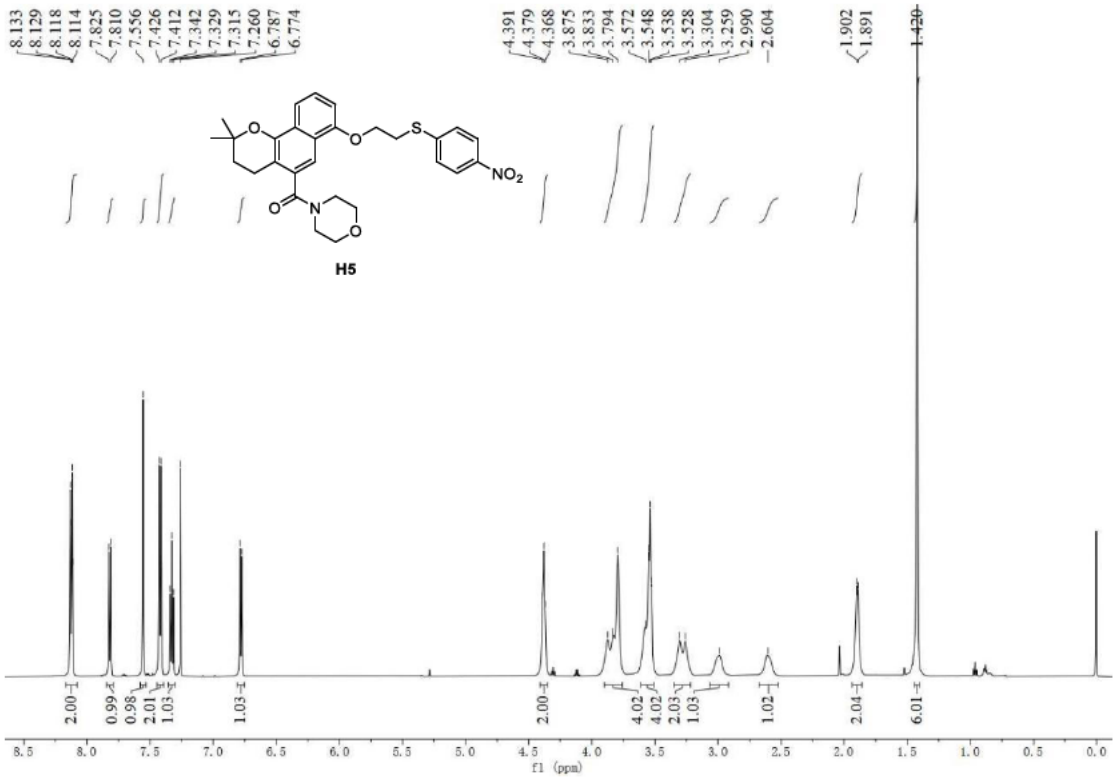


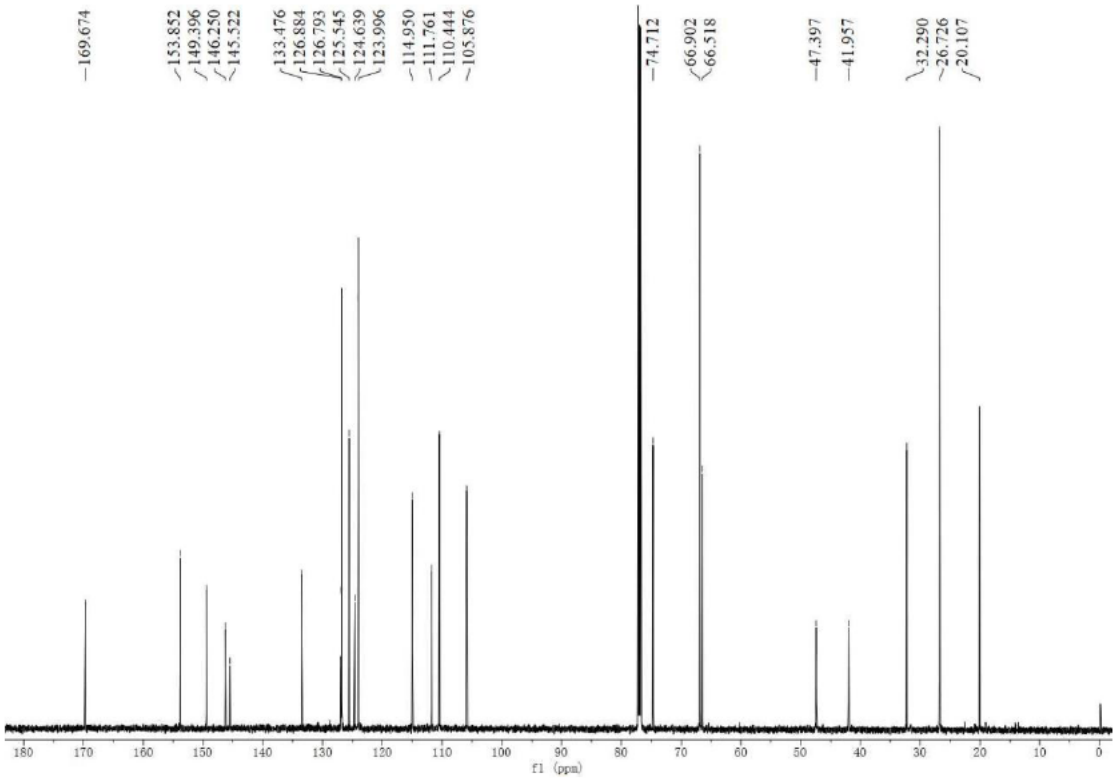
^{1}H-NMR and ^{13}C-NMR of **H4**



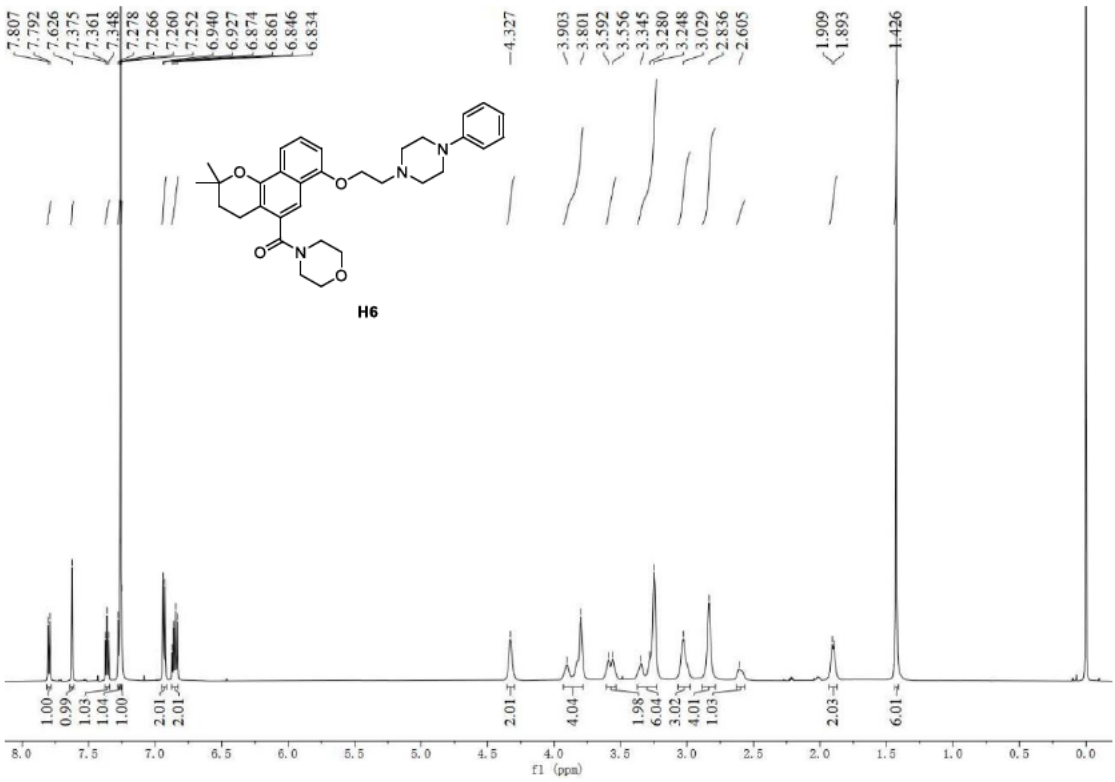


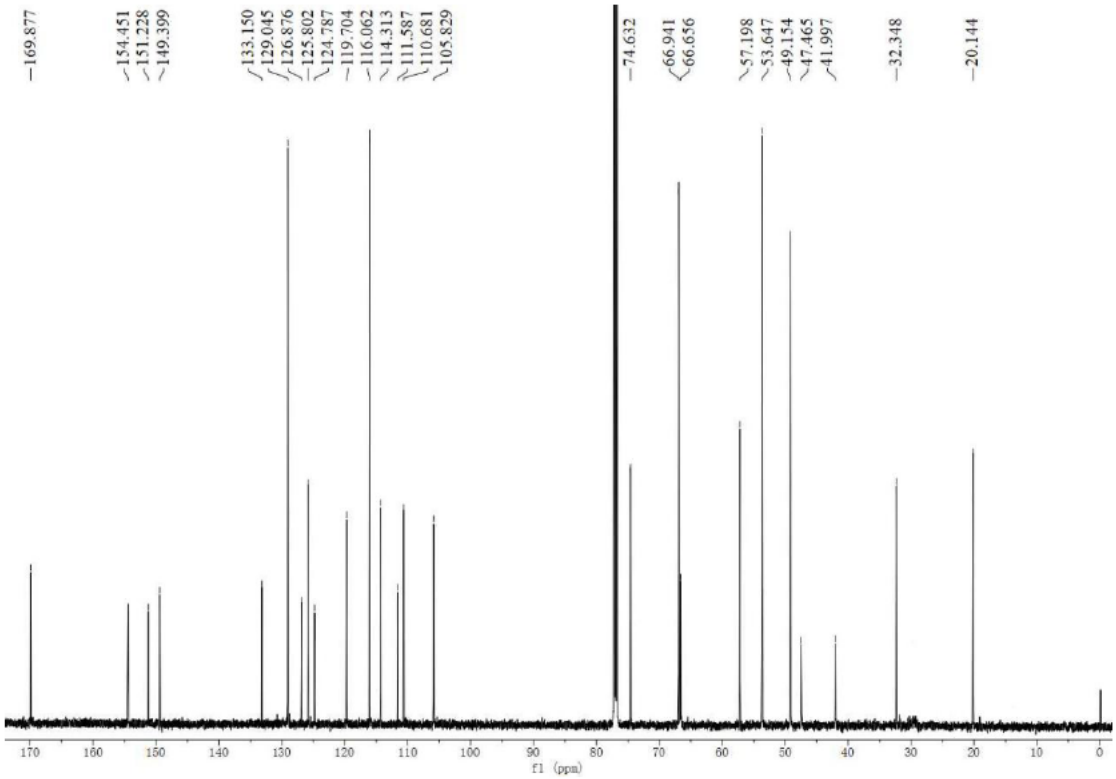
^{1}H-NMR and ^{13}C-NMR of **H5**



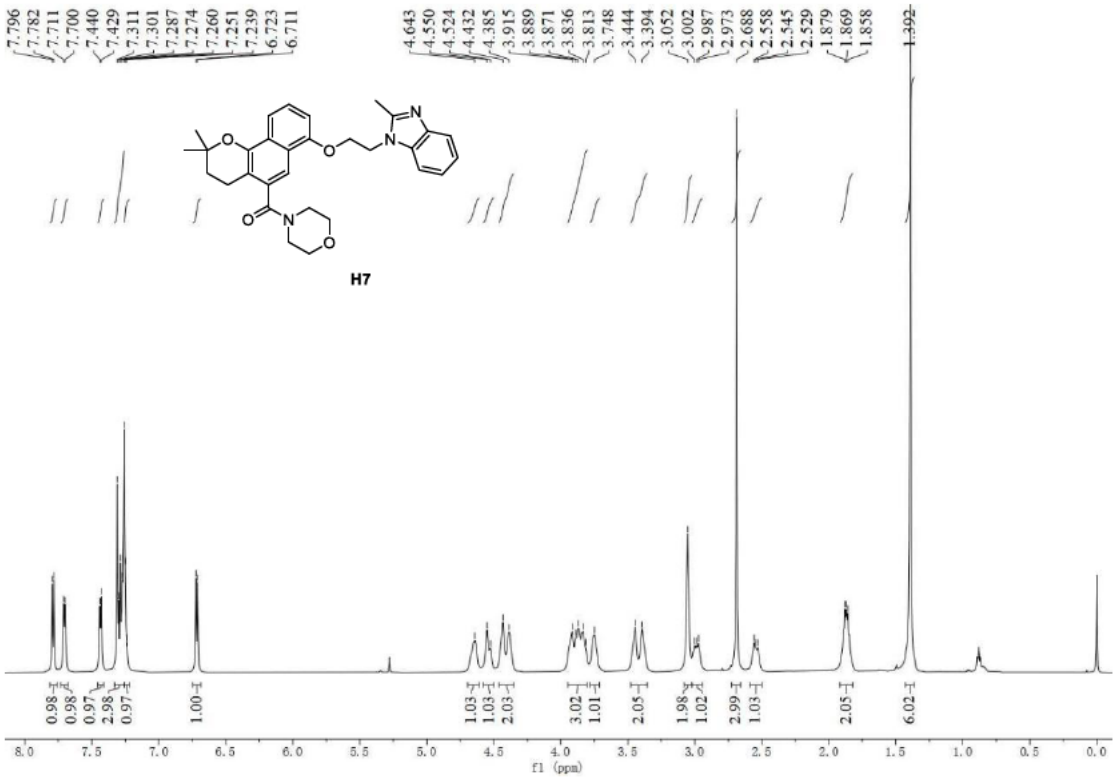


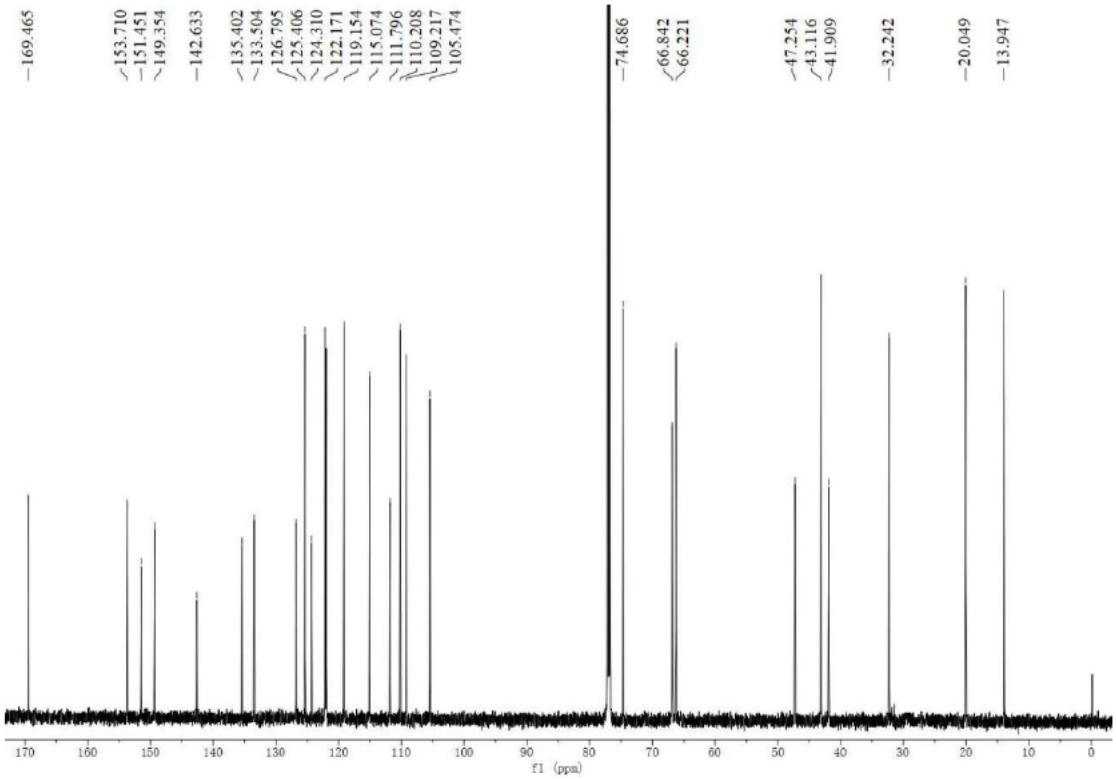
^{1}H-NMR and ^{13}C-NMR of **H6**



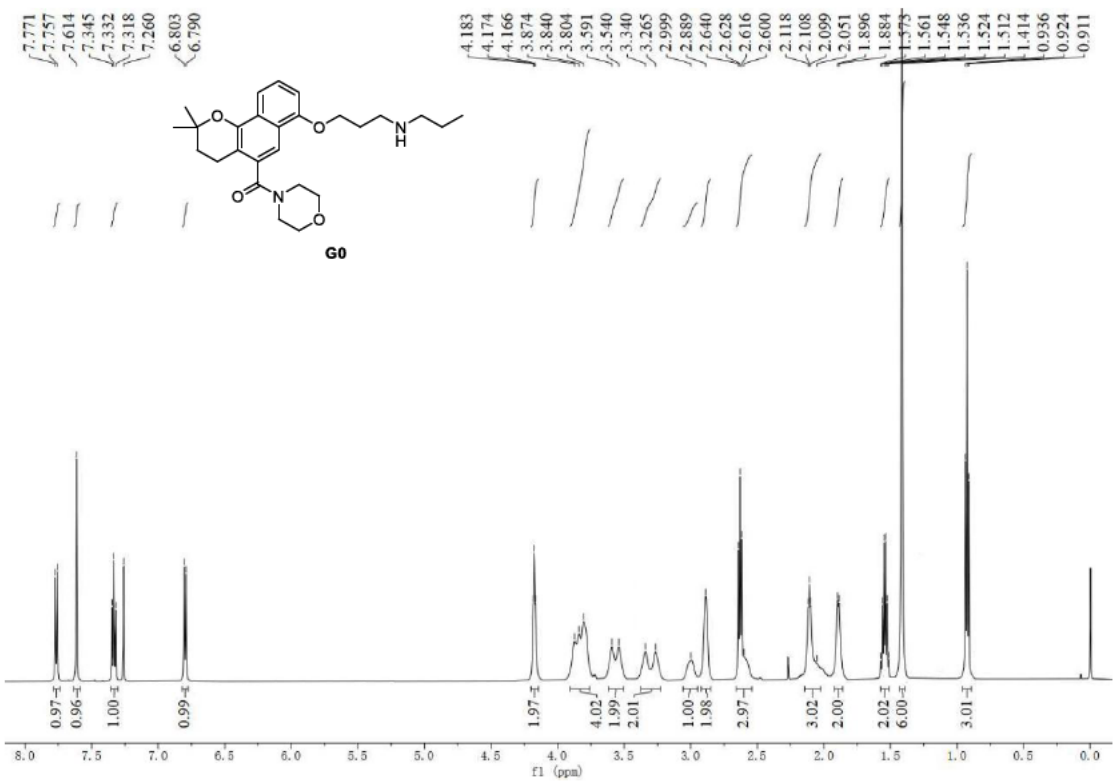


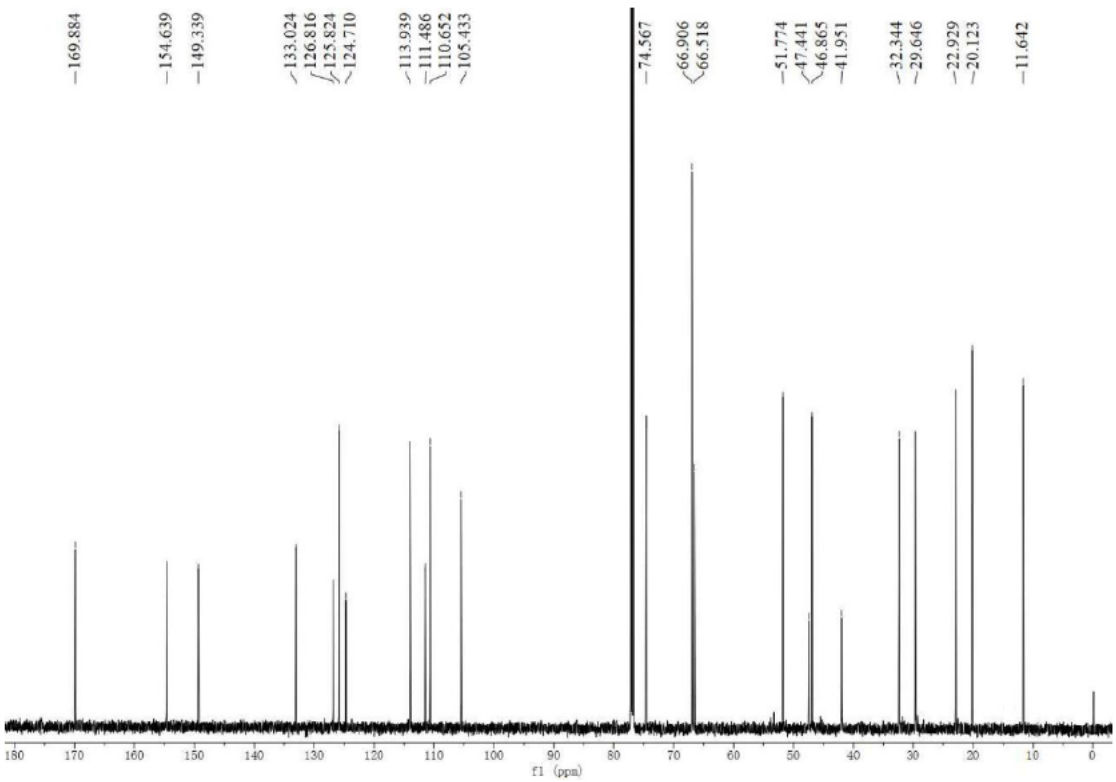
^{1}H-NMR and ^{13}C-NMR of **H7**



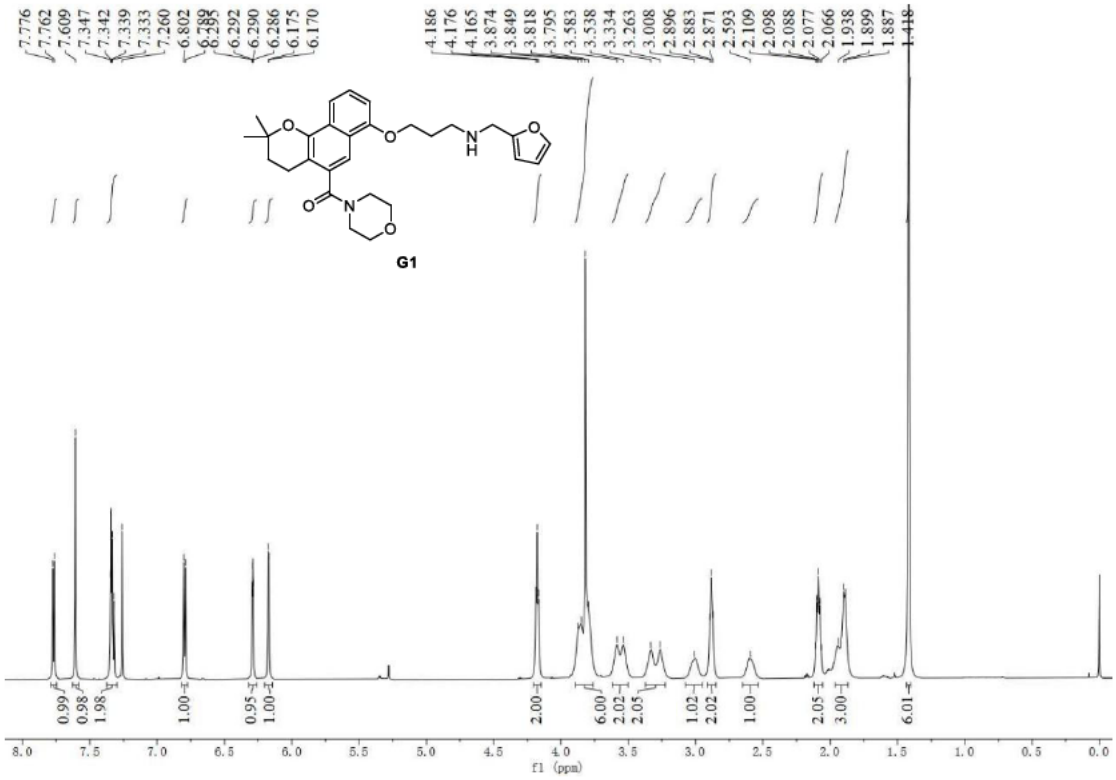


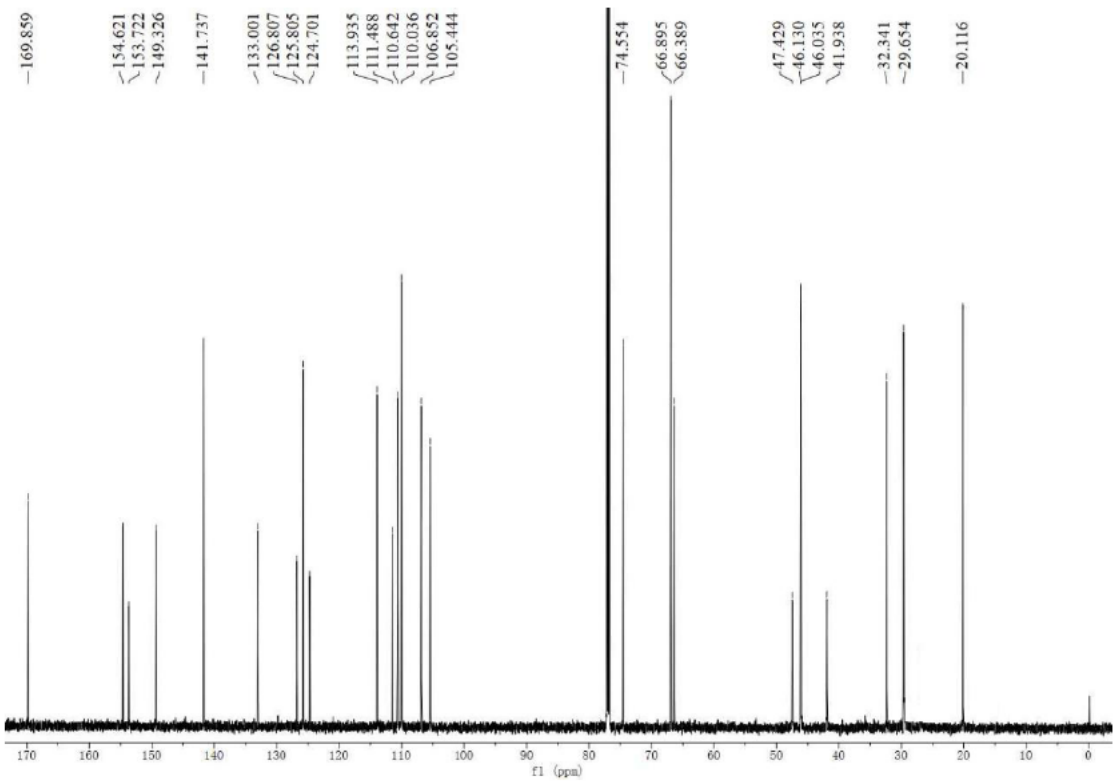
^{1}H-NMR and ^{13}C-NMR of **G0**



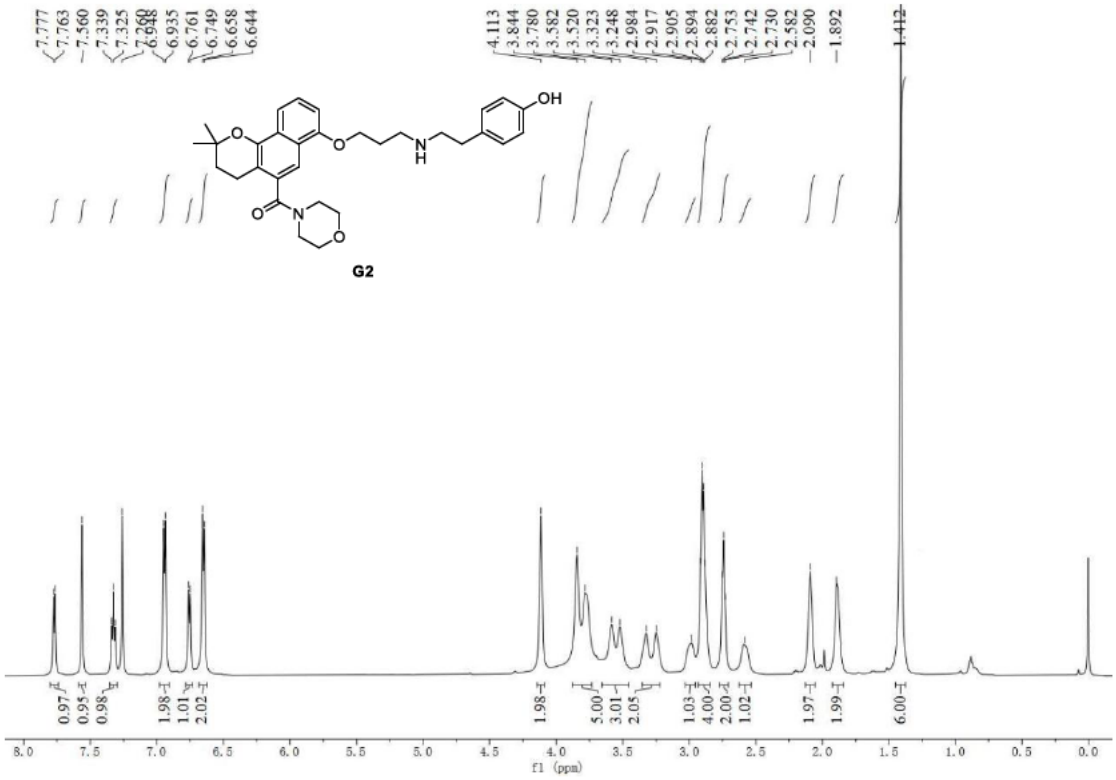


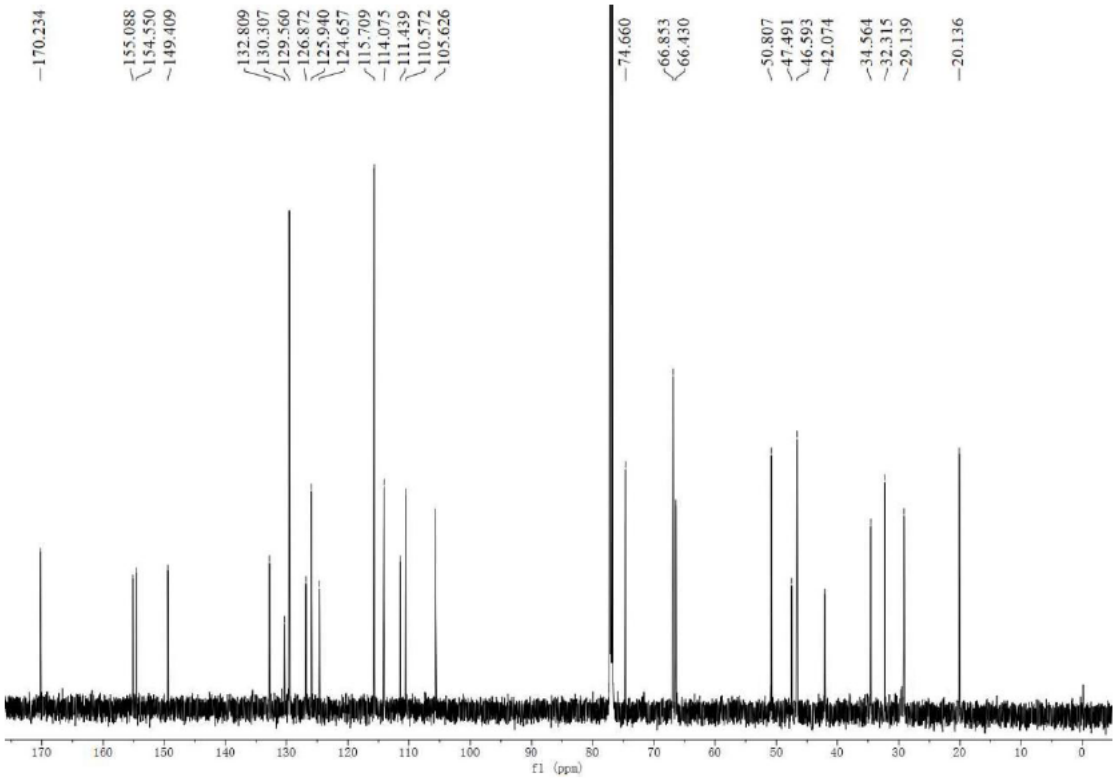
^{1}H-NMR and ^{13}C-NMR of **G1**



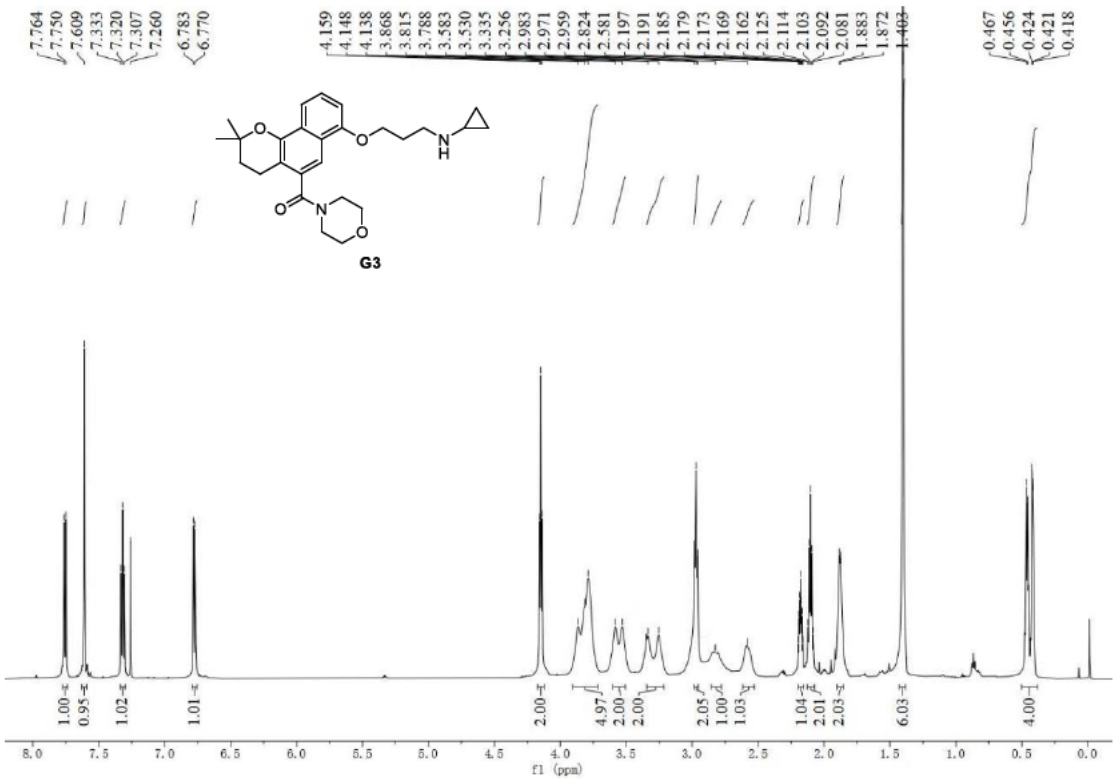


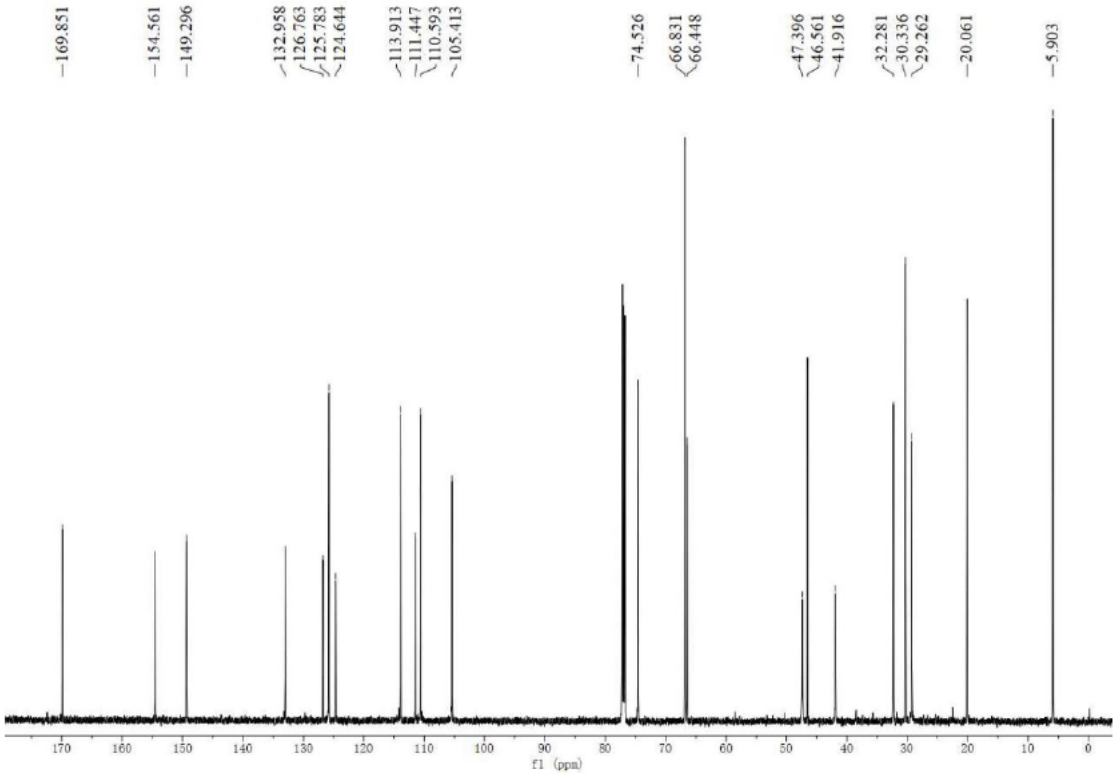
^{1}H-NMR and ^{13}C-NMR of **G2**



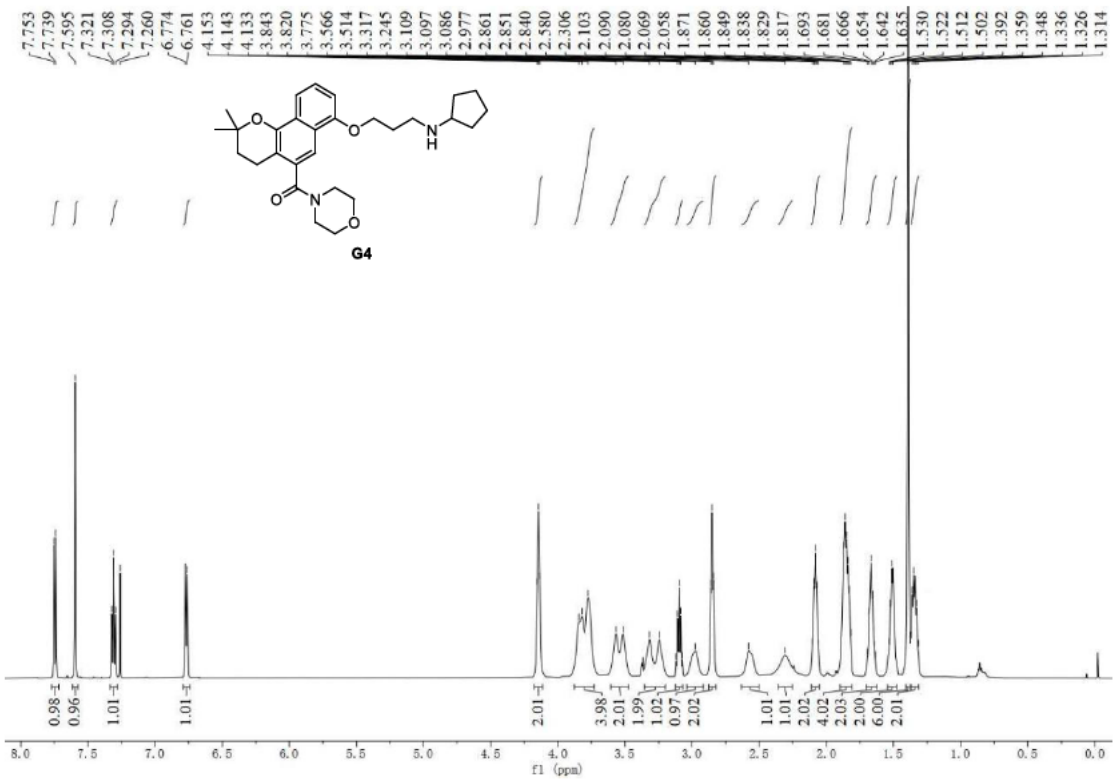


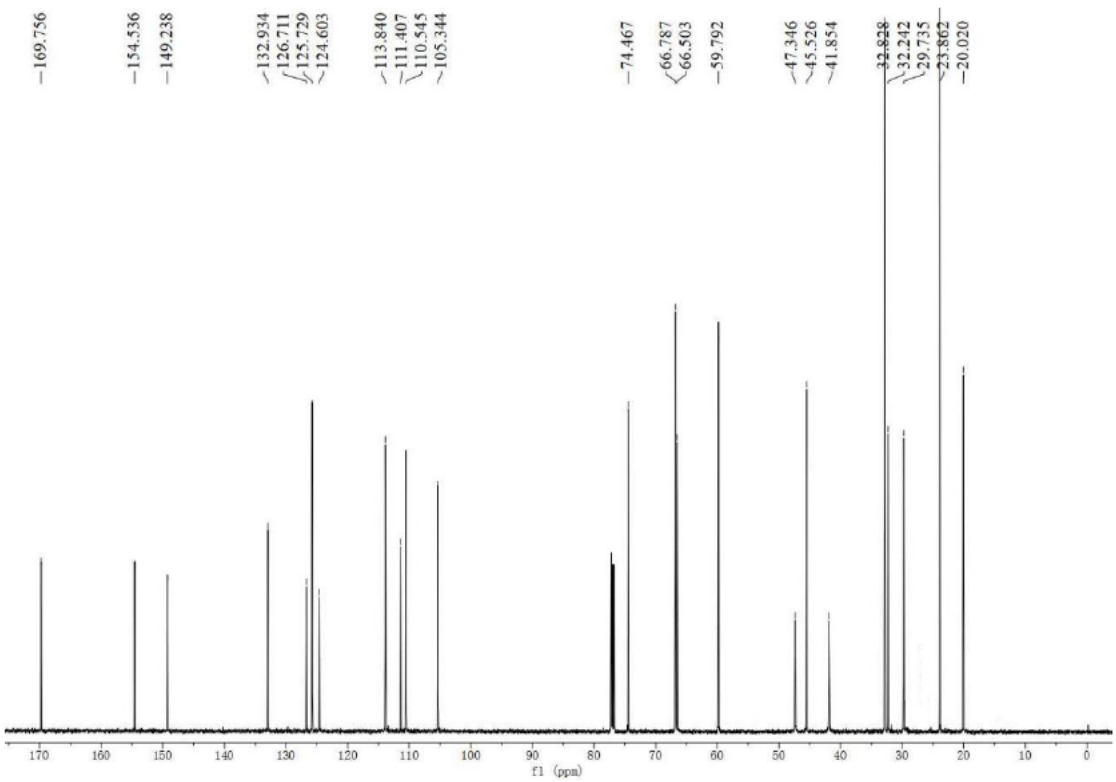
^{1}H-NMR and ^{13}C-NMR of **G3**



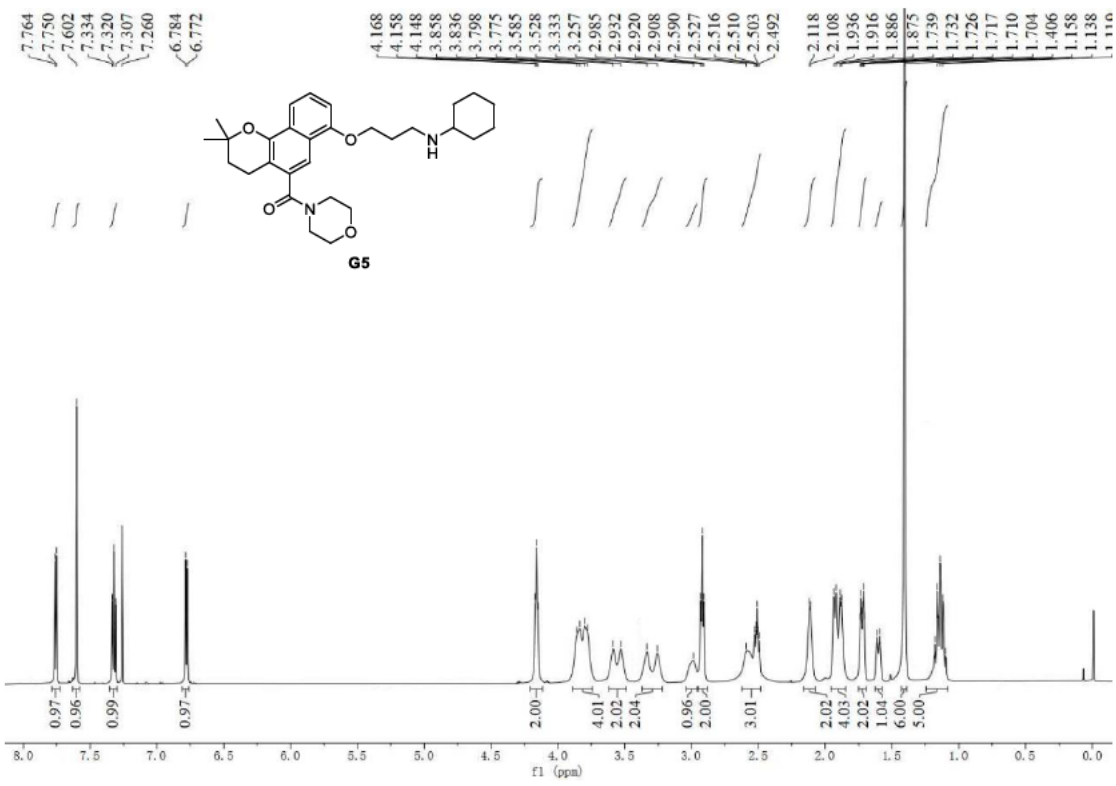


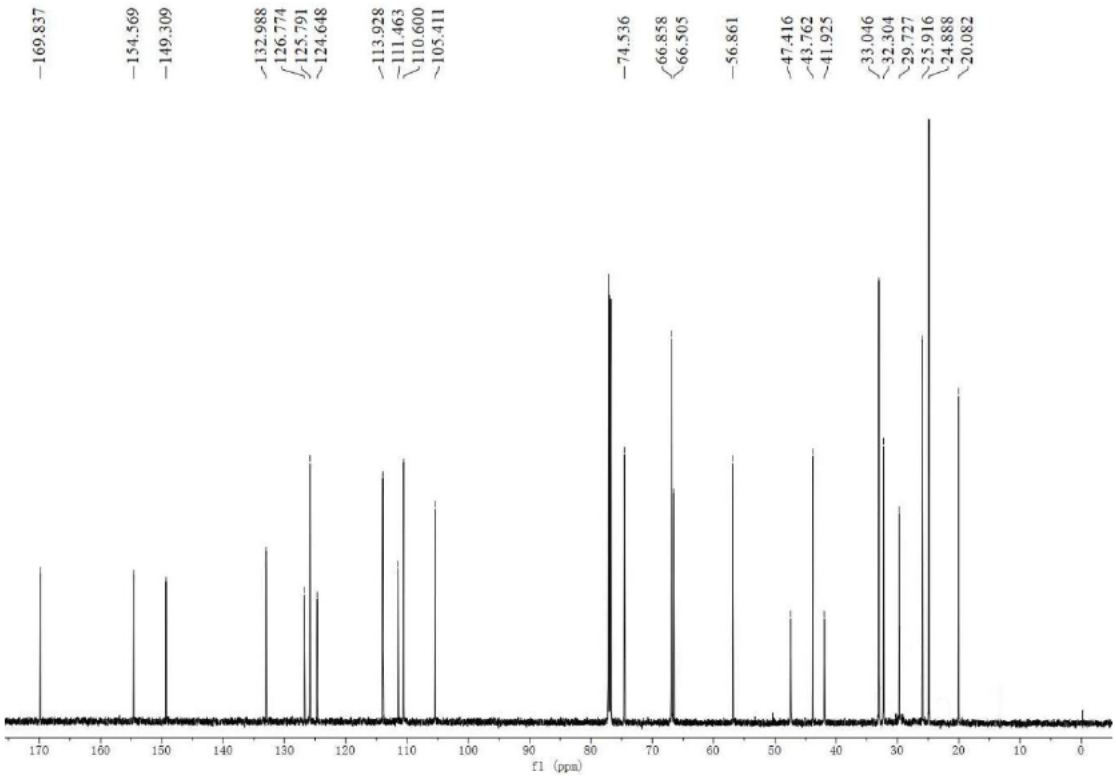
^{1}H-NMR and ^{13}C-NMR of **G4**



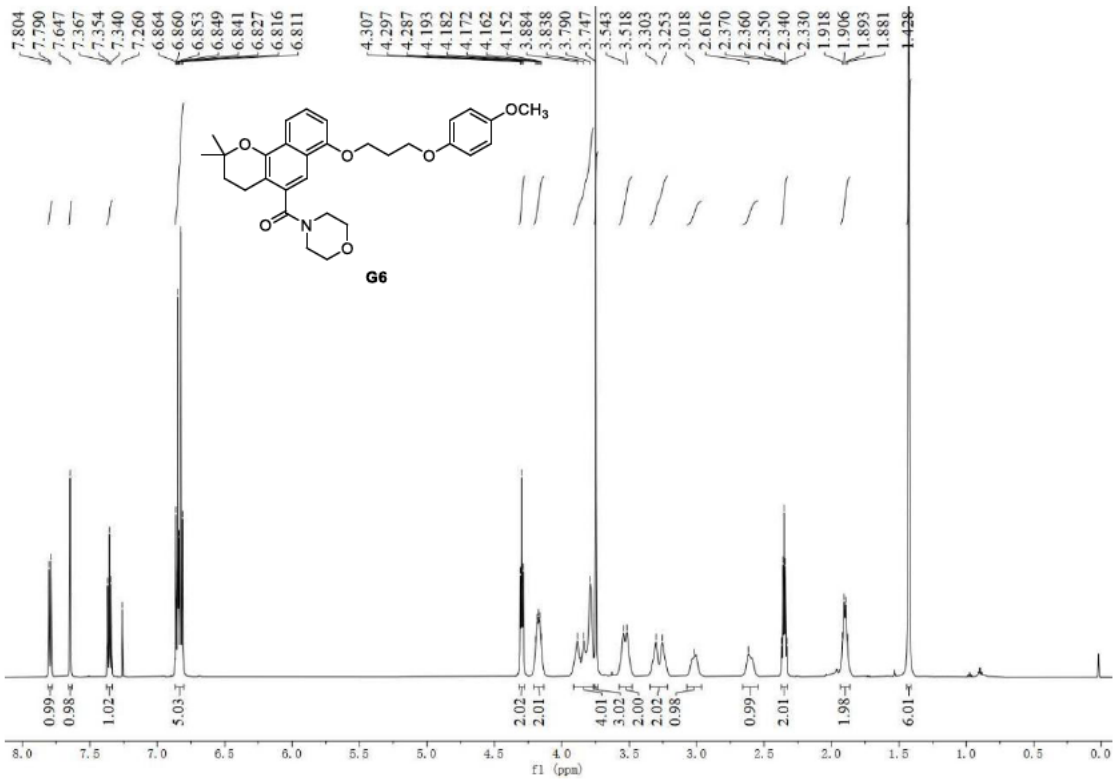


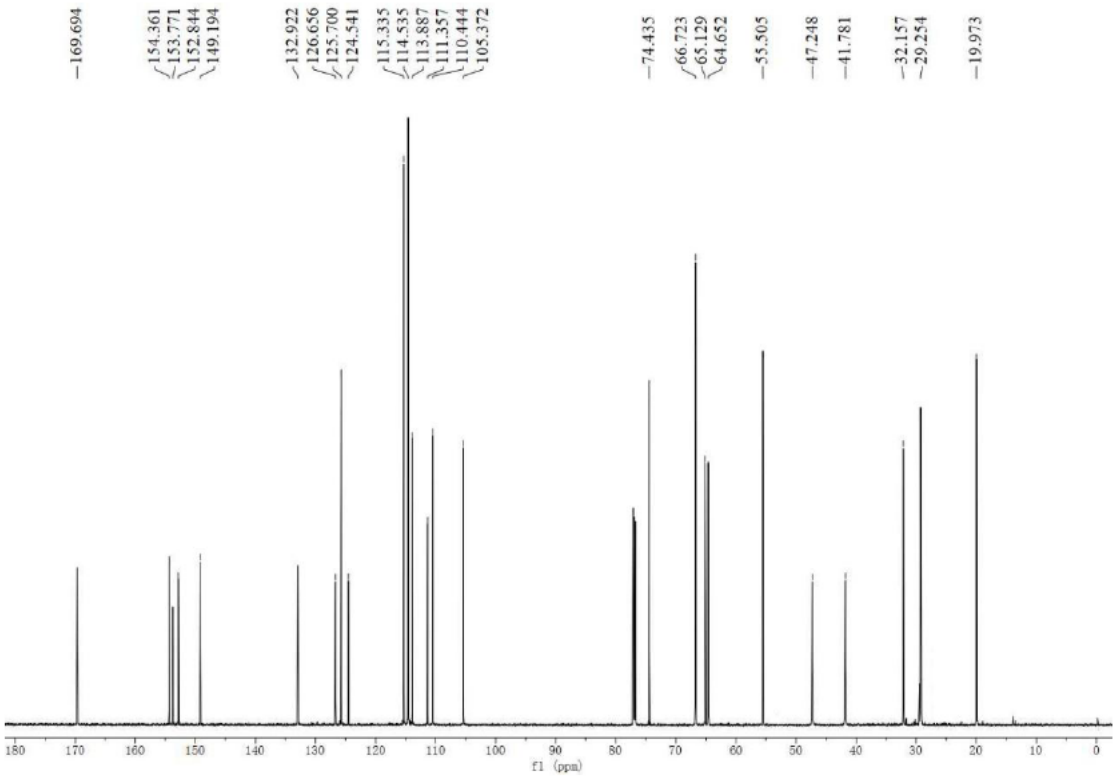
^{1}H-NMR and ^{13}C-NMR of **G5**



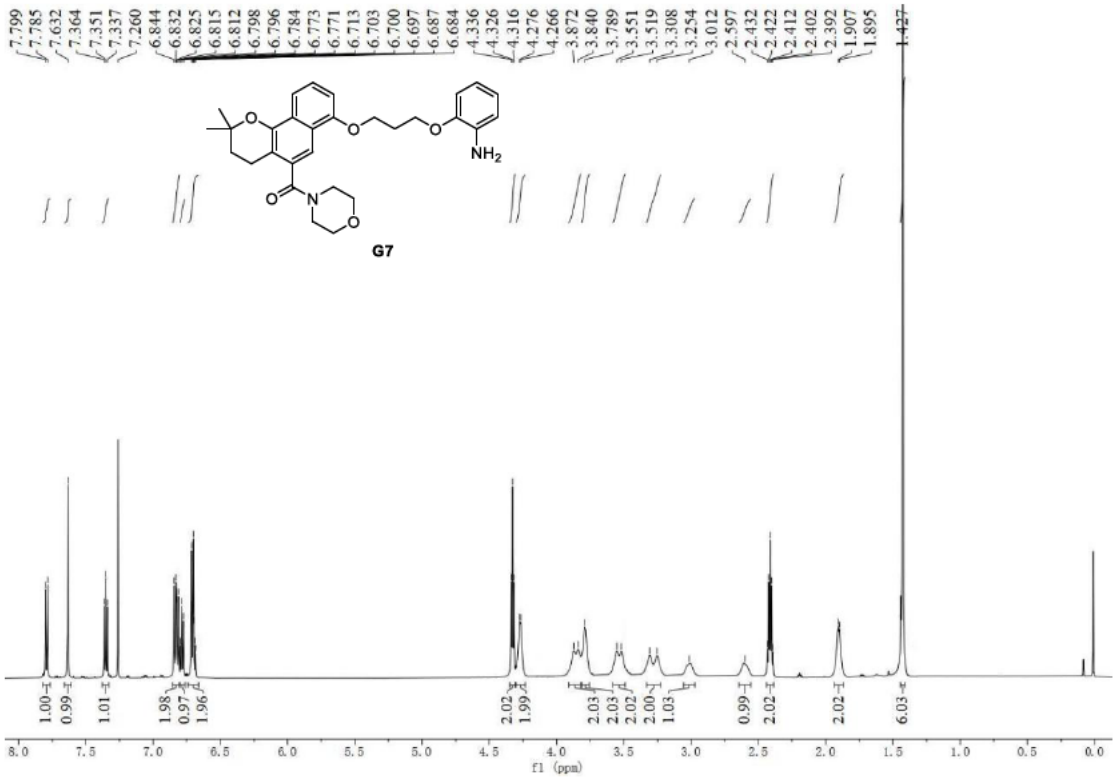


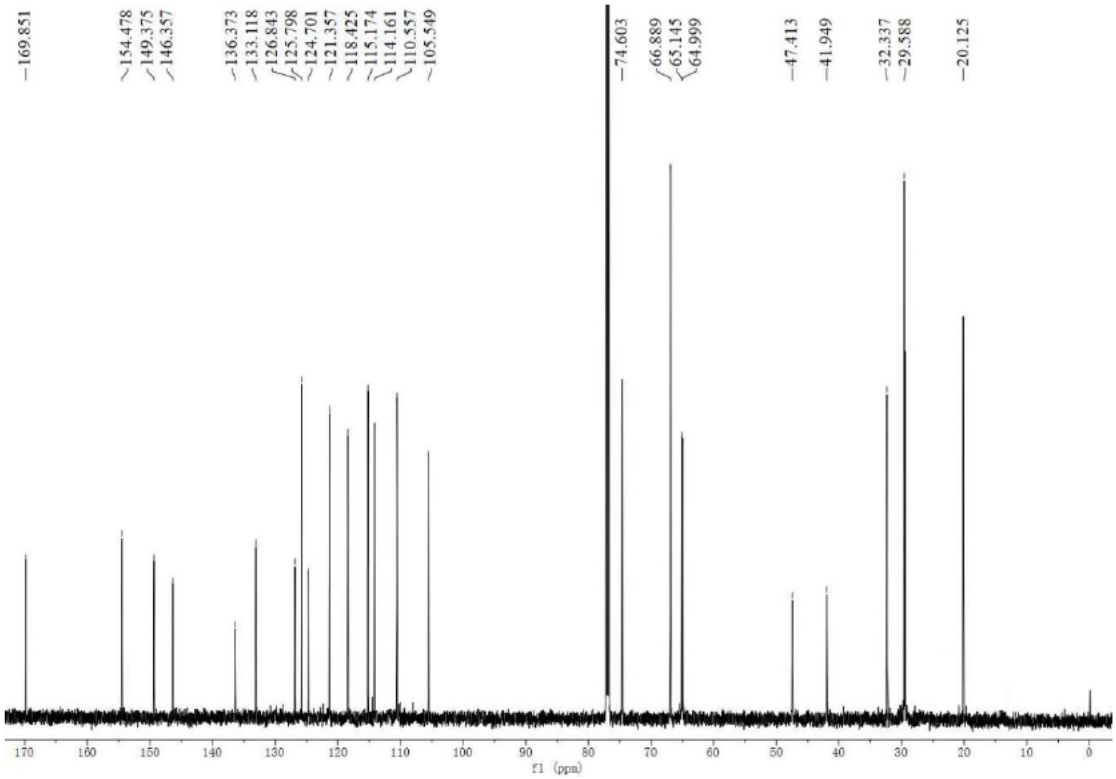
^{1}H-NMR and ^{13}C-NMR of **G6**



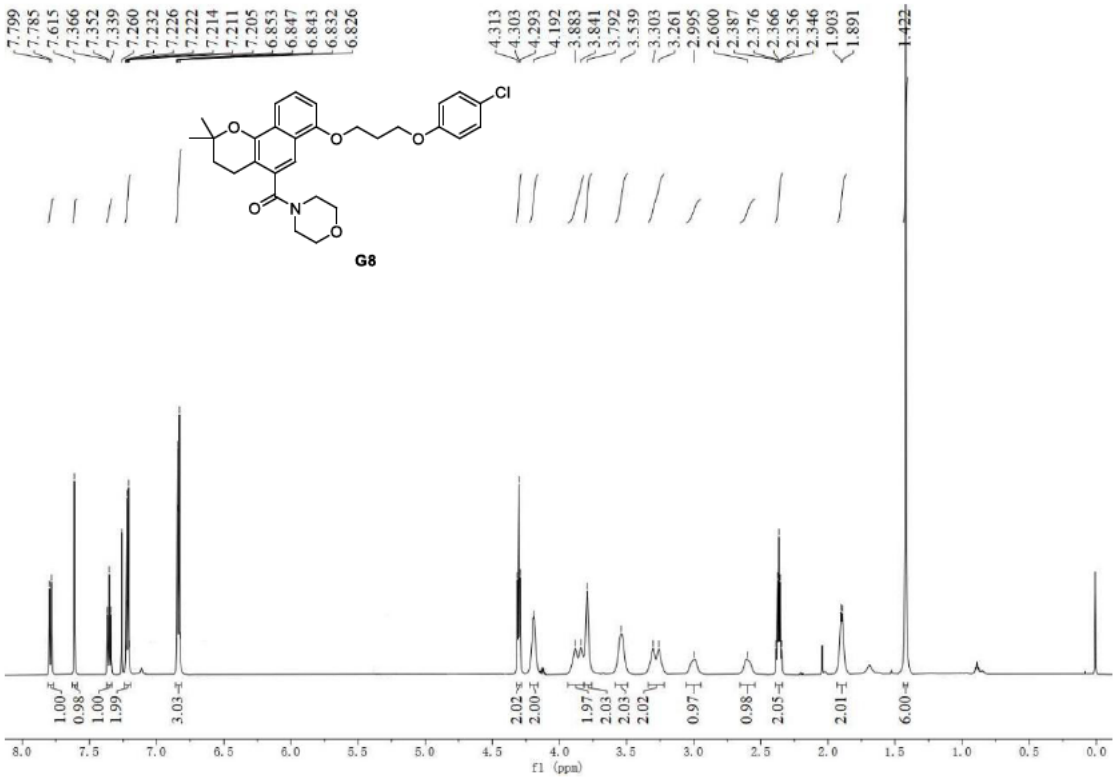


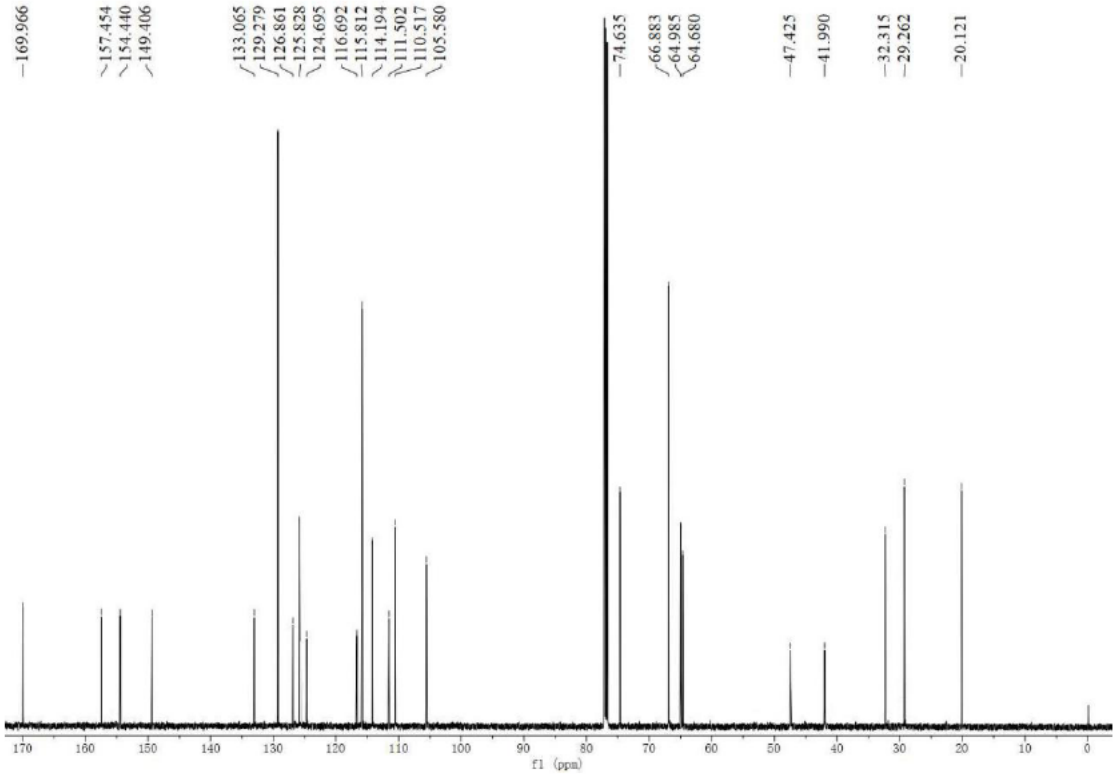
^{1}H-NMR and ^{13}C-NMR of **G7**



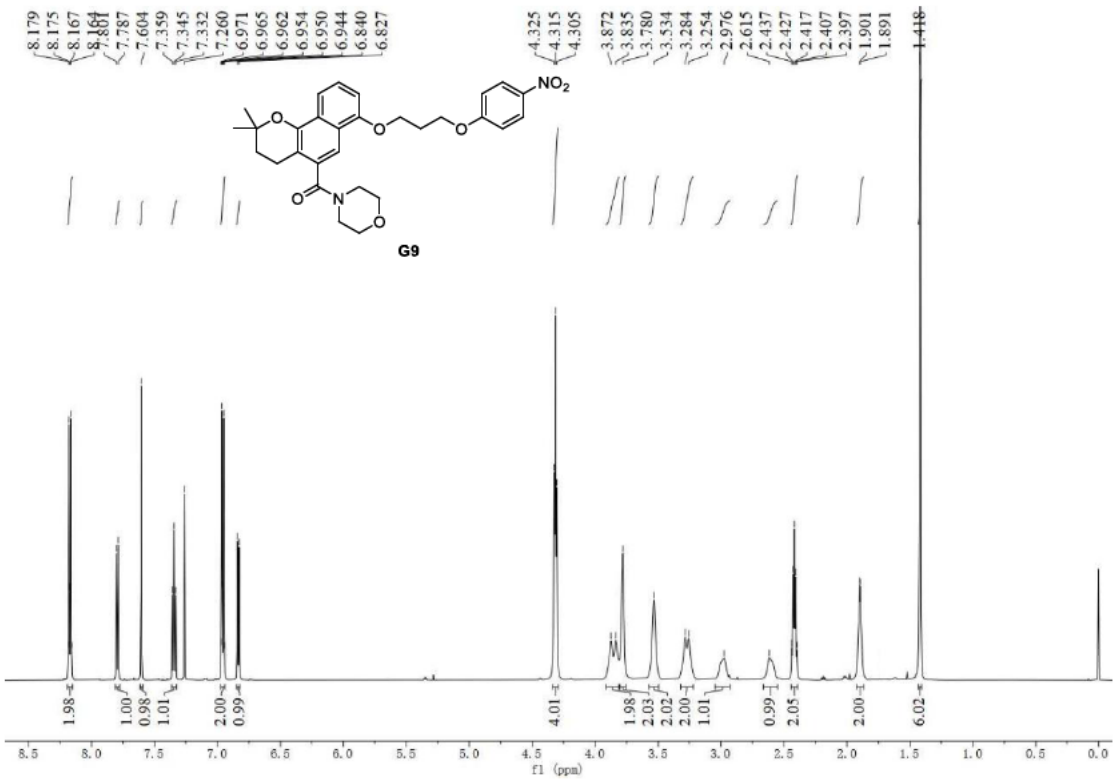


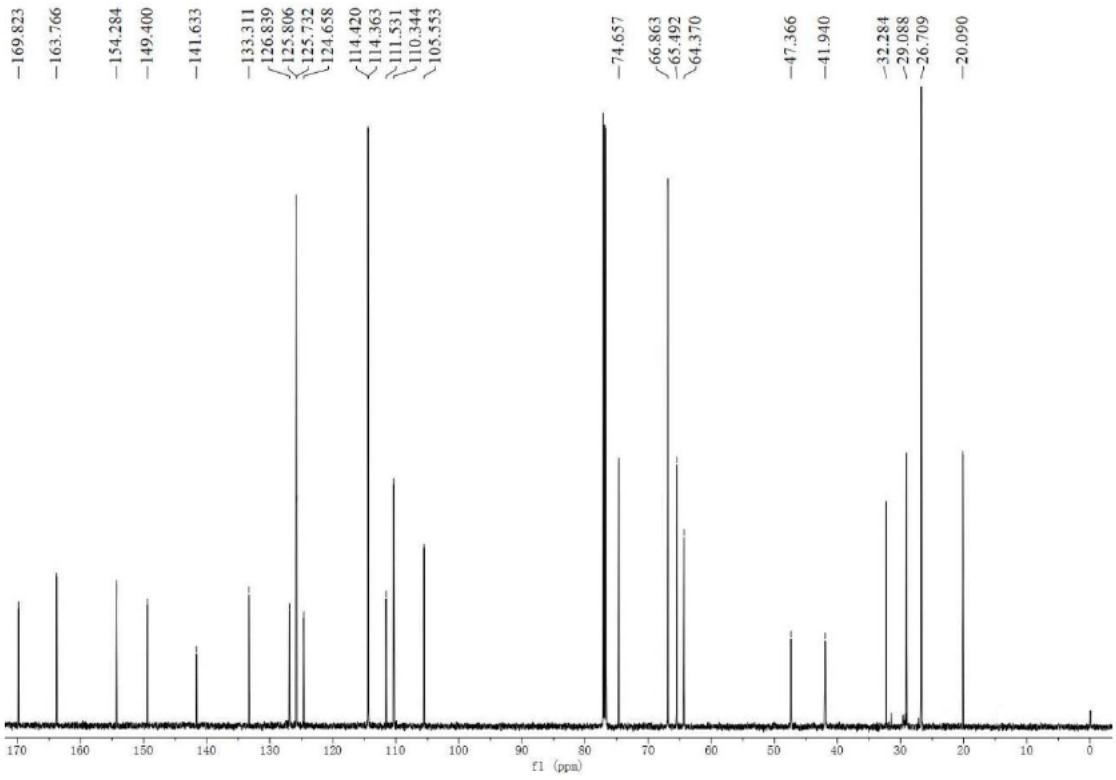
^{1}H-NMR and ^{13}C-NMR of **G8**



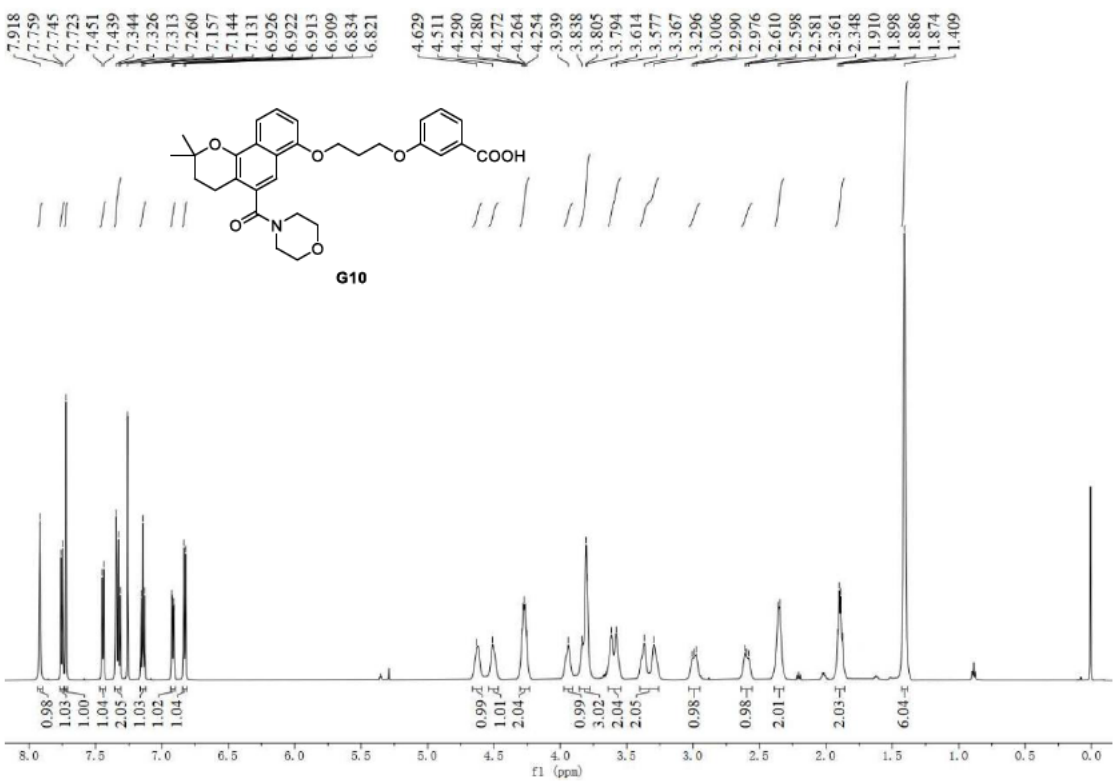


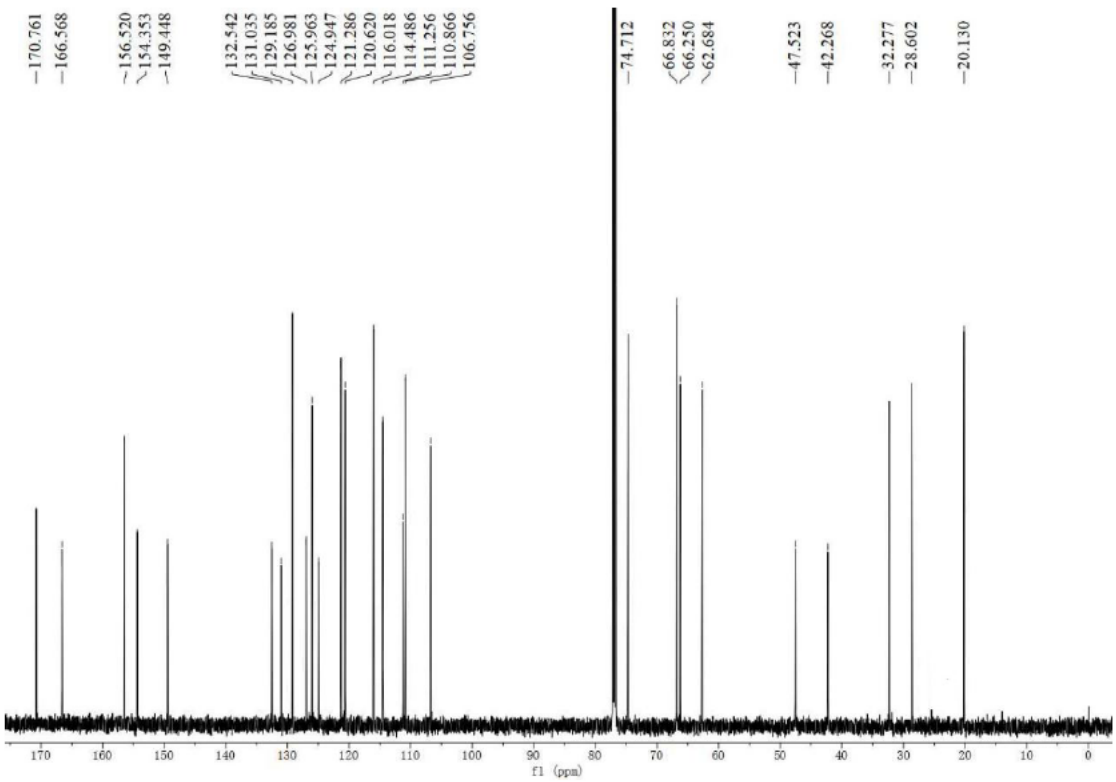
^{1}H-NMR and ^{13}C-NMR of **G9**



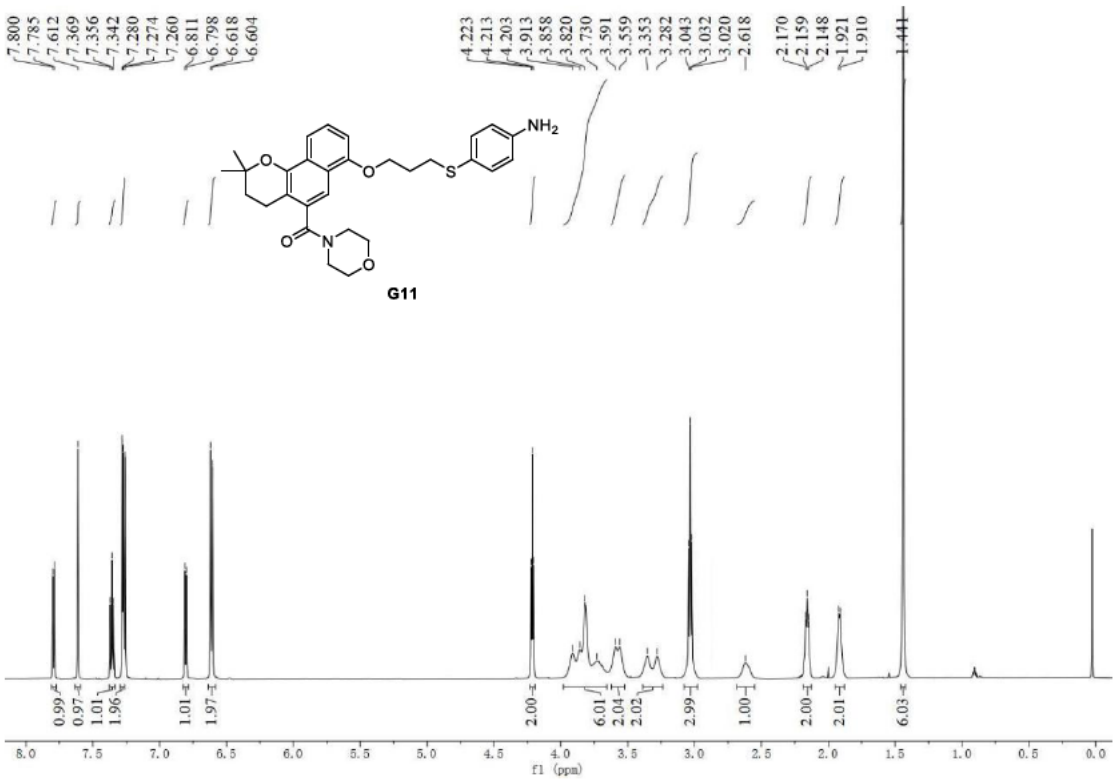


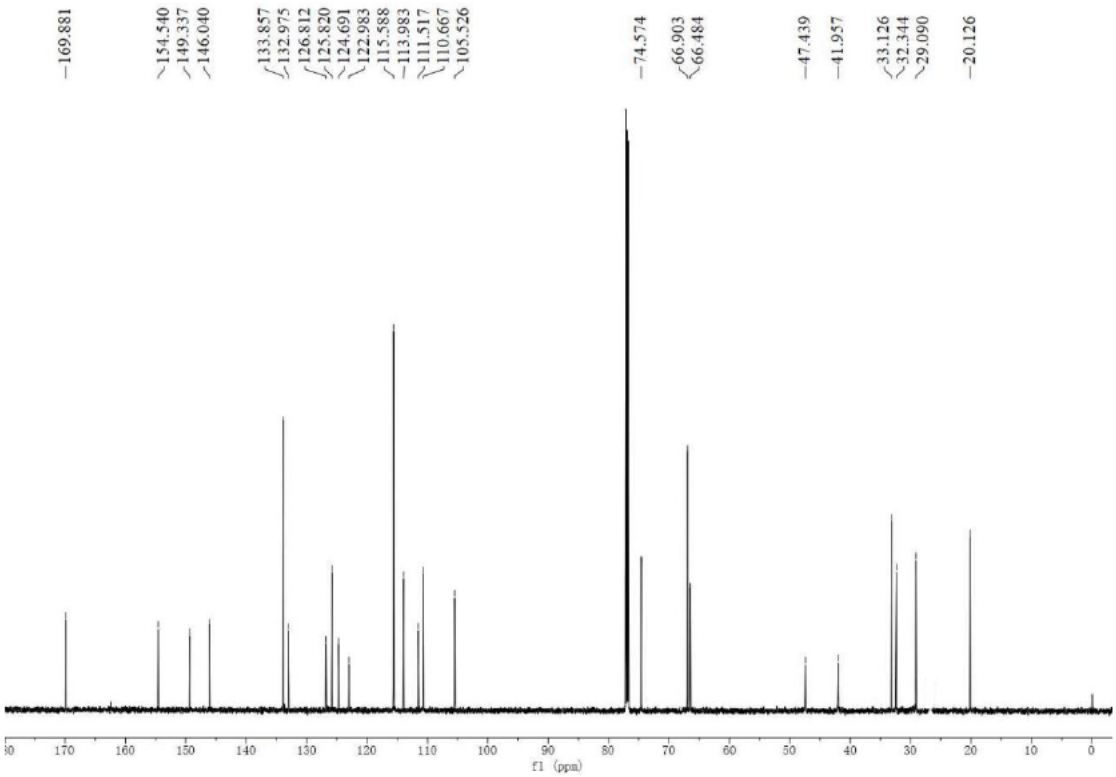
^{1}H-NMR and ^{13}C-NMR of **G10**



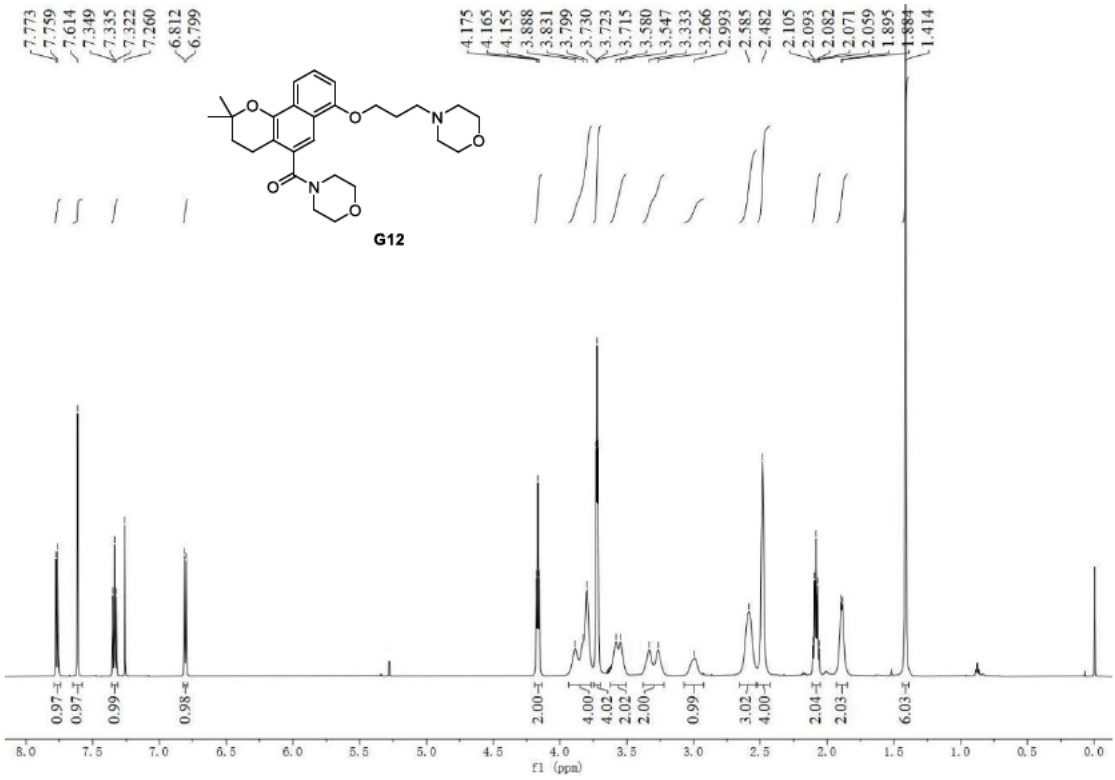


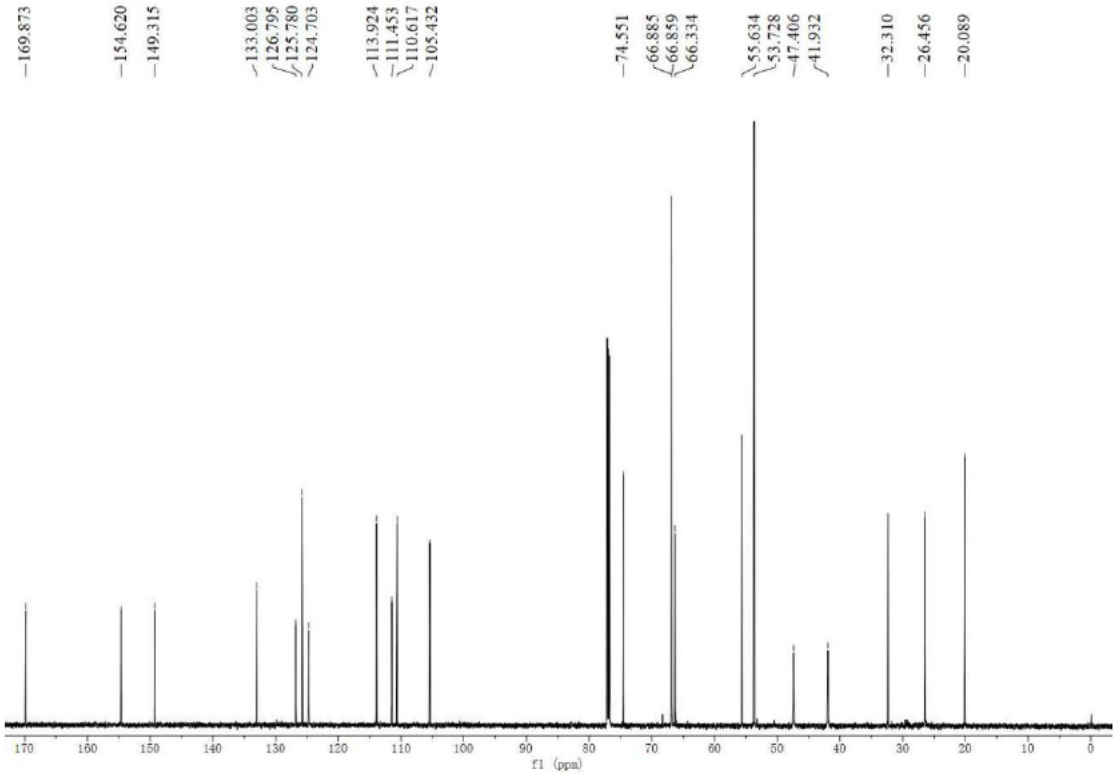
^{1}H-NMR and ^{13}C-NMR of **G11**



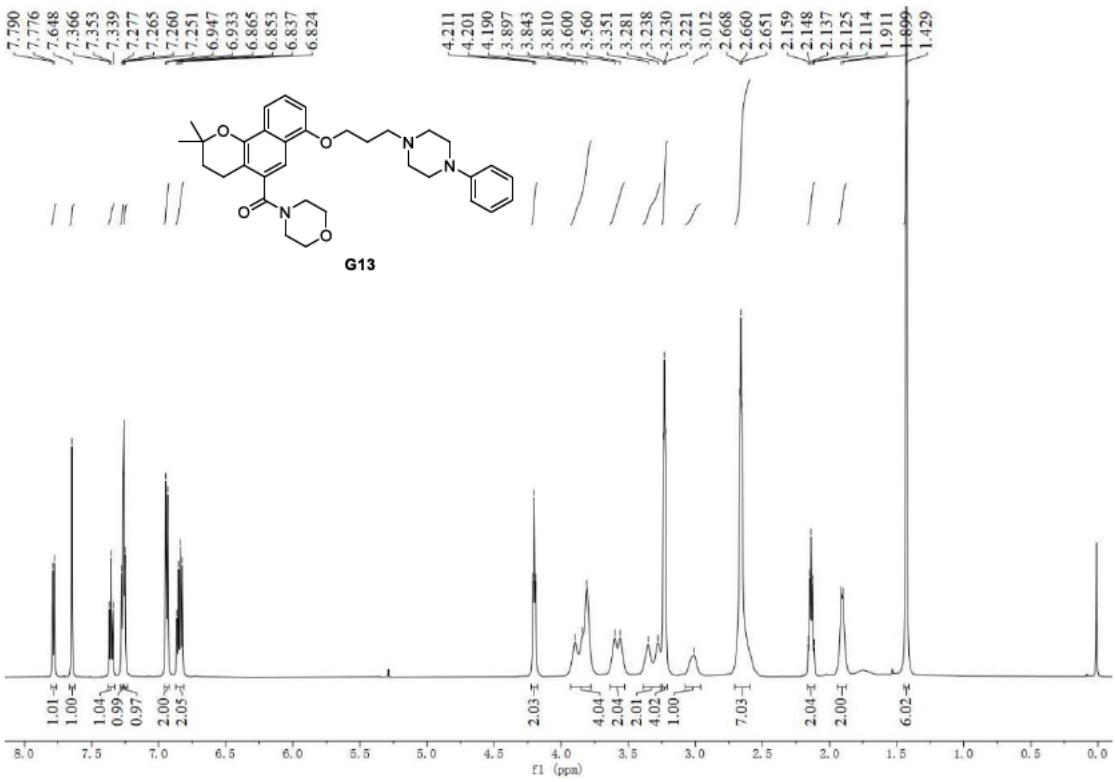


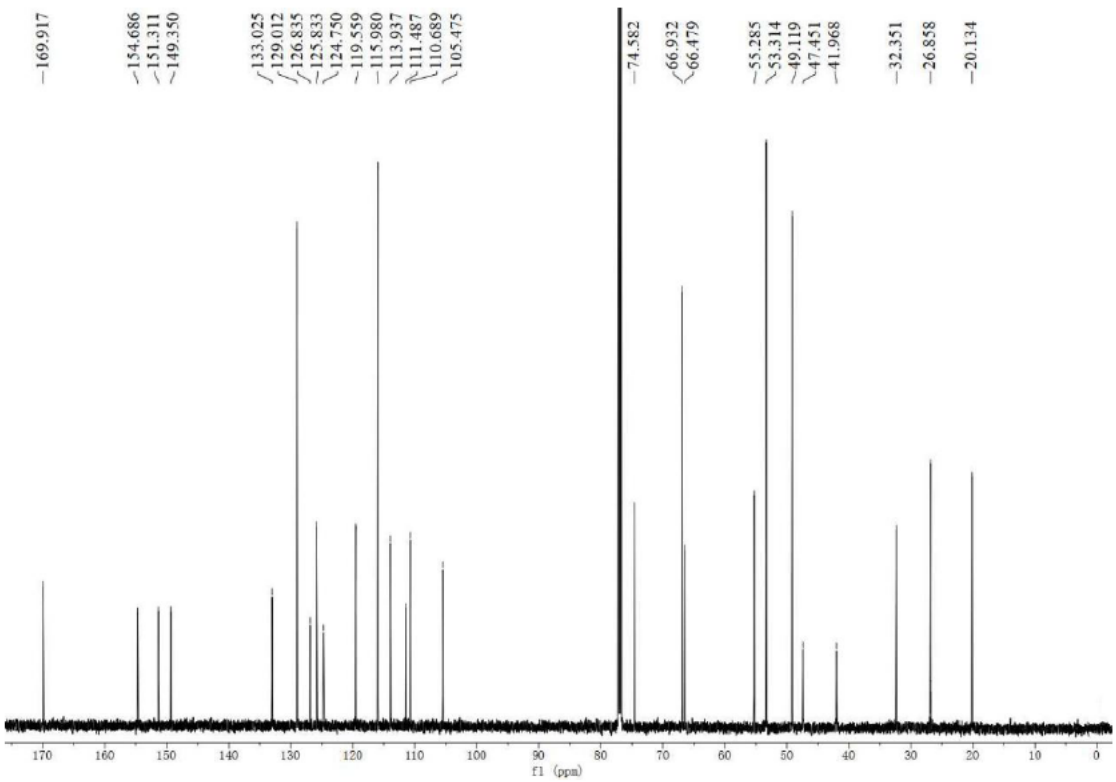
^{1}H-NMR and ^{13}C-NMR of **G12**



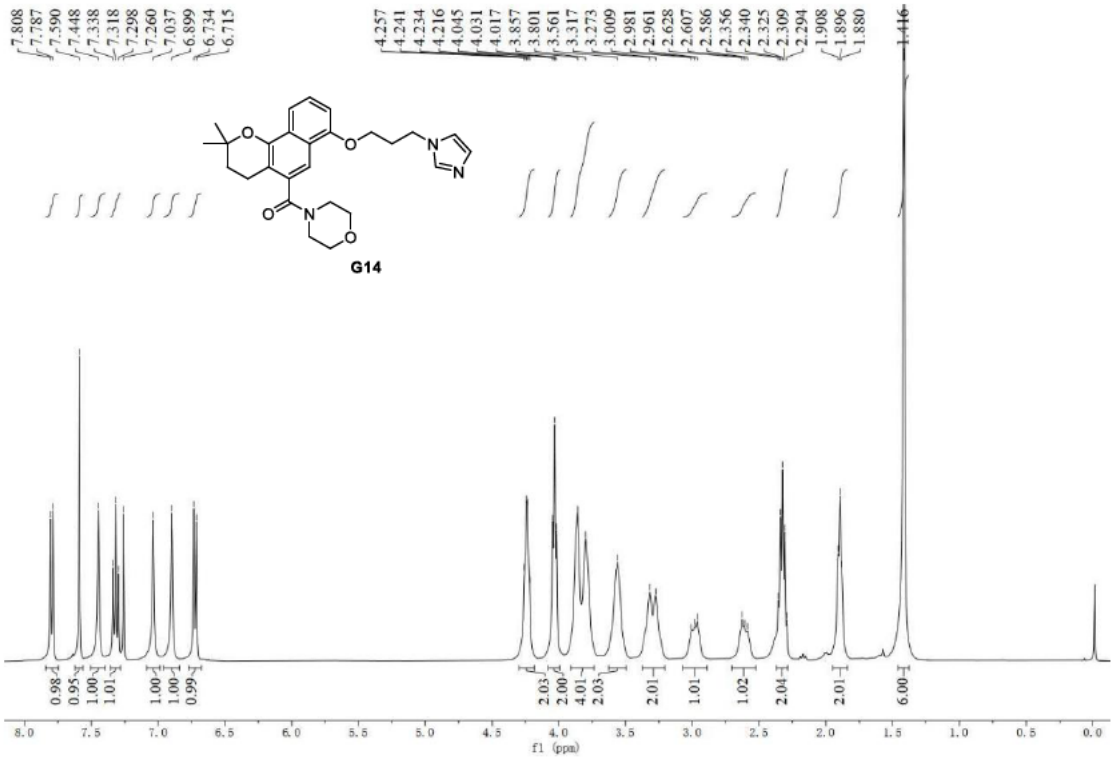


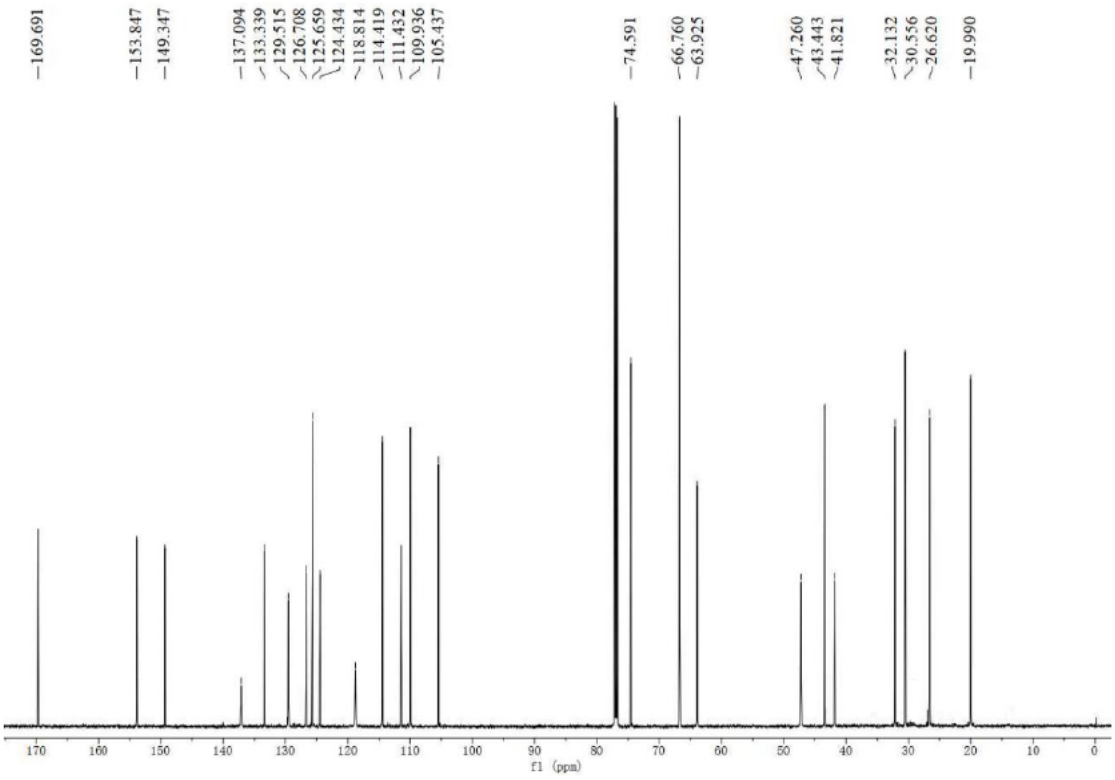
^{1}H-NMR and ^{13}C-NMR of **G13**



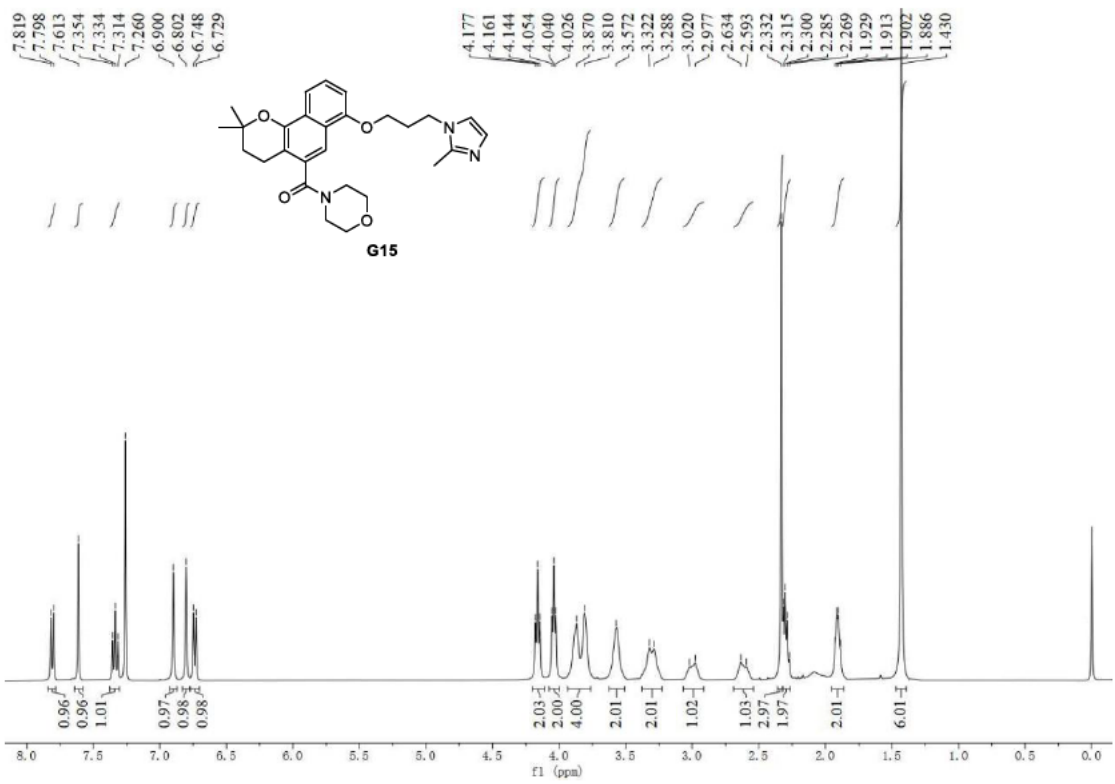


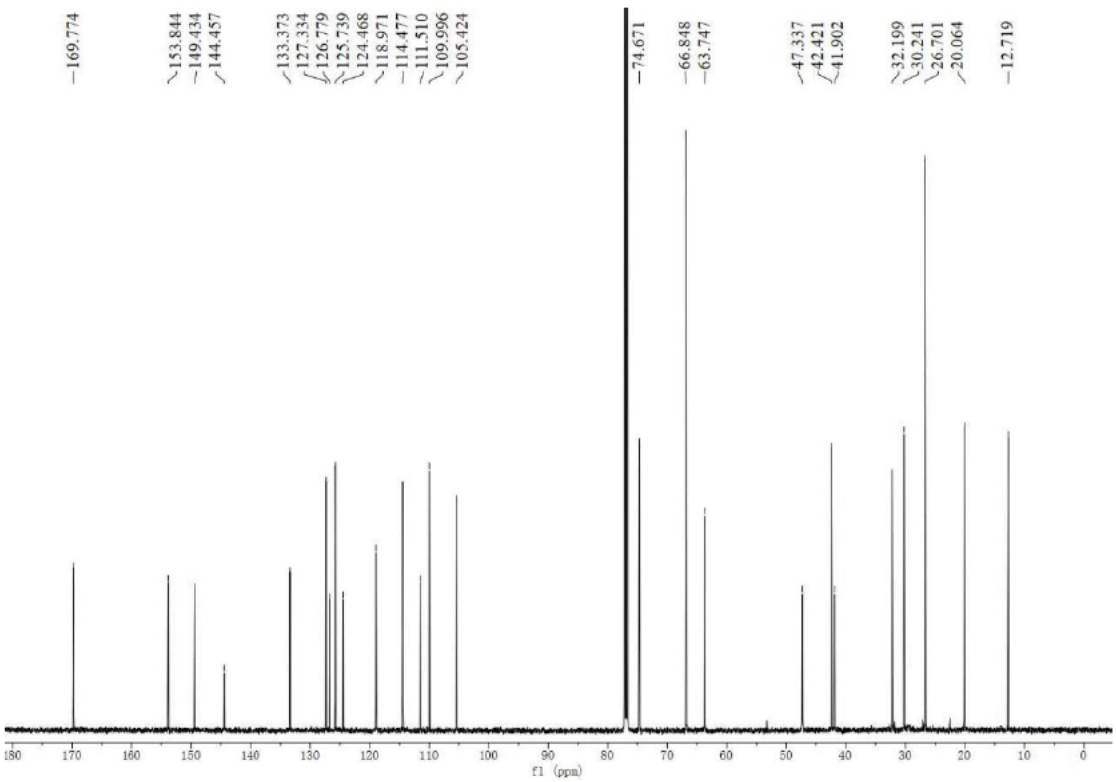
^{1}H-NMR and ^{13}C-NMR of **G14**



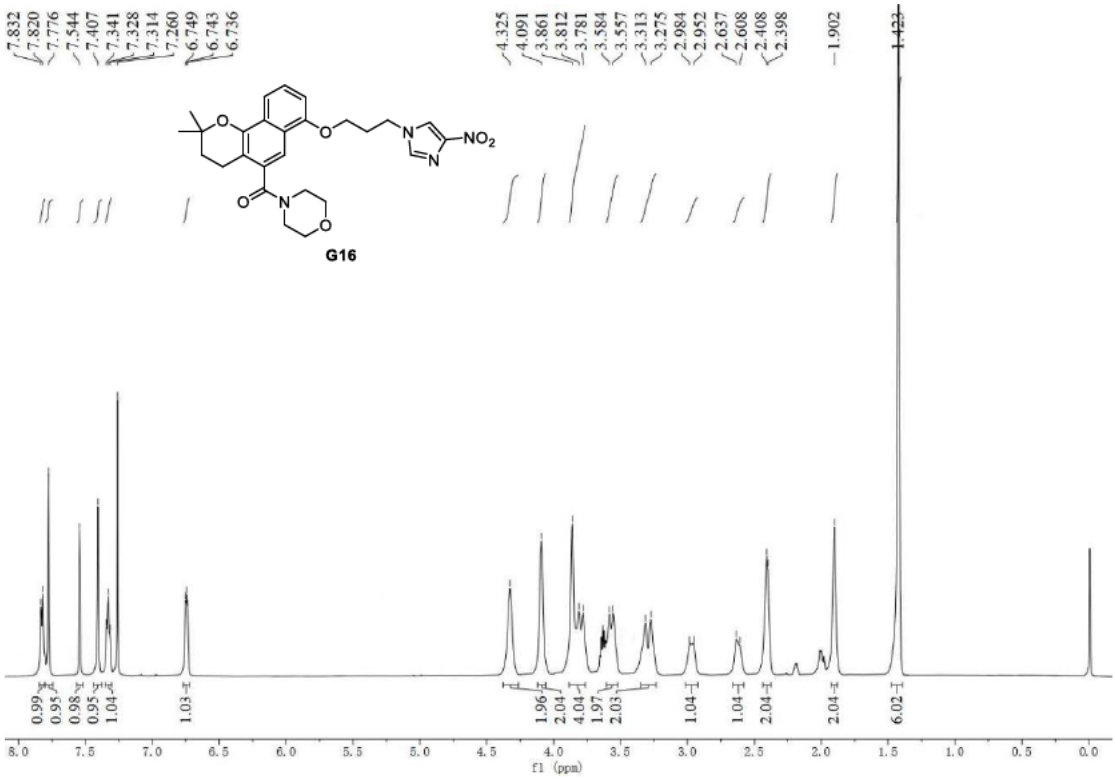


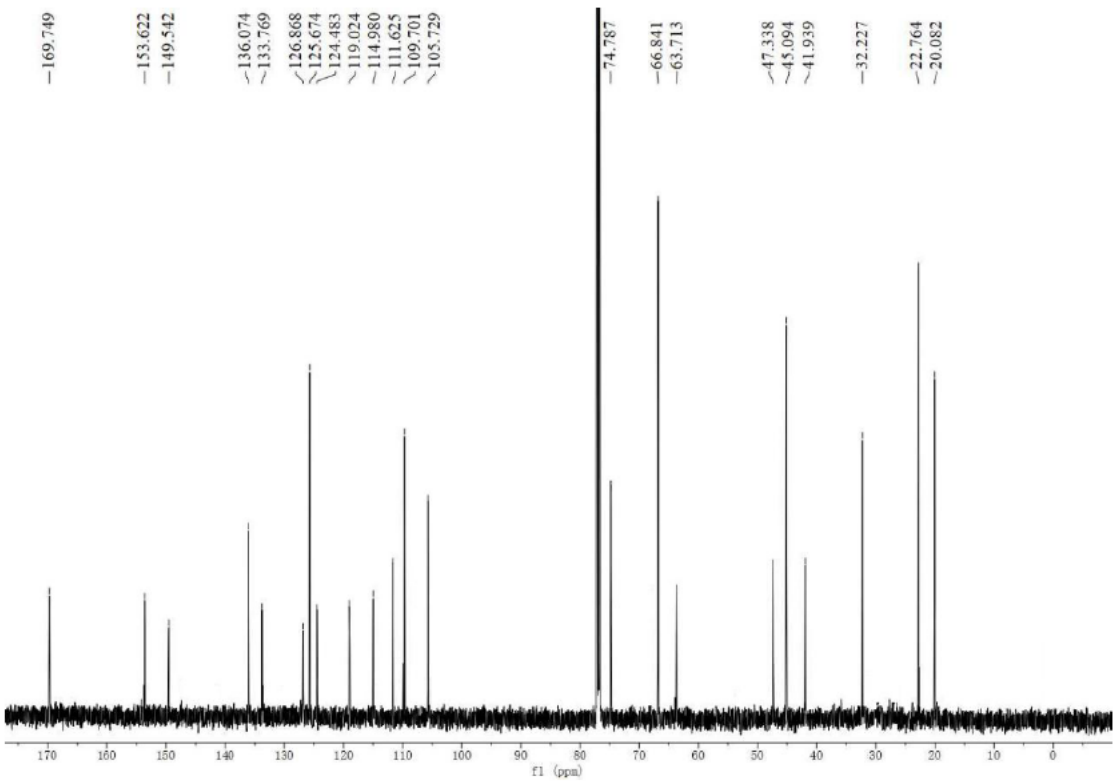
^{1}H-NMR and ^{13}C-NMR of **G15**



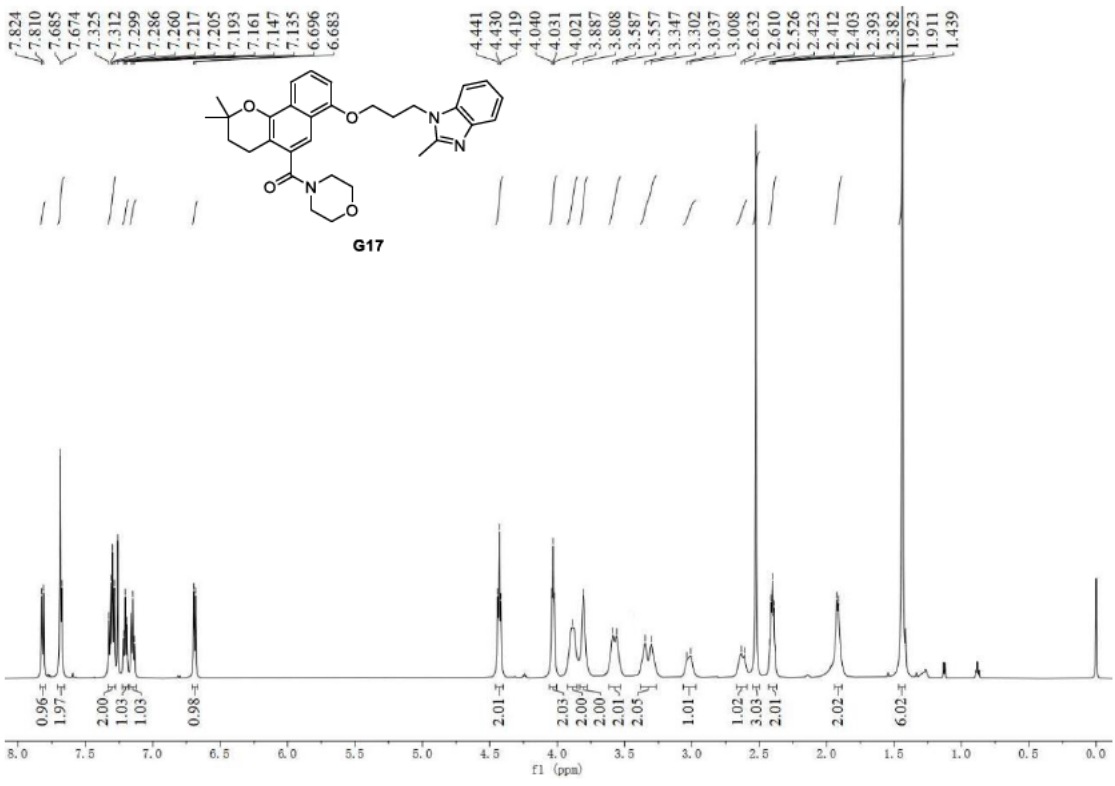


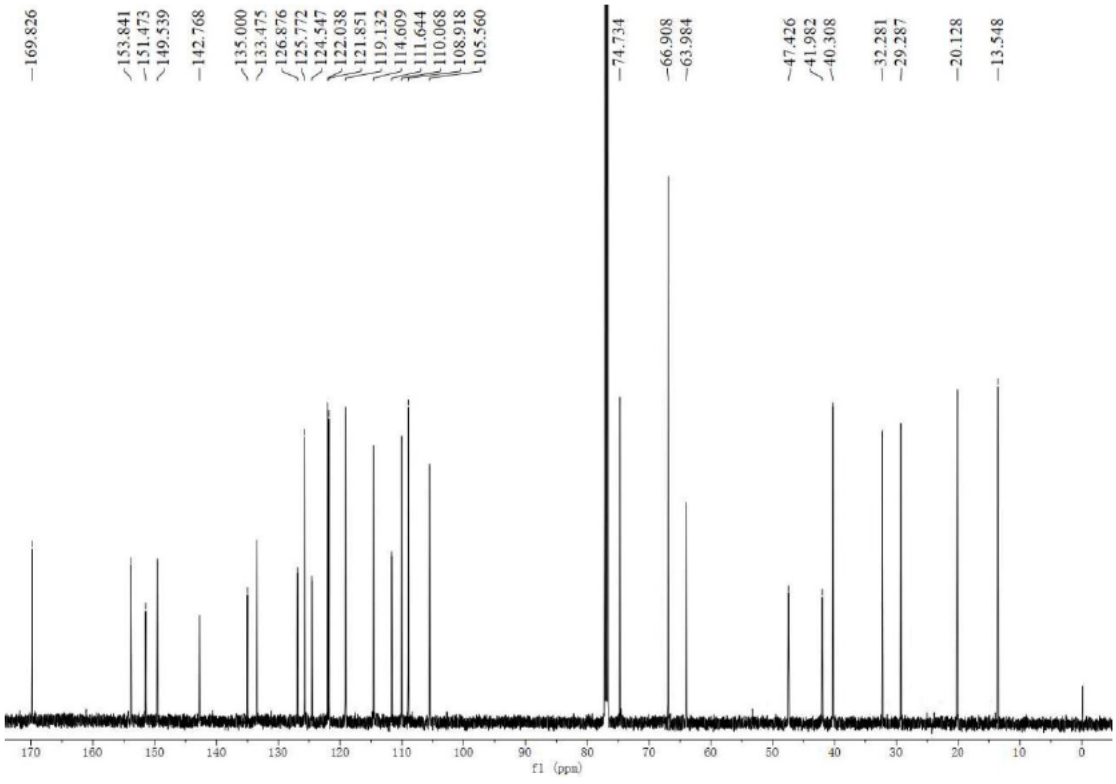
^{1}H-NMR and ^{13}C-NMR of **G16**



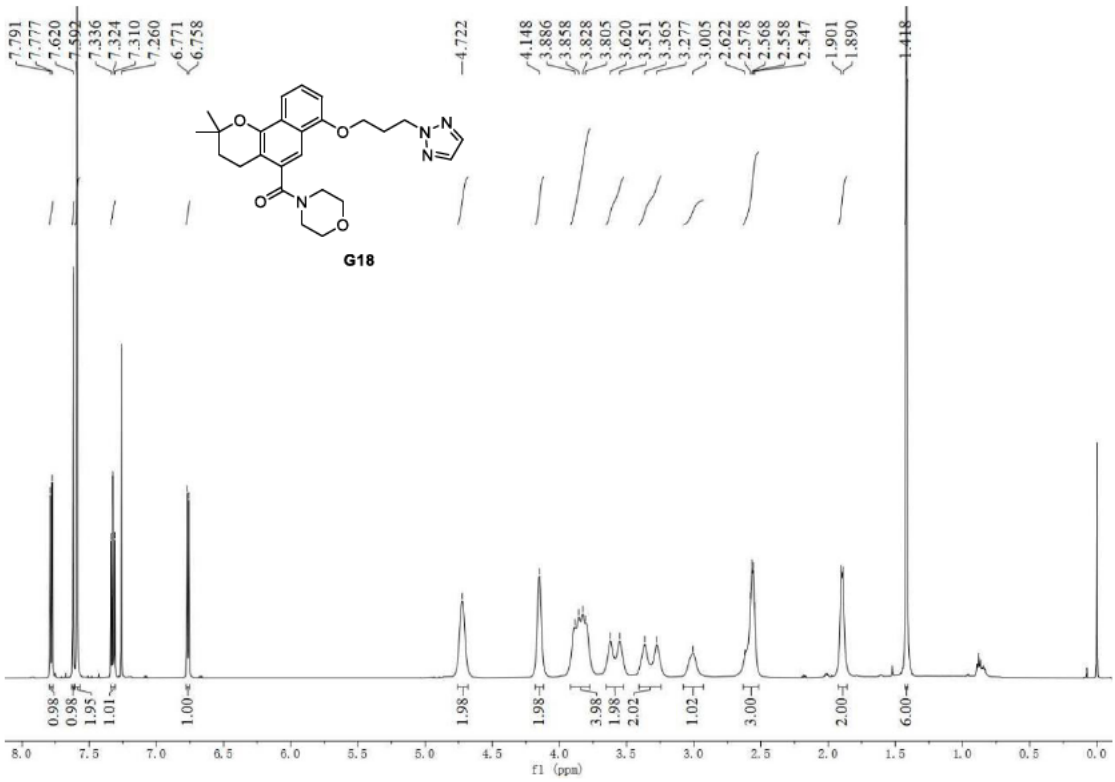


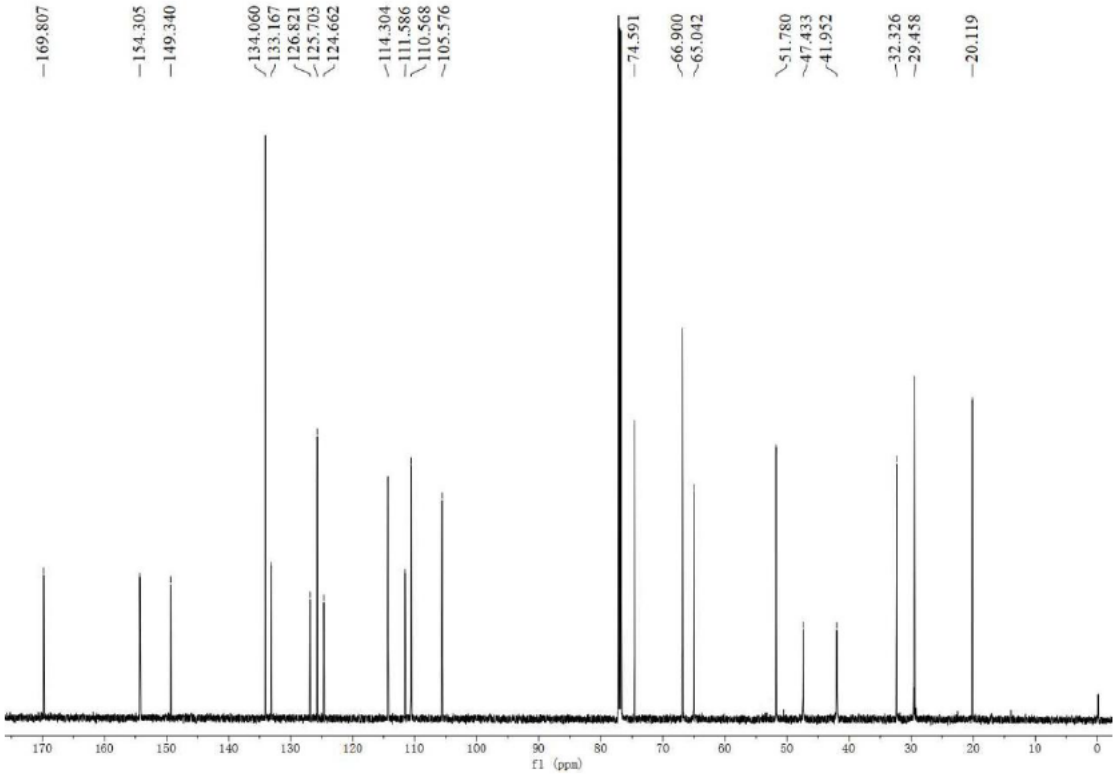
^{1}H-NMR and ^{13}C-NMR of **G17**



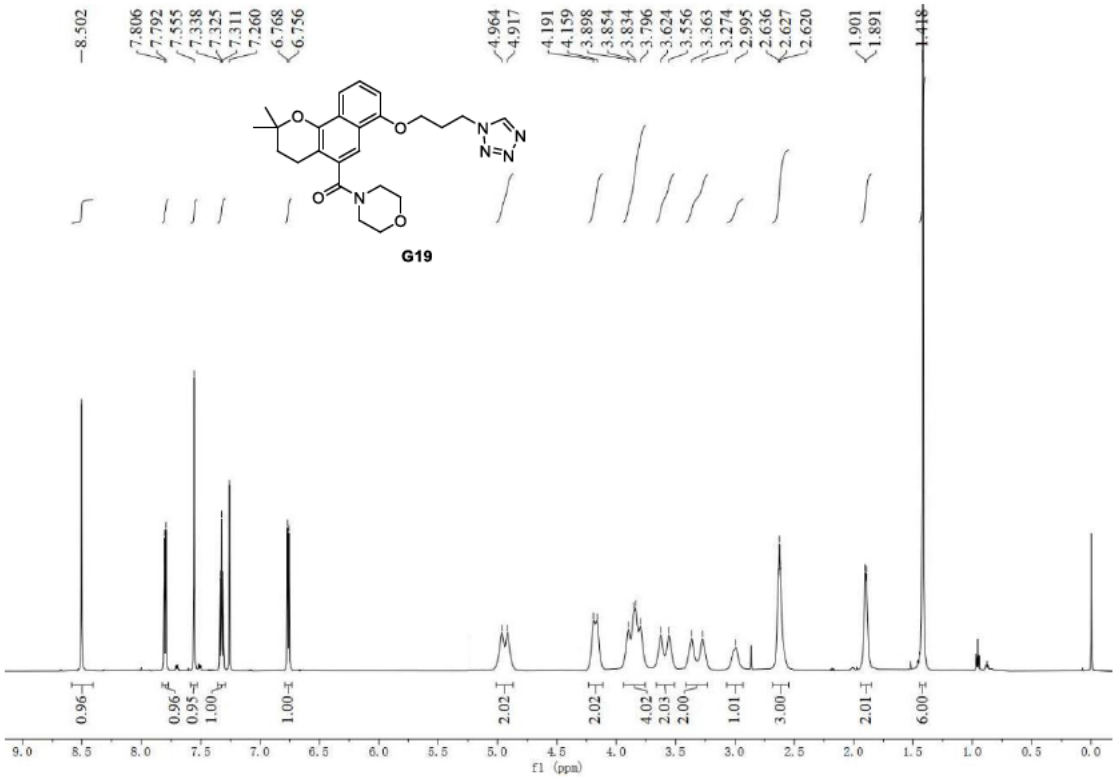


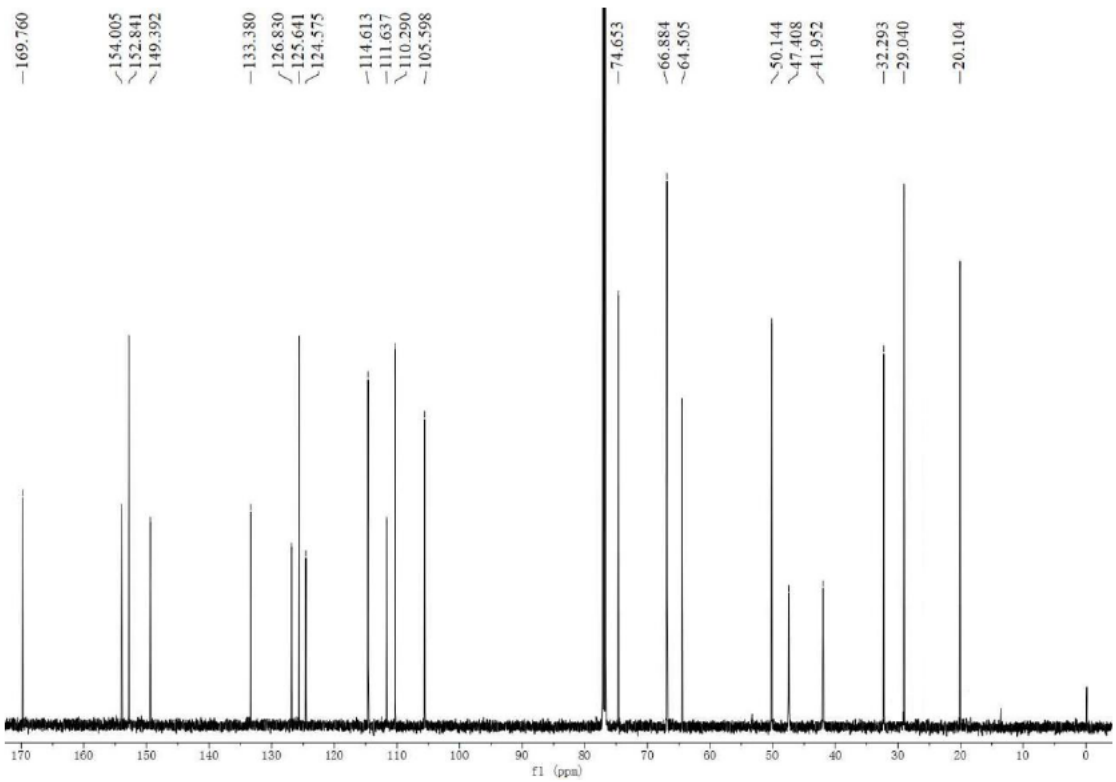
^{1}H-NMR and ^{13}C-NMR of **G18**



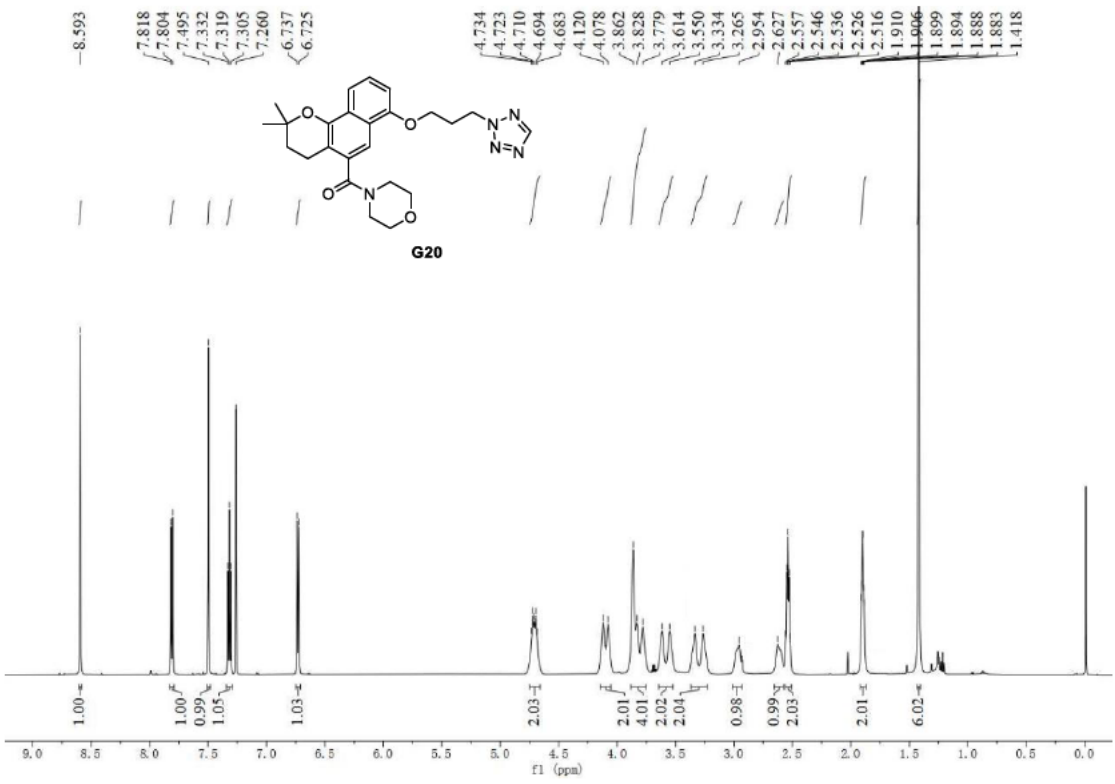


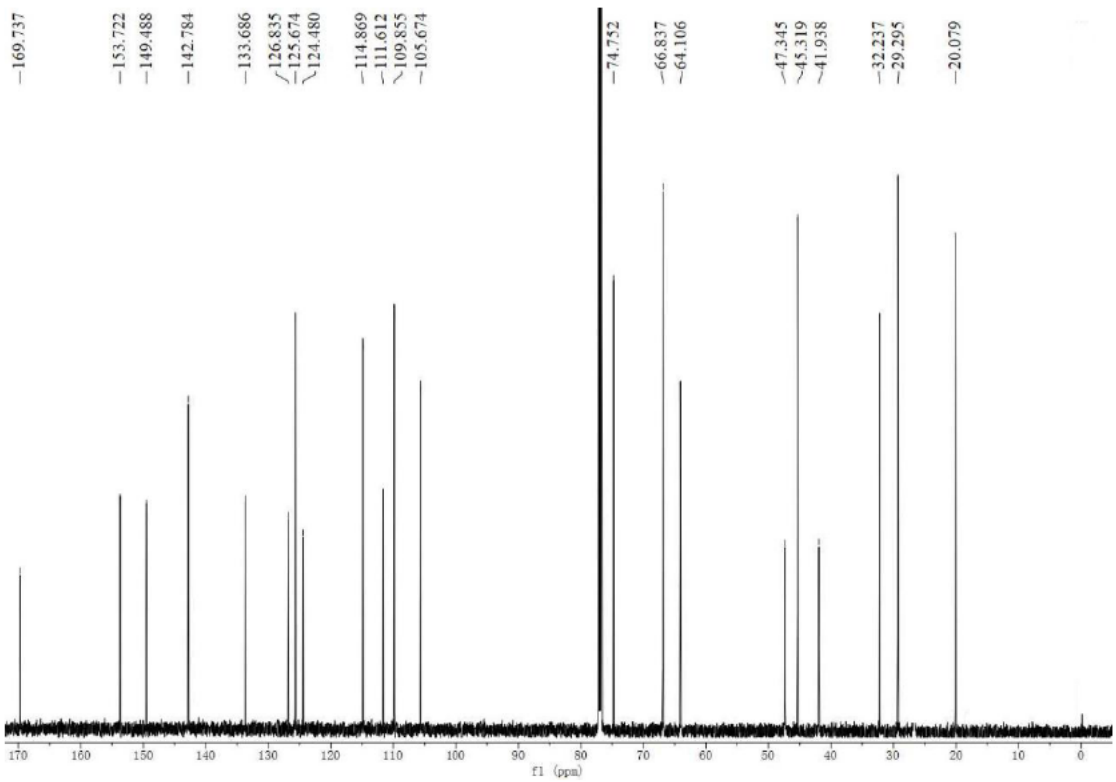
^{1}H-NMR and ^{13}C-NMR of **G19**



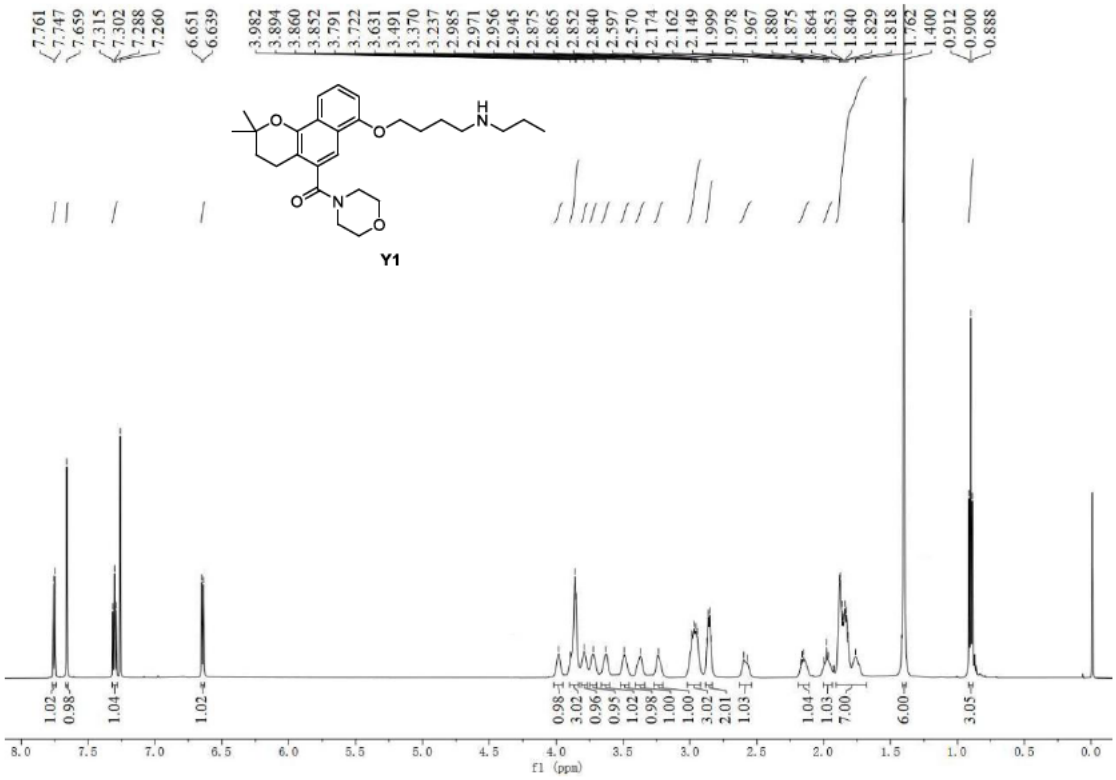


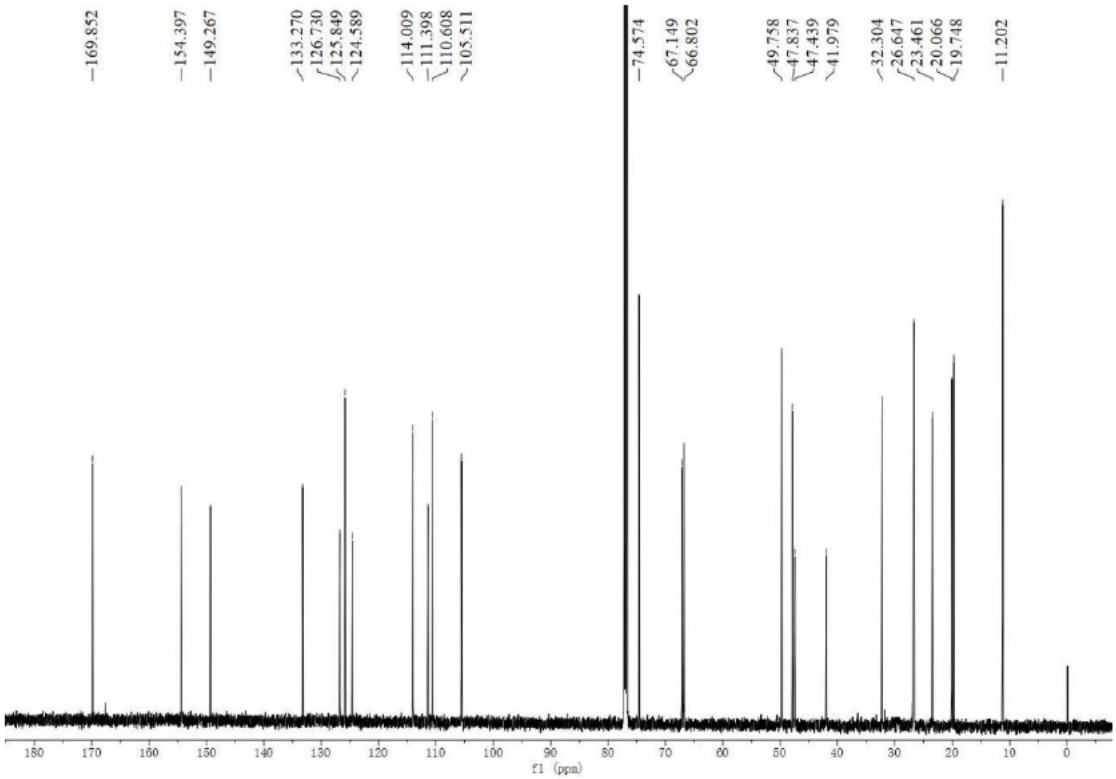
^{1}H-NMR and ^{13}C-NMR of **G20**



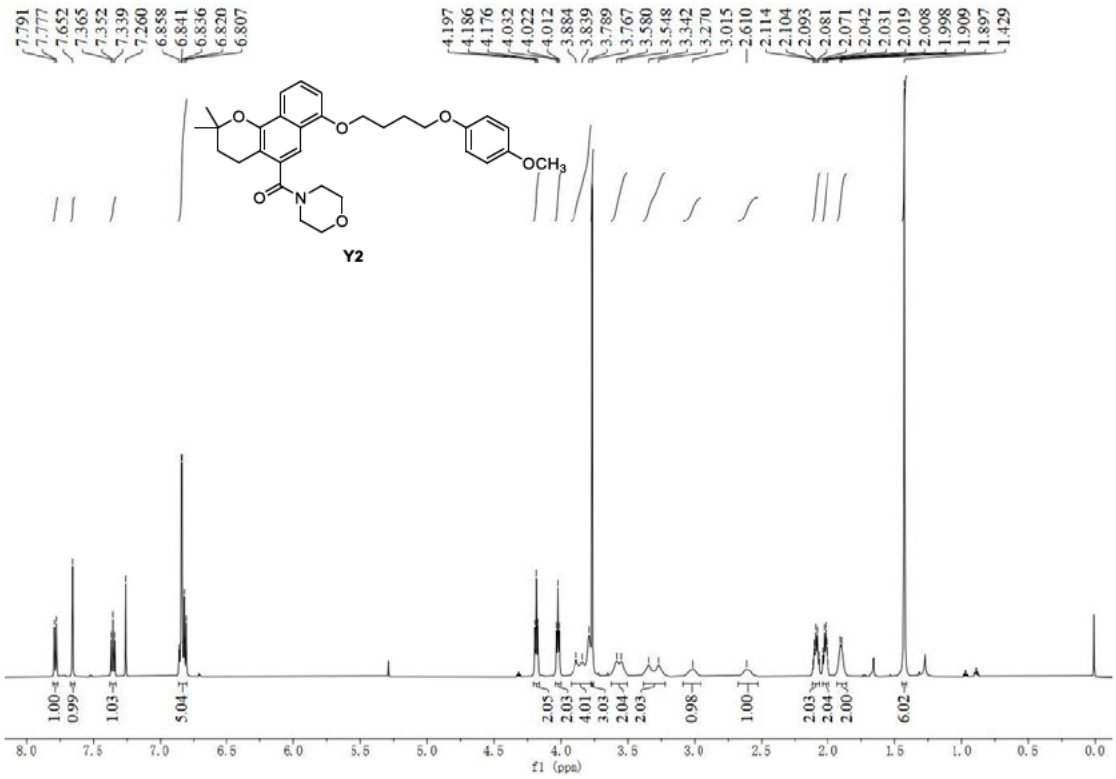


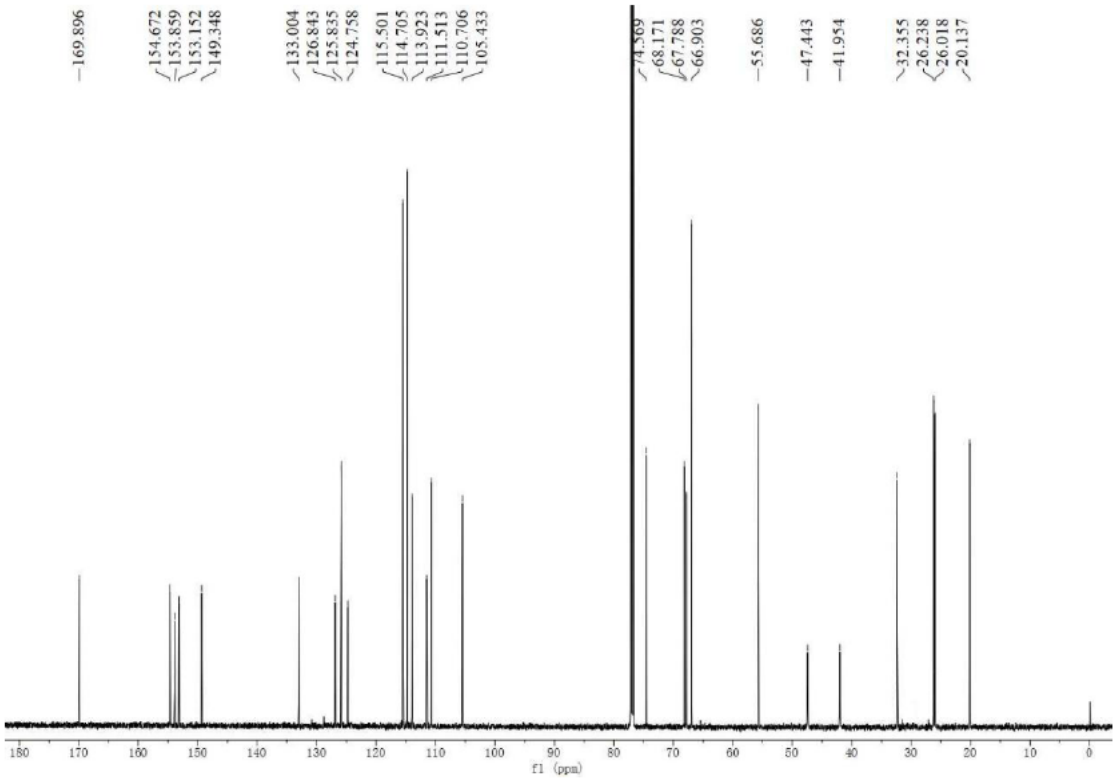
^{1}H-NMR and ^{13}C-NMR of **Y1**



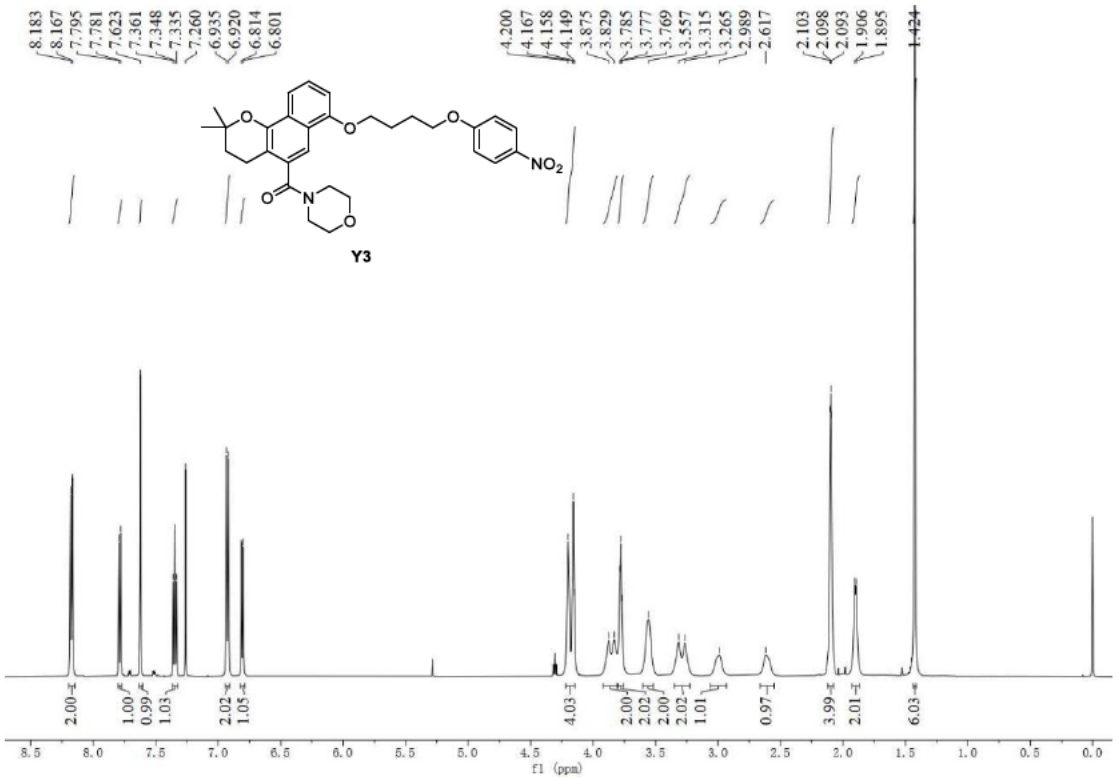


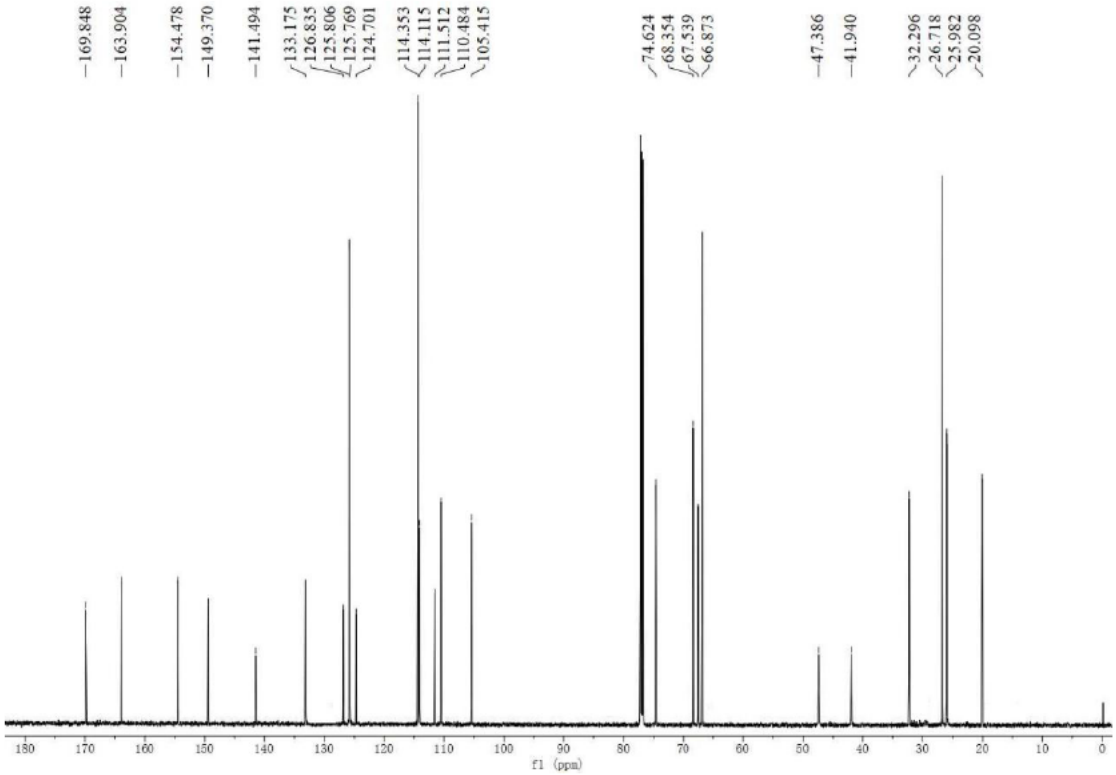
^{1}H-NMR and ^{13}C-NMR of **Y2**



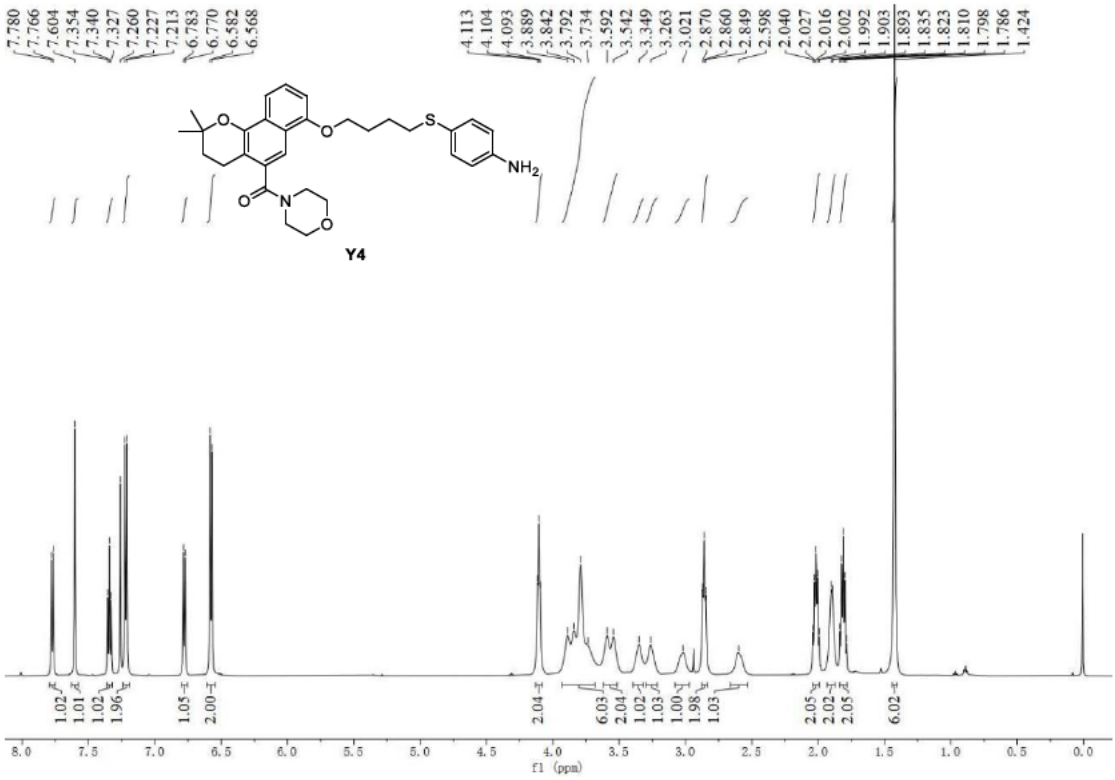


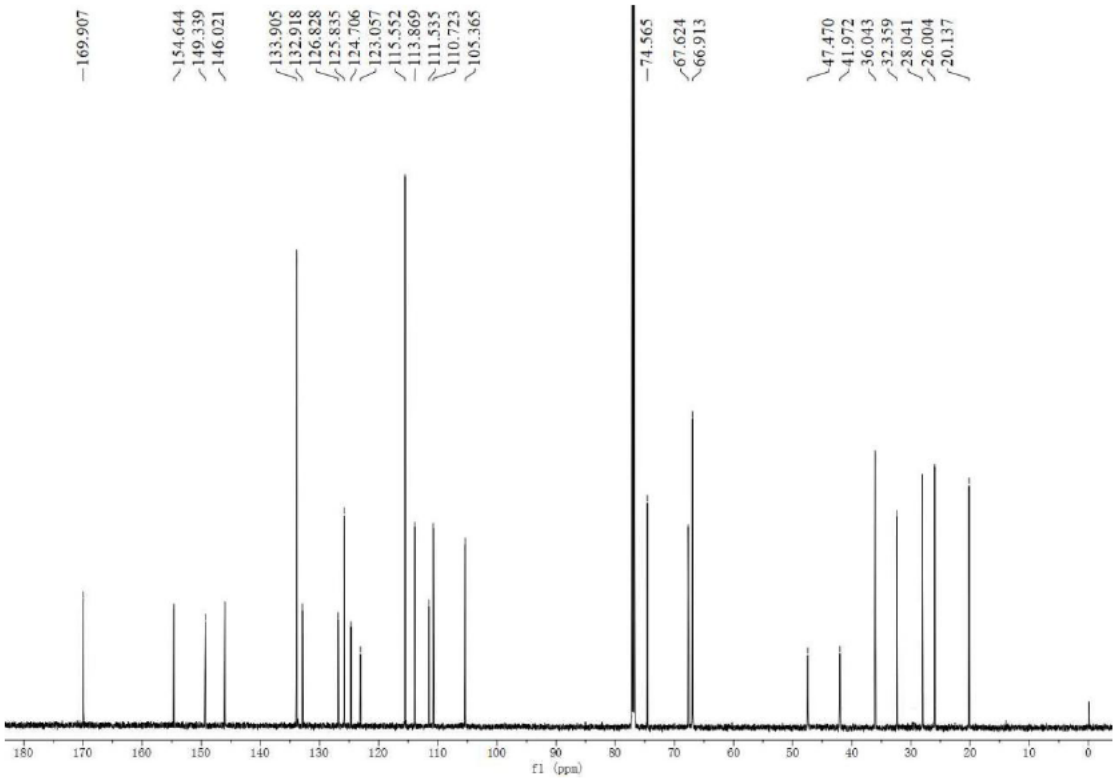
^{1}H-NMR and ^{13}C-NMR of **Y3**



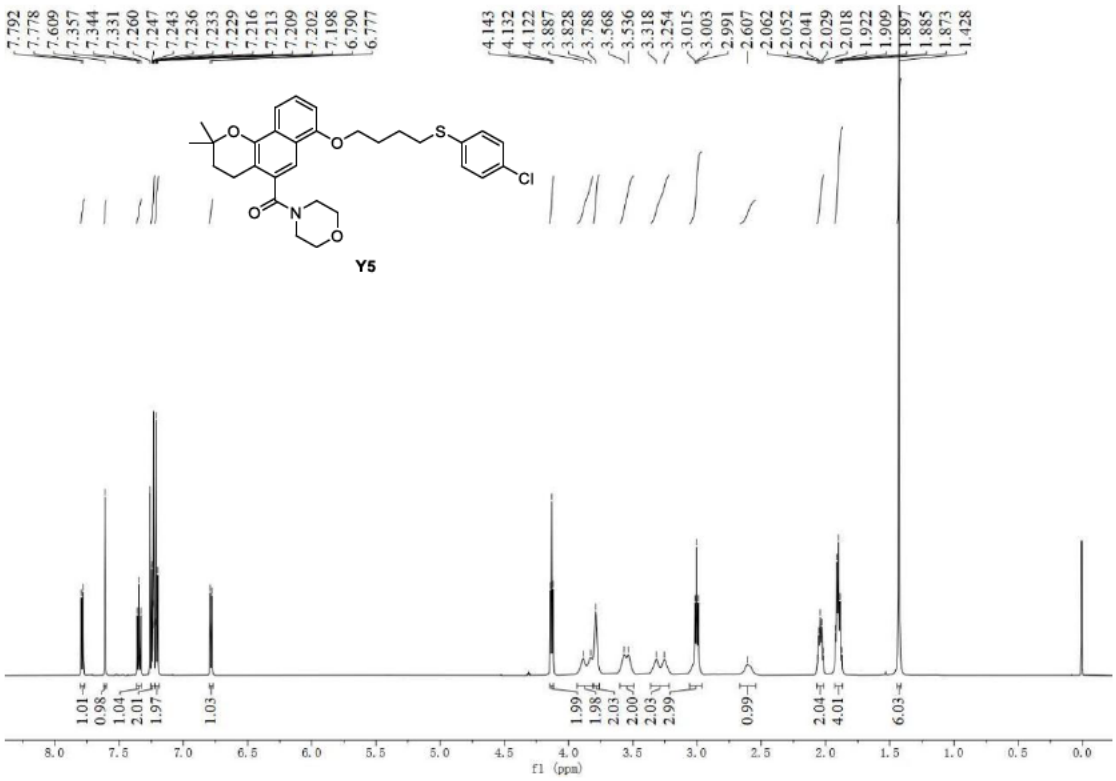


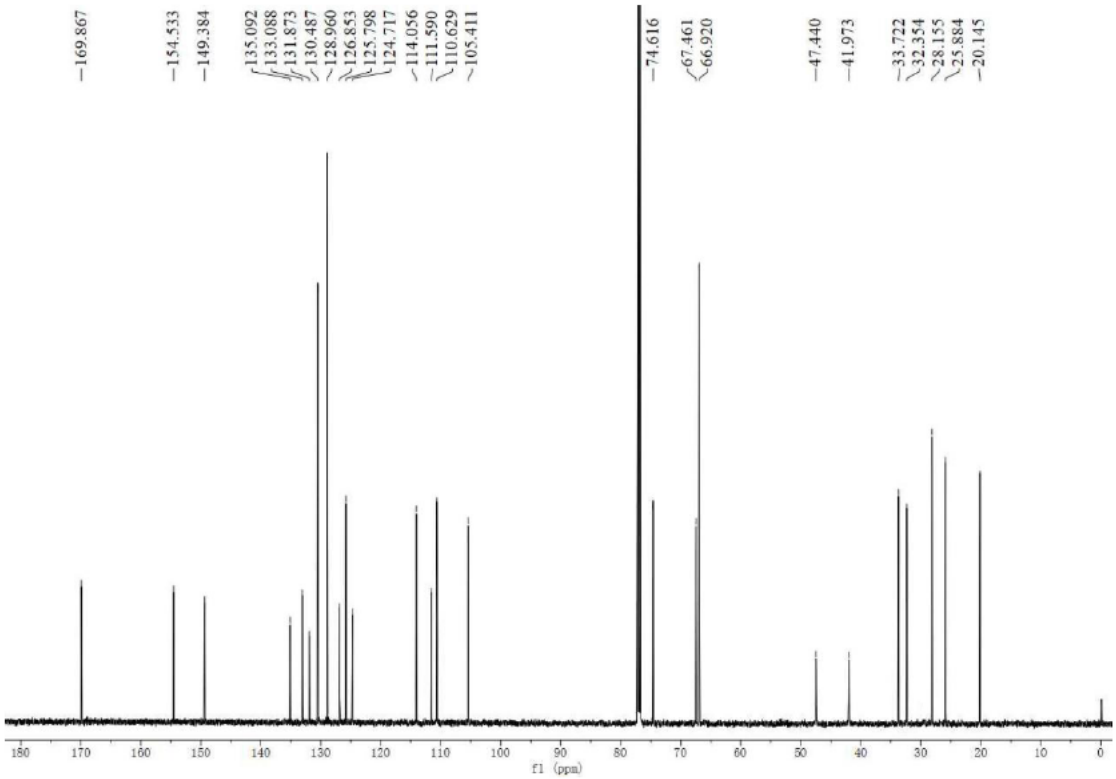
^{1}H-NMR and ^{13}C-NMR of **Y4**



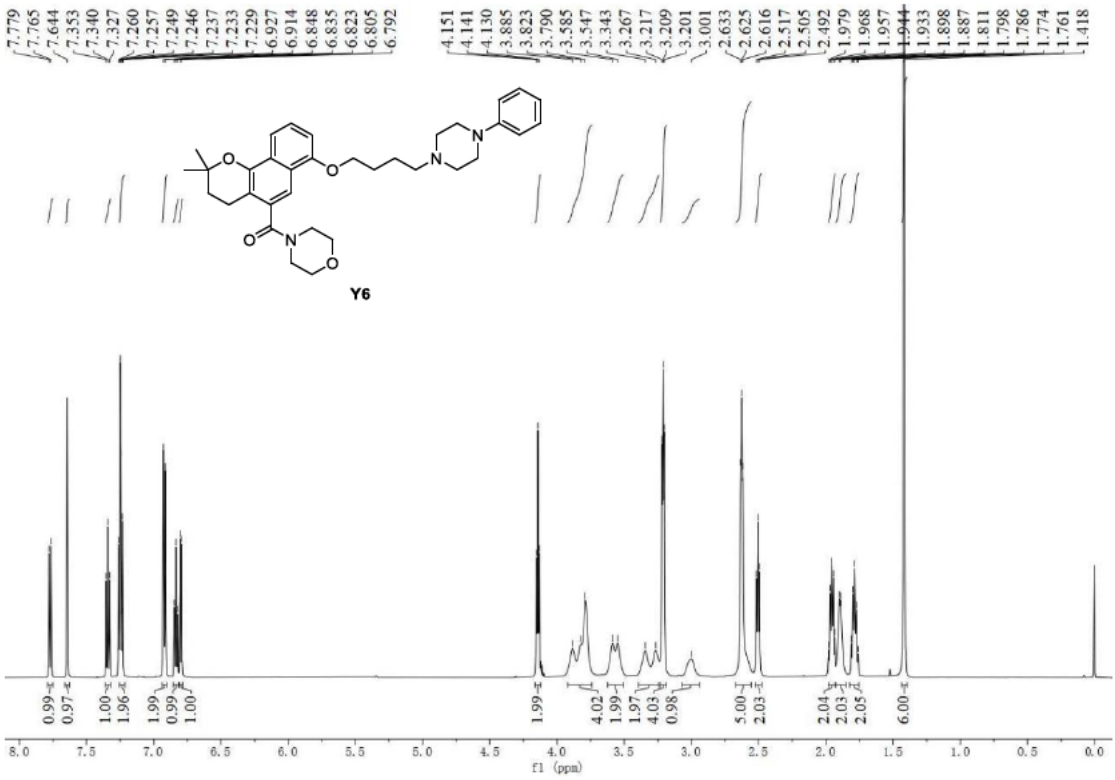


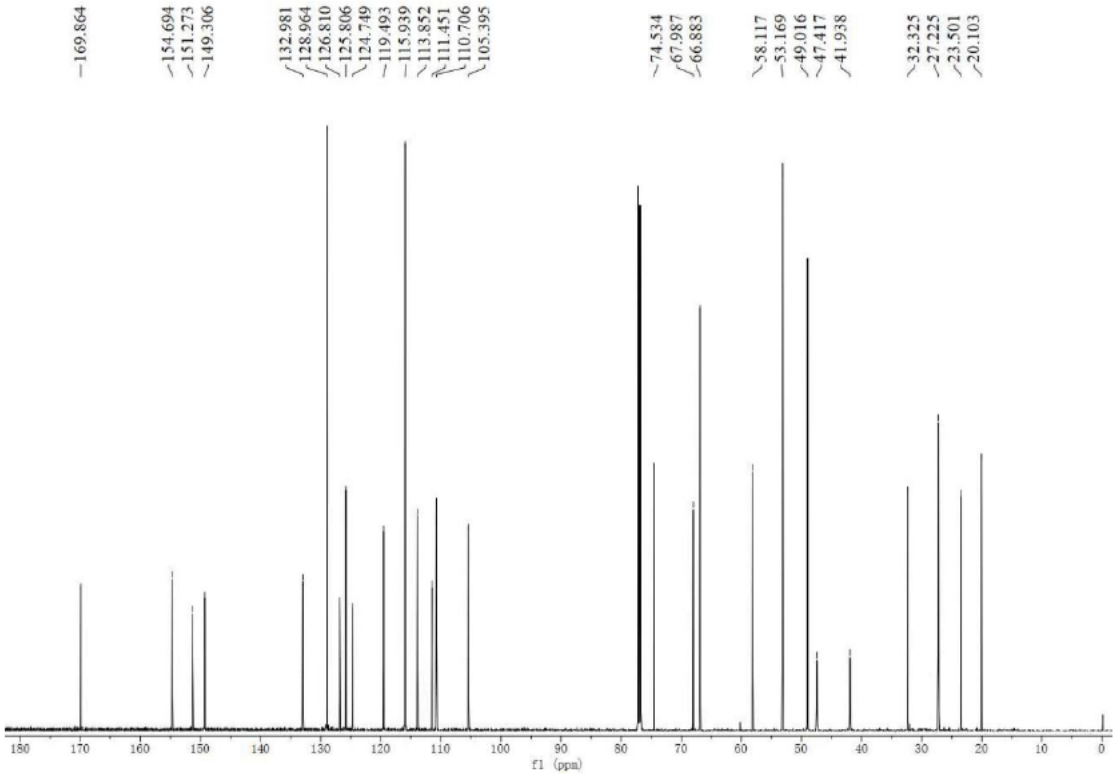
^{1}H-NMR and ^{13}C-NMR of **Y5**





^{1}H-NMR and ^{13}C-NMR of **Y6**





^{1}H-NMR and ^{13}C-NMR of **Y7**

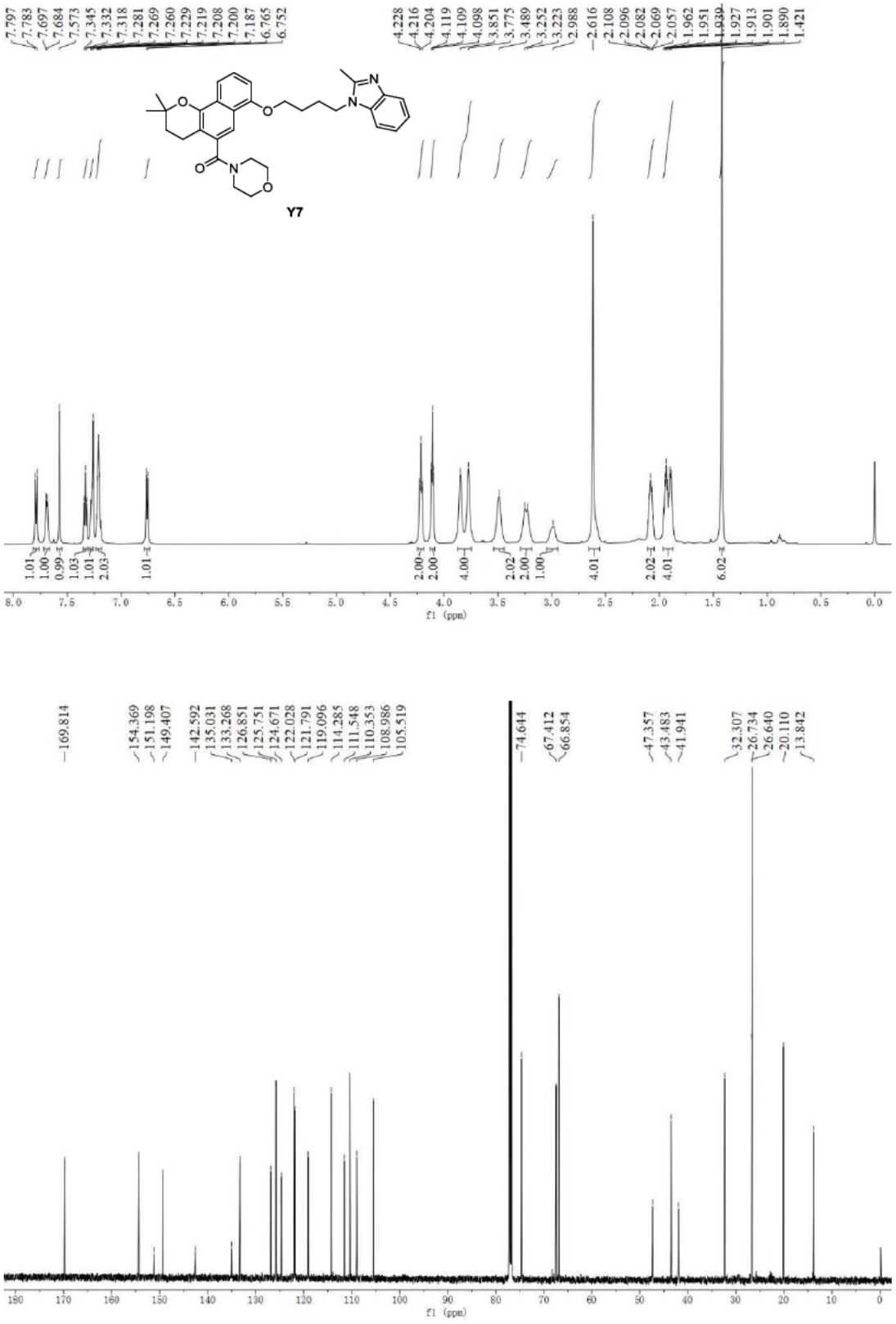
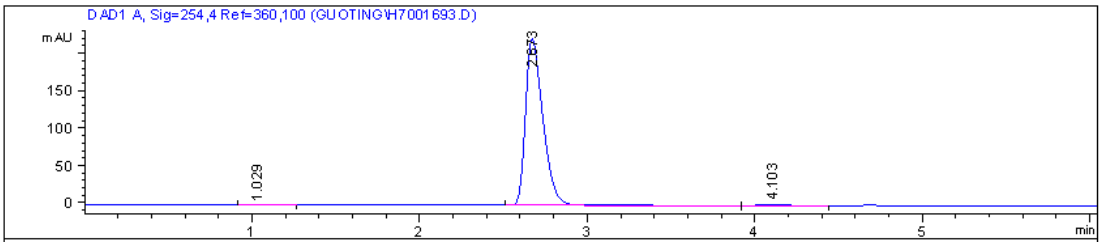


Figure A.4 ^{1}H NMR and ^{13}C NMR Spectra

HPLC chromatogram of **H1**

Signal 1: DAD1 A, Sig=254,4 Ref=360,100

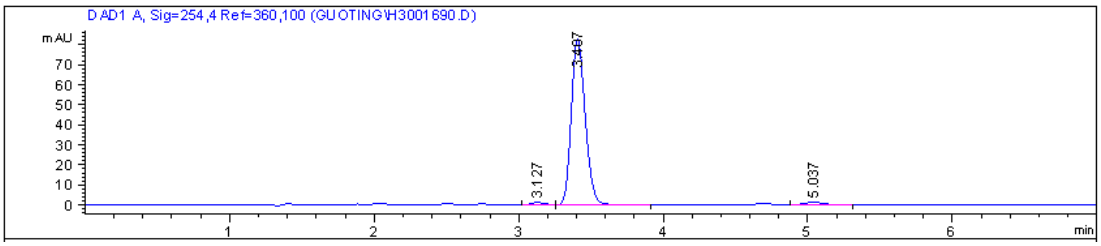
Peak #	RetTime [min]	Type	Width [min]	Area [mAU*s]	Height [mAU]	Area %
1	1.029	BB	0.2066	5.00908	3.27199e-1	0.3062
2	2.673	BB	0.1104	1611.99084	222.94366	98.5482
3	4.103	BB	0.1379	18.73910	2.10344	1.1456
Totals :				1635.73902	225.37430	



HPLC chromatogram of **H2**

Signal 1: DAD1 A, Sig=254,4 Ref=360,100

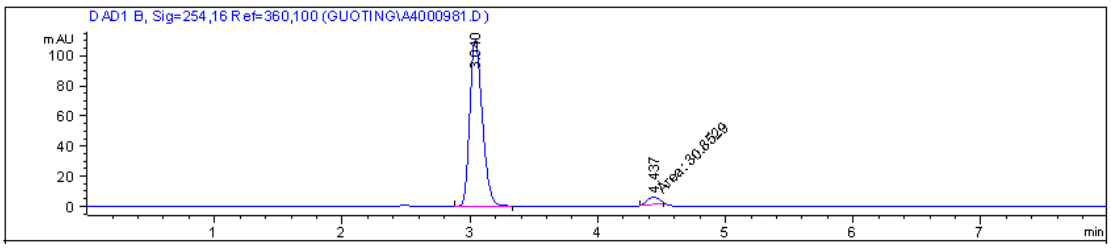
Peak #	RetTime [min]	Type	Width [min]	Area [mAU*s]	Height [mAU]	Area %
1	3.127	BV	0.0941	6.63768	1.10424	1.1677
2	3.407	VB	0.1036	551.12201	82.80500	96.9515
3	5.037	BB	0.1259	10.69145	1.32823	1.8808
Totals :				568.45114	85.23747	



HPLC chromatogram of **H3**

Signal 1: DAD1 B, Sig=254,16 Ref=360,100

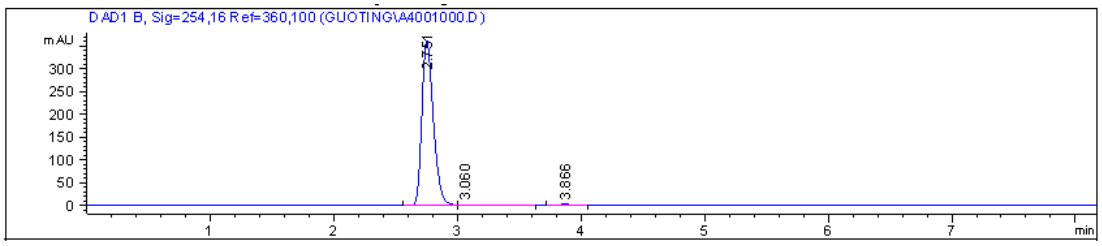
Peak #	RetTime [min]	Type	Width [min]	Area [mAU*s]	Height [mAU]	Area %
1	3.040	BB	0.1053	750.99420	110.53982	96.0538
2	4.437	MM	0.1046	30.85290	4.91641	3.9462
Totals :				781.84710	115.45623	



HPLC chromatogram of **H4**

Signal 1: DAD1 B, Sig=254,16 Ref=360,100

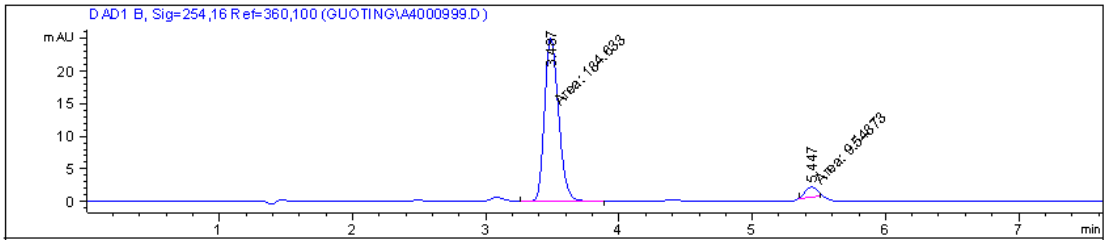
Peak #	RetTime [min]	Type	Width [min]	Area [mAU*s]	Height [mAU]	Area %
1	2.751	BV	0.0991	2335.57349	362.59955	98.2609
2	3.060	VB	0.1759	23.57500	1.81082	0.9918
3	3.866	BB	0.1127	17.76247	2.44560	0.7473
Totals :				2376.91096	366.85598	



HPLC chromatogram of **H5**

Signal 1: DAD1 B, Sig=254,16 Ref=360,100

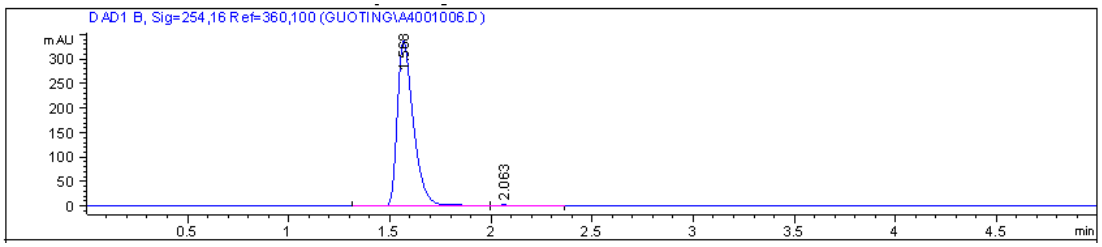
Peak #	RetTime [min]	Type	Width [min]	Area [mAU*s]	Height [mAU]	Area %
1	3.487	MM	0.1227	184.63341	25.06951	95.0826
2	5.447	MM	0.1032	9.54873	1.54144	4.9174
Totals :				194.18214	26.61095	



HPLC chromatogram of **H6**

Signal 1: DAD1 B, Sig=254,16 Ref=360,100

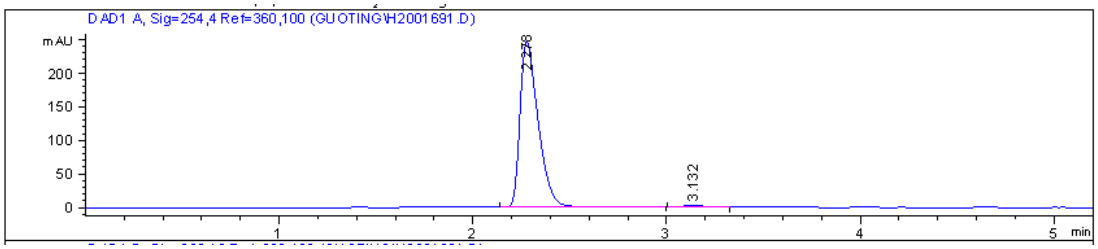
Peak #	RetTime [min]	Type	Width [min]	Area [mAU*s]	Height [mAU]	Area %
1	1.568	BV	0.0833	1887.87207	337.34442	99.0057
2	2.063	VB	0.1257	18.96032	2.09206	0.9943
Totals :				1906.83239	339.43648	



HPLC chromatogram of **H7**

Signal 1: DAD1 A, Sig=254,4 Ref=360,100

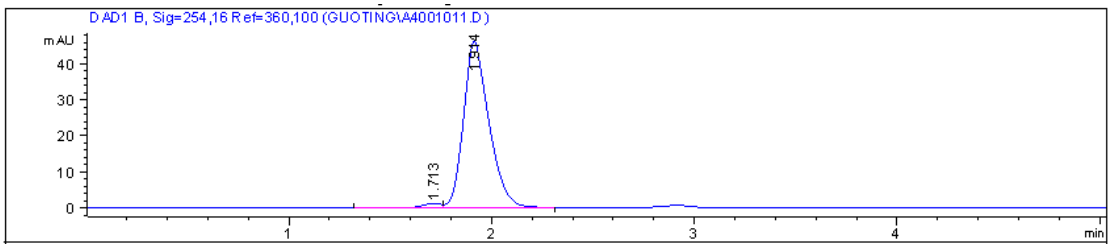
Peak #	RetTime [min]	Type	Width [min]	Area [mAU*s]	Height [mAU]	Area %
1	2.278	BB	0.1002	1611.29675	246.56415	98.5691
2	3.132	BB	0.1099	23.39058	3.33227	1.4309
Totals :				1634.68733	249.89642	



HPLC chromatogram of **G0**

Signal 1: DAD1 B, Sig=254,16 Ref=360,100

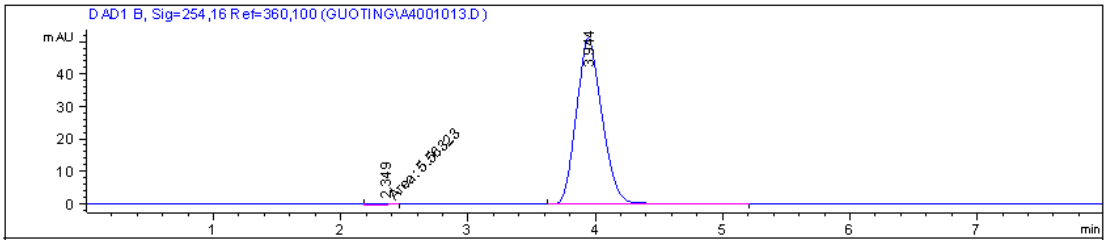
Peak #	RetTime [min]	Type	Width [min]	Area [mAU*s]	Height [mAU]	Area %
1	1.713	BV	0.1009	7.82287	1.15674	1.9171
2	1.914	VB	0.1269	400.23276	46.27472	98.0829
Totals :				408.05563	47.43146	



HPLC chromatogram of **G1**

Signal 1: DAD1 B, Sig=254,16 Ref=360,100

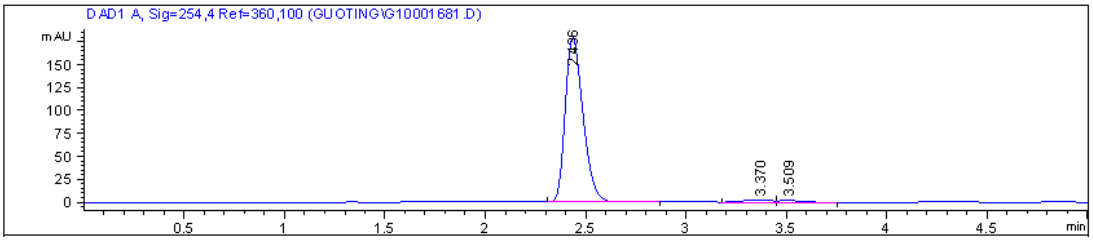
Peak #	RetTime [min]	Type	Width [min]	Area [mAU*s]	Height [mAU]	Area %
1	2.349	MM	0.1887	5.56323	3.90632e-1	0.7735
2	3.944	BB	0.2163	713.62927	51.29977	99.2265
Totals :				719.19250	51.69040	



HPLC chromatogram of **G2**

Signal 1: DAD1 A, Sig=254,4 Ref=360,100

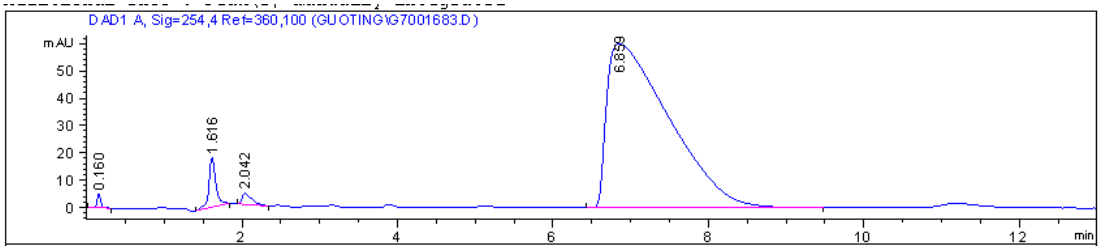
Peak #	RetTime [min]	Type	Width [min]	Area [mAU*s]	Height [mAU]	Area %
1	2.436	VB	0.0935	1100.20923	179.45274	97.1405
2	3.370	BV	0.1315	19.62969	2.09118	1.7332
3	3.509	VB	0.1079	12.75643	1.77347	1.1263
Totals :				1132.59535	183.31739	



HPLC chromatogram of **G3**

Signal 1: DAD1 A, Sig=254,4 Ref=360,100

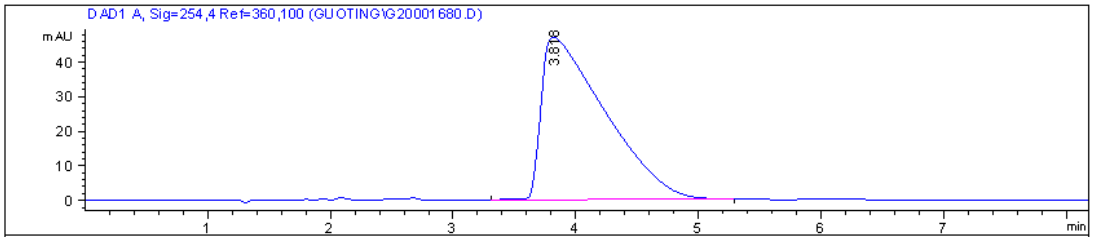
Peak #	RetTime [min]	Type	Width [min]	Area [mAU*s]	Height [mAU]	Area %
1	0.160	BB	0.0524	16.71953	5.07901	0.4764
2	1.616	BB	0.0907	109.96596	18.15289	3.1332
3	2.042	BB	0.1228	35.43434	4.09952	1.0096
4	6.859	BB	0.8139	3347.61743	60.09534	95.3809
Totals :				3509.73726	87.42677	



HPLC chromatogram of **G5**

Signal 1: DAD1 A, Sig=254,4 Ref=360,100

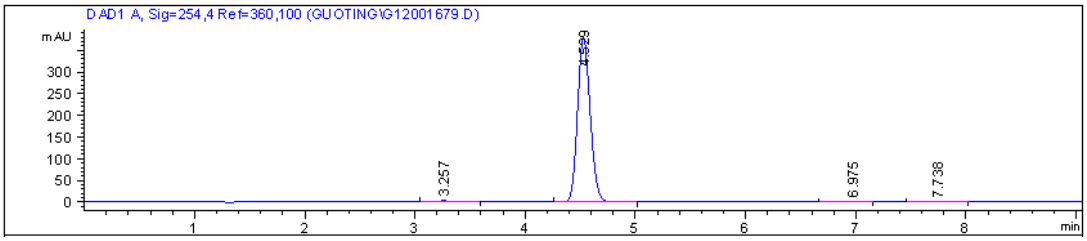
Peak #	RetTime [min]	Type	Width [min]	Area [mAU*s]	Height [mAU]	Area %
1	3.818	BB	0.5196	1692.89795	46.85187	100.0000
Totals :				1692.89795	46.85187	



HPLC chromatogram of **G6**

Signal 1: DAD1 A, Sig=254,4 Ref=360,100

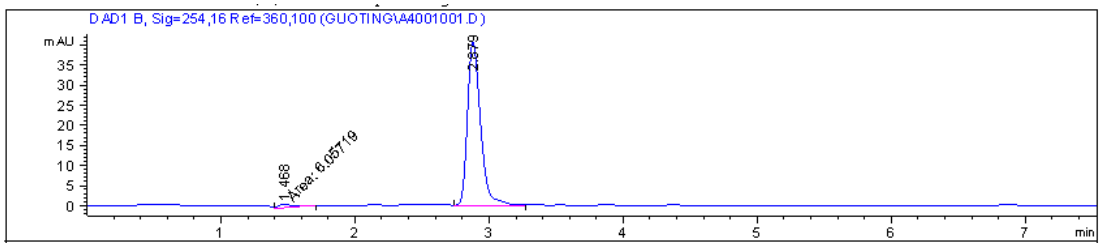
Peak #	RetTime [min]	Type	Width [min]	Area [mAU*s]	Height [mAU]	Area %
1	3.257	BB	0.1370	32.99414	3.34669	1.0639
2	4.529	BB	0.1230	3023.25488	379.31616	97.4887
3	6.975	BB	0.1951	29.09247	2.13273	0.9381
4	7.738	BB	0.1979	15.79227	1.26320	0.5092
Totals :				3101.13377	386.05879	



HPLC chromatogram of **G7**

Signal 1: DAD1 B, Sig=254,16 Ref=360,100

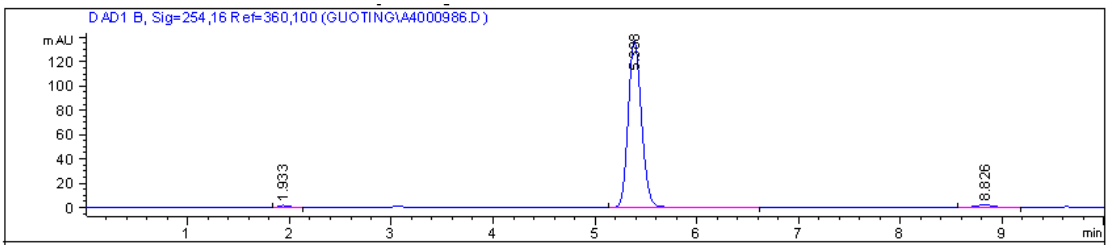
Peak #	RetTime [min]	Type	Width [min]	Area [mAU*s]	Height [mAU]	Area %
1	1.468	MM	0.1193	6.05719	8.46272e-1	2.1631
2	2.879	BB	0.1026	273.97061	40.68226	97.8369
Totals :				280.02780	41.52853	



HPLC chromatogram of **G8**

Signal 1: DAD1 B, Sig=254,16 Ref=360,100

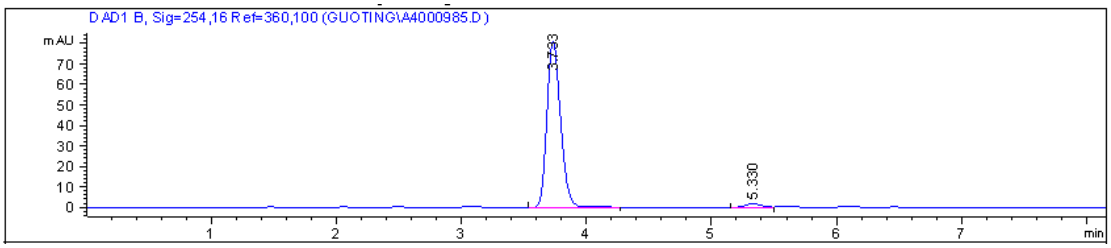
Peak #	RetTime [min]	Type	Width [min]	Area [mAU*s]	Height [mAU]	Area %
1	1.933	BB	0.1054	9.40790	1.38249	0.7333
2	5.388	BB	0.1426	1249.58130	136.76649	97.4009
3	8.826	BB	0.1920	23.93723	1.91263	1.8658
Totals :				1282.92643	140.06162	



HPLC chromatogram of **G9**

Signal 1: DAD1 B, Sig=254,16 Ref=360,100

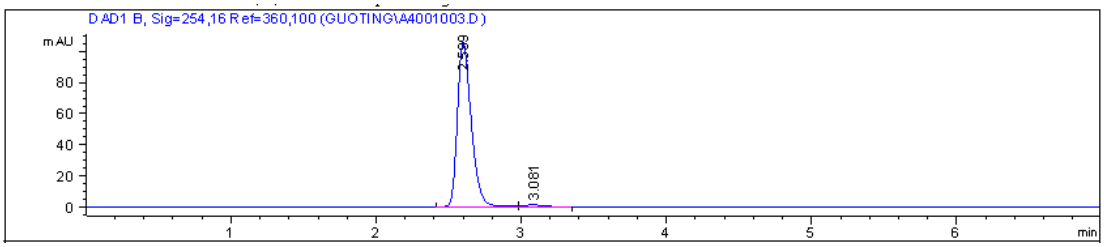
Peak #	RetTime [min]	Type	Width [min]	Area [mAU*s]	Height [mAU]	Area %
1	3.733	BB	0.1179	610.01770	81.00011	97.7021
2	5.330	BB	0.1345	14.34745	1.69969	2.2979
Totals :				624.36515	82.69979	



HPLC chromatogram of **G10**

Signal 1: DAD1 B, Sig=254,16 Ref=360,100

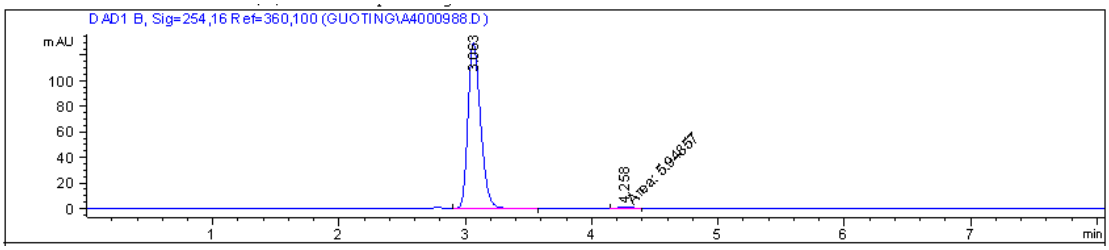
Peak #	RetTime [min]	Type	Width [min]	Area [mAU*s]	Height [mAU]	Area %
1	2.599	BV	0.1009	698.72083	105.98871	98.6366
2	3.081	VB	0.1229	9.65790	1.16316	1.3634
Totals :				708.37872	107.15187	



HPLC chromatogram of **G11**

Signal 1: DAD1 B, Sig=254,16 Ref=360,100

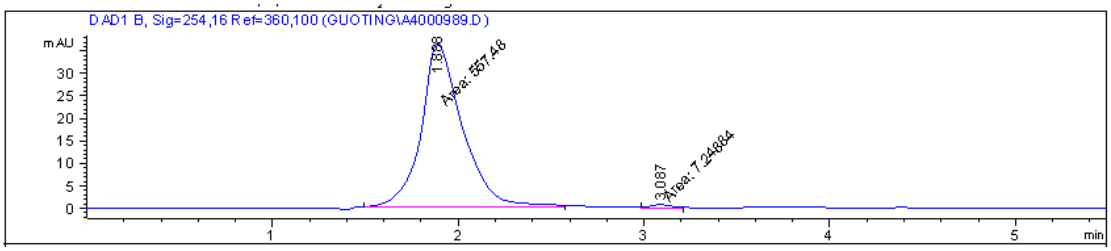
Peak #	RetTime [min]	Type	Width [min]	Area [mAU*s]	Height [mAU]	Area %
1	3.063	VB	0.1062	891.76782	129.72475	99.3374
2	4.258	MM	0.1456	5.94857	6.80881e-1	0.6626
Totals :				897.71639	130.40563	



HPLC chromatogram of **G12**

Signal 1: DAD1 B, Sig=254,16 Ref=360,100

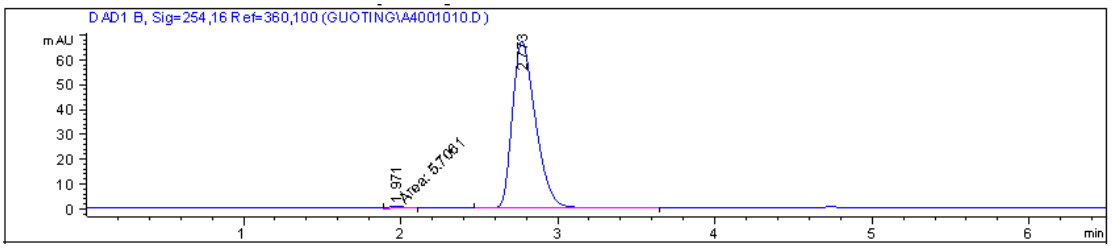
Peak #	RetTime [min]	Type	Width [min]	Area [mAU*s]	Height [mAU]	Area %
1	1.888	MM	0.2561	557.48041	36.28623	98.7164
2	3.087	MM	0.1381	7.24884	8.74575e-1	1.2836
Totals :				564.72925	37.16081	



HPLC chromatogram of **G13**

Signal 1: DAD1 B, Sig=254,16 Ref=360,100

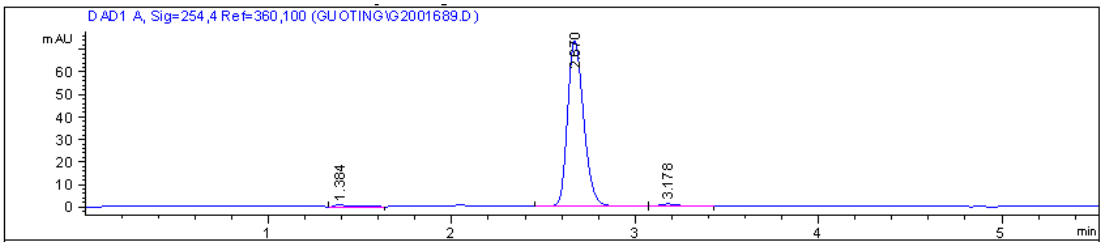
Peak #	RetTime [min]	Type	Width [min]	Area [mAU*s]	Height [mAU]	Area %
1	1.971	MM	0.1259	5.70610	7.55591e-1	0.8254
2	2.773	BB	0.1571	685.61237	67.15976	99.1746
Totals :				691.31846	67.91535	



HPLC chromatogram of **G14**

Signal 1: DAD1 A, Sig=254,4 Ref=360,100

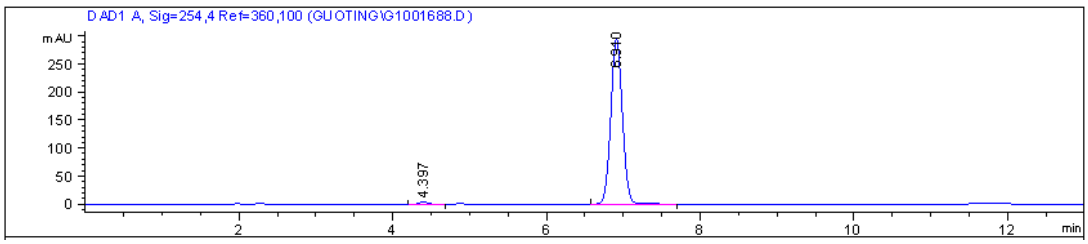
Peak #	RetTime [min]	Type	Width [min]	Area [mAU*s]	Height [mAU]	Area %
1	1.384	BB	0.0830	6.02455	1.04843	1.2963
2	2.670	BV	0.0931	450.70905	73.95541	96.9775
3	3.178	VB	0.1232	8.02261	1.02647	1.7262
Totals :				464.75621	76.03031	



HPLC chromatogram of **G16**

Signal 1: DAD1 A, Sig=254,4 Ref=360,100

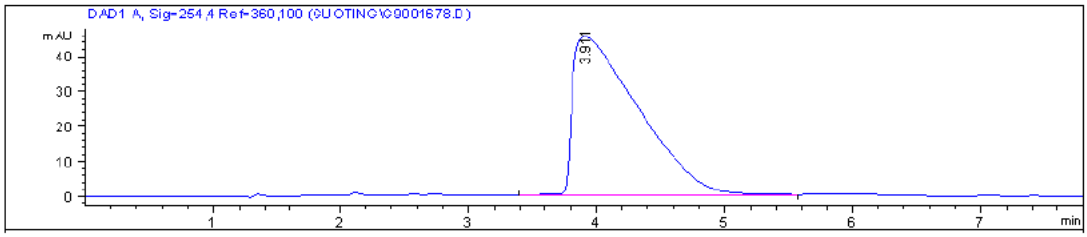
Peak #	RetTime [min]	Type	Width [min]	Area [mAU*s]	Height [mAU]	Area %
1	4.397	BB	0.1214	26.48578	3.30930	0.8535
2	6.910	BB	0.1621	3076.77856	293.99014	99.1465
Totals :				3103.26434	297.29944	



HPLC chromatogram of **G17**

Signal 1: DAD1 A, Sig=254,4 Ref=360,100

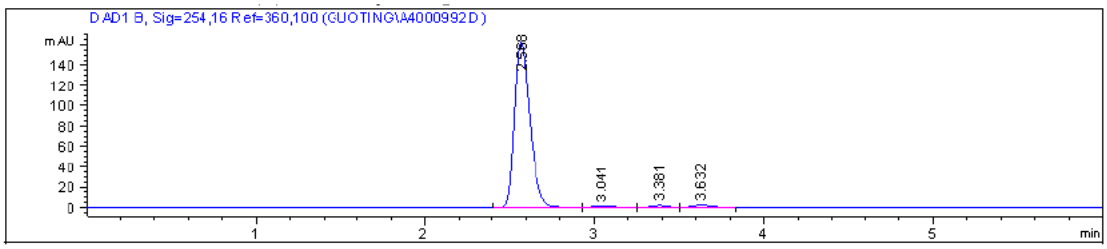
Peak #	RetTime [min]	Type	Width [min]	Area [mAU*s]	Height [mAU]	Area %
1	3.911	BB	0.5250	1611.31555	45.29570	100.0000
Totals :				1611.31555	45.29570	



HPLC chromatogram of **G18**

Signal 1: DAD1 B, Sig=254,16 Ref=360,100

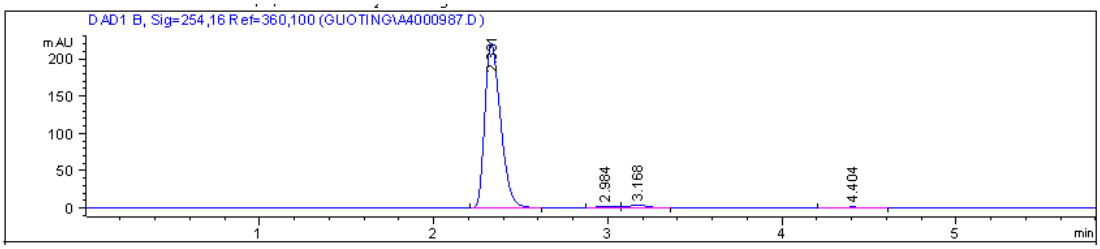
Peak #	RetTime [min]	Type	Width [min]	Area [mAU*s]	Height [mAU]	Area %
1	2.568	BV	0.0981	1033.85413	162.87801	96.2267
2	3.041	VB	0.1333	11.63547	1.26510	1.0830
3	3.381	BV	0.1046	12.04919	1.78883	1.1215
4	3.632	VB	0.1342	16.85541	2.00287	1.5688
Totals :				1074.39419	167.93480	



HPLC chromatogram of **G19**

Signal 1: DAD1 B, Sig=254,16 Ref=360,100

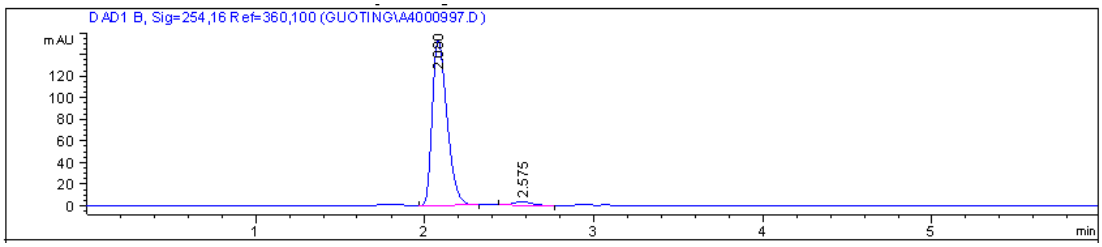
Peak #	RetTime [min]	Type	Width [min]	Area [mAU*s]	Height [mAU]	Area %
1	2.331	BB	0.0971	1379.37183	220.21931	96.4839
2	2.984	BV	0.1045	13.88099	1.96343	0.9709
3	3.168	VB	0.1172	27.18794	3.55713	1.9017
4	4.404	BB	0.1186	9.19895	1.21176	0.6434
Totals :				1429.63971	226.95163	



HPLC chromatogram of **G20**

Signal 1: DAD1 B, Sig=254,16 Ref=360,100

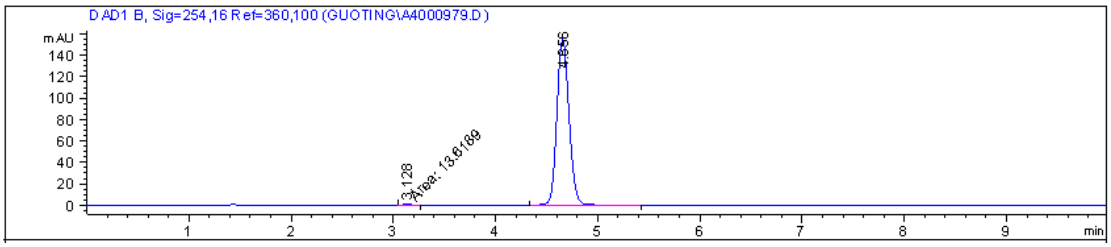
Peak #	RetTime [min]	Type	Width [min]	Area [mAU*s]	Height [mAU]	Area %
1	2.080	BB	0.0925	922.06226	152.55000	97.4562
2	2.575	BB	0.1291	24.06797	3.01730	2.5438
Totals :				946.13023	155.56730	



HPLC chromatogram of **Y2**

Signal 1: DAD1 B, Sig=254,16 Ref=360,100

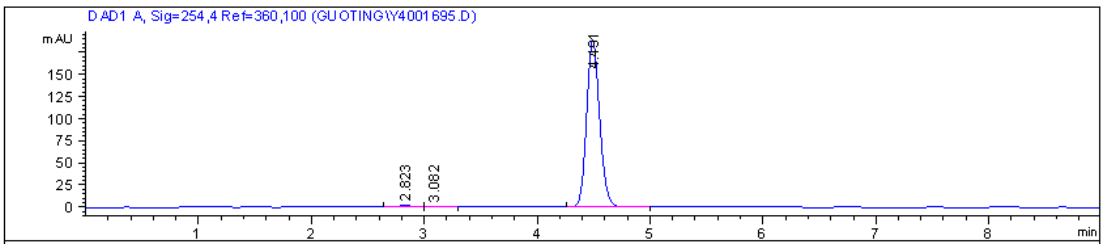
Peak #	RetTime [min]	Type	Width [min]	Area [mAU*s]	Height [mAU]	Area %
1	3.128	MM	0.1438	13.61885	1.57884	1.0493
2	4.656	BB	0.1265	1284.26147	155.30644	98.9507
Totals :				1297.88033	156.88528	



HPLC chromatogram of **Y3**

Signal 1: DAD1 A, Sig=254,4 Ref=360,100

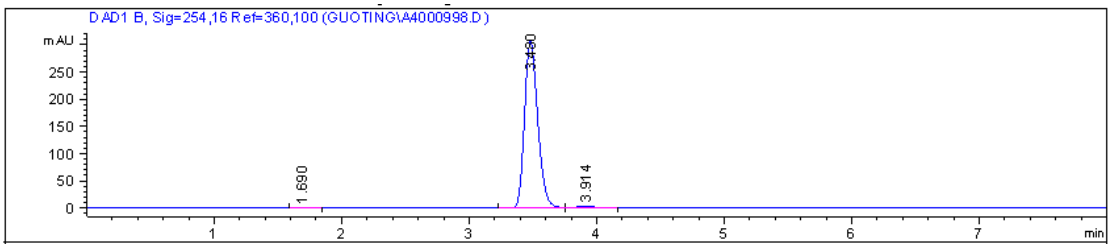
Peak #	RetTime [min]	Type	Width [min]	Area [mAU*s]	Height [mAU]	Area %
1	2.823	BV	0.0980	16.24786	2.49288	1.0546
2	3.082	VB	0.1006	6.99242	1.06455	0.4539
3	4.491	BB	0.1235	1517.38013	189.39934	98.4915
Totals :				1540.62041	192.95677	



HPLC chromatogram of **Y4**

Signal 1: DAD1 B, Sig=254,16 Ref=360,100

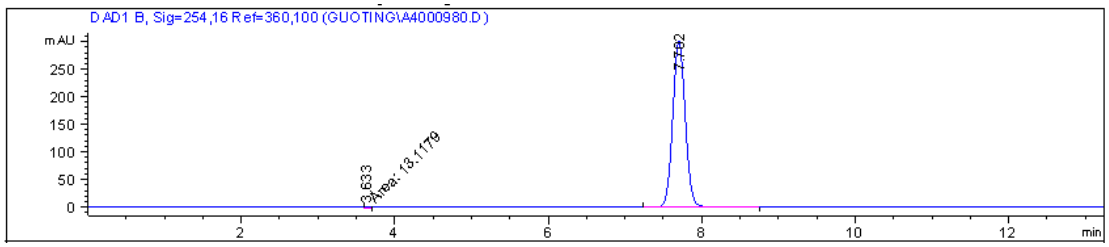
Peak #	RetTime [min]	Type	Width [min]	Area [mAU*s]	Height [mAU]	Area %
1	1.690	VB	0.0950	7.04884	1.09653	0.3147
2	3.480	BV	0.1117	2201.00732	306.70547	98.2688
3	3.914	VB	0.1425	31.72733	3.29015	1.4165
Totals :				2239.78349	311.09216	



HPLC chromatogram of **Y5**

Signal 1: DAD1 B, Sig=254,16 Ref=360,100

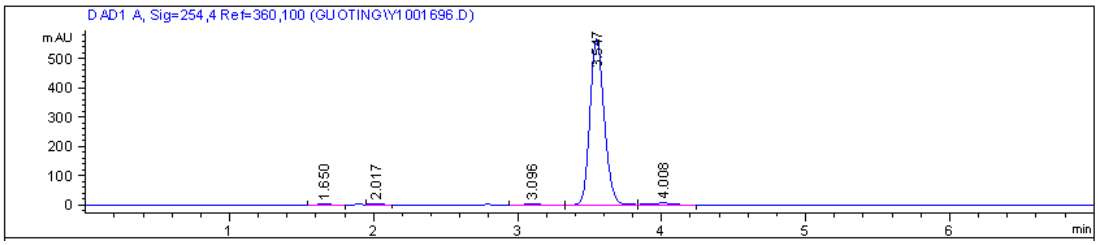
Peak #	RetTime [min]	Type	Width [min]	Area [mAU*s]	Height [mAU]	Area %
1	3.633	MM	0.0939	13.11794	2.32905	0.3836
2	7.702	BB	0.1761	3406.30908	300.80563	99.6164
Totals :				3419.42702	303.13468	



HPLC chromatogram of **Y6**

Signal 1: DAD1 A, Sig=254,4 Ref=360,100

Peak #	RetTime [min]	Type	Width [min]	Area [mAU*s]	Height [mAU]	Area %
1	1.650	VB	0.0845	12.13426	2.19353	0.3061
2	2.017	VB	0.0851	10.37359	1.86015	0.2617
3	3.096	BB	0.1140	11.68280	1.58491	0.2947
4	3.547	BV	0.1058	3883.18530	567.59570	97.9677
5	4.008	VB	0.1277	46.36473	5.42672	1.1697
Totals :				3963.74069	578.66103	



HPLC chromatogram of **Y7**

Signal 1: DAD1 A, Sig=254,4 Ref=360,100

Peak #	RetTime [min]	Type	Width [min]	Area [mAU*s]	Height [mAU]	Area %
1	3.729	BB	0.1539	2535.56836	238.76187	100.0000
Totals :				2535.56836	238.76187	

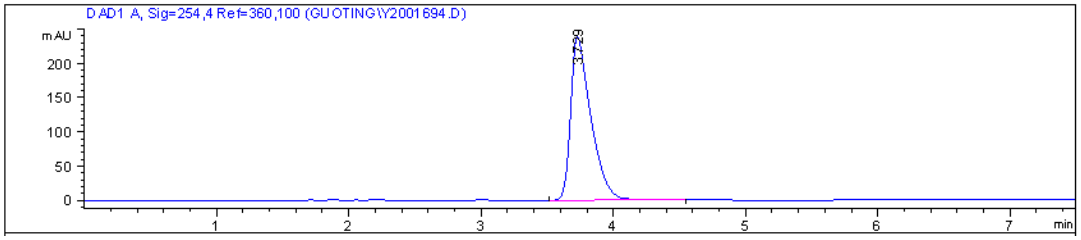


Figure A.5 HPLC spectra of representative compounds.

Agilent Technologies 1200 series HPLC with Diamonsil C18 column (150 × 4.6mm, 5 μm) at UV detection of 254 nm. Injection volume is 5 μL, and it was maintained at ambient temperature. The effective chromatogram was obtained using the mobile phase of acetonitrile-water or acetonitrile-0.025 mol/L potassium dihydrogen phosphate buffer and the pH value was adjusted to 3 with phosphoric acid at the flow rate of 1.0 mL/min.

Appendix 3. Checkerboard assay results for synthetic compounds not reported in Chapter 3

Table A.3 Minimum inhibitory concentration (MIC) of erythromycin (ERY), levofloxacin (LEV) and minocycline (MIN) against *E. coli* BW25113 in the presence of synthetic compounds (G, H, Y and S series) and positive control phenylalanine-arginine beta-naphthylamide (PAβN).

Results are from assays performed in duplicate on at least three different days with different batches of cells.

Compound and concentration (μg/mL)		**MIC (μg/mL)**			**Compound and concentration (μg/mL)**		**MIC(μg/mL)**		
		ERY	LEV	MIN			ERY	LEV	MIN
G0	8	64	0.063	2	G1	8	32	0.063	1
	16	64	0.063	2		16	32	0.063	1
	32	64	0.063	2		32	32	0.063	1
	64	64	0.063	2		64	32	0.063	1
	128	64	0.063	2		128	32	0.063	1
G2	8	64	0.063	2	G3	8	64	0.0315	2
	16	64	0.0315	2		16	64	0.0315	2
	32	64	0.0315	2		32	64	0.0315	1
	64	64	0.0315	1		64	64	0.0315	1
	128	64	0.0315	1		128	64	0.0315	1
G4	8	64	0.0315	2	G5	8	64	0.0315	2
	16	64	0.0315	2		16	64	0.063	2
	32	64	0.0315	2		32	64	0.0315	2
	64	64	0.063	2		64	64	0.063	2
	128	64	0.0315	1		128	64	0.063	1

G7	8	64	0.0315	2	G8	8	64	0.0315	2
	16	64	0.0315	2		16	64	0.0315	2
	32	64	0.0315	2		32	64	0.0315	2
	64	64	0.0315	2		64	64	0.0315	1
	128	64	0.0315	2		128	64	0.0315	1
G9	8	64	0.063	2	G12	8	64	0.063	2
	16	64	0.0315	2		16	64	0.063	1
	32	64	0.063	2		32	64	0.0315	1
	64	64	0.0315	2		64	64	0.063	2
	128	64	0.0315	2		128	128	0.0315	1
G13	8	64	0.0315	2	G14	8	64	0.063	2
	16	64	0.0315	1		16	64	0.0315	2
	32	64	0.0315	1		32	64	0.0315	2
	64	64	0.0315	1		64	64	0.0315	1
	128	32	0.0315	1		128	64	0.0315	2
G15	8	64	0.063	4	G16	8	64	0.0315	2
	16	64	0.128	4		16	64	0.063	2
	32	64	0.063	4		32	64	0.063	2
	64	64	0.063	4		64	64	0.0315	2
	128	64	0.063	4		128	32	0.0315	1
G17	8	64	0.063	2	G18	8	64	0.063	2
	16	64	0.128	1		16	64	0.063	2
	32	64	0.063	1		32	64	0.0315	1
	64	64	0.063	1		64	64	0.0315	1
	128	64	0.063	2		128	64	0.0315	2
G19	8	64	0.063	1	G20	8	64	0.063	4
	16	64	0.063	2		16	64	0.063	2
	32	64	0.063	1		32	64	0.063	2

	64 128	64 64	0.063 0.063	2 1		64 128	32 32	0.0315 0.0315	2 2
H1	8 16 32 64 128	64 64 64 64 64	0.063 0.063 0.063 0.063 0.063	2 2 2 2 2	H2	8 16 32 64 128	64 64 64 64 64	0.063 0.063 0.063 0.063 0.063	2 2 2 2 2
H4	8 16 32 64 128	64 64 64 64 64	0.063 0.063 0.063 0.063 0.063	2 2 2 2 2	H7	8 16 32 64 128	64 64 64 64 64	0.128 0.063 0.063 0.063 0.063	2 2 2 2 2
S1	8 16 32 64 128	64 64 64 64 64	0.063 0.063 0.063 0.063 0.063	2 2 2 2 2	S2	8 16 32 64 128	64 64 64 64 64	0.063 0.063 0.063 0.063 0.063	2 2 2 2 2
S3	8 16 32 64 128	64 64 64 64 64	0.063 0.063 0.063 0.063 0.063	2 2 2 2 2	PAβN	8 16 32 64 128	16 8 4 2 2	0.032 0.016 0.016 0.016 0.002	0.5 0.5 0.5 0.5 0.25
None (+) AcrB	0	64	0.063	2	None (-) AcrB	0	4	0.004	0.25

Appendix 4. Copyright permission

SPRINGER NATURE LICENSE
TERMS AND CONDITIONS

Apr 27, 2023

This Agreement between Mrs. YANG CHEN ("You") and Springer Nature ("Springer Nature") consists of your license details and the terms and conditions provided by Springer Nature and Copyright Clearance Center.

License Number	5536890491193
License date	Apr 27, 2023
Licensed Content Publisher	Springer Nature
Licensed Content Publication	Nature Reviews Microbiology
Licensed Content Title	Multidrug efflux pumps: structure, function and regulation
Licensed Content Author	Dijun Du et al
Licensed Content Date	Jul 12, 2018
Type of Use	Thesis/Dissertation
Requestor type	non-commercial (non-profit)
Format	electronic
Portion	figures/tables/illustrations
Number of figures/tables/illustrations	1
Would you like a high resolution image with your order?	no
Will you be translating?	no

Circulation/distribution	1 - 29
Author of this Springer Nature content	no
Title	Reversing antimicrobial resistance with inhibitors of drug efflux pumps
Institution name	University of South Australia
Expected presentation date	Apr 2023
Order reference number	123
Portions	Fig. 1 on page 2
Requestor Location	Mrs. YANG CHEN Jinsejiaoxiang Garden, Panlong Kunming, Yunnan 650000 China Attn: Mrs. YANG CHEN
Total	0.00 AUD

Terms and Conditions

Springer Nature Customer Service Centre GmbH Terms and Conditions

The following terms and conditions ("Terms and Conditions") together with the terms specified in your [RightsLink] constitute the License ("License") between you as Licensee and Springer Nature Customer Service Centre GmbH as Licensor. By clicking 'accept' and completing the transaction for your use of the material ("Licensed Material"), you confirm your acceptance of and obligation to be bound by these Terms and Conditions.

1. Grant and Scope of License

1. 1. The Licensor grants you a personal, non-exclusive, non-transferable, non-sublicensable, revocable, world-wide License to reproduce, distribute, communicate to the public, make available, broadcast, electronically transmit or create derivative works using the Licensed Material for the purpose(s) specified in your RightsLink Licence Details only. Licenses are granted for the specific use requested in the order and for no other use, subject to these Terms and Conditions. You acknowledge and agree that the rights granted to you under this License do not include the right to modify, edit, translate, include in collective works, or create derivative works of the Licensed Material in whole or in part unless expressly stated in your RightsLink

Licence Details. You may use the Licensed Material only as permitted under this Agreement and will not reproduce, distribute, display, perform, or otherwise use or exploit any Licensed Material in any way, in whole or in part, except as expressly permitted by this License.

1. 2. You may only use the Licensed Content in the manner and to the extent permitted by these Terms and Conditions, by your RightsLink Licence Details and by any applicable laws.

1. 3. A separate license may be required for any additional use of the Licensed Material, e.g. where a license has been purchased for print use only, separate permission must be obtained for electronic re-use. Similarly, a License is only valid in the language selected and does not apply for editions in other languages unless additional translation rights have been granted separately in the License.

1. 4. Any content within the Licensed Material that is owned by third parties is expressly excluded from the License.

1. 5. Rights for additional reuses such as custom editions, computer/mobile applications, film or TV reuses and/or any other derivative rights requests require additional permission and may be subject to an additional fee. Please apply to journalpermissions@springernature.com or bookpermissions@springernature.com for these rights.

2. Reservation of Rights

Licensor reserves all rights not expressly granted to you under this License. You acknowledge and agree that nothing in this License limits or restricts Licensor's rights in or use of the Licensed Material in any way. Neither this License, nor any act, omission, or statement by Licensor or you, conveys any ownership right to you in any Licensed Material, or to any element or portion thereof. As between Licensor and you, Licensor owns and retains all right, title, and interest in and to the Licensed Material subject to the license granted in Section 1.1. Your permission to use the Licensed Material is expressly conditioned on you not impairing Licensor's or the applicable copyright owner's rights in the Licensed Material in any way.

3. Restrictions on use

3. 1. Minor editing privileges are allowed for adaptations for stylistic purposes or formatting purposes provided such alterations do not alter the original meaning or intention of the Licensed Material and the new figure(s) are still accurate and representative of the Licensed Material. Any other changes including but not limited to, cropping, adapting, and/or omitting material that affect the meaning, intention or moral rights of the author(s) are strictly prohibited.

3. 2. You must not use any Licensed Material as part of any design or trademark.

3. 3. Licensed Material may be used in Open Access Publications (OAP), but any such reuse must include a clear acknowledgment of this permission visible at the same time as the figures/tables/illustration or abstract and which must indicate that the Licensed Material is not part of the governing OA license but has been reproduced with permission. This may be indicated according to any standard referencing system but must include at a minimum 'Book/Journal title, Author, Journal Name (if applicable), Volume (if applicable), Publisher, Year, reproduced with permission from SNCSC'.

4. STM Permission Guidelines

4. 1. An alternative scope of license may apply to signatories of the STM Permissions Guidelines ("STM PG") as amended from time to time and made available at https://www.stm-assoc.org/intellectual-property/permissions/permissions-guidelines/.

4. 2. For content reuse requests that qualify for permission under the STM PG, and which may be updated from time to time, the STM PG supersede the terms and conditions contained in this License.

4. 3. If a License has been granted under the STM PG, but the STM PG no longer apply at the time of publication, further permission must be sought from the Rightsholder. Contact journalpermissions@springernature.com or bookpermissions@springernature.com for these rights.

5. Duration of License

5. 1. Unless otherwise indicated on your License, a License is valid from the date of purchase ("License Date") until the end of the relevant period in the below table:

Reuse in a medical communications project	Reuse up to distribution or time period indicated in License
Reuse in a dissertation/thesis	Lifetime of thesis
Reuse in a journal/magazine	Lifetime of journal/magazine
Reuse in a book/textbook	Lifetime of edition
Reuse on a website	1 year unless otherwise specified in the License
Reuse in a presentation/slide kit/poster	Lifetime of presentation/slide kit/poster. Note: publication whether electronic or in print of presentation/slide kit/poster may require further permission.
Reuse in conference proceedings	Lifetime of conference proceedings
Reuse in an annual report	Lifetime of annual report
Reuse in training/CME materials	Reuse up to distribution or time period indicated in License
Reuse in newsmedia	Lifetime of newsmedia
Reuse in coursepack/classroom materials	Reuse up to distribution and/or time period indicated in license

6. Acknowledgement

6. 1. The Licensor's permission must be acknowledged next to the Licensed Material in print. In electronic form, this acknowledgement must be visible at the same time as the figures/tables/illustrations or abstract and must be hyperlinked to the journal/book's homepage.

6. 2. Acknowledgement may be provided according to any standard referencing system and at a minimum should include "Author, Article/Book Title, Journal name/Book imprint, volume, page number, year, Springer Nature".

7. Reuse in a dissertation or thesis

7. 1. Where 'reuse in a dissertation/thesis' has been selected, the following terms apply: Print rights of the Version of Record are provided for; electronic rights for use only on institutional repository as defined by the Sherpa guideline

(www.sherpa.ac.uk/romeo/) and only up to what is required by the awarding institution.

7. 2. For theses published under an ISBN or ISSN, separate permission is required. Please contact journalpermissions@springernature.com or bookpermissions@springernature.com for these rights.

7. 3. Authors must properly cite the published manuscript in their thesis according to current citation standards and include the following acknowledgement: '*Reproduced with permission from Springer Nature*'.

8. License Fee

You must pay the fee set forth in the License Agreement (the "License Fees"). All amounts payable by you under this License are exclusive of any sales, use, withholding, value added or similar taxes, government fees or levies or other assessments. Collection and/or remittance of such taxes to the relevant tax authority shall be the responsibility of the party who has the legal obligation to do so.

9. Warranty

9. 1. The Licensor warrants that it has, to the best of its knowledge, the rights to license reuse of the Licensed Material. **You are solely responsible for ensuring that the material you wish to license is original to the Licensor and does not carry the copyright of another entity or third party (as credited in the published version).** If the credit line on any part of the Licensed Material indicates that it was reprinted or adapted with permission from another source, then you should seek additional permission from that source to reuse the material.

9. 2. EXCEPT FOR THE EXPRESS WARRANTY STATED HEREIN AND TO THE EXTENT PERMITTED BY APPLICABLE LAW, LICENSOR PROVIDES THE LICENSED MATERIAL "AS IS" AND MAKES NO OTHER REPRESENTATION OR WARRANTY. LICENSOR EXPRESSLY DISCLAIMS ANY LIABILITY FOR ANY CLAIM ARISING FROM OR OUT OF THE CONTENT, INCLUDING BUT NOT LIMITED TO ANY ERRORS, INACCURACIES, OMISSIONS, OR DEFECTS CONTAINED THEREIN, AND ANY IMPLIED OR EXPRESS WARRANTY AS TO MERCHANTABILITY OR FITNESS FOR A PARTICULAR PURPOSE. IN NO EVENT SHALL LICENSOR BE LIABLE TO YOU OR ANY OTHER PARTY OR ANY OTHER PERSON OR FOR ANY SPECIAL, CONSEQUENTIAL, INCIDENTAL, INDIRECT, PUNITIVE, OR EXEMPLARY DAMAGES, HOWEVER CAUSED, ARISING OUT OF OR IN CONNECTION WITH THE DOWNLOADING, VIEWING OR USE OF THE LICENSED MATERIAL REGARDLESS OF THE FORM OF ACTION, WHETHER FOR BREACH OF CONTRACT, BREACH OF WARRANTY, TORT, NEGLIGENCE, INFRINGEMENT OR OTHERWISE (INCLUDING, WITHOUT LIMITATION, DAMAGES BASED ON LOSS OF PROFITS, DATA, FILES, USE, BUSINESS OPPORTUNITY OR CLAIMS OF THIRD PARTIES), AND WHETHER OR NOT THE PARTY HAS BEEN ADVISED OF THE POSSIBILITY OF SUCH DAMAGES. THIS LIMITATION APPLIES NOTWITHSTANDING ANY FAILURE OF ESSENTIAL PURPOSE OF ANY LIMITED REMEDY PROVIDED HEREIN.

10. Termination and Cancellation

10. 1. The License and all rights granted hereunder will continue until the end of the applicable period shown in Clause 5.1 above. Thereafter, this license will be terminated and all rights granted hereunder will cease.

10. 2. Licensor reserves the right to terminate the License in the event that payment is not received in full or if you breach the terms of this License.

11. General

11. 1. The License and the rights and obligations of the parties hereto shall be construed, interpreted and determined in accordance with the laws of the Federal Republic of Germany without reference to the stipulations of the CISG (United Nations Convention on Contracts for the International Sale of Goods) or to Germany's choice-of-law principle.

11. 2. The parties acknowledge and agree that any controversies and disputes arising out of this License shall be decided exclusively by the courts of or having jurisdiction for Heidelberg, Germany, as far as legally permissible.

11. 3. This License is solely for Licensor's and Licensee's benefit. It is not for the benefit of any other person or entity.

Questions? For questions on Copyright Clearance Center accounts or website issues please contact springernaturesupport@copyright.com or +1-855-239-3415 (toll free in the US) or +1-978-646-2777. For questions on Springer Nature licensing please visit https://www.springernature.com/gp/partners/rights-permissions-third-party-distribution

Other Conditions:

Version 1.4 - Dec 2022

Questions? customercare@copyright.com.